

Alma Mater Studiorum – Università di Bologna

DOTTORATO DI RICERCA IN

Meccanica e Scienze Avanzate dell'Ingegneria

Ciclo XXX

Settore Concorsuale: 09/C1

Settore Scientifico Disciplinare: ING-IND/08

OPTIMIZATION STRATEGIES FOR COMPLEX ENERGY NETWORKS
WITHIN DISTRIBUTED GENERATION

Presentata da: Maria Alessandra Ancona

Coordinatore Dottorato

Prof. Marco Carricato

Supervisore

Prof. Francesco Melino

Esame finale anno 2018

Contents

Introduction	1
Structure of the manuscript	3
Nomenclature	5
1. Complex Energy Networks and Distributed Generation	6
<i>References</i>	12
2. District Heating Networks	14
<i>References</i>	21
3. DHNs design and analysis	24
3.1 <i>The Todini-Pilati algorithm</i>	24
3.2 <i>Software Ca.R.Di.F.</i>	27
3.3 <i>Software validation.</i>	30
<i>References</i>	34
4. Smart District Heating	35
4.1 <i>Users substations in Smart District Heating Networks</i>	35
4.2 <i>Software IHENA</i>	38
4.3 <i>Thermodynamic considerations on the proposed schemes</i>	40
4.4 <i>Transformation hypothesis for the conversion of an existing user substation into a smart one</i>	45
4.4.1 <i>Case 1</i>	50
4.4.2 <i>Case 2</i>	58
<i>References</i>	68

5. Scheduling optimization methods in complex energy networks	69
5.1 <i>Genetic algorithms</i>	69
5.2 <i>Mixed Integer Linear Programming models</i>	72
5.3 <i>Mixed Integer Non-Linear Programming models</i>	74
<i>References</i>	76
6. Software EGO	78
6.1 <i>Calculation model</i>	78
6.2 <i>Software test versus alternative approach</i>	83
<i>References</i>	88
7. Optimization analysis – case study I	89
7.1 <i>DHN current set-up</i>	89
7.2 <i>Phase I: thermal needs fulfillment</i>	91
7.2.1 <i>Thermal needs profile definition</i>	92
7.2.2 <i>Case studies: characteristics and assumptions</i>	94
7.2.3 <i>Results and discussion</i>	98
7.3 <i>Phase II: thermal, electrical and cooling energy fulfillment</i>	105
7.3.1 <i>Energy needs analysis</i>	105
7.3.2 <i>Optimal management strategies – Case studies</i>	111
7.3.3 <i>Results and discussion</i>	117
<i>References</i>	135
8. Optimization analysis – case study II	137
8.1 <i>Case Study</i>	137
8.2 <i>Energy Systems</i>	140
8.3 <i>Energy Systems Off-design Operation and Others Assumptions</i>	145
8.4 <i>Energy Results</i>	148
8.5 <i>Economic and Environmental Results</i>	153
<i>References</i>	158

9. MILP optimization – comparison	160
9.1 Case Study	160
9.2 Software MEGS	161
9.3 Results	163
9.3.1 DHN design.....	163
9.3.2 Energy systems operation	164
9.3.3 Computational time	165
9.3.4 Integration between GA and MILP approaches	165
References	167
Conclusions	168
List of Tables	172
List of Figures	173
Appendix A	180
Appendix B	183
Appendix C	187

Introduction

In many European countries, the amount of distributed generation systems has been considerably increased in the last years, mainly due to the EU energy targets – first of all the so-called “20-20-20” strategy – and to the related national energy policies enforcement. Furthermore, the European strategy 20-20-20 – providing for energy efficiency increase, pollutant emissions reduction and fossil fuel consumption reduction – leads to an increasing attention on the concept of smart cities.

In the next years energy grids are expected to become increasingly complex, due to the integration between traditional generators (operating with fossil fuels, especially natural gas), renewable energy production systems and storage devices. In addition to the well-known and largely diffused electricity smart grids, the new concept of smart thermal network – and, in particular, smart district heating – has been recently developed. In fact, the possibility to allow a bidirectional heat exchange at final users, where solar thermal panels or small-size combined heat and power units are installed, seems to be a promising solution for the global conversion efficiency increase.

On the other hand, the increase in installed distributed generation systems is posing new issues for the existing grids. The integration involves both electric grids and thermal networks, such as district heating networks. As it regards electricity grids, the presence of non-programmable renewable sources causes some issues on grid frequency and stability, as well as the possibility of black-out events in case of wrong demand forecast and plants management. On the other hand, relating to thermal distribution networks (*i.e.* district heating networks), the idea of directly integrating distributed systems entails – in particular – the temperature levels of the network and, consequently, a correct district heating management is required.

In this scenario, it is fundamental to optimize the production mix and the operation of each system, in order to maximize the renewable energies exploitation, minimize the economic costs (in particular the fossil fuel consumption) and the environmental impact. As a result, one of the main purposes relating to the smart grids is the optimization of the scheduling (*i.e.* the load distribution) of the various energy production systems, which concur to the satisfaction of energy demand.

The determination of ideal systems set-up, as well as the control and operation of the integrated network, is not easy. With this purpose, several optimization algorithms can be applied, such as genetic algorithm (GA), particle swarm optimization and firefly algorithm – as it concerns heuristic models – or Linear Programming, Mixed Integer Linear Programming (MILP) and Mixed Integer Non Linear Programming (MINLP) models, as it regards exact methods. As it concerns energy networks, genetic algorithms and MILP based models are the most widely used for the scheduling optimization problems. Furthermore, MINLP models are considered as an interesting way, but further efforts have to be made in order to maintain the nonlinear complexity of the problem and an admissible computation time (the temporal horizon is usually 1 year of operation).

The aim of this Ph. D thesis is to investigate the complex energy networks scenario and elaborate innovative strategies and methods for the optimization of the energy systems scheduling (*i.e.* the optimal load allocation), in order to fulfill given electric, thermal and cooling needs of the users.

To this purpose, specific calculation codes have been developed and applied. The main objectives at the basis of the here presented work have been: (i) the minimization (or avoidance) of the electricity exchange with the national grid, (ii) the minimization (or avoidance) of the heat dissipations through the chimney, (iii) the minimization of the auxiliary boilers employment, (iv) the optimization of the cogeneration units operation and (v) the maximization of the renewable sources exploitation.

Innovative aspects of the work stand also in the definition of new configurations for user substation within district heating networks, in order to allow the bidirectional heat exchange and the transformation of the traditional networks into smart district heating networks.

Structure of the manuscript

This thesis is divided into four main parts:

Part I. The first part presents an overview of the scenarios of interest and motivates the work by outlining the fundamental key aspects concerning the integration between energy distribution networks and distributed generation systems. In particular, Chapter 1 presents an overview of the concept of complex energy networks and distributed generation technologies. Chapter 2, instead, focuses on the state of the art of district heating networks, considering both the World and the Italian context.

Part II. In this section a thermo-hydraulic analysis on district heating has been carried out. In particular, in Chapter 3 the mathematical model of an in-house developed software (called Ca.R.Di.F. – Calcolo Reti Distribuzione Fluidi) for the design and analysis of district heating and cooling networks is presented, along with its validation. To this purpose, a comparison with a commercial software on a case study is presented and discussed. Then, in Chapter 4 the concept of smart district heating is deeply investigated. In detail, four elaborated innovative configurations for users substations, able to guarantee the bidirectional heat exchange, are described and their implementation into the Ca.R.Di.F. software is shown, giving birth to the new software IHENA (Intelligent Heat Network Analysis). Furthermore, the effects of the four configurations on the network have been thermodynamically analyzed, with the help of a case study, and two different transformation hypotheses for the conversion of an existing user substation into a smart one have been conceived. For each of the proposed transformation hypotheses, a specific logic of operation has been elaborated and a techno-economic analysis has been carried out.

Part III. The third part of this thesis focuses on the scheduling optimization within complex energy networks. In Chapter 5 the state of the art of the main algorithms currently applied for the optimization of the energy systems load allocation is discussed, while in Chapter 6 the mathematical model of the in-house developed software EGO (Energy Grid Optimizer), based on genetic algorithms, is presented. This software has been applied to several case studies: the most representatives are discussed in Chapter 7 (middle size district energy network) and in Chapter 8 (isolated grid). In detail, indeed, in Chapter 7, starting from the current configuration and operation set-up, new optimized strategies for users' needs fulfillment in an existing middle size district heating network have been evaluated. Two different approaches have been investigated: the first one considers the fulfillment only of the thermal needs of the users while the second one adds the electricity and cooling energy fulfillment. For both of these approaches, various energy systems set-up have been hypothesized (including renewable energy systems, heat pumps, cogenerators, compression and absorption chillers, etc.) and the energy systems scheduling has been optimized by means of EGO. A comparison – from both economic and environmental points of view – has been carried out in order to define the most suitable technologies for the analyzed

case study. On the other hand, in Chapter 8 a particular application of isolated grid, *i.e.* a cruise ship, has been analyzed. As for the previous case, several energy systems set-up have been proposed, operationally optimized with the software EGO and comparatively analyzed, in order to find the best solution for the given cruise demand profile (in terms of electrical, thermal and cooling energy).

Part IV. Chapter 9 describes the comparison between genetic algorithms and MILP models to solve scheduling optimization problems, carried out during the PhD period abroad, at the École Polytechnique Fédérale de Lausanne (EPFL) – Valais offices. In more detail, the main characteristics of the MEGS software, developed by EPFL, are described and the results of its application to a case study are compared to the ones of the software EGO, outlining pro and cons of both the approaches.

Acknowledgments

A number of persons have directly or indirectly contributed to this research. I thank in particular my advisor, Prof. Francesco Melino, and the whole research group, Prof. Michele Bianchi, Prof. Antonio Peretto and Prof. Andrea De Pascale. I would like to thank also my colleagues, in particular Lisa Branchini and Valentina Orlandini, for their continuous support and friendship during my PhD years.

Nomenclature

Abbreviations

AB	Auxiliary Boiler
AC	Absorption Chiller
BB	Biomass Boiler
CaRDIF	Calcolo Reti Distribuzione Fluidi
CC	Compression Chiller
CHP	Combined Heat and Power
DG	Distributed Generation
DH	District Heating
DHN	District Heating Network
EES	Electrical Energy Storage
EGO	Energy Grid Optimizer
FC	Fuel Cell
FF	Fitness Function
FFA	FireFly Algorithm
GA	Genetic Algorithm
GT	Gas Turbine
HE	Heat Exchanger
HP	Heat Pump
ICE	Internal Combustion Engine
ICT	Information & Communication Technology
IHENA	Intelligent Heat Network Analysis
LP	Linear Programming
MDO	Marine Diesel Oil
MEGS	Multi Energy Grid Systems
MGT	Micro Gas Turbine
MILP	Mixed Integer Linear Programming
MINLP	Mixed Integer Non Linear Programming
PM	Prime Mover
PSO	Particle Swarm Optimization
PV	PhotoVoltaic
RES	Renewable Energy Source
RG	Renewable Generator
SDHN	Smart District Heating Network
SST	Storage Tank
TES	Thermal Storage
TSP	Thermal Solar Panels

Symbols

A	area [m ²]
CF	fixed cost [€]
c_l	liquid specific heat [kJ/kg°C]
COP	Coefficient Of Performance [-]
CT	total cost [€]
CV	variable costs [€]
ΔH	pressure losses [Pa]
D	diameter [m]
E	energy [kWh]
EER	Energy Efficiency Ratio [-]
F	fuel consumption [kWh]
f	drag coefficient

H	energy content of fluid [Pa]
I	solar irradiation [W/m ²]
IC	incremental cost [€/kW]
L	length [m]
\dot{m}	mass flow rate [kg/s]
v	mean velocity [m/s]
p	pressure [bar]
P	perimeter [m]
P	electrical power [kW]
Q	thermal power
ROI	return of investment [y]
Re	Reynolds number [-]
S	surface [m ²]
T	temperature [°C]
U	global heat exchange coefficient [W/m ² K]
V	volume [m ³]

Greek symbols

α	convection coefficient [W/m ² K]
β	coeff. of concentrated pressure losses [-]
ε	roughness [mm]
H	efficiency [-]
λ	conduction coefficient [W/mK]
μ	dynamic viscosity [Pa·s]
ζ	specific cost [€/kW]
ρ	density [kg/m ³]

Subscripts and superscripts

<i>conc</i>	concentrated
<i>des</i>	design
<i>dis</i>	distributed
<i>diss</i>	dissipated
<i>e</i>	electrical
<i>ext</i>	external
<i>F</i>	fictitious
<i>h</i>	hydraulic
<i>IN</i>	at the inlet
<i>ins</i>	insulating
<i>int</i>	internal
M	maintenance
<i>m</i>	mean
max	maximum
min	minimum
<i>OUT</i>	at the outlet
<i>p</i>	pipe
P	purchase
S	sale
th	thermal
<i>u</i>	user

1. Complex Energy Networks and Distributed Generation

In the last years, energy grids became a central issue for the achievement of the standards imposed by international regulations on environment preservation matter. With this purpose, the integration between distributed generation systems (in particular renewable energy sources generators) and traditional production systems has been promoted for the fulfillment of the users need [1, 2]. The consequent increase in the complexity of the energy networks develops new challenges in energy sector.

In more detail, the integration involves both electric grids and thermal networks, such as district heating networks. Consequently, as shown in Figure 1.1, at present a complex energy grid may be defined as a network for energy supply, consisting in electrical, thermal and cooling networks with centralized and distributed generation. The presence of storage systems – particularly suitable for renewable non-programmable sources, as better explained in the following of the chapter – has to be considered for this kind of networks. Furthermore, in the next years, the possibility to produce (from renewables, by means of electrolysis and methanation reactions) and distribute methane throughout the natural gas grid can be forecasted. As a consequence, also fuel networks are expected to be part of the future complex energy networks.

The evolution of energy networks' concept is presented in Figure 1.2: at the beginning electric grids and thermal networks (*i.e.* district heating) were conceived as completely separate distribution networks supplied by centralized electric or thermal power plants. However, the introduction of combined heat and power systems and distributed generation had led to several modifications. In the electricity grid scenario, the installation of distributed generators gave birth to the well-known *smart grids*, allowing the bidirectional electricity exchange at the final users. A subsequent step, which – at present – is not yet largely diffused, was the replication of the idea of smart grid in the heat sector, considering the possibility to interconnect district heating networks and thermal energy distributed generators (*smart district heating*). This innovative concept will be deeply discussed in the following chapters. Based on the concepts of smart grids and smart district heating, and aiming to focus on an energy district, the idea of complex energy network can be elaborated. The target of these kind of networks is mainly a neighborhood, thus they belongs to small-medium size networks. As for electricity generation, the main involved technologies are the ones shown in Figure 1.3 for domestic/residential and industry applications (*i.e.* for sizes up to around 1 MW_e).

Possible further modifications, in future, may led to the communication and integration between different complex energy network, as well as to the inclusion of distributed methane production and distribution. This latter technology, based on electrolysis and methanation processes starting from renewable sources (both programmable, such as biomass, and non-programmable, such as wind and solar), is at present mainly applied at a laboratory scale but future applications are expected [3].

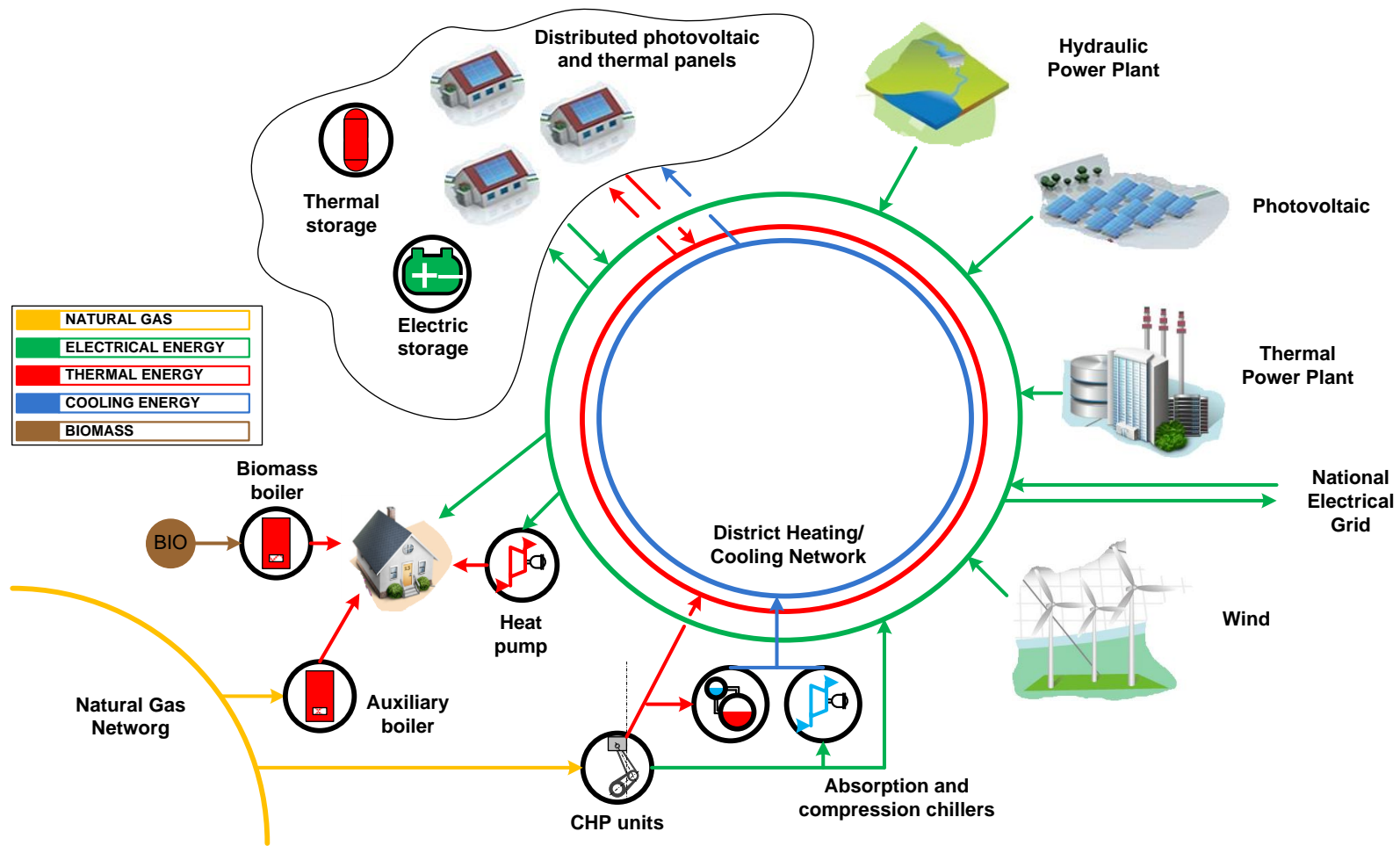


Figure 1.1 – Example of a complex energy networks.

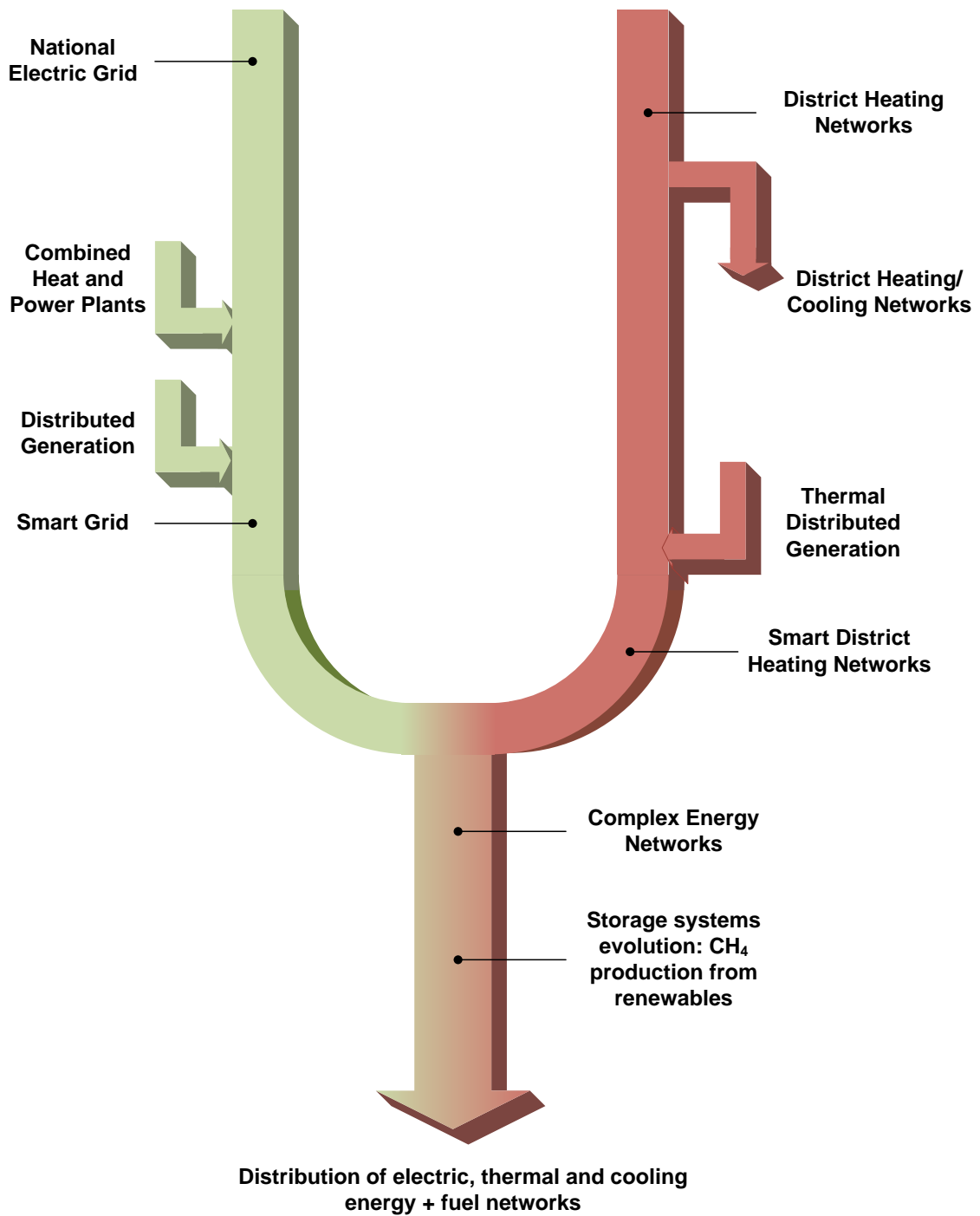


Figure 1.2 – Evolution of energy networks concept.

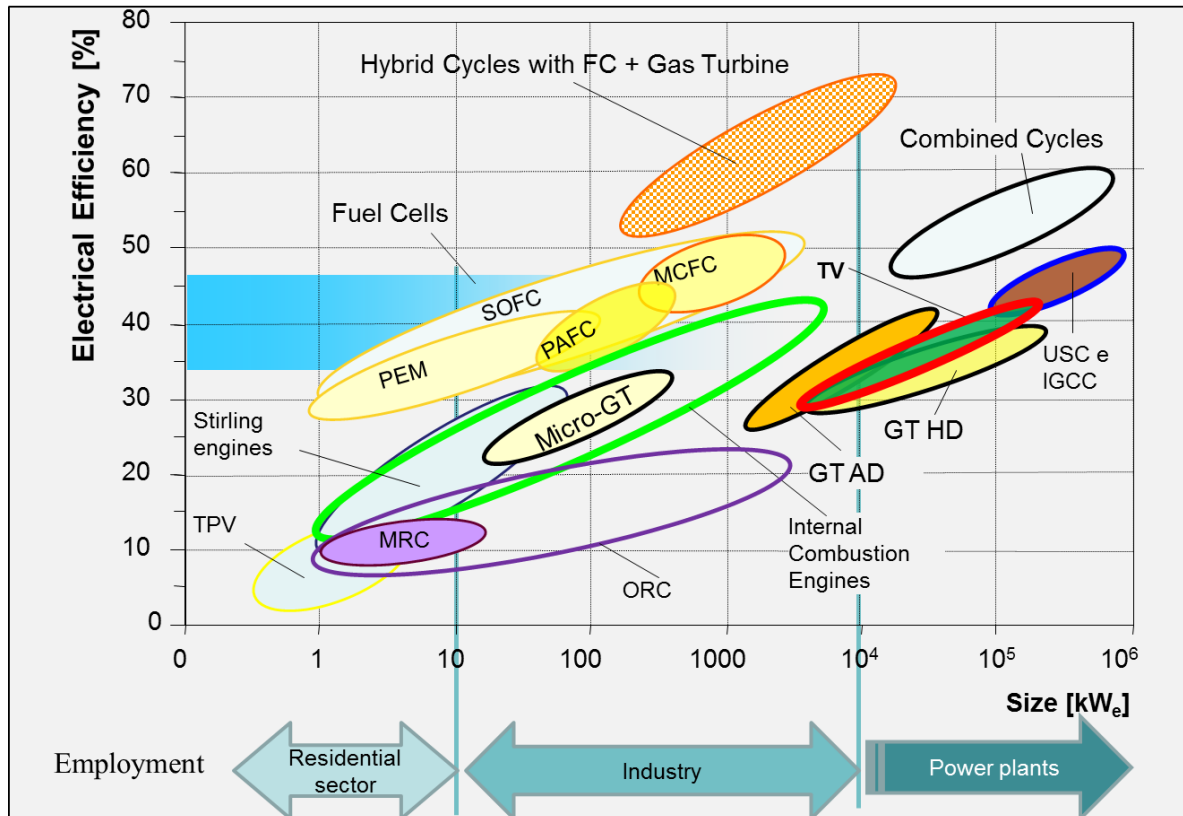


Figure 1.3 – Technologies for electrical energy generation as function of the size.

In this scenario, it is fundamental to optimize the energy production mix and the operation of each system, in order to maximize the renewable energies exploitation, minimize the economic costs (in particular the fossil fuel consumption) and the environmental impact.

In particular, as it regards the residential sector, it has been estimated that cities are responsible for the 67% of the world's energy demand and are the major contributors of CO₂ emissions, producing more than the 70% of the global CO₂ emissions [4]. Furthermore, it is expected that the world population who lives in the cities will increase in the next years, from the current percentage of 55% to a percentage equal to 66% in 2050. As a consequence, urban areas will have a crucial role in the climate change contrast [5]. For these reasons, governments and researchers promote energy policy initiatives focused on the increase in the sustainability of urban areas. Furthermore, the rational exploitation of renewable sources, the improvement in conversion efficiencies, the reduction of wasted energy and the minimization of pollutant emissions are the crucial purposes of any energy policy, whether applied at local, national or global level [2].

Relating to the electric smart grids, the diffusion of distributed energy production systems on territory has been recognized as a cost-effective solution [6, 7]. In fact, the installation of distributed generators within the cities enables to reduce the losses related to energy transportation and distribution, contemporarily allowing for the consumers the exchange of their own produced energy. Moreover, the installation of FC of small size generators close to users (both in

residential and industrial buildings) is expected to improve fuel energy exploitation through cogeneration and tri-generation plants.

Distributed Generation (DG) plays a fundamental role also in rural areas, where power delivery over long distance is difficult and/or uneconomical [8]. In those areas, energy supply requirements must be guaranteed taking advantage from stand-alone hybrid systems typically dependent on renewable sources [9]. As a consequence, a key role in the DG network is played by renewables and, in particular, by the non-programmable sources such as solar and wind [10, 11]. As known, the characteristics of non-programmable sources are adverse to the diffusion of renewable energy: in particular, intermittency presents a great challenge in energy generation and load balance maintenance to ensure power network stability and reliability [12-15]. Great efforts have been made in searching for viable solutions, including Electrical Energy Storage (EES), load shifting through demand management, interconnection with external grids, etc. Among all, EES has been recognized as one of the most promising solution with a huge potential in meeting renewable challenges [10, 16]. In Figure 1.4 the top ten Countries for federal smart grid investment at 2010 is presented [17].

In addition to renewables based energy conversion systems, other traditional technologies are usually considered as optimal solutions, in terms of cost performance, maintenance, future perspectives and environmental issues. Among the others, micro-gas turbines [18, 19] and internal combustion engines [20] are predicted to be essential because of their features in terms of costs (particularly advantageous for internal combustion engines), maintenance (in particular for micro-gas turbines), emissions (considering natural gas as fuel) and total efficiency (cogeneration or tri-generation application). Furthermore, as it regards electricity generation, fuel cells [21-23] and hybrid systems [24-27] are expected to be a good near term solution due to their high electrical efficiency conditions, even though some technical and cost issues must still be solved (*e.g.* cost and reliability aspects [28, 29], component integration [30, 31] and control system problems [32-34]).

All of the aforementioned technologies, as well as the distribution networks themselves need to be optimized in terms of size and management, in order to guarantee the complete fulfillment of users' needs and to minimize primary energy consumption and environmental impact.

Various publications investigate the optimal design of a single technology or the optimal choice of sets of technologies. Examples of the first typology of investigation can be found in [35-38], for what concerns thermal solar or photovoltaic energy systems, or in [39, 40] for tri-generation systems. Relating to the choice of sets of technologies, instead, Zhou et al. [41] propose a model for the optimal design of DGs considering the possibility to install a wide set of distributed energy systems. Furthermore, in [42] an advanced model for the optimal design and operation of distributed generators integrated with energy distribution networks is developed. Similarly, but considering the energy hub concept, the optimized installation of DGs in a neighborhood and the resulting energy distribution is evaluated in [43]. Finally, the study presented in [44] introduces a Distributed Energy Network Optimization model in order to choose the optimal set-up of energy production systems and evaluate the energy fluxes among the different users.

It should be noted that all the aforementioned models are technology driven, *i.e.* the design and the optimization mainly regard the choice of the technology to be integrated within the energy distribution network. They consider both economic and environmental aspects, being very useful for the design of distributed generators, but the operation of these systems is not optimized. Furthermore, due to the high level of detail of the models, they have a high computational complexity, which grows with the increase in the number of technologies involved in the design

optimization process and the number of buildings considered in the exchange. As a consequence, the previous models are not able to find optimal distributed configurations when a large amount of consumers and producers are considered.

The load allocation optimization between the energy systems connected to complex networks, being fundamental to reach the economic and environmental goals, will be discussed in detail in the second part of this PhD thesis (Chapters from 5 to 9).



Figure 1.4 – Top ten Countries for federal smart grid investment at 2010 [17].

References

- [1] International Energy Agency. Renewable energy medium-term market report 2014 – market analysis and forecast to 2020. Paris, France; 2014.
- [2] Directive 2009/28/EC of the European Parliament and of the Council of 23 April 2009 on the promotion of the use of energy from renewable sources and amending and subsequently repealing Directives 2001/77/EC and 2003/30/EC (Text with EEA relevance).
- [3] Ancona MA, De Pascale A, Melino F. Analisi delle prestazioni di un Sistema di Accumulo energetico alimentato da fonte rinnovabile e basato su: la generazione di H₂, l'utilizzo della CO₂, la conversione in CH₄ e l'immissione nella rete del gas naturale. PAR CNR 2012-2014.
- [4] Fifth Assessment Report, AR5, available at <<http://www.ipcc.ch/report/ar5/index.shtml>>.
- [5] Lindseth G. The cities for climate protection campaign (CCPC) and the framing of local climate policy. *Local Environ*, 9 (2004) 325-36.
- [6] Fichera A, Frasca M, Volpe R. Complex networks for the integration of distributed energy systems in urban areas. *Applied Energy*, 193 (2017) 336-345.
- [7] Bayod-Rujula AA. Future development of the electricity systems with distributed generation. *Energy*, 34 (2009) 377-383.
- [8] Bianchi M, Branchini L, De Pascale A, Peretto A. Application of environmental performance assessment of CHP systems with local and global approaches. *Applied Energy*, 130 (2014) 774-782.
- [9] Abd-el-Motaleb AM, Kazem Bekdach S. Optimal sizing of distributed generation considering uncertainties in a hybrid power system, *International Journal of Electrical Power & Energy Systems*, 82 (2016) 179-188.
- [10] Bianchi M, Branchini L, Ferrari C, Melino F. Optimal sizing of grid-independent hybrid photovoltaic–battery power systems for household sector. *Applied Energy*, 136 (2014) 805-816.
- [11] Ancona MA, Bianchi M, Branchini L, De Pascale A, Melino F, Peretto A. Generation Side Management In Smart Grid. *Proceedings of ASME ATI-UIT Conference on Thermal Energy Systems: Production, Storage, Utilization and the Environment*, 2015.
- [12] Branchini L, Perez-Blanco H. Handling Wind Variability Using Gas Turbine. *Proceedings of ASME Turbo Expo 2012*, 6 (2012) 727-734. 11-12 June 2012, Copenhagen, Denmark.
- [13] Branchini L, Perez-Blanco H. Computing Gas Turbine Fuel Consumption To Firm Up Wind Power. *Proceedings of ASME Turbo Expo 2012*, 6 (2012) 735-741. 11-12 June 2012, Copenhagen, Denmark.

- [14] Bianchi M, Branchini L, Cavina N, Cerofolini A, Corti E, De Pascale A, Orlandini V, Melino F, Moro D, Peretto A, Ponti F. Managing wind variability with pumped hydro storage and gas turbines. *Energy Procedia*, 45 (2014) 22-31.
- [15] Bianchi M, Branchini L, Cavina N, Cerofolini A, De Pascale A, Melino F. Wind-hydro-gas turbine unit commitment to guarantee firm dispatchable power, *Proceedings of ASME Turbo Expo 2014*, 16 - 20 June, 2014, Dusseldorf, Germany.
- [16] Bianchi M, Branchini L, De Pascale A, Melino F. Storage Solutions for Renewable Production in Household Sector. *Energy Procedia*, 61 (2014) 242-245.
- [17] Zpryme Research and Consulting.
- [18] Wang W, Cai R, Zhang N. General characteristics of single shaft microturbine set at variable speed operation and its optimization. *Applied Thermal Engineering*, 24 (2004) 1851-1863.
- [19] Al-attab KA, Zainal ZA. Externally fired gas turbine technology: a review. *Applied Energy*, 138 (2015) 474-487.
- [20] Fragaki A, Andersen AN, Toke D. Exploration of economical sizing of gas engine and thermal store for combined heat and power plants in the UK. *Energy*, 33 (2008) 1659-1670.
- [21] Singhal SC. Advances in solid oxide fuel cell technology. *Solid State Ionics*, 135 (2000) 305-313.
- [22] Massardo AF, Bosio B. Assessment of molten carbonate fuel cell models and integration with gas and steam cycles. *Journal of Engineering for Gas Turbines and Power*, 124 (2002) 103-109.
- [23] Baba S, Kobayashi N, Takahashi S, Hirano S. Development of anode gas recycle system using ejector for 1 KW solid oxide fuel cell. *Journal of Engineering for Gas Turbines and Power*, 137 (2015).
- [24] Veyo S, Shockling LA, Dederer JT, Gillett JE, Lundberg WL. Tubular solid oxide fuel cell/gas turbine hybrid cycle power systems: status. *Journal of Engineering for Gas Turbines and Power*, 124 (2002) 845-849.
- [25] Ferrari ML, Massardo AF. Cathode-anode interaction in SOFC hybrid systems. *Applied Energy*, 105 (2013) 369-379.
- [26] Bakalis DP, Stamatis AG. Incorporating available micro gas turbines and fuel cell: matching considerations and performance evaluation. *Applied Energy*, 103 (2013) 607-617.
- [27] Jia Z, Sun J, Dobbs H, King J. Feasibility study of solid oxide fuel cell engines integrated with sprinter gas turbines: modeling, design and control. *Journal of Power Sources*, 275 (2015) 111-125.
- [28] Wang J. Barriers of scaling-up fuel cells: cost, durability and reliability. *Energy*, 80 (2015) 509-521.

- [29] Mostofi F, Safavi M. Application of ABC algorithm for grid-independent hybrid hydro/photovoltaic/wind/fuel cell power generation system considering cost and reliability. *International Journal of Renewable Energy Research*, 3 (2013) 928-940.
- [30] Peters R, Deja R, Blum L, Pennanen J, Kiviaho J, Hakala T. Analysis of solid oxide fuel cell system concepts with anode recycling. *International Journal of Hydrogen Energy*, 38 (2013) 6809-6820.
- [31] Ferrari ML, Traverso A, Pascenti M, Massardo AF. Early start-up of SOFC hybrid systems with ejector cathodic recirculation: experimental results and model verification. Proceedings of the institution of mechanical engineers, Part A. *J Power Energy*, 221 (2007) 627-635.
- [32] McLarty D, Brouwer J, Samuelsen S. Fuel cell-gas turbine hybrid system design part II: Dynamics and control. *Journal of Power Sources*, 254 (2014) 126-136.
- [33] Ferrari ML. Advanced control approach for hybrid systems based on solid oxide fuel cells. *Applied Energy*, 145 (2015) 364-373.
- [34] Ferrari ML. Solid oxide fuel cell hybrid system: control strategy for stand-alone configurations. *Journal of Power Sources*, 196 (2011) 2682-2690.
- [35] La Gennusa M, Lascari G, Rizzo G, Scaccianoce G, Sorrentino G. A model for predicting the potential diffusion of solar energy systems in complex urban environments. *Energy Policy*, 39 (2011) 5335-5343.
- [36] Kanters J, Wall M. A planning process map for the solar buildings in urban environments. *Renewable and Sustainable Energy Reviews*, 57 (2016) 173-185.
- [37] Humada AM, Hojabri M, Hamada HM, Samsuri FB, Ahmed MN. Performance evaluation of two PV technologies (c-Si and CIS) for building integrated photovoltaic based on tropical climate condition: a case study in Malaysia. *Energy Build*, 119 (2016) 233-241.
- [38] Ren H, Gao W, Ruan Y. Economic optimization and sensitivity analysis of photovoltaic system in residential buildings. *Renewable Energy*, 34 (2009) 883-889.
- [39] Ascione F, Canelli M, De Masi RF, Sasso M, Vanoli GP. Combined cooling, heating and power for small urban districts: an Italian case study. *Applied Thermal Engineering*, 71 (2013) 705-713.
- [40] Chmielewski A, Guminski R, Maczak J, Radkowski S, Szulim P. Aspects of balanced developments of RES and distributed micro-cogeneration use in Poland: case study of a I-CHP with Stirling engine. *Renewable and Sustainable Energy Reviews*, 60 (2016) 930-952.
- [41] Zhou Z, Liu P, Li Z, Ni W. An engineering approach to the optimal design of distributed energy systems in China. *Applied Thermal Engineering*, 53 (2013) 387-396.
- [42] Yang Y, Zhang S, Xiao Y. Optimal design of distributed energy resource systems coupled with energy distribution networks. *Energy*, 85 (2015) 433-448.

- [43] Orehounig K, Evins R, Dorer V. Integration of decentralized energy systems in neighborhoods using the energy hub approach. *Applied Energy*, 154 (2015) 277–289.
- [44] Omu A, Choudhary R, Boies A. Distributed energy resource system optimization using mixed integer linear programming. *Energy Policy*, 61 (2013) 249-266.

2. District Heating Networks

In order to increase the efficiency and the safety of energy networks, District Heating Networks (DHNs) are promoted by European and national regulations [1, 2], as well as by United Nations [3]. In fact, with the aim to obtain several advantages, with regard to either practical or environmental and safety aspects, the direct production of thermal energy for hot water and space heating can be replaced with the district heating.

District Heating Networks, indeed, have found a large development after the World War II. The main advantage of DHNs is the reduction of pollutant and thermal emissions in the city area. Further, the large use of DHNs increases the safety, due to the absence of combustion systems at the final users of thermal energy. For the same reason, also the transportation of fuel in the city area can be drastically reduced by the use of DHNs. Last but not least, the district heating allows to achieve high conversion efficiencies by centralizing in few large power plants the need of thermal energy in household sector. Usually, the power plants that feed the District Heating Networks work by combined heat and power set-up and the network is crossed by hot water or steam, ranging from 90 to 130°C [4].

Often, in order to promote an efficient thermal energy production, DHNs are supplied with the heat produced by means of Combined Heat and Power (CHP) units. For example, in Finland the 80% of the heat distributed through DHN is produced by centralized CHP units [5, 6], while in China about the 62.9% of district heat is produced in cogeneration [7]. In this kind of networks, an energy efficiency improvement and a costs reduction can be reached with an optimal location of the peak boilers, as reported in [8]. For further efficiency improvement, however, the integration of Renewable Energy Sources (RES) in the CHP-DH scenario can be seen as an interesting solution. The intermittent and non-programmable nature of this typology of energy source can be overcome with the introduction of opportune storage systems [9]. In Europe, some instances of integrated thermal grids are present, considering the integration of different technologies – such as heat pumps, solar panels, waste-to-energy systems, CHP, etc. – with renewable sources for the production of thermal energy [10, 11]. As an example, at the Delft University of Technology the 17% of thermal and cooling needs is currently provided by a system which includes CHP units, geothermal systems and aquifer thermal storage [12], allowing an energy saving equal to about the 10%. Particularly, the positive effect of the introduction of heat pumps in district heating networks has been studied and confirmed [13, 14].

The world data, in terms of percentage of population supplied by district heating and thermal energy supplied to the users via DHN, are shown for several Countries respectively in Figure 2.1 and in Figure 2.2 [15].

As it regards the Italian scenario, nowadays 216 DHNs are present in 182 cities for a total connected volumetry of 330'000'000 m³ [16]. Figure 2.3 shows the increase of connected DHN volumetry since 1972 to 2015.

Currently, the thermal energy provided is about 10'491 GWh, combined with 6'212 GWh of electrical energy and 127 GWh of cooling energy. In this scenario, District Heating (DH) allows to save 506'000 toe and to avoid about 1'600'000 tons of CO₂ emissions [16]. The comparisons, in terms of primary energy and emissions of CO₂, between traditional production systems and systems in the service of DHNs are shown respectively in Figure 2.4 and Figure 2.5.

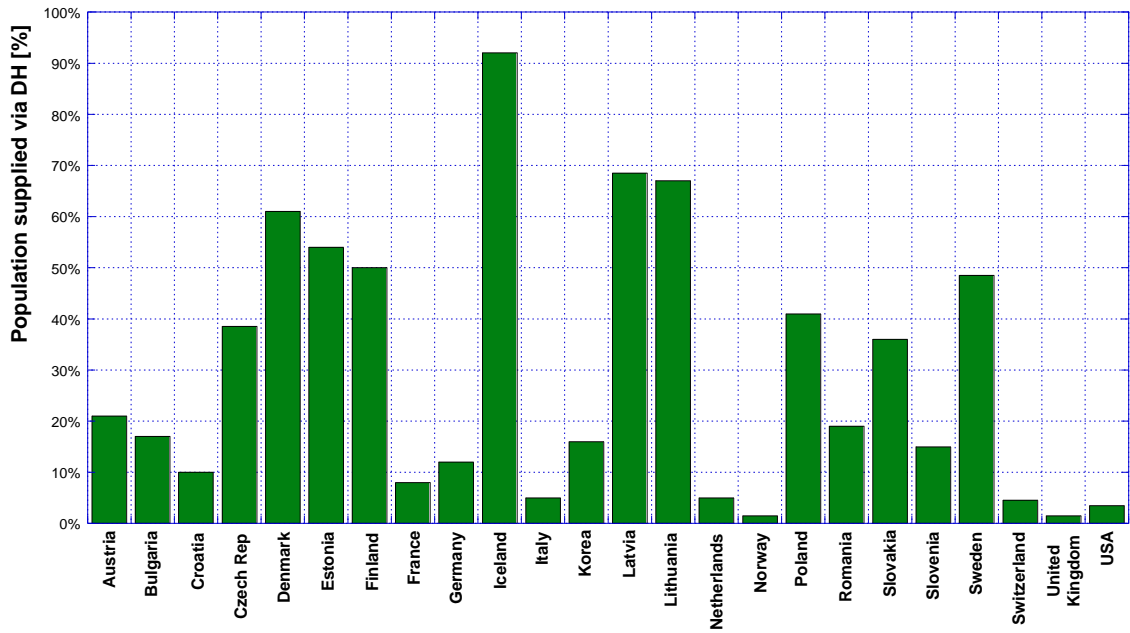


Figure 2.1 – Percentage of population supplied by district heating [15].

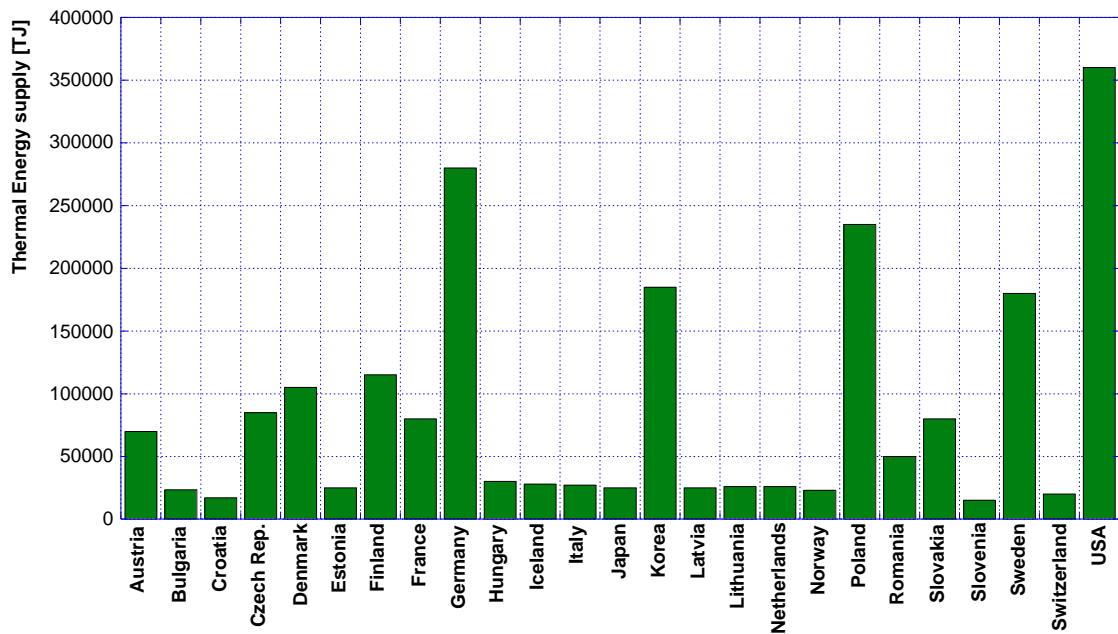


Figure 2.2 – Thermal energy supplied to the users via DHN in 2011, for several Countries [15].

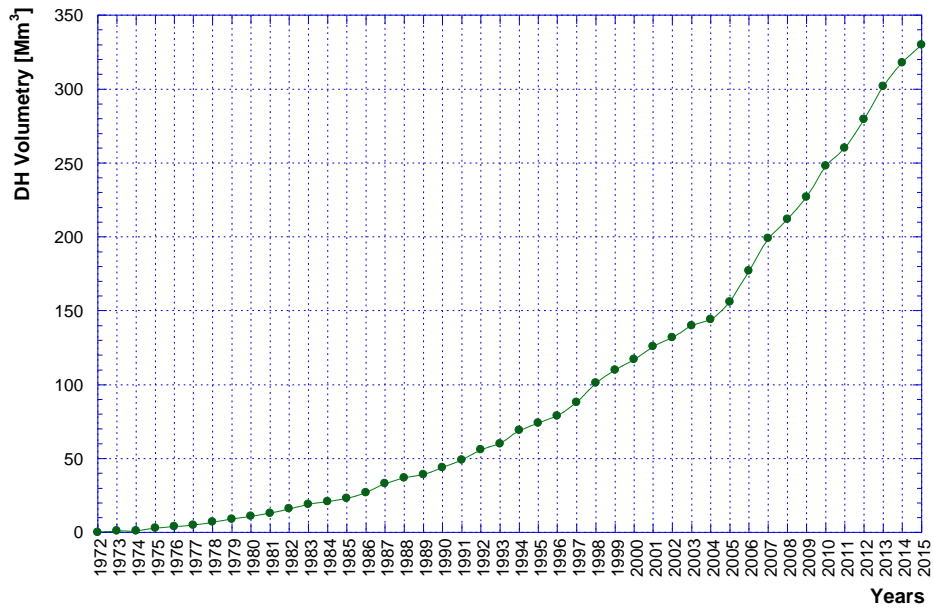


Figure 2.3 – Trend of the DHN connected volumetry in Italy from 1972 to 2015 [16].

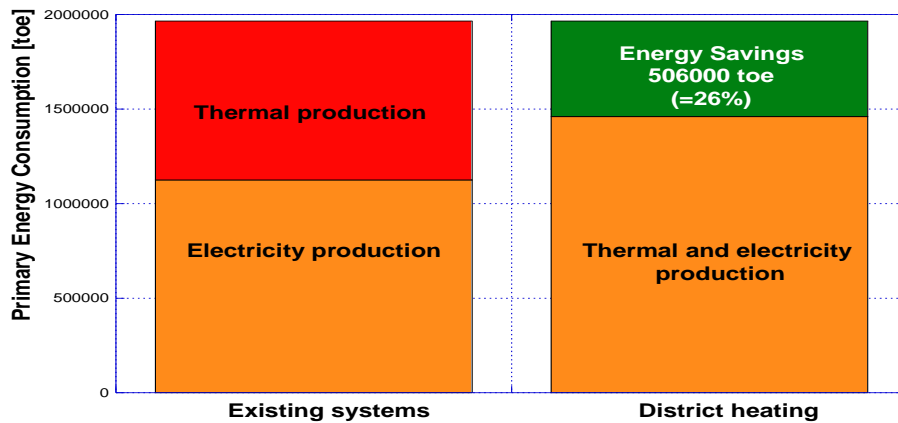


Figure 2.4 – Fossil primary energy savings with DHNs [16].

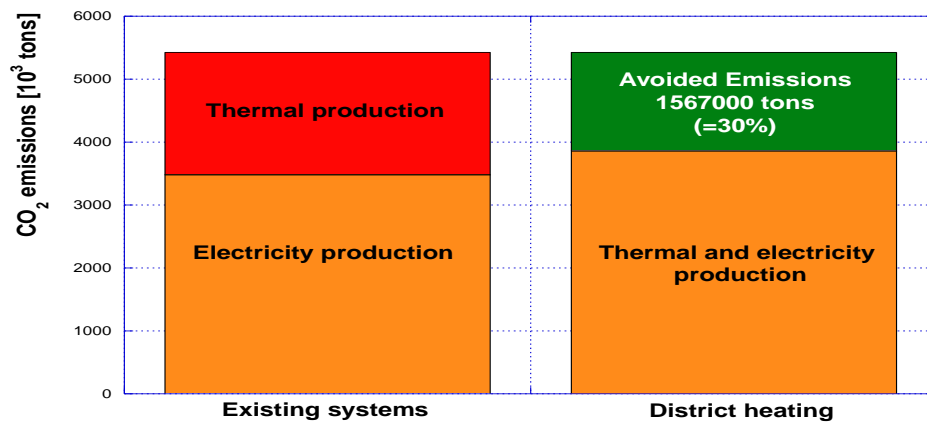


Figure 2.5 – CO₂ emissions [16].

In this context, several studies analyze and forecast the possible enhancements in district heating and cooling sector [17-20], highlighting the efforts to be made in order to maintain in the future this technology competitive as it concerns environmental and economic aspects.

With this purpose, in the last years a new concept of DHNs has been developed, that is the so called 4th generation District Heating (DH) [21]¹ or Smart District Heating Network (SDHN). This kind of networks replies, in heat sector, the concepts of distributed generation and of energy exchange between a prosumer (*i.e.* a producer and consumer of energy) and the grid, already known for the electrical sector. The basic idea, indeed, is the realization of a smart network, through the integration of distributed generation systems (from both renewable sources and/or fossil fuels) into the thermal network, in order to reproduce the well-known concept of electric smart grid [21]. In this way, a bidirectional thermal energy exchange can occur at final user: from the network to the user when the user need cannot be completely met by the distributed generator, from the user to the network when the decentralized production exceed with respect to the user need. Furthermore, the integration between DHNs and distributed generation systems allows to both increase the exploitation of renewable sources and reduce the thermal dissipations through the network, with consequent benefits on the whole integrated system efficiency [22-24].

Examples of SDHNs can be found in Central and Northern of Europe, such as in Sweden, Denmark [25], etc.; in particular, the distributed generation systems in these smart networks are often thermal solar generators. In this respect, it can be seen that, during the winter period, the solar generator satisfies only a fraction of the thermal energy need of the utility: the remaining part has to be supplied by the thermal distribution network. On the contrary, during the summer, it usually occurs that the solar production overcomes the thermal need: in this case the excess of production can be sold to the distribution network. It follows a bidirectional exchange of thermal energy between the distribution network and the user. In this case, the network can be used as seasonal storage: of course this can increase the efficiency of the whole system.

Obviously, also the cogeneration units can be used as decentralized thermal production systems in SDHNs. The only constraint to the bidirectional exchange regards the temperature at which the decentralized system produces the thermal energy with reference to the temperature of distribution network. For this reason, Combined Heat and Power (CHP) units, such as micro-turbines and internal combustion engines, can be easily integrated with DHN.

On the contrary, other systems such as micro Rankine cycles, solar thermal plates and Stirling engines could be characterized by a thermal production at temperature levels lower than the typical values of DHN. In this case the integration can occur only with particular configurations and/or under certain boundary conditions, as will be better explained in the following chapters.

Furthermore, the integration between DH and renewable sources has been deeply investigated in the last period [26], since it become one of the future major challenges in heat sector, even for the will of reaching the 100% renewable production [27]. Sayegh et al. [28] produced a report on European district heating current status and future expected modifications for a sustainable development, where Renewable Energy Sources (RES) are expected to play a key role. With this purpose, different kind of systems are considered, such as heat pumps, geothermal systems, solar collectors as well as combined heat and power units - representing a consolidated technology for

¹ The main characteristic of the first generation DH system was that the heat was transported with steam. In the second generation, instead, the heat is transported by pressurized super-heated water at temperatures above 100°C. The main difference of the 3rd generation DH system, finally, is the material and labor lean components applied combined with general lower temperatures.

the integration with DH. The overview proposed in [28] clearly confirms the necessity to realize smart DHNs in order to reach the sustainability goals imposed by the regulations.

CHP-DH integration [29-31], on the other hand, represents an economic and environmental viable solution to meet the climate change targets, as demonstrated in [29] for the United Kingdom context. This study shows how CHP-DH systems can potentially prevent important CO₂ emissions and allow an improvement in energy security due to the distributed generation and the increased energy efficiency. Furthermore, the importance of CHP technology in SDHNs is demonstrated in [32], where the role of cogeneration units and heat pumps is shown in order to balance the intermittency of renewable sources production.

Brand et al. [33] investigated the effect of the decentralized production on the network's technical parameters and, in particular, the modification in the network temperature levels due to the SDHN. This is a central issue for smart thermal grid, essentially for two reasons: *(i)* the distributed generation systems must be able to produce thermal energy with a temperature level higher than the network one, in order to make the heat introduction into the DH feasible; *(ii)* the management of the centralized thermal station becomes complex, since the temperature variation of the network piping could be frequent and important. For this reason, the modality of thermal exchange is a key point and possible typologies of utilities substation in SDHNs will be proposed and investigated in Chapter 4 [34]. As for the best Author's knowledge, indeed, there is a literature lack on technical modalities to practically convert existing DH utility substations in smart substations, able to guarantee a bidirectional thermal energy exchange for final users. The main researches, in fact, analyze possible configurations of DG systems substations focusing only on the production systems; in other words, they consider a DHN with a principal centralized production and with the addition of some DG systems scattered around the network, without the contextual presence of a thermal user. As an example, in [35] several configurations, for a solar collectors-based decentralized substation, are compared in order to analyze the interaction between DG and network. Similar considerations can be made about the study presented in [36]. However, this kind of decentralized substations can be considered as similar to the centralized one, while the presence of a final user poses new issues.

References

- [1] Directive 2009/28/EC of the European Parliament and of the Council of 23 April 2009 on the promotion of the use of energy from renewable sources and amending and subsequently repealing Directives 2001/77/EC and 2003/30/EC (Text with EEA relevance).
- [2] Connolly D, Lund H, Mathiesen BV, Werner S, Möller B, Persson U, et al. Heat roadmap Europe: combining district heating with heat savings to decarbonise the EU energy system. *Energy Policy*, 65 (2014) 475-89.
- [3] District energy in cities: unlocking the potential of energy efficiency and renewable energy. *United Nations Environment Programme* (UNEP), 2015.
- [4] Annuario Associazione Italiana Riscaldamento Urbano – 2011.
- [5] Statistics Finland. Energy. 2012 [assessed 17.03.15] http://www.stat.fi/til/ene_en.html.
- [6] Ortiga J, Bruno JC, Coronas A. Operational optimisation of a complex trigeneration system connected to a district heating and cooling network. *Applied Thermal Engineering*, 51 (2013) 1536-1542.
- [7] Wang H, Yin W, Abdollahi E, Lahdelma R, Jiao W. Modelling and optimization of CHP based district heating system with renewable energy production and energy storage. *Applied Energy*, 159 (2015) 401-421.
- [8] Wang H, Lahdelma R, Wang X, Jiao W, Zhu C, Zou P. Analysis of the location for peak heating in CHP based combined district heating systems. *Applied Thermal Engineering*, 87 (2015) 402-411.
- [9] Arteconi A, Hewitt NJ, Polonara F. Domestic demand-side management (DSM): role of heat pumps and thermal energy storage (TES) systems. *Applied Thermal Engineering*, 51 (2013) 155-165.
- [10] Böttger D, Götz M, Lehr N, Kondziella H, Bruckner T. Potential of the power-to heat technology in district heating grids in Germany. *Energy Procedia*, 46 (2014) 246-253.
- [11] Sartor K, Quoilin S, Dewallef P. Simulation and optimization of a CHP biomass plant and district heating network. *Applied Energy*, 130 (2014) 474-483.
- [12] Schmidt RF, Fevrier N, Dumas P. Smart cities and communities, key to innovation integrated solution – smart thermal grids; 2013.
- [13] Ommen T, Markussen WB, Elmegaard B. Heat pumps in combined heat and power systems. *Energy*, 76 (2014) 989-1000.
- [14] Bach B, Werling J, Ommen T, Münster M, Morales JM, Elmegaard B. Integration of largescale heat pumps in the district heating systems of Greater Copenhagen. *Energy*, 107 (2016) 321-334.
- [15] Ancona MA, Melino F. Analisi di soluzioni tecniche e gestionali che favoriscano l'implementazione di nuovi servizi energetici nelle reti termiche in presenza di sistemi di

generazione distribuita. Report Ricerca di Sistema Elettrico, Accordo di Programma Ministero dello Sviluppo Economico – ENEA, Piano Annuale di Realizzazione 2013. http://www.enea.it/it/Ricerca_sviluppo/documenti/ricerca-di-sistema-elettrico/risparmio-energia-settore-civile/2013/rds-par2013-053.pdf.

- [16] Annuario Associazione Italiana Riscaldamento Urbano – 2016.
- [17] Rezaie B, Rosen MA. District heating and cooling: review of technology and potential enhancements. *Applied Energy*, 93 (2012) 2-10.
- [18] Persson U, Werner S. Heat distribution and the future competitiveness of district heating. *Applied Energy*, 88 (2011) 568-76.
- [19] Nielsen S, Möller B. GIS based analysis of future district heating potential in Denmark. *Energy*, 57 (2013) 458-68.
- [20] Lake A, Rezaie B, Beyerlein S. Review of district heating and cooling systems for a sustainable future. *Renewable and Sustainable Energy Reviews*, 67 (2017) 417-425.
- [21] Lund H, Werner S, Wiltshire R, Svendsen S, Thorsen JE, Hvelplund F and Mathiesen BV. 4th Generation District Heating (4GDH) Integrating smart thermal grids into future sustainable energy systems. *Energy*, 68 (2014) 1-11.
- [22] Jiang XS, Jing ZX, Li YZ, Wu QH, Tang WH. Modelling and operation optimization of an integrated energy based direct district water-heating system. *Energy*, 64 (2014) 375-88.
- [23] Yang L, Entchev E, Rosato A and Sibilio S. Smart thermal grid with integration of distributed and centralized solar energy systems. *Energy*, 122 (2017) 471-481.
- [24] Jing ZX, Jiang XS, Wu QH, Tang WH, Hua B. Modelling and optimal operation of a small-scale integrated energy based district heating and cooling system. *Energy*, 73 (2014).
- [25] Schafer K, Schlegel F, Pauschinger T. Decentralized feed-in of solar heat into district heating networks – a technical analysis of realized plants. *Book of papers of the 2nd International Solar District Heating Conference*, 3-4 June 2014, Hamburg, Germany.
- [26] Li Y, Rezgui Y, Zhu H. District heating and cooling optimization and enhancement - Towards integration of renewables, storage and smart grid. *Renewable and Sustainable Energy Reviews*, 72 (2017) 281-294.
- [27] Mathiesen BV, Lund H, Connolly D, Wenzel H, Østergaard P, Möller B, Nielsen S, Ridjan I, Karnøe P, Sperling K, Hvelplund FK. Smart Energy Systems for coherent 100% renewable energy and transport solutions. *Applied Energy*, 145 (2015) 139-54.
- [28] Sayegh MA, Danielewicz J, Nannou T, Miniewicz M, Jadwiszczak P, Piekarska K and Jouhara H. Trends of European research and development in district heating technologies. *Renewable and Sustainable Energy Reviews*, 68 (2017) 1183-1192.
- [29] Kelly S and Pollitt M. An assessment of the present and future opportunities for combined heat and power with district heating (CHP-DH) in the United Kingdom. *Energy Policy*, 38 (2010) 6936–6945.

- [30] Karschin I, Geldermann J. Efficient cogeneration and district heating systems in bioenergy villages: an optimization approach. *J Clean Prod*, 104 (2015) 305–14.
- [31] Bracco S, Dentici G, Siri S. Economic and environmental optimization model for the design and the operation of a combined heat and power distributed generation system in an urban area. *Energy*, 55 (2013) 1014–24.
- [32] Levihn F. CHP and heat pumps to balance renewable power production: Lessons from the district heating network in Stockholm. *Energy* (2017), <http://dx.doi.org/10.1016/j.energy.2017.01.118>.
- [33] Brand L, Calvén A, Englund J, Landersjö H and Lauenburg P. Smart district heating networks - A simulation study of prosumers' impact on technical parameters in distribution networks. *Applied Energy*, 129 (2014) 39-48.
- [34] Ancona MA, Branchini L, Di Pietra B, Melino F, Puglisi G and Zanghirella F. Utilities Substations In Smart District Heating Networks. *Energy Procedia*, 81 (2015) 597-605.
- [35] Paulus C and Papillon P. Substations for decentralized solar district heating: design, performance and energy cost. *Energy Procedia*, 48 (2014) 1076-1085.
- [36] Schafer K, Schlegel F and Pauschinger T. Decentralized feed-in of solar heat into district heating networks – a technical analysis of realized plants. Book of papers of the 2nd International Solar District Heating Conference, 3-4 June 2014, Hamburg, Germany.

3. DHNs design and analysis

In order to analyze district heating networks, a calculation code has been developed in Visual Basic for Application (VBA). The first version of this code was called Ca.R.Di.F. (Calcolo Reti Distribuzione Fluidi, *i.e.* Calculation of Fluids Distribution Networks) and it is able to design and/or analyze a traditional DHN. Subsequently, with the purpose of modeling the bidirectional energy exchange which can occur in Smart District Heating (SDH), four different schemes for the users' substations have been defined and a new version of the software has been developed (renamed as IHENA – Intelligent Heat Energy Network Analysis).

The realized calculation codes are both based on the Todini – Pilati algorithm [1, 2] as it concerns the hydraulic resolution of the network. Other methods were defined by Wood and Charles [3], by Epp and Fowler [4] and later by Kesavan and Chandrashekar [5] or by Martin and Peters [6] and by Shamir and Howard [7]. The choice of Todini – Pilati algorithm has been done considering the fast convergence and the robustness of this resolution method [1].

In this chapter the Todini-Pilati algorithm and the software Ca.R.Di.F. will be described, along with the validation of the realized code. Chapter 4 will provide for SDH evaluations and case studies.

3.1 The Todini-Pilati algorithm

Generally speaking, an hydraulic network – such as a district heating network – can be represented by means of a given number of nodes (NN) and a given number of pipes (NP). As an example, in Figure 3.1 a portion of a generic district heating network is presented: as it can be easily seen, in this case $NN = 6$ and $NP = 5$. Furthermore, with reference to Figure 3.1, it can be observed that a general node can be:

- i. a mixer: see nodes 2 or 5 in Figure 3.1, in which the sum of the inlet mass flow rates is equal to the sum of the outlet mass flow rates;
- ii. a user: see nodes 3, 4 or 6, for which the difference between the inlet and outlet mass flow rate to the node is equal to the required flow, q_3 , q_4 and q_6 in Figure 3.1;
- iii. a source: which allows the introduction of the flow into the network.

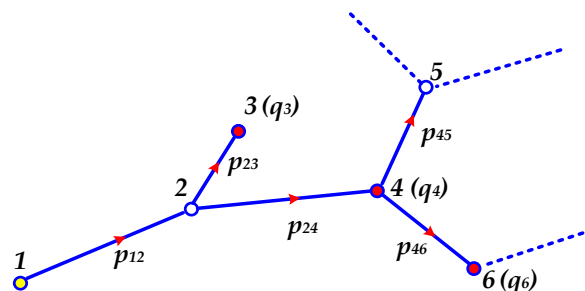


Figure 3.1 – Example of a portion of a DHN.

For each pipe (p_{ij}) of the network, the energy balance, being i and j respectively the upstream and the downstream nodes, can be written as:

$$\Delta H_{p_{ij}} - (H_i - H_j) = 0 \quad \text{E3.1}$$

where:

- $\Delta H_{p_{ij}}$ represents the total pressure losses through the pipe p_{ij} ;
- H_i and H_j are the energy content of the liquid, respectively in node i and in node j .

Obviously, $\Delta H_{p_{ij}}$ can be expressed as the sum of the distributed and concentrated pressure losses. The distributed pressure losses, which consists in the losses through the straight distances of the networks, are calculated with the Darcy-Weisbach equation:

$$\Delta H_{dis} = f \frac{L}{D} \rho \frac{v^2}{2} \quad [\text{Pa}] \quad \text{E3.2}$$

where:

- f is the drag coefficient (Darcy coefficient);
- L is the length of the pipe;
- D is the diameter of the pipe;
- ρ is the density of the fluid;
- v is the mean velocity of the fluid.

The drag coefficient f can be evaluated with the following expression, proposed by Colebrook and White:

$$f = \left[-2 \cdot \log \left(\frac{2.51}{Re \cdot f^{1/2}} + \frac{1}{3.71} \frac{\varepsilon}{D_h} \right) \right]^{-2} \quad \text{E3.3}$$

where:

- ε the roughness;
- D_h is the hydraulic diameter, which is equal to the pipe internal diameter for circular sections and equal to $4 \cdot A/P$ (A is the pipe section area and P is the section wet perimeter) in the other cases;
- $Re = \rho v D / \mu$ is the Reynolds number (being μ the dynamic viscosity).

Since the form of the expression introduced by Colebrook and White is implicit, the determination of f requires an iterative procedure. The relationship can be converted in an explicit form with the substitution of f_0 instead of f within the second member of the equation:

$$f = \left[-2 \cdot \log \left(\frac{2.51}{Re \cdot f_0^{1/2}} + \frac{1}{3.71} \frac{\varepsilon}{D_h} \right) \right]^{-2} \quad \text{E3.4}$$

in which f_0 is calculated as:

$$f_0 = 0.0055 \cdot \left[1 + \left(20000 \frac{\varepsilon}{D} + \frac{10^6}{Re} \right)^{1/3} \right] \quad \text{E3.5}$$

As it regards the concentrated pressure losses – namely all those losses due to valves, curves, instrumentation, sudden section variations, etc. – instead the equation is:

$$\Delta H_{conc} = \beta \rho \frac{v^2}{2} \quad [\text{Pa}] \quad \text{E3.6}$$

where:

- β is the coefficient of the concentrated pressure losses, usually available in literature and listed as function of the geometry.

Further, for each node of the considered network, the balance of the mass flow rate can be written as:

$$\sum_{IN} Q_{IN} - \sum_{OUT} Q_{OUT} - \sum_U q_U = 0 \quad \text{E3.7}$$

where:

- $\sum_{IN} Q_{IN}$ is the sum of the mass flow rates entering into the node;
- $\sum_{OUT} Q_{OUT}$ is the sum of the mass flow rates leaving the node;
- $\sum_U q_U$ is the sum of the mass flow rates eventually required by the users.

From the energy balances (see Eq. E3.1) a number of NP equations is obtained. In matrix form it results:

$$F_P(Q, H) = A_{11}Q + A_{12}H = 0 \quad \text{E3.8}$$

In the same way, from the mass balances (see Eq. E3.7), NN equations can be written as:

$$F_Q = A_{21}Q - q = 0 \quad \text{E3.9}$$

It follows a system of $NP + NN$ equations where mass flow rates (Q) and energy contents of the liquid (H) are the unknowns of the problem:

$$\begin{cases} F_P(Q, H) = A_{11}Q + A_{12}H = 0 \\ F_Q(Q, H) = A_{21}Q - q = 0 \end{cases} \quad \text{E3.10}$$

In equation E3.10, the term $A_{11} = [NP \times NP]$ is a diagonal matrix in which the non-null terms can be expressed as:

$$A_{11}(j, j) = \frac{\partial F_{Pj}}{\partial Q_j} = \frac{\partial \Delta H_j}{\partial Q_j} \quad \text{E3.11}$$

In the same equation E3.10, the term $A_{21} = [NN \times NP]$ is the so called topological matrix; the rows of the topological matrix represent the nodes of the network, while the columns are the pipes. As a consequence, the generic term $A_{21}(i, j)$ is equal to:

- +1 if the mass flow rate q_j (flowing through the pipe j) enters into the node i : it means that the node i is downstream with respect to the pipe j considering the direction of the flow;
- -1 if the mass flow rate q_j (flowing through the pipe j) exits from the node i : it means that the node i is upstream with respect to the pipe j considering the direction of the flow;
- 0 if there is no connection between the node i and the pipe j .

Finally the matrix $A_{12} = [NP \times NN]$ is the transpose of A_{21} .

The system can be iteratively solved with Newton-Raphson method generalized in matrix form by Todini-Pilati. At the beginning of the iterative process NP mass flow rates, NN energy contents of the liquid and the direction of the flow for each pipe have to be supposed. With these supposed values, the matrices A_{12} , A_{21} and A_{11} can be written. It follows, for the generic iteration (m):

$$\begin{cases} F_P(Q, H) = A_{11}Q^{(m)} + A_{12}H^{(m)} = 0 \\ F_Q(Q, H) = A_{21}Q^{(m)} - q = 0 \end{cases} \quad \text{E3.12}$$

By applying the Newton-Raphson method to solve the previous systems, the following problem can be obtained:

$$\begin{cases} F_P(Q, H) = A_{11}\Delta Q^{(m)} + A_{12}\Delta H^{(m)} = -dE \\ F_Q(Q, H) = A_{21}\Delta Q^{(m)} = -dq \end{cases} \quad \text{E3.14}$$

where dE and dq are the residual of the balances of mass and energy respectively, at the iteration ($m - 1$):

$$-dq_i = -[\Sigma_{IN}Q_{IN} - \Sigma_{OUT}Q_{OUT} - \Sigma_U Q_U] \quad \text{E3.15}$$

$$-dE = -[\Delta H_{pij} - (\Delta H_i - \Delta H_j)] \quad \text{E3.16}$$

The system in E3.14 needs to be solved in $\Delta H^{(m)}$ and $\Delta Q^{(m)}$. After each iteration the values of energy and mass flow rate can be updated as follows:

$$H^{(m)} = H^{(m-1)} + \Delta H^{(m)} \quad \text{E3.17}$$

$$Q^{(m)} = Q^{(m-1)} + \Delta Q^{(m)} \quad \text{E3.18}$$

If, from the calculation, a negative value is obtained for a mass flow rate, it means that the associated pipe is crossed by the flow in the opposite direction and, thus, the first attempt flow direction chosen for that pipe was wrong. Consequently, the topological matrix and its transpose must be updated.

Finally, in the developed calculation code the iterative procedure goes on until the convergence is reached, namely until each of the terms $\Delta H^{(m)}$ and $\Delta Q^{(m)}$ are greater than 10^{-9} .

3.2 Software Ca.R.Di.F.

The developed software, called Ca.R.Di.F. (Calcolo Reti Distribuzione Fluidi, *i.e.* Calculation of Fluids Distribution Networks), can simulate the behavior of a District Heating Network working under given conditions. Thus, this software can be applied for the analysis of an existing DHN, by simulating its behavior, or for the design of a new DHN, by defining a layout and starting a *trial and error* procedure.

Normally, a distribution network for district heating can be divided into two parts: the DHN feed and the DHN return lines. The system of equations determined in the previous paragraph must be

solved for both the feed and the return lines. Starting from the feed line, the working structure of this software can be represented with the flow chart reported in Figure 3.2.

It can be observed that the flow chart in Figure 3.2 strictly follows the mathematical model presented from Eq. E3.1 to Eq. E3.18 of the previous paragraph.

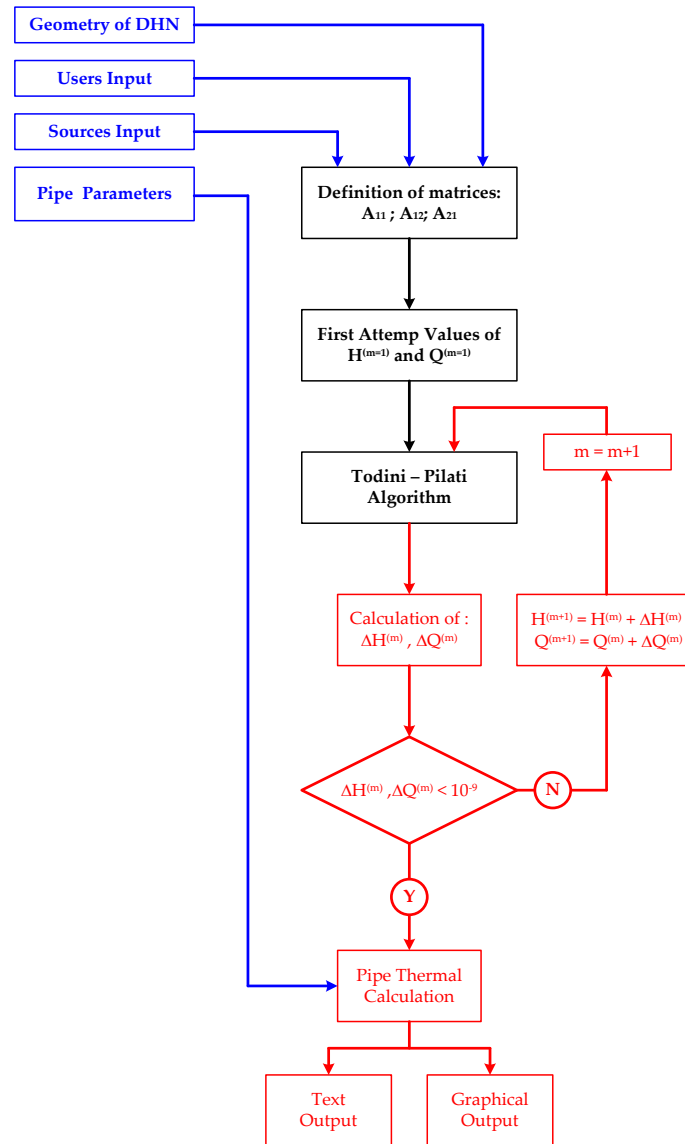


Figure 3.2 – Main Calculation code flow chart.

In more detail, in order to define the matrices A_{11} , A_{12} and A_{21} , a list of input of the DHN must be defined so they can be read from the software. The main input are listed below:

- Geometrical input: Cartesian coordinates (x, y, z) for each node, inside and external diameter of each pipe including the insulating material, length of the pipes, pumps position and operational characteristics, etc.. In this section also the nodes typology can be defined (user, source or mixer).

- Users input: thermal power required by each of the defined users and/or the required mass flow rate, temperature difference between the inlet and the outlet of the primary user circuit, etc..
- Sources input: number and position of sources, feed pressure, feed temperature, pressure at the expansion vessel, pumping station operational characteristics and performance, etc..
- Pipe parameters: conduction coefficient of each pipe, roughness, conduction coefficient of the insulating material, etc..
- Additional pumps: pressure increase, design efficiency and off-design performance of pumps eventually installed along the DHN.

Similarly, same inputs have to be defined for the return line of the network. In this connection, it is important to point up that the software, once defined a feed layout of the network, considers the same geometry for the return, simply reversing the direction of the flow. Thus, the nodes that for the feed line are sources for the return are considered as users; in the same way, the users are considered as sources, while the mixers remain the same. With this approach, the flow chart in Figure 3.2 can be used for both “feed” and “return” calculation.

Furthermore, from Figure 3.2 it can be seen that the application of the Todini-Pilati algorithm consists in the thermodynamic calculation of the pipes. In more detail, referring to a DHN composed by a source and a certain number of users, this procedure consists for the feed line in the determination of the pressure losses for each pipe, starting from the source until the users. Then, the same procedure is applied to the return line, from the users to the source. This procedure guarantee the convergence of the calculation, but, if the pressure increase at the source is not appropriate for the characteristics of the network and the users, negative pressure drops at the users heat exchangers are generated. As a consequence, the calculation of the pressure losses is a key point for the correct resolution of a district heating network. With respect to the expressions given in the previous paragraph for the pressure losses determination, the software Ca.R.Di.F. do not implement the analytic calculation of the concentrated pressure losses. This choice is motivated considering that – excepting for some specific cases in which the DHN has a particularly curvy path, due to constraints such as streets or wildlife conservation – the straight parts of the networks counts in a predominant manner in the computation of the total pressure losses. However, concentrated pressure losses are not generally negligible, so they are accounted with a specific increasing coefficient (often equal to the 30%) of the distributed pressure losses in each pipe. The application of this coefficient is usually sufficiently adequate, allowing in fact to have precautionary conditions.

Another important aspect of the software to be highlighted is the calculation of the thermal dissipations through the pipes walls. This calculation is made by applying the equation which governs the thermal exchange phenomenon between the fluid going through the network and the external air:

$$Q_{th,dis} = \sum_{i=1}^{NP} U_i L_i (T_{m,i} - T_{ext}) \quad [W] \quad E3.19$$

where:

- U_i is the global heat exchange coefficient, [W/mK]
- L_i is the length of the pipe i , [m]
- $T_{m,i}$ is the mean temperature of the fluid in the pipe i , [K]
- T_{ext} is the temperature of the ambient air, [K]

The global heat exchange coefficient for a horizontal pipe with insulation and circular section can be expressed with the following relation:

$$U = \frac{\pi}{\frac{1}{\alpha_1 D_{int}} + \frac{1}{2\lambda_1} \ln\left(\frac{D_{ext}}{D_{int}}\right) + \frac{1}{2\lambda_2} \ln\left(\frac{D_{ins}}{D_{ext}}\right) + \frac{1}{\alpha_2 D_{ins}}} \quad \text{E3.20}$$

where D_{int} , D_{ext} and D_{ins} are respectively the internal and external diameters of the pipe and the insulating material diameter; α_1 and α_2 are the coefficients of internal and external convection thermal exchange respectively; finally, λ_1 and λ_2 are the conduction coefficients for the pipe and the insulation respectively.

The external convection coefficient is univocally determined from the input given for the external air, while the internal convection coefficient is function of the fluid velocity through the network. Once fixed the diameters for each pipe, in order to guarantee the required mass flow rates to the users, the velocities (and thus also the coefficients α) are determined, while the remaining parameters are given to the software as input.

On the other hand, the main outputs of the software, for both feed and return lines of the DHN, are:

- inlet and outlet temperature and pressure, mass flow rate, velocity, pressure drop for each pipe;
- total mass flow rate supplied from the sources;
- total electrical power for the sources pumping stations;
- total heat dissipation across the network;
- pressure drops at each of primary circuits of the users.

Moreover, the developed software enables to visualize the network's layout, both for the feed and for the return lines, with pointers on each pipe to indicate the direction of flow.

With the software Ca.R.Di.F., finally, it is possible to calculate and graph the distributions of velocity, mass flow rates, pressure losses and diameters. The understanding of the representation is immediate, thanks to the use of different colors for the different ranges of the considered quantity.

3.3 Software validation

With the aim to validate the software Ca.R.Di.F., an existing district cooling network is considered (see Figure 3.3). The network behavior has been evaluated with the Ca.R.Di.F. and the obtained results have been compared with the ones of the commercial tool Termis [8].

The analyzed network is composed by 95 pipes and 96 nodes (34 users, 61 mixers and 1 source). No additional pumps are present nor on the feed or on the return lines, but a pumping station with an efficiency equal to the 90% is considered at the source. The results of the comparison between Ca.R.Di.F. and Termis are listed in Table 3.1, in terms of mean value, standard deviation and variance of the ratios between mass flow rates (\dot{m}), temperatures and pressures at the inlet (T_{in} , p_{in}) and at the outlet (T_{out} , p_{out}) of each pipe, obtained with Termis and Ca.R.Di.F. respectively. The values shown in the table account for both the feed and the return line of the network.

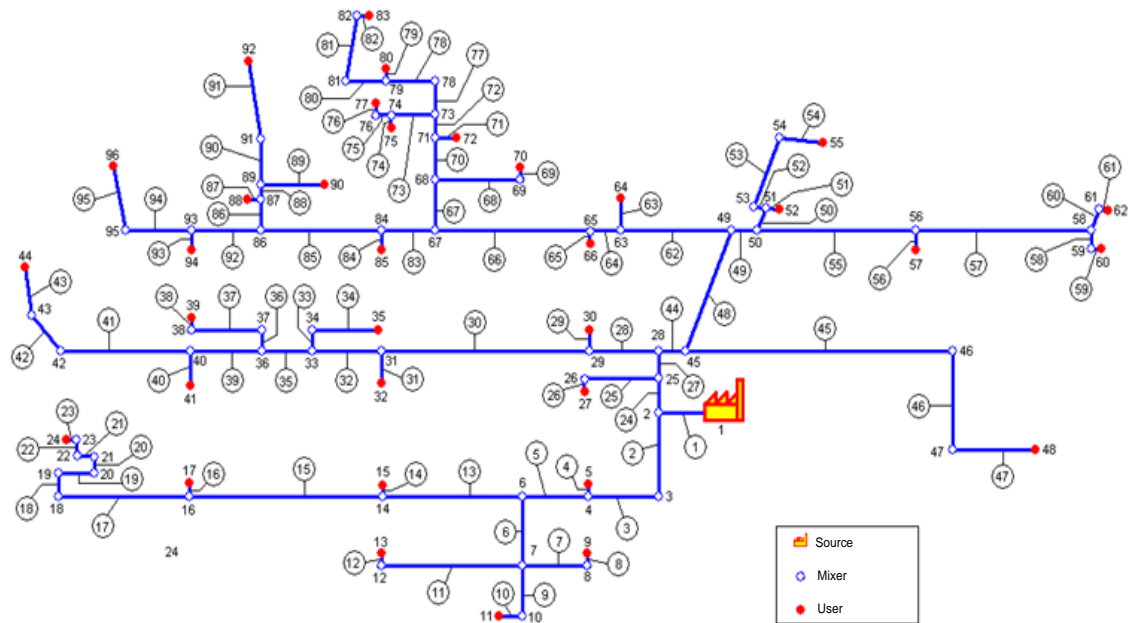


Figure 3.3 – Case study layout selected for software validation.

Table 3.1 – Comparison between Termis and Ca.R.Di.F. software.

	Mean Value [%]	Standard Deviation [%]	Variance [%]
$(\dot{m})_{Termis} / (\dot{m})_{Ca.R.Di.F.}$	100.00	0.58	0.34
$(p_{in})_{Termis} / (p_{in})_{Ca.R.Di.F.}$	99.48	1.11	1.23
$(p_{out})_{Termis} / (p_{out})_{Ca.R.Di.F.}$	99.59	1.09	1.19
$(T_{in})_{Termis} / (T_{in})_{Ca.R.Di.F.}$	99.96	0.05	0.00
$(T_{out})_{Termis} / (T_{out})_{Ca.R.Di.F.}$	99.96	0.05	0.00

As it can be seen in Table 3.1, there is a strong accord between Termis and Ca.R.Di.F. results. The mean value of the ratio between the general quantity obtained with Termis and the one obtained with Ca.R.Di.F., indeed, is always higher than the 99%. Furthermore, the maximum values of standard deviation and variance are respectively equal to 1.11% and 1.23%. As a consequence, the results of the comparison confirm the effectiveness of the developed software.

As an example, in Figure 3.4, in Figure 3.5 and in Figure 3.6 are shown respectively the trends of the mass flow rate, pressure and temperature – evaluated with the two considered software – at the inlet of the pipes, considering the network path from the source to the user #43.

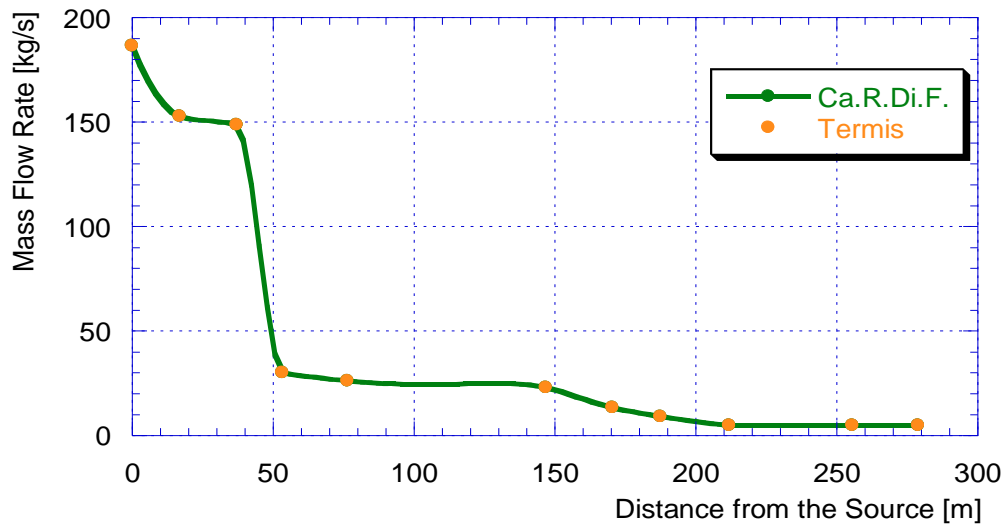


Figure 3.4 – Comparison between the mass flow rates results of the two considered software.

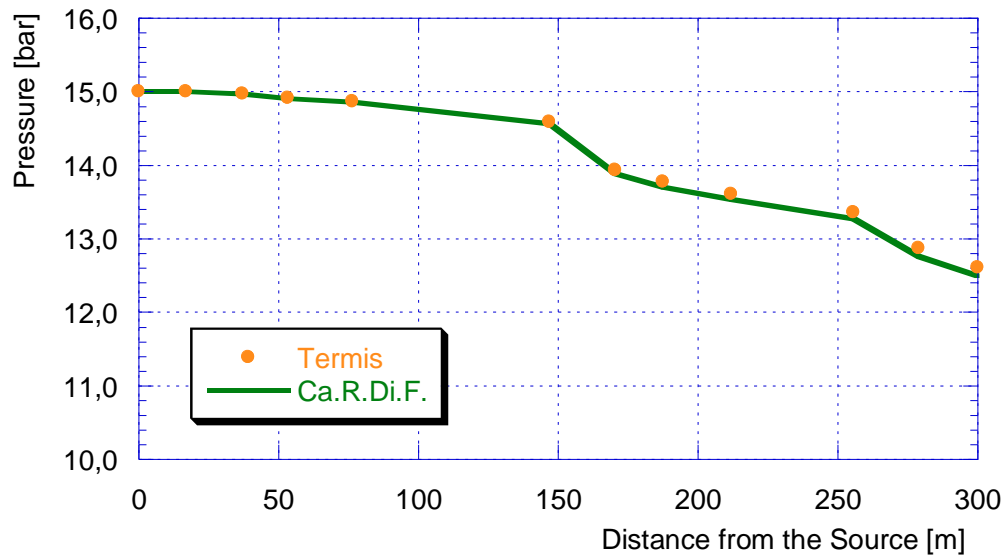


Figure 3.5 – Comparison between the pressure results of the two considered software at the inlet of the pipes, considering the network path from the source to the user #43.

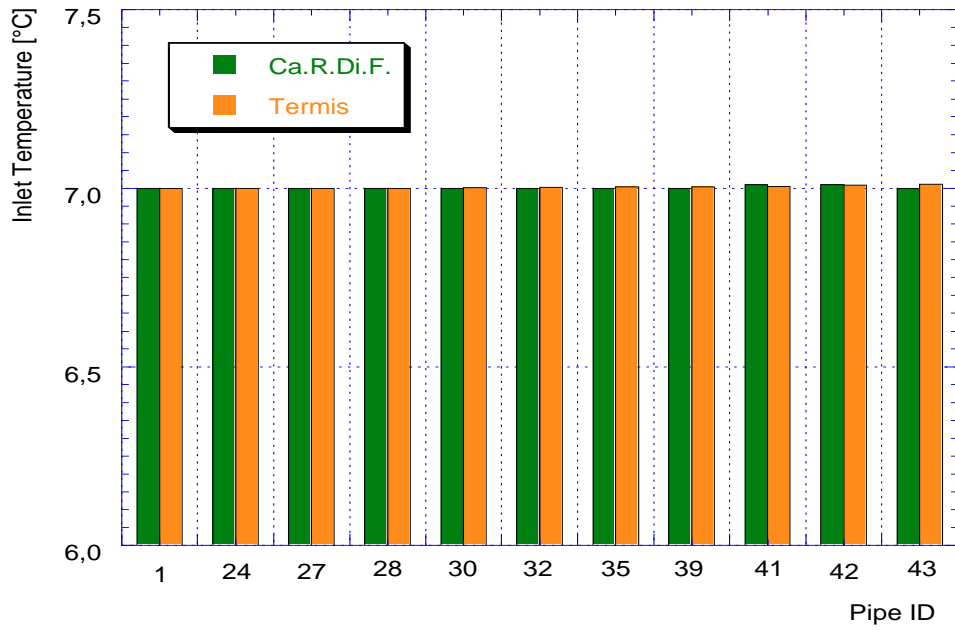


Figure 3.6 – Comparison between the temperature results of the two considered software at the inlet of the pipes, considering the network path from the source to the user #43.

References

- [1] Todini E. On the Convergence Properties of the Different Pipe Network Algorithms.
- [2] Todini E. Towards Realistic Extended Period Simulations (Eps) in Looped Pipe Networks. *Proc. 8th Annual Int. Symp. On Water Distribution Systems Analysis*, ASCE, Reston, VA; 2006.
- [3] Wood DJ and Charles COA. "Hydraulic network analysis using linear theory. *Journal of the Hydraulics Division*, ASCE, Vol. 98, No. HY7, 1972.
- [4] Epp R and Fowler AG. Efficient code for steady-state flows in networks. *Journal of the Hydraulics Division*, ASCE, Vol. 96, No. HY1, 1970.
- [5] Kesavan HK and Chandrashekar M. Graph-theoretic models for pipe network analysis. *Journal of the Hydraulics Division*, ASCE , Vol. 98, 1972.
- [6] Martin DW and Peters G. The application of Newton's method to network analysis by digital computers. *IWES Journal*, 1963.
- [7] Shamir U and Howard CDD. Water distribution network analysis. *Journal of the Hydraulics Division*, ASCE , Vol. 94, No. HY1, 1968.
- [8] <http://www.schneider-electric.com/products/ww/en/5100-software/5125-information-management/61418-termis-software/>

4. Smart District Heating

In this chapter the four different schemes, proposed as innovative solutions for the integration of distributed generation systems within DHNs, will be presented and discussed. Furthermore, software IHENA realized by their implementation into the Ca.R.Di.F. calculation code will be described and its application to a case study will be presented.

4.1 Users substations in Smart District Heating Networks

In order to allow a bidirectional energy flux, the users substations are one of the most important components in the SDHNs, because they represent the transfer of thermal energy from the grid to the users. Usually, a traditional user's substation mainly consists in a heat exchanger which allows the thermal energy exchange between the primary circuit (directly connected to the DHN) and the secondary circuit (user side). If a distributed generation system is installed at the final user, the user substation must be modified and a further circuit (called tertiary circuit) is introduced in order to connect the distributed generation system with both the user and the network. As for the bidirectional heat exchange there are different possibilities, thus in this perspective four configurations have been elaborated and proposed [1].

The proposed four different users substations layouts are presented in Figures from 4.1 to 4.4:

1. scheme 1 (feed to return): a mass flow rate is extracted from the feed line of the network and it is heated by decentralized production system before the reintroduction in the return line (see Figure 4.1);
2. scheme 2 (feed to feed): the thermal energy transfer from the decentralized production system towards the distribution network concerns only the feed line (see Figure 4.2);
3. scheme 3 (return to return): the transfer of thermal energy from the user to the network involves only the return line (see Figure 4.3);
4. scheme 4 (return to feed): a mass flow rate is taken from the return line, heated from the decentralized production system and reintroduced in the feed line of the network (see Figure 4.4).

In all of the presented layouts three different circuits are accounted and can be defined as it follows: a primary circuit, which connects the distribution network to the substation; a secondary circuit, which is internal to the user and, finally, a tertiary circuit, which exchanges the heat produced by the decentralized generator. Furthermore, a common assumption has been made for the development of the four proposed schemes, *i.e.* that only the excess of thermal production can be introduced into the distribution network. Therefore, the regulation strategy imposes that the produced thermal energy is always firstly used for the fulfillment of the user needs.

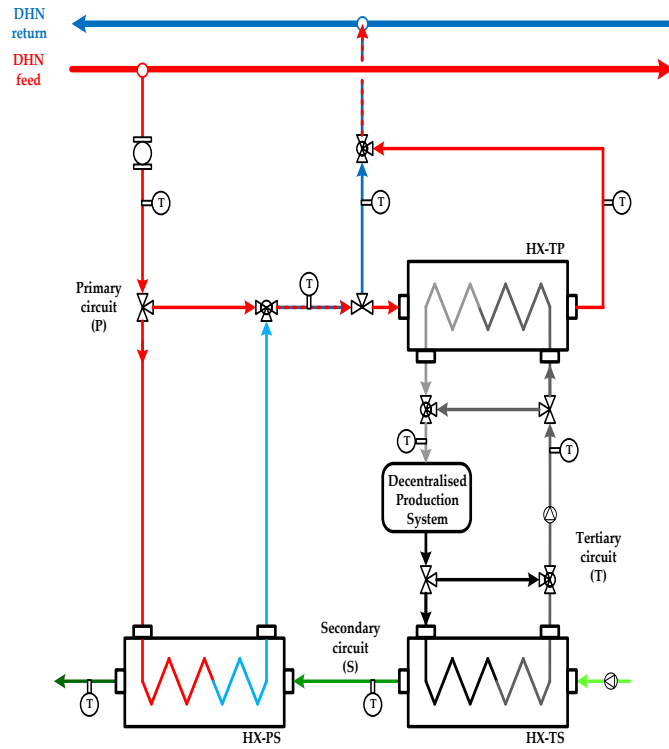


Figure 4.1 – Scheme 1, feed to return configuration.

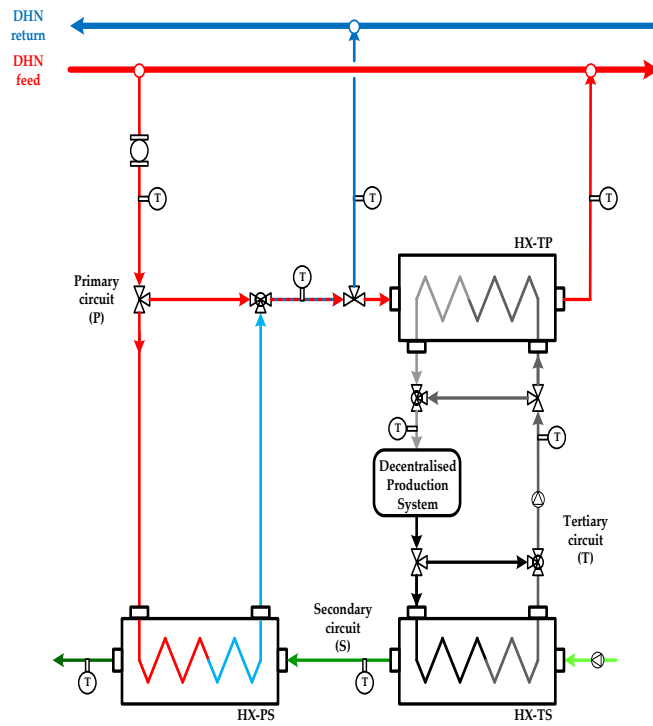


Figure 4.2 – Scheme 2, feed to feed configuration.

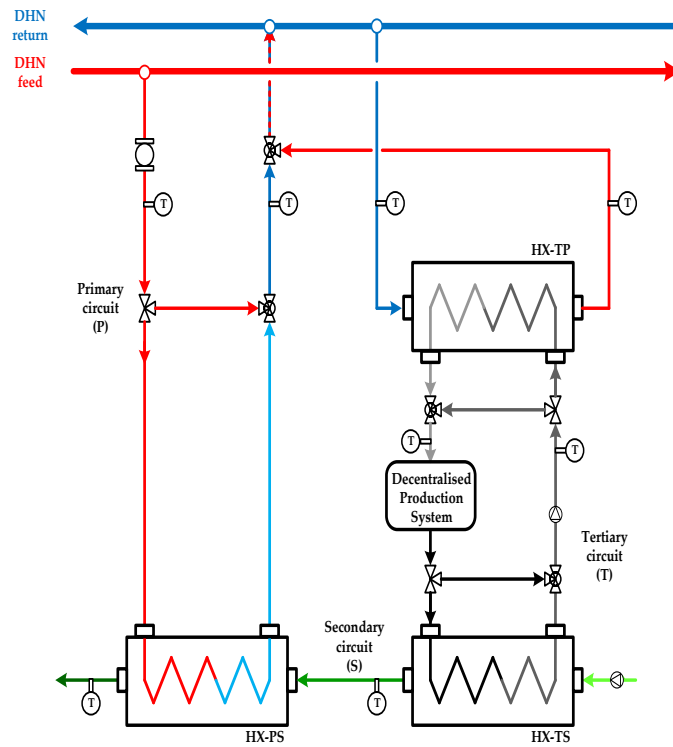


Figure 4.3 – Scheme 3, return to return configuration.

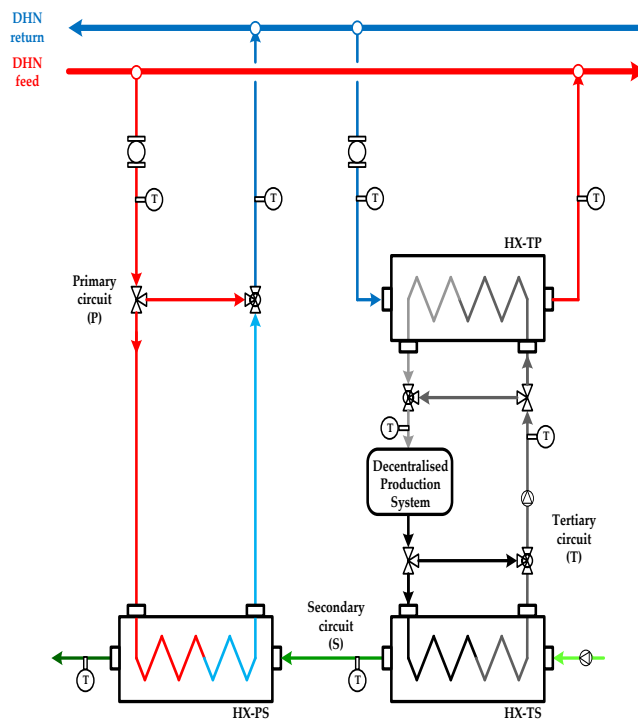


Figure 4.4 – Scheme 4, return to feed configuration.

Obviously, the introduction of heat into the network produces a temperature modification and – in some cases – a change in the network flows. Firstly, the following general considerations can be made before a deep thermodynamic analysis on the proposed layouts. First of all, the increase in the temperature on the return circuit of the distribution network is not appreciated by the network management: in fact, it implies the necessity of modifications in control and regulation strategy of the whole network (with a consequent reduction of the conversion efficiency for the centralized production plant). This characteristic entails schemes 1 and 3, which are at present rarely adopted. Secondly, with the scheme 2 an increase in the temperature on the feed line is obtained; this effect could not be optimal for downstream users if they need a constant temperature flow and/or for other distributed generation systems which can be excluded from the possibility of thermal energy feed-in. Finally, scheme 4 is the more complex configuration and it is the only one which modifies the current flow of the network, due to the flow from the return to the feed of the network. However, this scheme does not necessary implies the increase in the feed temperature (see Figure 4.4), avoiding particular regulation problems related to the temperature profile. For instance, scheme 4 is widely adopted in existing SDHNs.

4.2 Software IHENA

In order to evaluate the performance of a SDHN, these proposed schemes have been implemented within the software Ca.R.Di.F., generating a new version of the code called IHENA (Intelligent Heat Energy Network Analysis). The algorithm applied for the network resolution is the Todini-Pilati algorithm, but the possibility of bidirectional thermal energy exchange at one or more users is now accounted. The main flow chart of the software is presented in Figure 4.5 and shows the main connections between required inputs, calculation routines and outputs.

In more detail, the flow chart can be divided into six main sections:

1. *network implementation*: this section concerns the introduction of the main input of network geometry, such as nodes coordinates and typology (mixer, utility, source), pipes length, users schemes (traditional or smart schemes and in this case which one), etc.;
2. *network input*: in this section the main network input, such as source temperature, source pressure and users thermal demand, etc., can be introduced;
3. *users fitting*: this routine realizes the balance among the decentralized thermal production system (in case of smart substations), the user need and the network feed. This balance represents the first attempt solution of the calculation code;
4. *network geometry implementation and operational parameters definition*: this is the routine which, on the basis of the previous input, draws the network and allows the definition of the regulation strategy (*i.e.* constant mass flow rate, constant temperature difference or a mix of this two regulation criteria);
5. *network calculation*: in this routine the Todini-Pilati algorithm is applied in order to calculate temperatures, pressures and mass flow rates of the whole network, including the bidirectional exchange with the smart users, if present;
6. *text and graphical output*: this section only provides for the writing of the output in both text and graphical form.

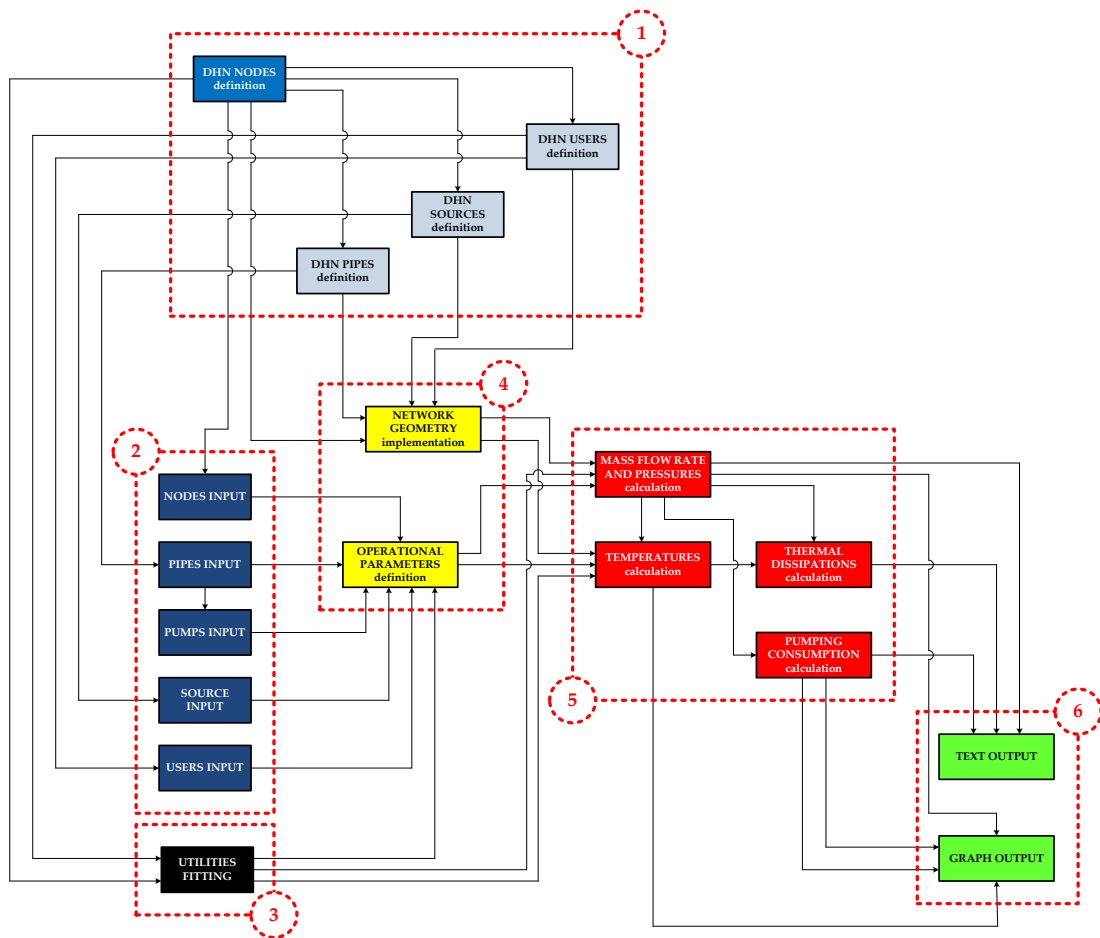


Figure 4.5 – Software IHENA main flow chart.

Network inputs and operational parameters have to be defined for both the feed and the return circuits. In this connection, as already explained for the software Ca.R.Di.F., it is important to remember that the software, once defined a feed layout of the network, considers the same geometry for the return, simply reversing the direction of the flow. Thus, the nodes that for feed are sources for the return are considered as “virtual” users; in the same way, the users are considered as “virtual” sources, while the mixers remain the same.

The main outputs of the software, for both feed and return of the DHN, are:

- inlet and outlet temperature and pressure, mass flow rate, velocity, pressure drop for each pipe;
- total mass flow rate supplied from the sources;
- total electrical power for the pumping stations;
- pressure drops at each of primary circuits of the users;
- heat exchanged between network and users.

Moreover, the developed software enables to visualize the network’s layout, both for the feed and for the return, with pointers on each pipe to indicate the direction of flow.

As well as for Ca.R.Di.F. software, finally, with the software IHENA it is possible to calculate and graph the distributions of velocity, mass flow rates, pressure losses and diameters. The

understanding of the representation is immediate, thanks to the use of different colors for the different ranges of the considered quantity.

4.3 Thermodynamic considerations on the proposed schemes

A series of simulations has been carried out in order to analyze the behavior of smart substations. The simulations have been initially carried out without considering a DHN, but only analyzing the user substation (*i.e.* simply considering a feed line and a return line).

In more detail, a parametric analysis has been conducted varying the ratio between the users need ($Q_{TH,U}$) and the thermal power available from the decentralized production system ($Q_{TH,SP}$). Furthermore, a modification in the ratio between the mass flow rate circulating in the primary circuit (M_P) and the one circulating in the tertiary circuit (M_T) has been considered.

The ratio $Q_{TH,U}/Q_{TH,SP}$ has been exclusively considered ranging between 0 and 1, in order to take into account only the case in which the thermal energy provided by the distributed generation system exceeds the user's needs, as described in Paragraph 4.1 as it regards the control strategy of the smart substations.

The further following boundary conditions have been assumed:

- temperature of the feed line of the DHN equal to 80°C or to 90°C;
- temperature available from the distributed production system (*i.e.* at the inlet of the tertiary circuit) equal to 110°C.

It should be pointed out that a feed line temperature ranging from 80°C to 90°C is typical and largely adopted for DHNs, especially in the South of Europe [2]. As a consequence, the temperature available from the distributed generation system has been chosen equal to 110°C, in order to guarantee a suitable temperature difference with the feed line of the distribution network. A temperature equal to 110°C for instance can be achieved with systems such as internal combustion engines, micro-gas turbines (among CHP units) or with vacuum solar thermal panels.

The results of the developed simulations are presented in Figures from 4.6 to 4.11, in terms of primary circuit temperature increase versus the ratio $Q_{TH,U}/Q_{TH,SP}$. In particular, in Figures 4.6, 4.8 and 4.10 the temperature increase is shown as function of M_P/M_T (varying from 0.5 to 2.0) with reference to a feed line temperature equal to 80 °C, while in Figures 4.7, 4.9 and 4.11 the comparison between the two different feed temperature – respectively equal to 80°C and 90°C – is considered, being constant the value of M_P/M_T (equal to 1.0).

It should be highlighted that the results presented in Figures from 4.6 to 4.11 relate only to the temperature variations on the primary circuit, without considering the effects of bidirectional exchange on the main network temperatures. This second aspect, indeed, will be investigated and discussed later in the following of this paragraph.

From the figures, it can be observed that the results for schemes 1 and 2 coincides. This evidence is due to the fact that both the configurations are characterized by the heat exchanger HX-TP fed from the supply circuit of the network. On the basis of the assumed hypothesis and boundary conditions, the maximum increase in the temperature of the primary circuit is equal to about 25°C

for a feed line temperature equal to 80°C. With the increase in the feed line temperature up to 90°C, the maximum increase reduces to 15°C. Obviously, with the increase in the ratios M_P/M_T and/or $Q_{TH,U}/Q_{TH,SP}$ the achievable temperature differences decreases. Going to the scheme 3, it can be seen that the achievable temperature increases are higher with respect to schemes 1 and 2, because it acts on the return circuit flow.

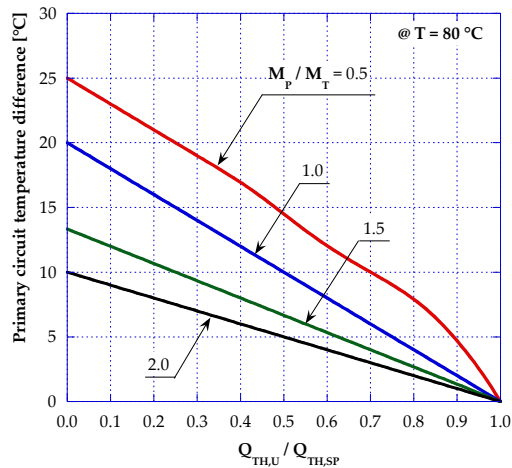


Figure 4.6 – Primary circuit temperature increase as function of the ratios $Q_{TH,U}/Q_{TH,SP}$ and M_P/M_T , in case of $T=80\text{ °C}$ and schemes 1 and 2.

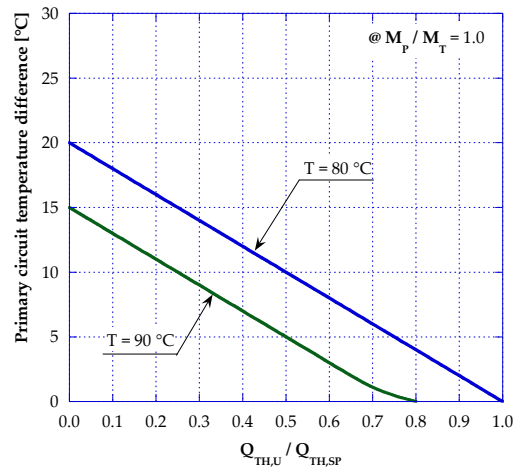


Figure 4.7 – Primary circuit temperature increase as function of the ratio $Q_{TH,U}/Q_{TH,SP}$ and of the primary circuit inlet temperature, in case of $M_P/M_T=1.0$ and schemes 1 and 2.

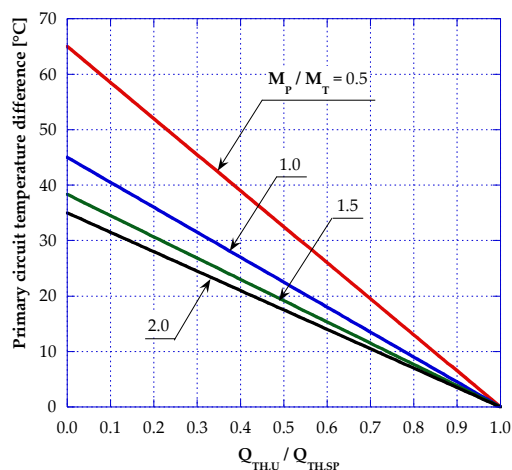


Figure 4.8 – Primary circuit temperature increase as function of the ratios $Q_{TH,U}/Q_{TH,SP}$ and M_P/M_T , in case of $T=80\text{ °C}$ and scheme 3.

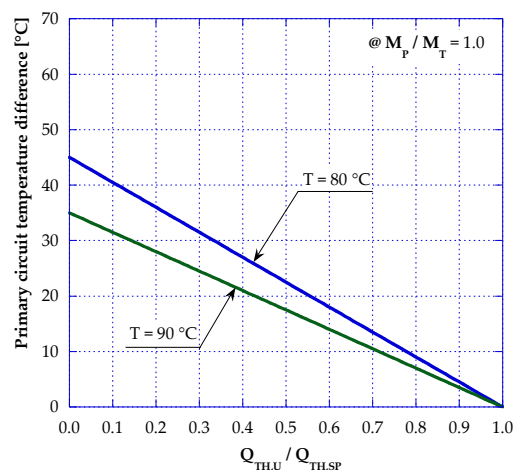


Figure 4.9 – Primary circuit temperature increase as function of the ratio $Q_{TH,U}/Q_{TH,SP}$ and of the primary circuit inlet temperature, in case of $M_P/M_T=1.0$ and scheme 3.

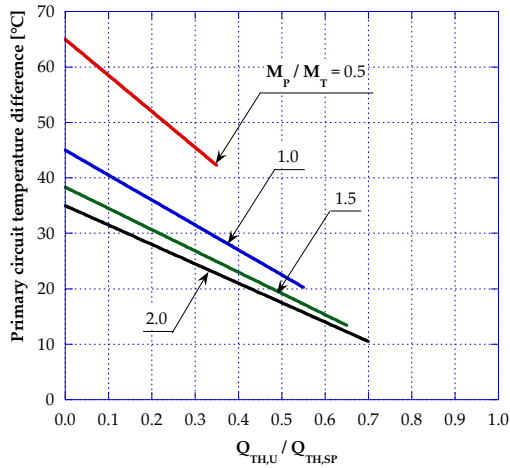


Figure 4.10 – Primary circuit temperature increase as function of the ratios $Q_{TH,U}/Q_{TH,SP}$ and M_P/M_T , in case of $T=80\text{ °C}$ and scheme 4.

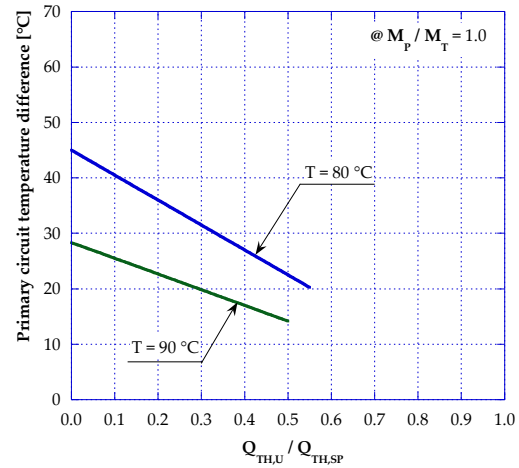


Figure 4.11 – Primary circuit temperature increase as function of the ratio $Q_{TH,U}/Q_{TH,SP}$ and of the primary circuit inlet temperature, in case of $M_P/M_T=1.0$ and scheme 4.

Finally, the curves related to the scheme 4 derives from the ones of scheme 3 – for the same reasons already explained in case of schemes 1 and 2 – but with a reduced admissible range of the ratio $Q_{TH,U}/Q_{TH,SP}$. The constraints are due to the temperature levels: in fact, in scheme 4 the heated mass flow rate has to be introduced on the feed line of the network, thus once reached the same temperature level of the feed line, the heat exchange stops.

After the results obtained for the users substations, in order to evaluate the effects of the smart thermal exchange on a district heating network, a case study has been chosen and simulated with the software IHENA. The layout of the network is proposed in Figure 4.12: it is composed of 26 pipes and 27 nodes (11 users, 1 source and 15 mixers) for a total length of 3036 m.

The developed software has been applied with the aim of studying the different behaviors of a district heating network when the various smart users substation schemes are considered. The network presented in Figure 4.12 has been chosen for the simulations. First of all, a simulation of the behavior of the chosen network has been carried out with the software IHENA, without considering thermal energy production at any user. This preliminary analysis enabled to individuate the critical path of the DHN – *i.e.* the path that, starting from the source, presents the higher pressure losses – highlighted in green color in Figure 4.12. The main hypothesis assumed for the simulation are summarized in Table 4.1.

Subsequently, the user represented by the node #12 has been selected as the one where a bidirectional heat exchange with the network can occur. This choice has been made focusing on the critical path and considering that the node #12 is contemporarily mixer and user, allowing therefore to generalize the developed analysis. The main characteristics of the distributed generation system, supposed to be installed at the user #12, are shown in Table 4.2.

In order to study the effect of the bidirectional thermal energy exchange on the network, several simulations have been carried out:

- the SDHN behavior has been analyzed by carrying out four set of simulations, each one considering a different smart user substation scheme (Figures from 4.1 to 4.4) in correspondence of the node #12;
- for fixed smart user substation scheme, the behavior of the network – when the ratio between the thermal power required by the user ($Q_{th,u}$) and the thermal power produced by the distributed generation system ($Q_{th,sp}$) varies from 0 to 1 – has been evaluated.

The results of the simulations, in terms of temperature profile along the critical path for the case $Q_{th,u}/Q_{th,sp} = 0.0$, are presented in Figure 4.13.

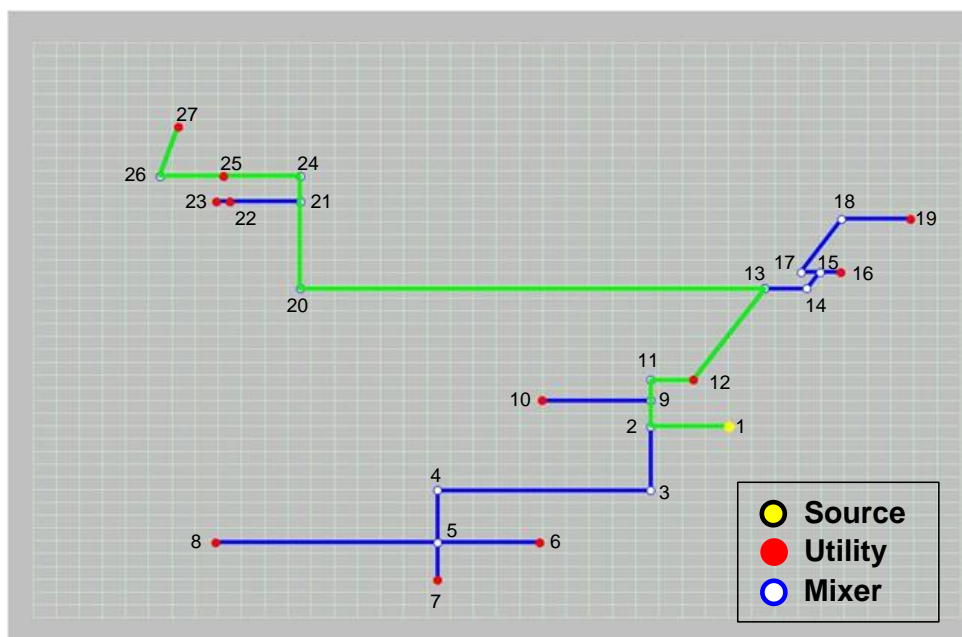


Figure 4.12 – Layout of the DHN chosen as case study.

Table 4.1 – Main users and source parameters assumed for the analysis.

Design thermal need of each user ($Q_{th,u,DES}$)	200 MW
Feed temperature (T_F)	80°C
Feed pressure (p_F)	18 bar
Return pressure (p_R)	4 bar

Table 4.2 – Distributed generation system parameters.

Design thermal power production ($Q_{th,sp,DES}$)	200 MW
Production temperature (T_{SP})	110°C

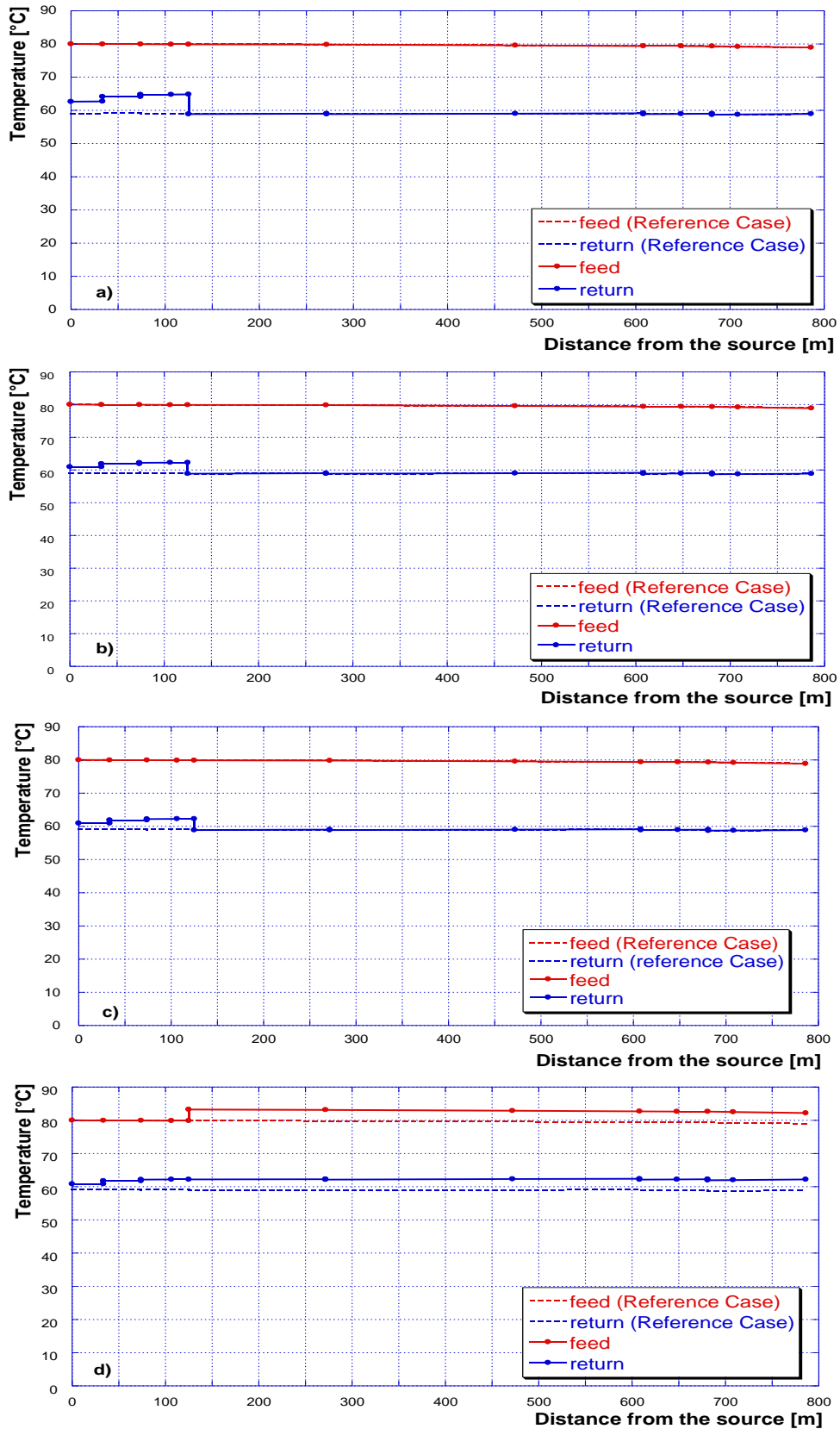


Figure 4.13 – Temperature profiles along the critical path of the network – for both the feed and the return lines – for the case $Q_{th,u}/Q_{th,sp} = 0.0$ and when the user substation at the node #12 can be represented with (a) scheme 1, (b) scheme 2, (c) scheme 3 or (d) scheme 4. In dotted lines the temperature profiles when no thermal production occurs are presented as comparison.

From Figure 4.13 it can be observed that:

- the scheme 1 entails the increase in the temperature on the DHN return line and, as a consequence, also the temperature at the inlet of the centralized production plant increases. This effect is unpleasant for the management of the network, due to the need of regulating the operating conditions according to the modified temperature, and so causing a consequent decrease in the centralized production system efficiency;
- with the scheme 2 the temperature increase occurs on the feed line of the network and, then, it propagates also on the network return line. However, due to the thermal dissipations across the network, the return temperature increase is lower than the one achieved with the scheme 1. On the other hand, with this second configuration, the inlet primary circuit temperature for the users located downstream – with respect to the considered smart user – results higher than the one in case without bidirectional heat exchange. As a consequence, this effect might be negative if the downstream users require particular temperature constraints and/or if these users are smart users too and the energy production occurs contemporarily;
- as it concerns the scheme 3, the same considerations already made for the scheme 1 can be repeated. Furthermore, the layout of the user substation is more complex and it is necessary to take a certain mass flow rate from the return line of the network with a consequent management complication;
- finally, with the scheme 4 the same qualitative effects observed for the scheme 2 occur. Furthermore, in this case even more than in the previous ones, the management of the network mass flows is critical and extremely delicate. On the other hand, the scheme 4 is the only scheme that – taking a mass flow rate from the return line of the network and introducing it into the feed line – allows to keep unchanged the temperature levels of both the feed and the return, only varying the mass flow rate.

Obviously, with the increase in the ratio $Q_{th,U}/Q_{th,SP}$ and with the increase in T_F , the achievable temperature differences decrease with respect to the case without smart users.

4.4 Transformation hypothesis for the conversion of an existing user substation into a smart one

With the aim to evaluate the possibility of implementing one of the proposed configurations in a real district heating network, an existing user substation has been selected and analyzed. The considered substation is placed in the North of Italy and it provides for hot water and space heating needs of an infant school. The simplified schematic of the utility substation, as currently designed, is shown in Figure 4.14. It is a traditional user substation, where the thermal energy exchange between the network (primary circuit) and the user (secondary circuit) occurs by means of a plate heat exchanger (HE1 in Figure 4.14). The space heating loads are met directly by the secondary circuit, while a thermal storage tank is interposed for the hot water needs supply. The main characteristics of the utility substation's heat exchanger HE1 are listed in Table 4.3.

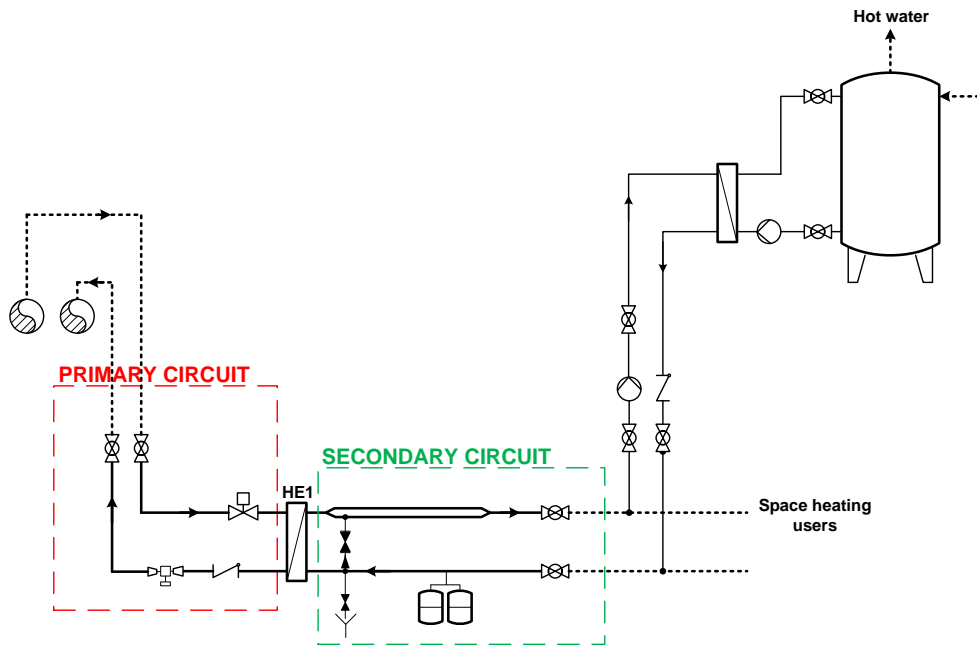


Figure 4.14 – Schematic of the current utility substation (traditional thermal exchange: from the network to the user).

Table 4.3 – Heat exchanger main characteristics.

PRIMARY CIRCUIT	
Fluid type	Industrial softened hot water
Rated thermal power	200 kW
Maximum temperature	120 °C
Feed temperature	80 °C
Return temperature	60 °C
Peak mass flow rate	2.39 kg/s
Certified pressure loss	5000 mm H ₂ O
Meter pressure loss	Kvs.6 – 3539 mm H ₂ O
Maximum allowed pressure	16 bar (PN16)
SECONDARY CIRCUIT	
Fluid type	Hot water
Maximum temperature	100 °C
Feed temperature	70 °C
Return temperature	55 °C
Mass flow rate	10090 kg/h
Maximum certified pressure loss	500 mm H ₂ O
Maximum allowed pressure	10 bar (PN10)
CONNECTIONS	
Primary circuit	Weld joint – ϕ 1'' 1/2
Secondary circuit	Threaded – UNI EN ISO 228 – F 2''

An experimental campaign has been conducted in the wintertime and springtime during 2015, allowing to collect the operational data (temperatures, mass flow rates, etc.) for the evaluation of the thermal needs hourly profile. In more detail, the feed and return temperatures (measured on the primary circuit of the heat exchanger HE1), the mass flow rate through the primary circuit and the flow velocity have been monitored by means of specific sensors. The time step for the data collection is one minute.

Based on the experimental campaign results, the heat exchanger (HE1 in Figure 4.14) of the user substation has been modeled, firstly in design operation, by means of in-house developed software. The rated power, as presented in Table 4.3, is 200 kW and the temperature difference operated on the primary circuit is equal to 20°C in design conditions. In more detail, the operating parameters for the design operation of the heat exchanger are listed in Table 4.4, while the thermal exchange diagram in design condition is shown in Figure 4.15. With reference to Figure 4.15, the following temperature differences can be defined:

- $\tau_1 = T_{IN,P} - T_{OUT,S}$
- $\tau_2 = T_{OUT,P} - T_{IN,S}$

The off-design operation of the heat exchanger has been analyzed by applying an in-house developed software considering the variation of thermal energy exchange, while keeping constant the feed temperature on the primary circuit (namely $T_{IN,P}$). In other words, the regulation strategy of the network considers the possibility of mass flow rate variation, while the feed temperature of the network is assumed as constant. The results of the off-design modeling are shown in Figure 4.16a and Figure 4.16b, respectively for the mass flow rate and for the primary circuit outlet temperature as function of the exchanged heat and of the primary circuit inlet temperature $T_{IN,P}$.

Table 4.4 – Heat exchanger design operation.

	PRIMARY CIRCUIT	SECONDARY CIRCUIT
Mass flow rate [kg/s]	2.389	2.803
Inlet temperature [°C]	80	55
Outlet temperature [°C]	60	72
Thermal power exchanged [kW]	200	
US [kW/°C]	31.18	
Thermal dissipations [kW]	2.015	

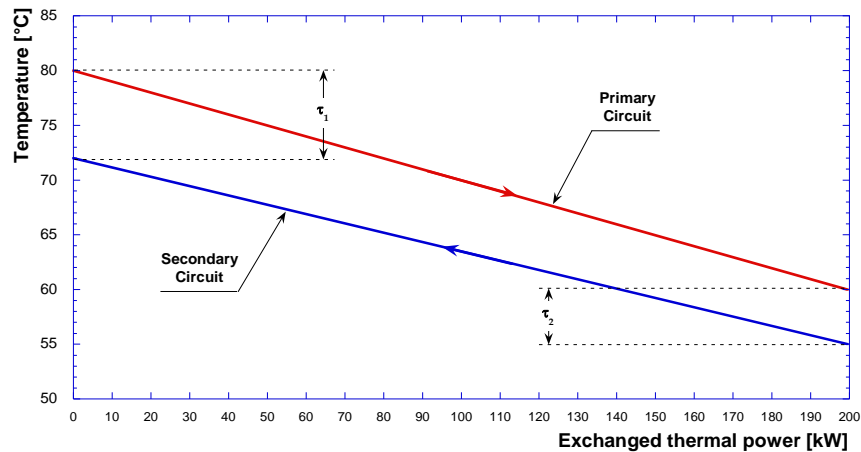


Figure 4.15 – Thermal exchange diagram for the heat exchanger HE1 in design conditions.

Afterwards, with the aim to evaluate the possibility of modifying the current user substation configuration in order to allow the bidirectional thermal energy exchange, two different smart scenarios have been defined and analyzed:

- I. Case 1 – plant integration with thermal solar panels: this configuration has been conceived with the purpose of minimizing the modification actions on the present user substation. For this reason, the scheme 1 (feed to return configuration) has been considered, heating – with the distributed generation system – a mass flow rate from the network feed line and re-introducing the same mass flow rate into the network return piping. As already explained, this scheme entails the temperature increase in the water at the inlet of the thermal power station with a consequent need of regulating the centralized production system. Furthermore, due to the considered configuration, the assumed distributed generation system has to produce heat with a temperature level higher than the one of the network feed, so that the thermal exchange can occur. As a consequence, evacuated tube solar collectors have been considered.
- II. Case 2 – plant integration with a micro-combined heat and power unit (micro-CHP): for this case, opposite to the previous case, the most complex layout has been selected, namely scheme 4 (return to feed configuration). Thus, with this configuration, the distributed system located at the final user allows to increase the temperature of a mass flow rate from the network return and introducing the same mass flow rate into the network feed piping. The main advantage of this configuration stands in the possibility of keeping unchanged the feed temperature level even with a thermal exchange. Indeed, the heat produced by the distributed thermal generation system could be eventually employed for the temperature increase from the return network temperature level until (and not beyond) the feed temperature level. However, the mass flow rates across the whole network result modified and, for this reason, the correct network management is essential. The proposed solution considers the integration between the present user substation and a micro-combined heat and power unit.

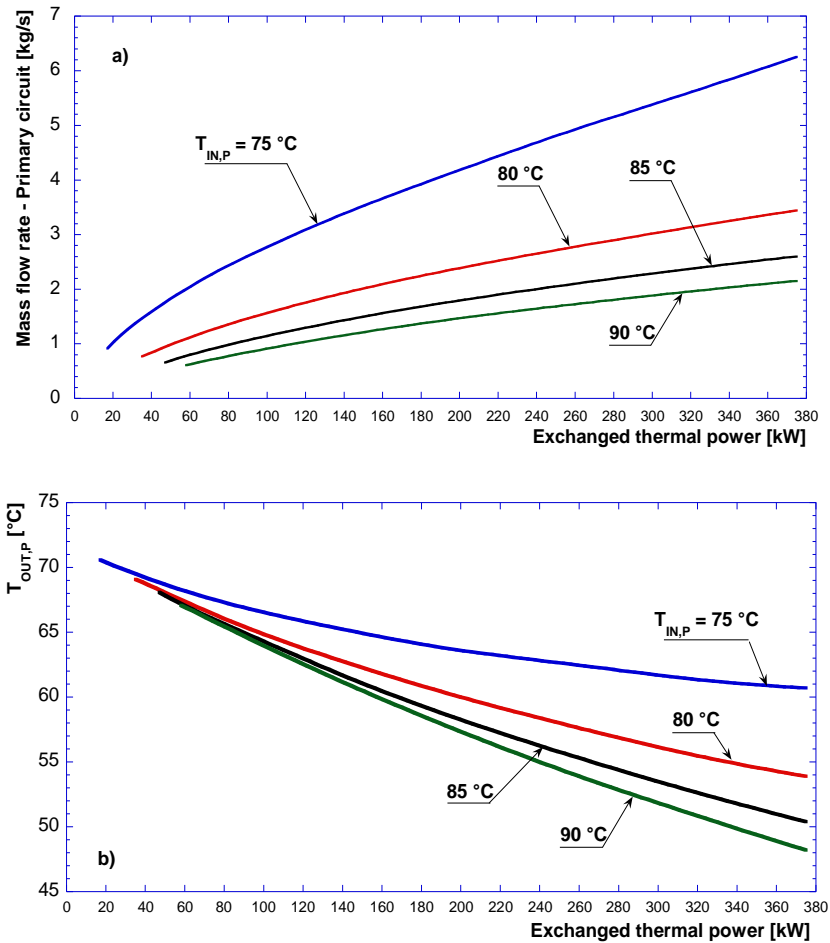


Figure 4.16 – Heat exchanger HE1 off-design operation: a) primary circuit mass flow rate and b) primary circuit outlet temperature as function of the exchanged heat, for different values of the primary circuit inlet temperature $T_{IN,P}$.

For each of the two proposed smart substation configurations, a calculation model has been specifically developed and applied for the simulation of the design and off-design operation of the considered substation during the year. The carried out simulations – for both the considered cases – allowed to determine the heat exchange of each heat exchanger under different operating conditions and the temperature variations on the network side as a result of the bidirectional heat exchange.

Furthermore, technical aspects have been considered and investigated, aiming to the development of preliminary technical schematic of the converted user substations able to guarantee the bidirectional heat exchange. The modifications required by the current substation have been identified and the economic costs related to the required technical actions have been evaluated. Based on the obtained results, a general discussion about the best way to follow depending on the boundary conditions has been reported.

4.4.1 Case 1

First of all, for a preliminary design of the thermal solar integrated utility substation, schematized through the scheme 1, the rooftop useful surface for the panels installation (S_{TSP}) has been estimated as:

$$S_{TSP} = S \cdot \alpha \cdot \beta \quad \text{E4.1}$$

where:

- S is the rooftop surface [m^2];
- α is a correction coefficient introduced for considerations related to the latitude and the corresponding optimal facing. In particular, only rooftop surfaces exposed to south, south-east and south-west (blue surface in Figure 4.17) have been considered for the determination of the useful surface [-];
- β is a reduction coefficient introduced to account the space necessary for installation and maintenance of the thermal solar panels [-].

On the basis of the evaluated rooftop useful surface, the thermal solar panels peak power can be calculated as:

$$Q_P = S_{TSP} \cdot I \cdot \eta_{TSP} \quad \text{E4.2}$$

where:

- I is the solar peak irradiance for the considered latitude [W/m^2];
- η_{TSP} is the thermal solar panels efficiency [-].

Based on the assumptions presented in Table 4.5, a rooftop useful surface equal to 360 m^2 and a solar panels peak power equal to about 200 kW have been calculated. As it regards the values of coefficients α and β , it must be pointed out that the choice has been made as usual in engineer practice and based on the real available information on the considered location.

Table 4.5 – Hypothesis and assumptions for the Case 1 – thermal solar panels integration.

S [m^2]	1800
α [-]	0.50
β [-]	0.60
I [W/m^2]	800
η_{TSP} [-]	0.70

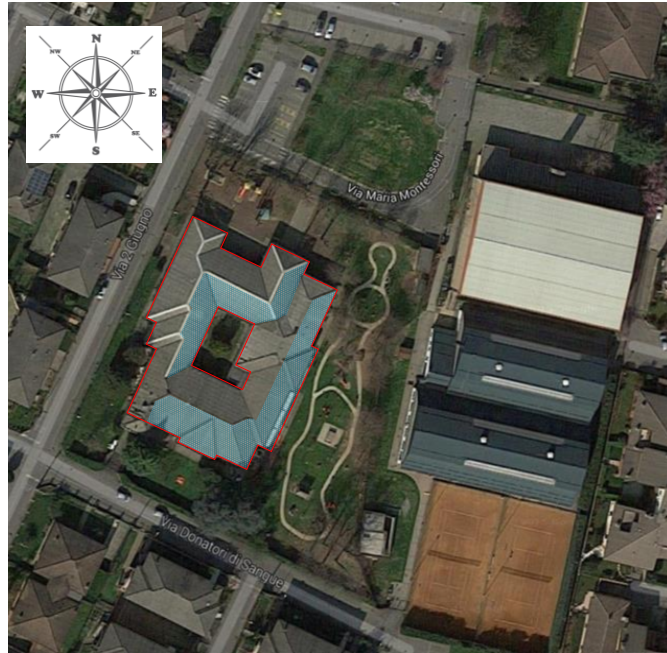


Figure 4.17 – Plant of the selected user for the implementation of smart user substations and rooftop surfaces exposed to south, south-east and south-west (highlighted in blue).

Due to the will of introducing less modifications as possible and considering that the estimated peak power of the thermal solar panels is equal to the rated power of the heat exchanger already installed, there is no need to add any further heat exchanger for the smart conversion of the considered utility substation. As a consequence – with reference to Figure 4.18 – the thermal energy exchange occurs always by means of the heat exchanger HE1: (i) in the direction from the DHN to the user whenever the distributed generation system is not able to meet the user needs, (ii) in the direction from the user to the DHN whenever the distributed production exceeds the user needs. Obviously, the further constraint of temperatures compatibility is present to guarantee the heat exchange. As it can be seen from Figure 4.18 the thermal solar panels are connected to the secondary circuit of the heat exchanger HE1 by means of a thermal storage tank. A further consideration about the primary circuit regulating valve should be made: the current control of this valve, indeed, is related to a maximum admissible temperature and would consequently avoid the bidirectional thermal exchange, as devised for this scenario. As a consequence, the control logic of the primary circuit regulating valve has to be modified in the design of the smart user substation.

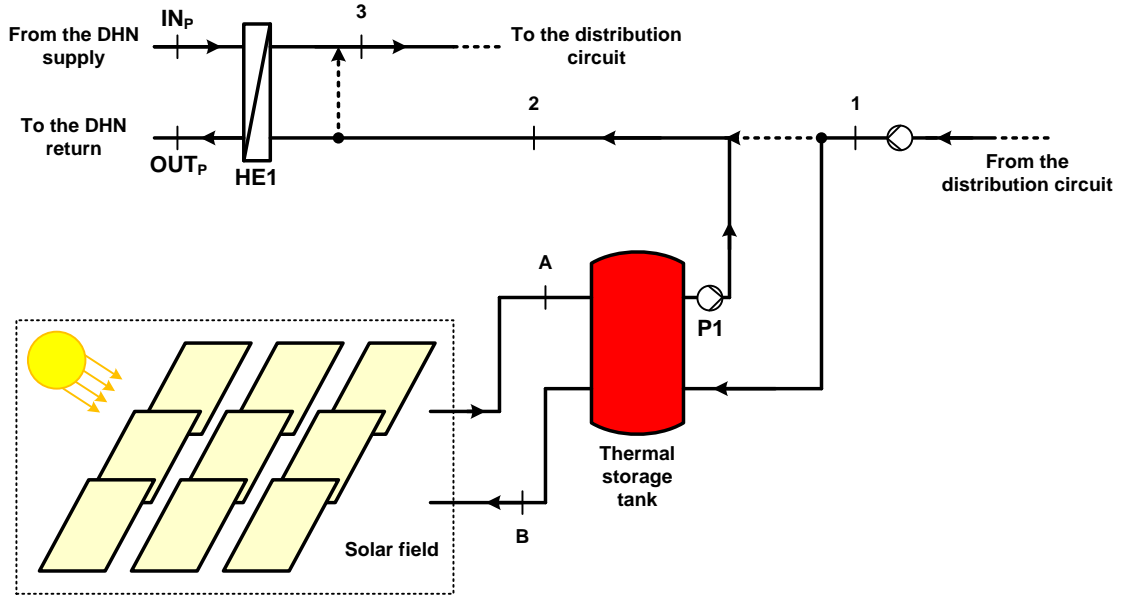


Figure 4.18 – Case 1: thermal solar panels integration: smart user substation schematic (scheme 1 – feed to return configuration).

The elaborated mode of operation of the smart user substation aims to keep unchanged – and equal to the design set values – the temperatures in sections 1 and 3 of the secondary circuit. In other words, the user is supplied by a constant temperature T_3 , while the measured T_1 is used to control the user need. This mode of operation has been chosen in order to employ the solar source to meet firstly the user needs and only the eventual excess is transferred to the DHN, thus the network operates as bidirectional back-up system for the solar field. In more detail:

1. on the basis of the measurement of the temperature in section 1 (T_1) and for known secondary circuit mass flow rate and temperature T_3 , the thermal power required by the user at the time $i - 1$ ($Q_{TH,i-1}$) can be evaluated as:

$$Q_{TH,i-1} = \dot{m}_{i-1} \cdot c_l \cdot (T_3 - T_{1,i-1}) \quad \text{E4.3}$$

where \dot{m}_{i-1} is the mass flow rate through the secondary circuit at the time $i - 1$ [kg/s] and c_l is the liquid specific heat [kJ/kg°C].

If the measured temperature in section 1 ($T_{1,i-1}$) is lower than the set value (T_1), then the user thermal need is increasing; otherwise, it is decreasing.

2. On the basis of the evaluated thermal power required by the user at the time $i - 1$, the mass flow rate to be sent to the user at the time i (by acting on the pump P1) can be calculated as:

$$\dot{m}_i = \frac{Q_{TH,i-1}}{c_l \cdot (T_3 - T_1)} \quad \text{E4.4}$$

being T_3 and T_1 equal to their corresponding set values.

3. Once defined the mass flow rate, the temperature in section 2 (*i.e.* the storage tank temperature) is measured, depending exclusively from the solar heat production:
 - a. if $T_{2,i} > T_3 > T_{IN,P}$, a part of the produced thermal power can be transferred to the DHN. It means:

$$Q_{TH,to\ the\ network} = \dot{m}_i \cdot c_l \cdot (T_3 - T_{2,i}) \quad E4.5$$

- b. if $T_{2,i} < T_3$, the traditional thermal exchange from the network to the user occurs:

$$Q_{TH,from\ the\ network} = \dot{m}_i \cdot c_l \cdot (T_{2,i} - T_3) \quad E4.6$$

In Figure 4.19 and in Figure 4.20 the obtained thermodynamic results of the Case 1 are shown, respectively in terms of temperature T_3 and heat transferred from the distributed generation system to the DHN, as function of the ratio between user need and thermal solar production, for different values of the primary circuit inlet temperature $T_{IN,P}$. The analysis has been carried out for three different values of the temperature at the inlet of the HE1 primary circuit (that is the temperature of the network feed line), since this parameter importantly affects the possibility for the distributed generation system of introducing heat into the network. Based on the current practice in district heating field, the chosen values for $T_{IN,P}$ are 75°C, 80°C and 85°C. Furthermore, in order to give a general result (as much as it is possible), the evaluation has been presented as function of the ratio between the user need and the thermal solar production, rather than as function of the only thermal solar production. The operational model, indeed, aims to firstly meet the user need with the distributed thermal energy production, while only the eventual excess is used to heat the network return. In this way, the presented results are independent from the user need.

As it can be seen from Figure 4.19, for given T_3 (*i.e.* for given thermal solar production) the higher is the temperature $T_{IN,P}$, the lower is the thermal energy exchange from the secondary to the primary circuit of the heat exchanger HE1. As a consequence, the trend of T_3 as function of the ratio between user need and thermal solar production is the same with the increase of $T_{IN,P}$, but it is shifted to the right. This means that, for constant value of T_3 , higher user need can be guarantee. On the contrary, for given ratio between user need and thermal solar production, the curve is up-shifted with the increase of $T_{IN,P}$.

On the other hand, Figure 4.20 shows that the trend of the heat – locally produced and then introduced into the network – remains unchanged on varying the primary circuit temperature $T_{IN,P}$. However, a modification can be found in the range of the ratio between user need and thermal solar production in which the thermal exchange in the direction from the user to the network can occur. Evidently, the higher $T_{IN,P}$, the lower the allowed thermal exchange range.

Moreover, from both the figures it can be observed that there is a minimum value for the ratio between user need and thermal solar production in order to allow the heat exchange. This minimum value, equal to 0.4, is due to the temperature level of the thermal solar production.

Finally, in Figure 4.21 the trend of the maximum thermal power transferred from the distributed generation system to the DHN as function of the network feed line temperature $T_{IN,P}$ is presented. As it can be seen, the maximum thermal power transferrable to the network decreases linearly with the increase of the network feed line temperature. For this reason, if the DHN is operated

with high feed temperature levels, a small amount of heat can be introduced into the network; consequently, it may not be convenient the installation of thermal solar panels for 200 kW of overall peak power. For the specific considered case, an alternative solution may be represented by a plant with a peak power equal to 100 kW: with this power the self-consumption can be opportunely met without an excessive investment cost. On the opposite, if the DHN is operated with a low temperature level (*i.e.* around 55°C for the network feed line), a thermal solar field with 200 kW of peak power would allow to introduce into the network a great amount of thermal energy, justifying the higher investment cost.

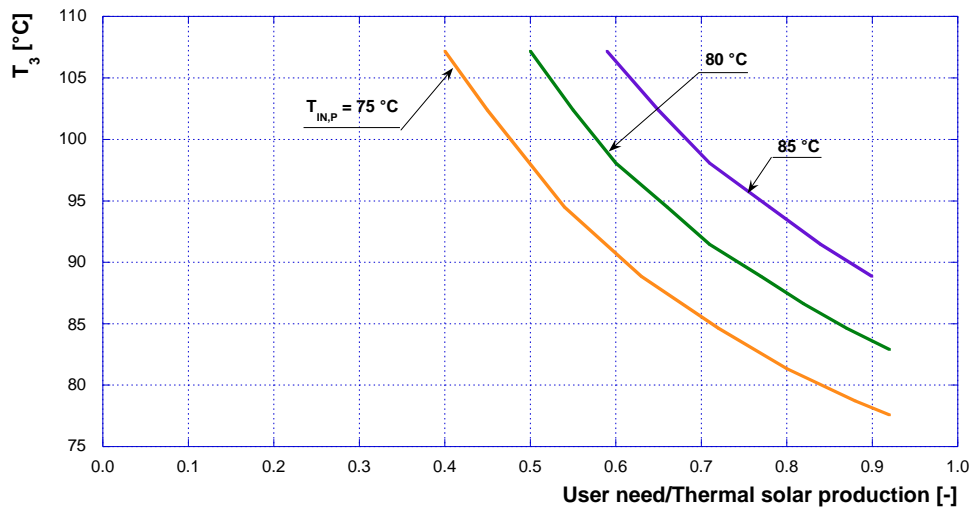


Figure 4.19 – Temperature T_3 as function of the ratio between user need and thermal solar production, for different values of the primary circuit inlet temperature $T_{IN,P}$.

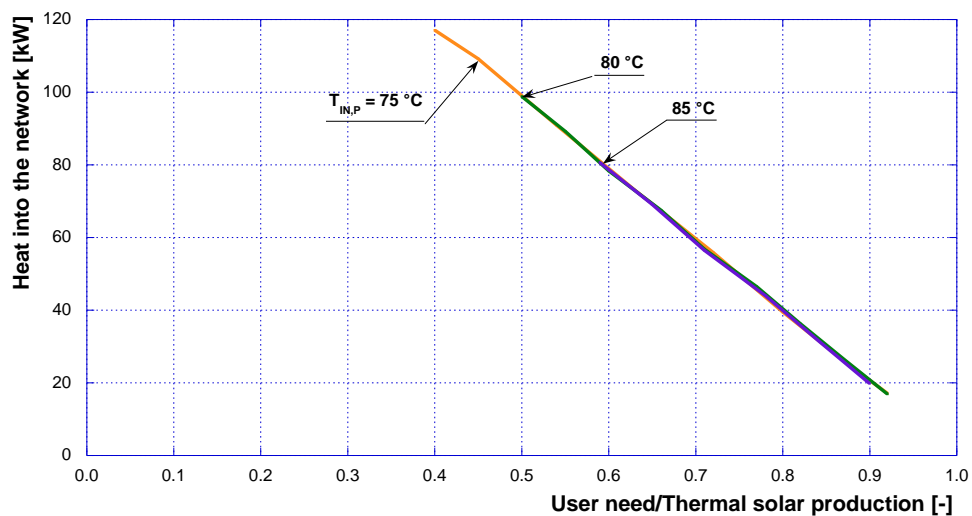


Figure 4.20 – Heat transferred from the distributed generation system to the DHN as function of the ratio between user need and thermal solar production, for different values of the primary circuit inlet temperature $T_{IN,P}$.

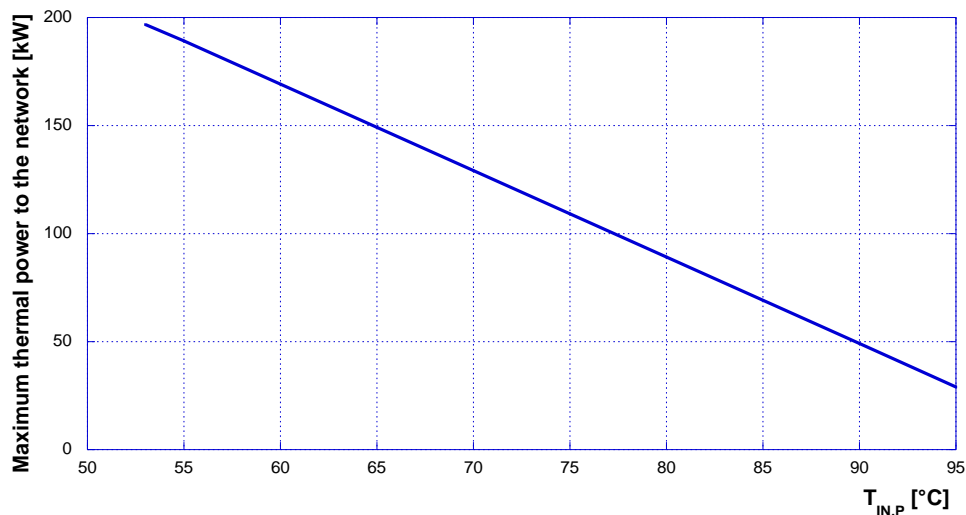


Figure 4.21 – Trend of the maximum thermal power transferred from the distributed generation system to the DHN as function of the network supply temperature $T_{IN,P}$.

The carried out technical analysis led, for the Case 1, to the schematic shown in Figure 4.22. As it regards the heat exchanger HE1, the instrumentation currently installed has been maintained. However, as previously highlighted, the operational mode of the thermostatic valve – located on the primary circuit for the mass flow rate control – must be modified, in order to allow the bidirectional thermal energy exchange. This valve, indeed, with the current control does not allow the introduction of thermal energy into the network. The main components to be added for the conversion of the utility substation are a storage tank (SST in Figure 4.22) and – obviously – the thermal solar panels. Furthermore, the instrumentation to be introduced has been defined. It includes temperature sensors, a mass flow rate sensor, a safety valve and check valves in order to guarantee the correct operation of the systems.

The complete list of the components to be added for the integration between the existing utility substation and the thermal solar panels is presented in Table 4.6 along with the investment costs for each component, determined by direct contact with the corresponding manufacturers and/or suppliers.

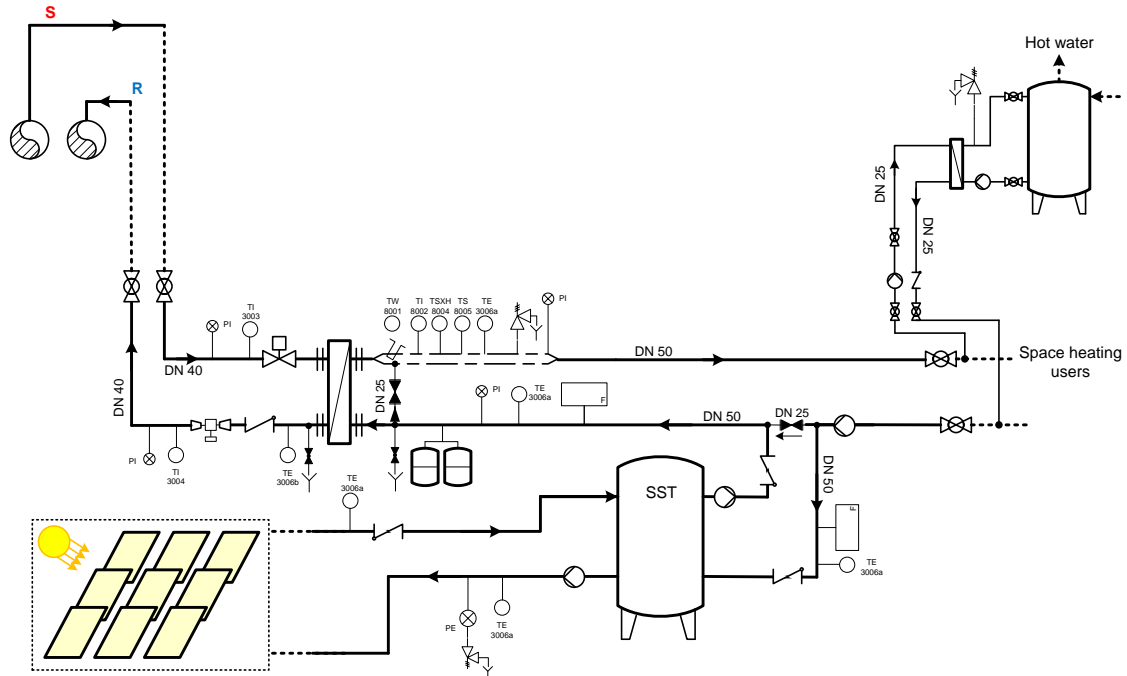


Figure 4.22 – Plant schematic for the Case 1 – integration with thermal solar panels.

Table 4.6 – List of components selected for the smart utility substation transformation - Case 1.

Component	Model/description	Cost ² [€]
Thermal solar panels + Piping for the connection between thermal solar panels and thermal storage tank	SKY 8 CPC 58, n° 250 – installed peak power 228 kW + Black steel piping S.S. (eventually threaded) UNI EN 10255 ex UNI 8863 – DN25 – possibility of taking advantage from an unemployed chimney for the piping installation	300'000
Thermal storage tank from solar energy	Stratified storage made of steel (S 235 JR) PH2000 produced by TiSUN	5'800
Piping for the connection between secondary circuit and thermal storage tank	Black steel piping S.S. (eventually threaded) UNI EN 10255 ex UNI 8863 – DN50	

² Reference year: 2015.

Component	Model/description	Cost ² [€]
Temperature measurement sensors for the solar circuit (T _B and T _A in Figure 8)	Quadrant gas expansion thermometers, DN100, stainless steel AISI 304, measurement scale 0...120°C, accuracy 1%, in compliance with ISPEL - back-end threaded connection M ½" UNI EN ISO 228	1'500
Pressure measurement sensor for the solar circuit return	Quadrant pressure gauge DN100, stainless steel AISI 304, measurement scale 0...10 bar, class 1.0, in compliance with ISPEL, radial threaded connection M ½" UNI EN ISO 228	
Mass flow measurement sensor for the secondary circuit - upstream of the solar storage tank	PROLINE PROMAG 10W ENDRESS HAUSER (electromagnetic sensor)	
Mass flow measurement sensor for the secondary circuit - downstream of the solar storage tank	PROLINE PROMAG 10W ENDRESS HAUSER (electromagnetic sensor)	
Temperature measurement sensor for the secondary circuit - upstream of the solar storage tank	Quadrant gas expansion thermometer, DN100, stainless steel AISI 304, measurement scale 0...120°C, accuracy 1%, in compliance with ISPEL - back-end threaded connection M ½" UNI EN ISO 228	
Temperature measurement sensor for the secondary circuit - downstream of the solar storage tank	Quadrant gas expansion thermometer, DN100, stainless steel AISI 304, measurement scale 0...120°C, accuracy 1%, in compliance with ISPEL - back-end threaded connection M ½" UNI EN ISO 228	
Safety valve for the solar circuit return	Certified PED, diameter 25 mm, calibration 3.5 bar - threaded connections FF 1"x1"1/2	1'400
Pump at the outlet of the solar storage tank	Wet rotor electric pump - variable mass flow	
Check valve for the solar circuit supply	Ball check valve - maximum pressure 16 bar	
Pump on the secondary circuit - upstream of the solar storage tank	Wet rotor electric pump - variable mass flow	
Pump on the secondary circuit - downstream of the solar storage tank	Wet rotor electric pump - variable mass flow	
By-pass valve for the solar storage tank exclusion	Bronze, maximum pressure 16 bar, threaded connections	
Check valve on the secondary circuit - upstream of the solar storage tank	Ball check valve - maximum pressure 16 bar	
Check valve on the secondary circuit - downstream of the solar storage tank	Ball check valve - maximum pressure 16 bar	

All the new components have been selected by means of a market survey, which also allowed the calculation of the total maximum investment cost for the conversion of the existing substation. The intervention cost results equal to 310'000 €, considering a peak power of 200 kW for the thermal solar field. This solution is very expensive and from Table 4.6 it can be noted that the major cost is due to the solar panels. Therefore, the obtained result probably suggests to halve the installed thermal solar power. In any case, it should not be neglected the simplicity for what concerns the network management, due to the choice of the scheme 1 for the smart substation realization.

4.4.2 Case 2

In this case the current user substation is supposed to be integrated with a micro-cogeneration unit. The bidirectional thermal energy exchange is schematized by means of the scheme 4 (return line to feed line configuration, that is the most complex of the proposed schemes). The proposed schematic of the modified utility substation is shown in Figure 4.23. As it can be seen, opposite to the Case 1, in this case the heat exchanger HE1 cannot be used for the bidirectional exchange due to the considered scheme for the smart substation. Two heat exchangers have been added: HE2 and HE3 in Figure 4.23, for the heat transfers from the distributed generation system to the network and from the distributed generation system to the user respectively. In greater detail, at the outlet of the CHP (section B) the fluid is firstly employed to meet (partially or completely) the user need by means of the heat exchanger HE3. Then, the eventual excess of thermal production can be transferred to the network, compatibly with the temperature levels.

In order to compare the two proposed solutions, the size of the micro-CHP unit has been imposed to have a rated thermal power equal to 200 kW (which is the design exchanged thermal power of HE1). With this assumption the user need can be largely met by the micro-CHP unit during the year. Similarly, the two heat exchangers to be introduced have been considered with a design heat exchange equal to 200 kW.

Among the micro-CHP technologies, micro-gas turbines (micro-GT) have been considered for the analysis, due to the advantages – in comparison to the internal combustion engines – of reducing pollutant emissions and noise, even if with a lower level of technologic development. Furthermore, micro-GTs have more architectural simplicity than internal combustion engines, thanks to the one level heat recovery: as a consequence, they result the recommended solution for the analyzed user typology. After a market survey (presented in Table 4.7), the micro-GT Elliott TA100 has been chosen being the only machine able to guarantee by itself the desired rated power (200 kW). From Table 4.7, indeed, it can be observed that the micro-GT Elliott TA100 enables to obtain a rated electric power equal to 100 kW (corresponding to a rated thermal power equal to 200 kW) with higher efficiency compared to the micro-GT Turbec T100.

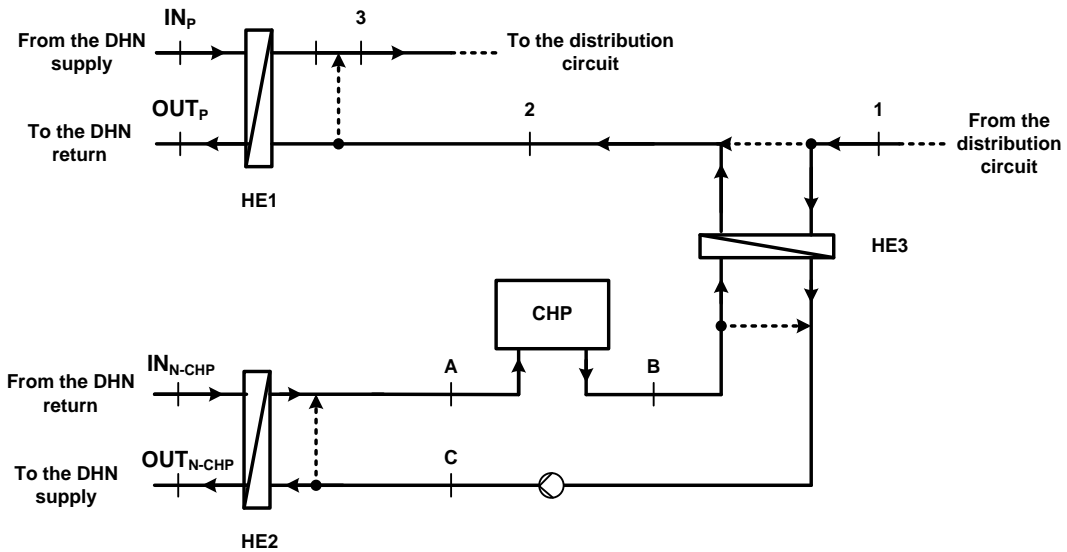


Figure 4.23 – Case 2: combined heat and power unit integration: smart user substation schematic (scheme 4 – return to feed configuration).

Table 4.7 – Micro-GT available on the market.

Manufacturer	Model	P_e [kW _e]	η_e [%]	η_{CHP} [%]	$\dot{m}_{\text{exhaust gas}}$ [kg/s]	Speed [rpm]	β [-]	$T_{\text{exhaust gas (no CHP)}}$ [°C]
Capstone	C30	30	26	-	0.31	96000	3.5	275
Capstone	C60*	60	28	53.7	0.49	96000	3.7	360
Capstone	C65	65	29	50.0	0.49	96000	3.7	309
Ingersoll Rand	MT70*	70	28	40.0	0.73	44000	-	210
Bowman	TG80CG	80	26	48.8	0.83	68000	-	278
Elliott	TA80*	80	28	60.0	0.77	-	4.0	230
Elliott	TA100	100	29	50.0	1.00	-	4.0	293
Turbec	T100	100	30	46.5	0.81	70000	4.5	270
Capstone	C200	190	31	40.0	1.30	65000	-	280
Ingersoll Rand	MT250	250	30	44.6	2.00	45000	-	249
Capstone	C1000**	1000	33	-	6.70	-	-	275

* old model, no more present in the manufacturer price list

** package composed of 5 units C200

The mode of operation of the smart user substation here described is based on the assumption of keeping constant the mass flow rate through the secondary circuit and the temperature T_3 , while the measurement of the temperature T_1 is used to control the user need. Relating to the micro-CHP unit, the temperatures T_A and T_B are assumed as constants in order to maximize the CHP heat recovery efficiency.

In more detail:

1. based on the measurement of the temperature in section 1 and for known mass flow rate through the secondary circuit (\dot{m}_S), the thermal power required by the user at the time $i - 1$ ($Q_{TH,i-1}$) can be evaluated as:

$$Q_{TH,i-1} = \dot{m}_S \cdot c_l \cdot (T_3 - T_{1,i-1}) \quad E4.7$$

if the temperature T_1 is lower than its set value, the thermal power need of the user is increasing, otherwise it is decreasing.

2. The heat exchanger HE3, between the CHP and the secondary circuits, is operated to keep constant (and equal to the set value) the temperature T_3 .
3. Based on the heat exchanged between CHP unit and user (*i.e.* by means of the heat exchanger HE3), a temperature variation in the section C can be observed. As a consequence, the heat exchanged between the CHP circuit and the network varies being equal the temperature T_A .

The thermodynamic results obtained for the Case 2 are presented in Figure 4.24 and in Figure 4.25. In detail, Figure 4.24 shows the trends of the mass flow rate through the heat exchanger HE3 on the secondary circuit (*i.e.* user side) – blue line in figure – and of the mass flow rate through the heat exchanger HE2 on the network side (*i.e.* the mass flow rate withdrawn from the DHN return line and introduced – after being heated – into the DHN feed piping) – red dotted line in figure. Evidently, as it can be seen in Figure 4.24, with the increase of the amount of thermal energy which is produced by the CHP unit and given to the user, the mass flow rate through the heat exchanger HE3 on the user side results increased. On the other hand, this entails the decrease in the mass flow rate through the heat exchanger HE2 on the network side, in order to keep constant the temperature at the end of the heat exchange. As already highlighted, indeed, one of the main advantages of the configuration scheme 4 for the smart user substation is the possibility of non-modifying the network temperature levels. For this reason, the simulations have been carried out with the constraint of heating the mass flow rate taken from the DHN return until (and not beyond) the temperature level of the DHN feed line. Thus, the mass flow rate involved in the heat exchange results as a consequence.

In Figure 4.25, instead, the trend of the HE2 inlet temperature on the CHP side (T_C), as function of the ratio between user need and CHP production is presented. As it can be seen, the increase in the thermal power from the CHP to the user causes the decrease of the temperature T_C , which varies from 90°C (when the whole CHP production is self-consumed) to 137°C (when the whole CHP production is introduced into the DHN).

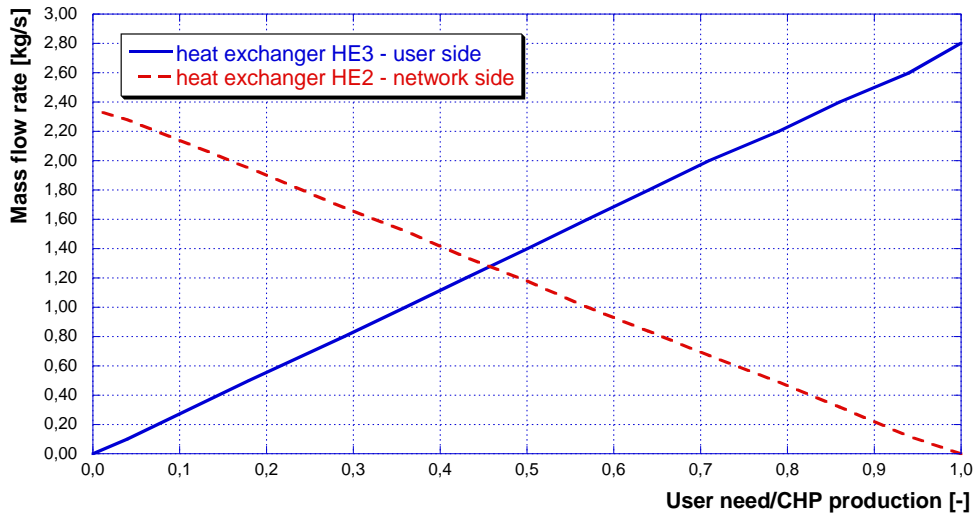


Figure 4.24 – Trends of the mass flow rate to the heat exchanger HE3 on the secondary circuit (*i.e.* user side) – blue line – and of the mass flow rate through the heat exchanger HE2 on the network side (*i.e.* the mass flow rate withdrawn from the DHN return and introduced – after being heated – into the DHN supply) – red dotted line.

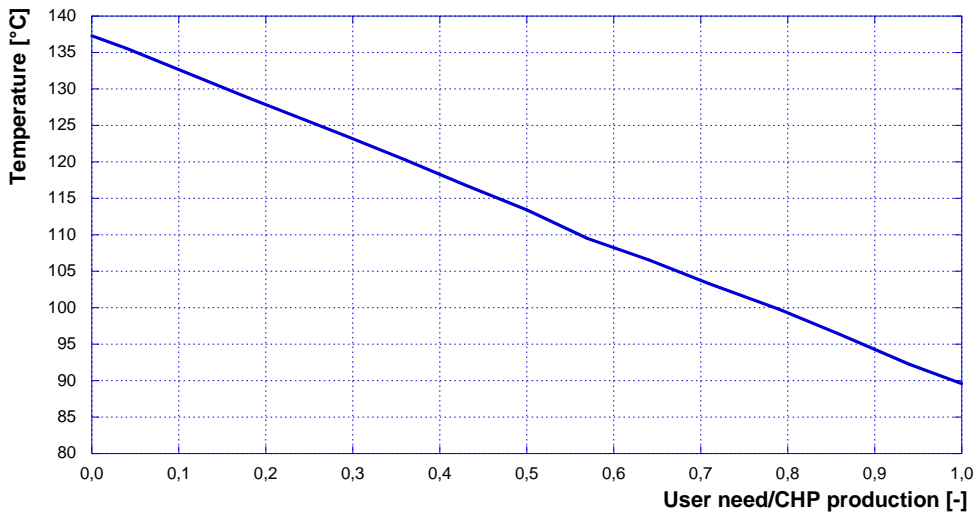


Figure 4.25 – Trend of the HE2 inlet temperature on the CHP side (TC), as function of the ratio between user need and CHP production.

The technical analysis for the Case 2, differently from what shown for the Case 1, have to consider the need of doubling the connection piping between the user substation and the DHN principal circuit, in order to allow the bidirectional exchange as schematized with the proposed scheme 4. With this purpose, in Figure 4.26 the portion of the district heating network circuit which involves the considered user (infant school), as currently set, is shown. As it can be seen

from the figure, the portion of the network between the point A and the point B is the one interested in the intervention required for the conversion of the utility substation. A further detail of this portion, including the distance measurements, is presented in Figure 4.27, along with the representations of the piping location sections, both for the street and for the greensward areas.

The developed hypothesis for the disposition of the two needed pipes to be added for the bidirectional heat exchange is shown in Figure 4.28. As it can be seen, the most viable solution considers the placement of the new piping next to the existing ones, being the available pavement space large enough for this modification.

Finally, analogous to Case 1, a techno-economic analysis has been repeated for the Case 2, leading to the definition of the project plant presented in Figure 4.29. In this case important modifications must be made to the current substation set-up, especially related to the network piping addition. Also the substation itself must be modified and the main introduced components are the combined heat and power unit and two heat exchangers. Furthermore the instrumentation for temperature and mass flow rate measurement has been included, as well as the required pumps and valves.

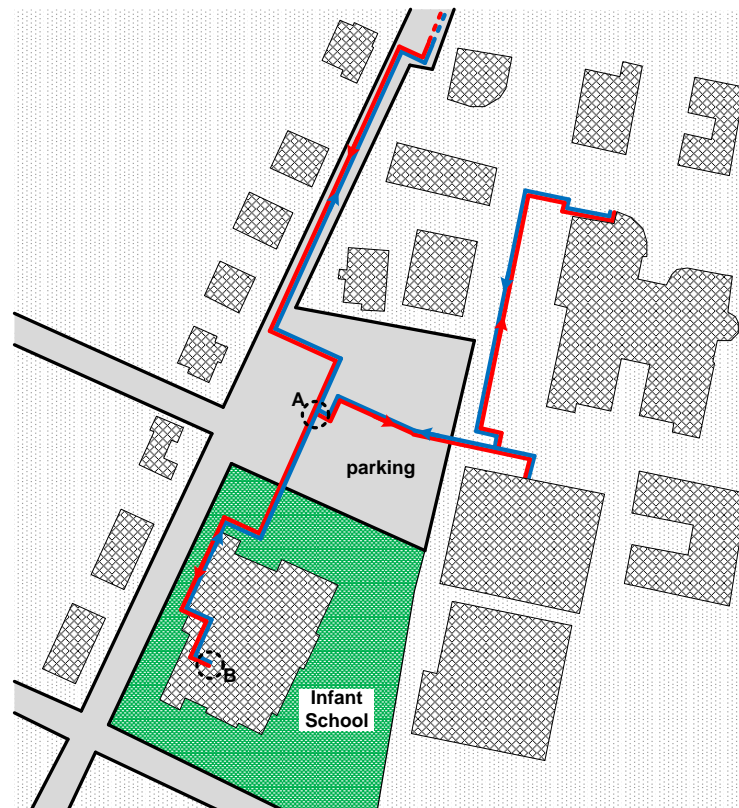


Figure 4.26 – Portion of the district heating network circuit which involves the considered user (infant school) as currently set.

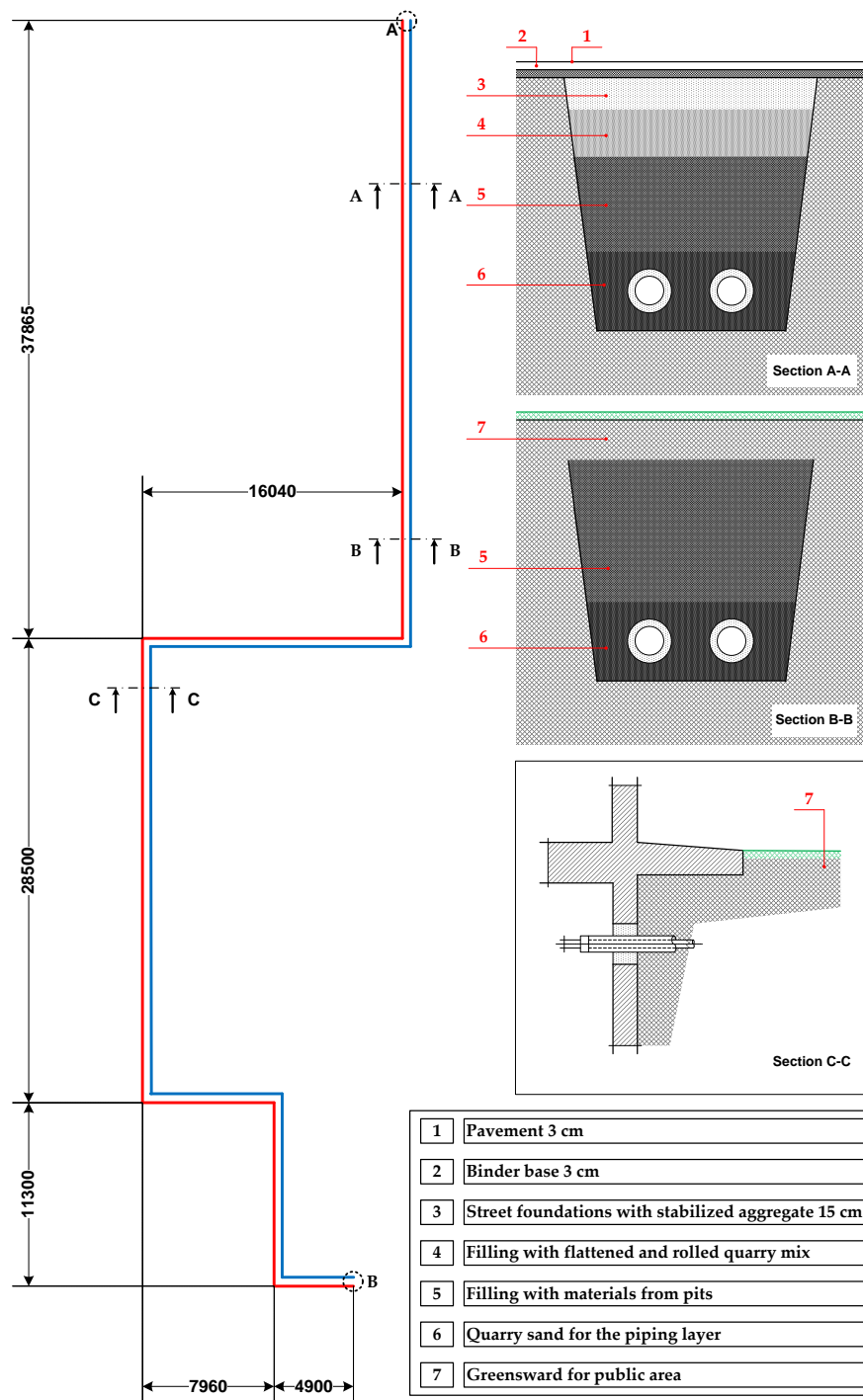


Figure 4.27 – Detail of the current status of the district heating network portion involved in the required modifications in order to convert the considered utility substation in a smart substation.

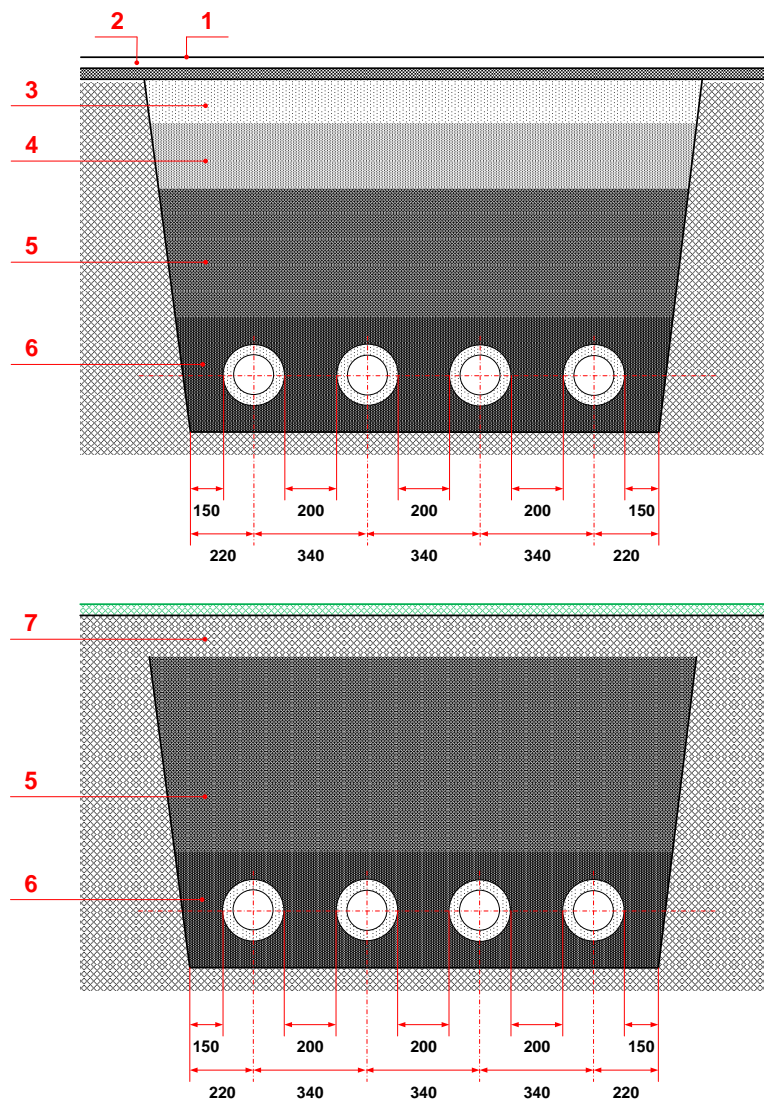


Figure 4.28 – Portion of the district heating network circuit which involves the considered user (infant school).

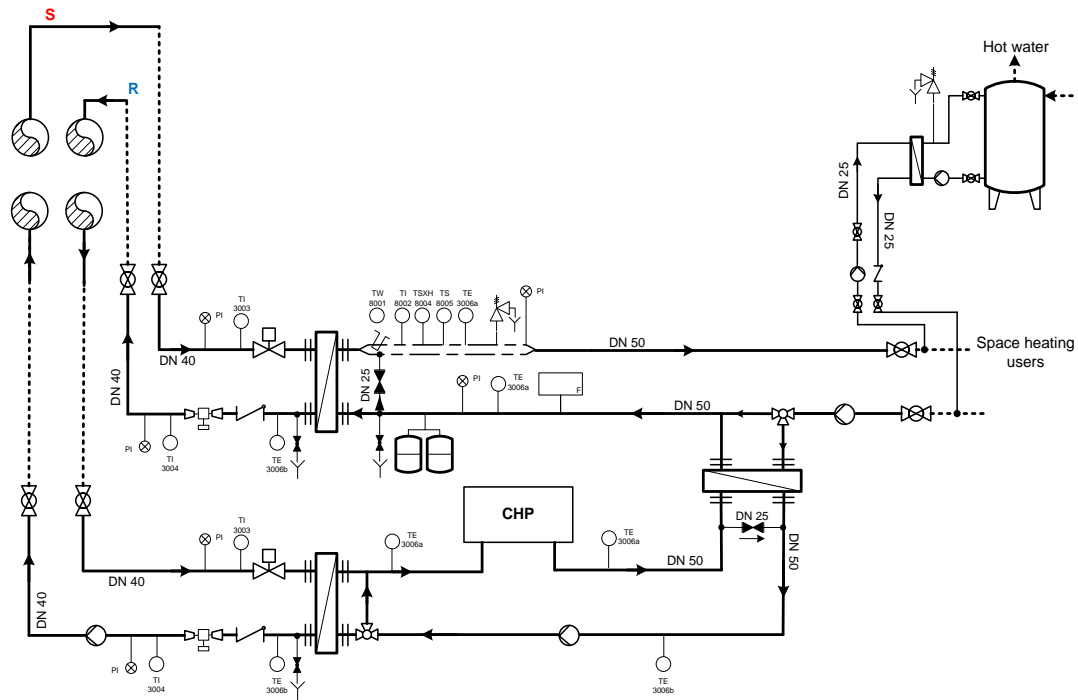


Figure 4.29 – Plant schematic for the Case 2 – integration with CHP unit.

The complete list of the components to be added for the integration between the existing utility substation and the combined heat and power unit is presented in Table 4.8, along with the investment costs for each component.

For the intervention, required to modify the current utility substation set-up in order to integrate the CHP unit, an overall cost equal to 180'000 € has been estimated. As it can be observed from Table 4.8, the major cost stands in the CHP unit installation. However, also the cost related to the installation and set-up of the new piping is not negligible. Even though this solution has much more complexity in comparison with the thermal solar panels integration (Case 1), it is economically preferable. Evidently, if the peak power of the thermal solar field is reduced to 100 kW, the two analyzed cases result comparable.

Table 4.8 – List of components selected for the smart utility substation transformation - Case 2.

Component	Model/description	Cost ³ [€]
Micro-CHP unit + piping for the CHP circuit	Micro gas turbine Elliott TA100 - 200 kW _{th} , $\eta_{\text{CHP}} = 50\%$ + Black steel piping S.S. (eventually threaded) UNI EN 10255 ex UNI 8863 – DN50	150'000
DHN connection piping	Insulated piping - DN65	22'000
Heat exchanger CHP - user (secondary circuit)	Alfa Laval heat exchanger - rated thermal power 200 kW	
Heat exchanger CHP - DHN	Alfa Laval heat exchanger - rated thermal power 200 kW	
Temperature measurement sensor at the inlet of the heat exchanger CHP-DHN, network side	Quadrant gas expansion thermometers, DN100, stainless steel AISI 304, measurement scale 0...120°C, accuracy 1%, in compliance with ISPEL - threaded back-end connection M ½" UNI EN ISO 228	1'200
Temperature measurement sensor at the outlet of the heat exchanger CHP-DHN, network side	Quadrant gas expansion thermometers, DN100, stainless steel AISI 304, measurement scale 0...120°C, accuracy 1%, in compliance with ISPEL - threaded back-end connection M ½" UNI EN ISO 228	
Pressure measurement sensor at the inlet of the heat exchanger CHP-DHN, network side	Quadrant pressure gauge DN100, stainless steel AISI 304, measurement scale 0...10 bar, class 1.0, in compliance with ISPEL, radial threaded connection M ½" UNI EN ISO 228	
Pressure measurement sensor at the outlet of the heat exchanger CHP-DHN, network side	Quadrant pressure gauge DN100, stainless steel AISI 304, measurement scale 0...10 bar, class 1.0, in compliance with ISPEL, radial threaded connection M ½" UNI EN ISO 228	
Temperature measurement sensor at the inlet of the heat exchanger CHP-DHN, network side	Quadrant gas expansion thermometer, DN100, stainless steel AISI 304, measurement scale 0...120°C, accuracy 1%, in compliance with ISPEL - back-end threaded connection M ½" UNI EN ISO 228	
Temperature measurement sensor at the outlet of the heat exchanger CHP-DHN, CHP side	Quadrant gas expansion thermometer, DN100, stainless steel AISI 304, measurement scale 0...120°C, accuracy 1%, in compliance with ISPEL - back-end threaded connection M ½" UNI EN ISO 228	
Temperature measurement sensor at the inlet of the heat exchanger user-CHP, CHP side	Quadrant gas expansion thermometer, DN100, stainless steel AISI 304, measurement scale 0...120°C, accuracy 1%, in compliance with ISPEL - back-end threaded connection M ½" UNI EN ISO 228	
Mass flow measurement sensor downstream of the heat exchanger user-CHP, user side	PROLINE PROMAG 10W ENDRESS HAUSER (electromagnetic sensor)	

³ Reference year: 2015.

Component	Model/description	Cost ³ [€]
Motor-driven two ways valve	Siemens VVF52 - threaded connection, maximum pressure 16 bar, stem stroke 20 mm, kvs m ³ /h	2·150
Check valve at the outlet of the heat exchanger CHP-DHN, network side	Ball check valve - maximum pressure 16 bar	
Thermostatic valve for mass flow limiting at the outlet of the heat exchanger CHP-DHN, network side	Danfoss - mass flow rate and temperature limit control	
Pump at the outlet of the heat exchanger CHP-DHN, network side	Wet rotor electric pump - variable mass flow	
Y filter	Steel body, stainless steel removable basket, filtration 1000 mm, threaded connections, maximum pressure 16 bar	
Two intercept valves for the heat exchanger CHP-DHN circuit, network side	Steel, maximum pressure 16 bar, welded connections	
Pump downstream of the heat user-CHP, CHP side	Wet rotor electric pump - variable mass flow	
By-pass valve for the solar storage tank exclusion	Bronze, maximum pressure 16 bar, threaded connections	
Pump upstream of the heat user-CHP, user side (secondary circuit)	Wet rotor electric pump - variable mass flow	
Two three-ways thermostatic valves	MK, DN50, maximum pressure 16 bar, operating temperature 4 °C - 150 °C	

References

- [1] Ancona MA, Melino F, Peretto A. An Optimization Procedure for District Heating Networks. *Energy Procedia*, 61 (2014) 278-281.
- [2] Ancona MA, Melino F. Analisi di soluzioni tecniche e gestionali che favoriscano l'implementazione di nuovi servizi energetici nelle reti termiche in presenza di sistemi di generazione distribuita. *Report Ricerca di Sistema Elettrico, Accordo di Programma Ministero dello Sviluppo Economico – ENEA, Piano Annuale di Realizzazione 2013*.

5. Scheduling optimization methods in complex energy networks

As introduced in Chapter 1, the optimal systems operation and management is a key point within complex energy networks. Furthermore, the integration of distributed generation (DG) technologies within the existing network is likely to create significant issues relating to the costs of energy provision, the price of electricity and fuel, power quality, infrastructure requirements and technical performance. In fact, the diffusion of DG has increasingly stressed the operation of distribution networks, originally conceived to operate as passive systems for delivering energy to loads. However, distributed generation supported by smart grids and Information and Communication Technology (ICT) can be the solution to actual energy problems such as the continuous rise in price of electricity, the availability of fossil fuels or the integration of conventional energy systems with non-programmable renewable resources [1, 2].

As a result, one of the main purposes relating to the smart grids is the optimization of the scheduling (*i.e.* the load distribution) of the various energy production systems, which concur to the satisfaction of energy demand. To achieve this goal various optimization techniques have been applied [3], such as genetic algorithm (GA), particle swarm optimization (PSO) and firefly algorithm (FFA) [4] – as it concerns heuristic models – or Linear Programming (LP), Mixed Integer Linear Programming (MILP) [5-9] and Mixed Integer Non Linear Programming (MINLP) problems [10], as it regards exact methods. As it concerns energy networks, genetic algorithms and MILP based models are the most widely used for the scheduling optimization problems. Furthermore, MINLP models are considered as an interesting way but further efforts have to be made in order to maintain the nonlinear complexity of the problem and an admissible computational time.

5.1 Genetic algorithms

In more detail, genetic algorithms allow to solve nonlinear problems obtaining good approximate solutions [11]. The computational time, due to nonlinearities, can be considerably high depending on the typology and complexity of the problem to be solved, ranging from few minutes (for medium size problems with low number of time steps) to several days (for large problems and large number of time steps).

This typology of algorithms belongs to artificial-evolution search methods and it is based on the concepts of natural selection and population genetics [12]. The first generation is composed by a set of candidate solutions (known as population), randomly or pseudo-randomly generated, each one representing a point in the space of potential solutions. Each individual of the population (see Figure 5.1) is characterized by a set of parameters, *i.e.* a set of *chromosomes*, which completely describe a solution. A binary alphabet is used in the majority of the cases for the chromosomes formation. Furthermore, in order to evaluate how good each candidate solution is, a fitness function is defined, which represents the objective function of the problem. Then, based on the fitness function value, an individuals' rank is created and a certain percentage of individuals (the

best rank solutions) is selected for the reproduction process. In other words, the reproduction is based on probabilities calculated from the individual's fitness value, which means that strings with higher values have a higher probability of participating in reproduction process. The new population is based on genetic rules and it can be created by applying one (or more) of the following criteria: (i) parent selection, (ii) crossover and (iii) mutation [13]. In particular, the first criterion is inspired by natural selection (*i.e.* the Darwin laws are accounted), while the other two by genetics.

The Darwinian selection supports the idea that “stronger” individuals have a major probability of survival within their living context and, as a consequence, a major probability of reproducing themselves. In the GA context, the stronger individuals are the ones with higher values of fitness function, since they solve in a better way the given search problem. For this reason, they should be favored during the phase of selection of those individuals which will be able to reproduce. The probability of success associated with each individual can be defined proportionally to the fitness function value. These probabilities are then used to create a sort of *roulette*, as for the example proposed in Figure 5.2: the four individuals A_1 , A_2 , A_3 and A_4 are characterized by probabilities respectively equal to 0.12, 0.18, 0.3 and 0.4 and they occupy a portion of the roulette corresponding to their probability. In the proposed example the selection operator generates the random number $c=0.78$, thus the individual A_4 is selected.

Population p of the GA

1	0	1	1	1	0	1				1	0	0	Individual 1
1	1	1	0	1	0	1				1	0	1	Individual 2
1	0	0	1	1	0	1				0	0	0	Individual 3
1	0	1	0	1	0	1				1	1	0	Individual n

Figure 5.1 – Example of the composition of a population in the GA model.

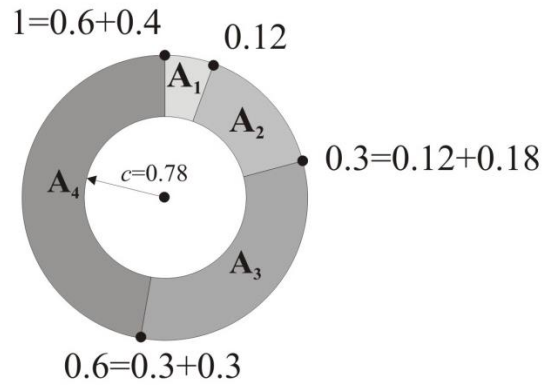


Figure 5.2 – Roulette structure in the GA model.

Every time an individual of the population is selected its copy is created and it is inserted in the so called mating pool. When the mating pool is filled with a number n of individuals (that is the number of the population individuals), new n descendants are created by means of genetics rules. One of these rules, as previously mentioned, is the crossover method: in this case, two individuals (which will be the parents) are randomly chosen in the mating pool. Furthermore, a cut point (crossover point) has to be selected for these individuals and the genotype portions located at the right of the crossover point are inverted, as graphically shown in Figure 5.3. The crossover operator is applied, accordingly with a fixed probability, $n/2$ times in order to obtain n descendants. In some models the crossover operator is not applied, thus in that cases the descendants coincide with the parents.

After the crossover application, a further modification can be introduced with the mutation process, which is the occasional random alternation of the value of a string position (see Figure 5.4). This process is particularly useful in order to avoid the losses of some potentially useful genetic materials after the crossover process.

For completeness, the summary of the whole explained process is presented in Figure 5.5.

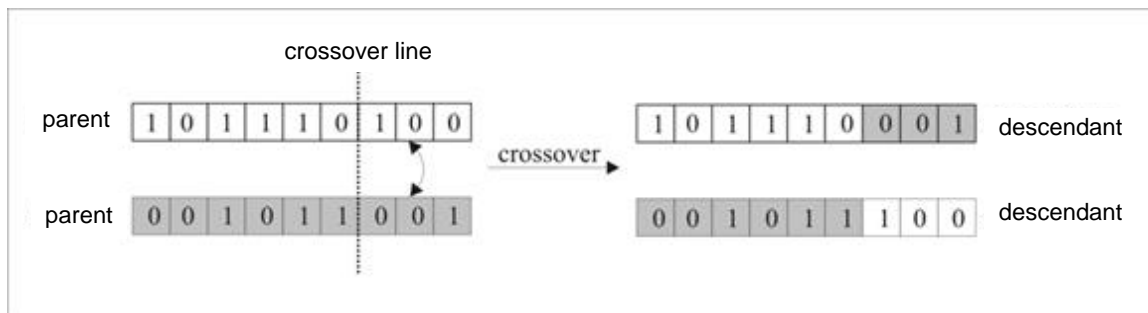


Figure 5.3 – Crossover process for new individuals creation in the GA model.

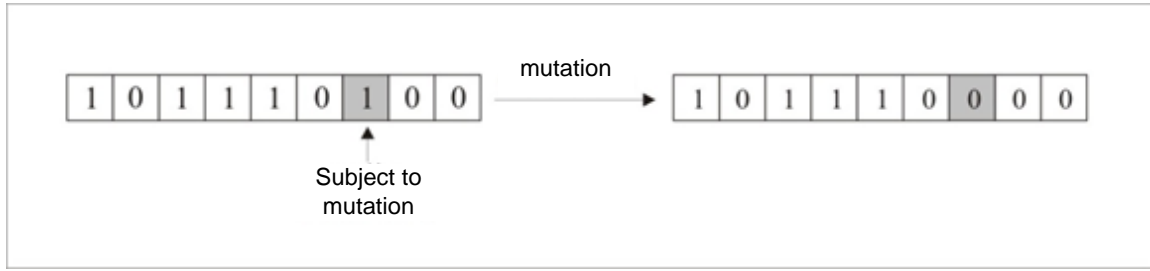


Figure 5.4 – Mutation process for new individuals creation in the GA model.

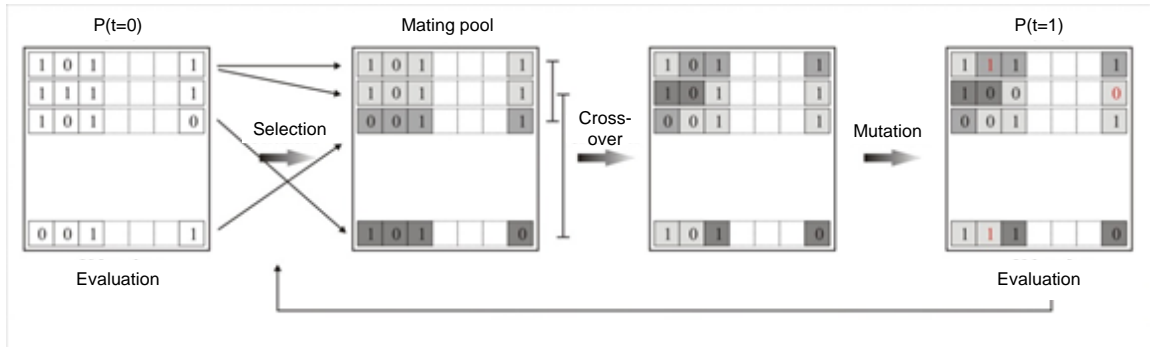


Figure 5.5 – Summary of the whole GA process.

5.2 Mixed Integer Linear Programming models

The MILP problems are characterized by linear functions and discrete variables. As a consequence, when a scheduling optimization problem is formulated with a MILP model, the nonlinearities are lost (*e.g.* pressure losses across DHNs or off-design behavior of the energy systems performance). On the other hand, the possibility of finding the exact solution of the problem with a low computational time also for a large number of time steps made this kind of problems particularly suitable in the complex energy network field. In detail, few seconds or minutes (depending on the energy network complexity) are needed to solve a MILP problem for the hourly-based yearly scheduling optimization.

A general formulation can be written as:

$$\begin{cases} \text{minimize } f(\mathbf{x}, \mathbf{y}) = \mathbf{c}^T \mathbf{x} + \mathbf{d}^T \mathbf{y}, \\ \text{subject to } \mathbf{A}\mathbf{x} + \mathbf{B}\mathbf{y} \leq \mathbf{b}, \\ \mathbf{x}_{\min} \leq \mathbf{x} \leq \mathbf{x}_{\max}, \mathbf{x} \in \mathbf{X}, \\ \mathbf{y} \in \{0,1\}^q \end{cases} \quad \text{E5.1}$$

where \mathbf{x} is a vector of n continuous variables, \mathbf{y} is a vector of q variables 0-1, \mathbf{b} represents the constraints vector and $\mathbf{X} \subset \mathbb{R}^n$ is a bounded polyhedral set.

As an example of MILP models application, the economic scheduling problem in cogeneration planning is proposed in [14, 15]. In these studies the nonlinear process behavior is approximated using linearized models for turbines and boilers with a constant efficiency.

Regarding the scheduling of micro-grids under limited resources, different formulations have been developed to minimize the operational cost of a network, considering the management of electricity and heat. Some works are focused on the energy generation management side. For example, Carrión and Arroyo [16] developed a discrete-time Mixed-Integer Linear Programming (MILP) formulation to minimize the operational cost for an established energy demand.

In the area of smart houses, Nistor et al. [17] presented an approach for the scheduling of tasks, where these tasks may be delayed according to the real-time energy price. Rastegar et al. [18] presented an MILP formulation in order to manage the human behavior and to better satisfy the energy demand to respond to real-time prices, by incorporating priority in the tasks. Zhang et al. [19] proposed a multi-criteria optimization model for the analysis of the trade-off between economics and environmental sustainability while scheduling the energy tasks within smart houses in a micro-grid.

The management of generation and demand has been investigated in a sequential way. This is given by adjusting the process schedule to the availability of energy. For instance, Nolde and Morari [20] developed a MILP formulation to minimize the energy cost by optimizing the schedule of energy tasks. The objective of the proposed model was to adjust the schedule of a steel plant. A penalization for deviations from the previously contracted energy consumption to the provider was introduced. Other works are based on adjusting the operation of a process to the variable real-time price of the energy. For example, Mitra et al. [21] presented a MILP for the generation planning based on the electricity price for a continuous process. Moreover, Hadera et al. [22] proposed a mathematical formulation to deal with the demand response, in order to minimize the energy costs, taking into account the schedule of a steel plant. Mohsenian-Rad and León-García [23] presented a residential energy task scheduling formulation considering energy pricing models for smart houses. Silvente et al. [24] presented a MILP formulation for the coordinated management of generation and demand in a micro-grid, taking into account renewable energy sources and the interconnection with the power grid. Penalty costs were applied in case of delays from the nominal target. In addition, Zhang et al. [25] contemplated non-constant profiles in the energy demand requirements.

Finally, a flow chart schematic of a MILP model developed in [26] is presented as an example in Figure 5.6. This study proposes an optimal operational planning model on the basis of mixed-integer linear programming, where energy loss characteristics of connecting pipes between storage tanks are originally modeled by considering the influence of hot water retention. The developed models are then applied to a residential energy supply network for a housing complex composed of multiple 1-kWe gas engine-based cogeneration systems and 20 residence units.

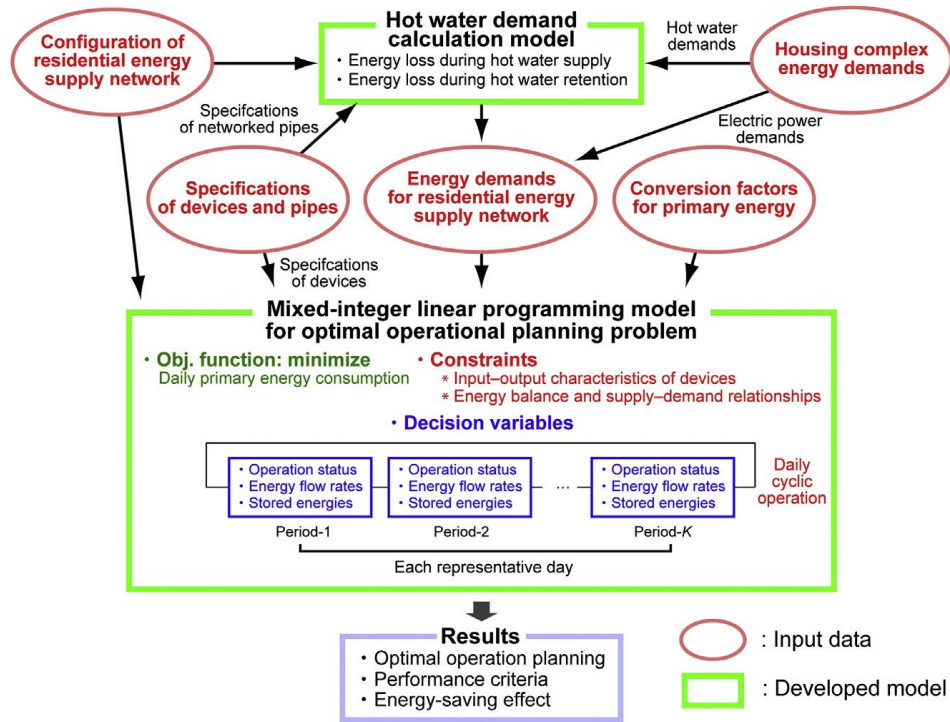


Figure 5.6 – Schematic of a MILP model for a cogeneration-based energy supply network [26].

5.3 Mixed Integer Non Linear Programming models

The MINLP problems are particularly interesting in complex energy networks' optimization applications, because they allow to combine the difficulty of optimizing over discrete variable sets with the challenges of handling nonlinear functions. The problem can be formulated as it follows [27]:

$$\begin{cases} \text{minimize } f(x), \\ \text{subject to } c(x) \leq 0, \\ x \in X, \\ x_i \in \mathbb{Z}, \forall i \in I \end{cases} \quad \text{E5.2}$$

where $f : \mathbb{R}^n \rightarrow \mathbb{R}$ and $c : \mathbb{R}^n \rightarrow \mathbb{R}^m$ are twice continuously differentiable functions, $X \subset \mathbb{R}^n$ is a bounded polyhedral set and $I \subseteq \{1, \dots, n\}$ is the index set of integer variables.

It should be highlighted that Equation E5.2 represents one of the possible formulations: indeed, as already discussed, the problem to be solved could be also a maximization problem (instead of a minimization one). In a similar way, different kind of constraints can be considered, such as equality constraints or lower and upper bounds $l \leq c(x) \leq u$.

The major advantage of the MINLP problems stands in the possibility of exactly solving the energy networks optimization problem, without the linearization simplification. However, at present this kind of formulation is not widely applied, mainly due to the very high computational time required when an extremely complex problem has to be solved. The main challenge, indeed, relates to the reduction in computational time when the design and annual systems scheduling

optimization problem is applied to smart grids with a high number of energy systems, users and constraints. The computational time depends on the problem complexity, in terms of time steps, number of users and energy production systems, as well as on the number of non-linear phenomena considered in the formulation. Considering a medium size energy network for electricity, thermal and cooling energy fulfillment with centralized and distributed production systems, several days can be necessary to run a simulation over a whole year of operation (hourly based time steps).

As an example, Elsidio et al. [10] proposes a MINLP model with a two-stage optimization algorithm developed for the purpose of determining the most profitable design of CHP units (in terms of minimum energy consumption and minimum total annual cost). The scenario includes a district heating network with heat storage and the optimal CHP units scheduling over the year is accounted. The upper level of the optimization consists in an evolutionary algorithm which allows to select and properly size the CHP units, while at the lower level the operational scheduling problem is linearized and optimized with a commercial MILP solver. Furthermore, a bounding technique is introduced in order to limit the computational time required to solve the lower-level problem. To this aspect the results of the test carried out in [10] seems to indicate that the continuous relaxation of the plant sizes significantly helps to improve the convergence rate of the tested evolutionary algorithm and to find improved solutions. However, the analyzed problem is limited in size and complexity, thus further efforts should be made for the application of MINLP models to the complex energy networks field.

References

- [1] Flores RJ, Shaffer BP, Brouwer J. Dynamic distributed generation dispatch strategy for lowering the cost of building energy. *Applied Energy*, 123 (2014) 196-208.
- [2] Picciariello A, Reneses J, Frias P, Söder L. Distributed generation and distribution pricing: Why do we need new tariff design methodologies?. *Electric Power Systems Research*, 119 (2015) 370-376.
- [5] Tan WS, Hassan MY, Majid MS, Rahman HA. Optimal distributed renewable generation planning: A review of different approaches. *Renewable and Sustainable Energy Reviews*, 18 (2013) 626-645.
- [6] Ul Haque A, Mandal P, Meng J, Pineda RL. Performance Evaluation of Different Optimization Algorithms for Power Demand Forecasting Applications in a Smart Grid Environment. *Procedia Computer Science*, 12 (2012) 320-325.
- [7] Wakui T, Kinoshita T, Yokoyama R. A mixed-integer linear programming approach for cogeneration based residential energy supply networks with power and heat interchanges. *Energy*, 68 (2014) 29-46.
- [8] Fazlollahi S, Becker G, Ashouri A, Maréchal F. Multi-objective, multi-period optimization of district energy systems: IV - A case study. *Energy*, 84 (2015) 365-381.
- [9] Bordin C, Gordini A, Vigo D. An optimization approach for district heating strategic network design. *European Journal of Operational Research*, 252 (2016) 296-307.
- [10] Elsidio C, Bischi A, Silva P, Martelli E. Two-stage MINLP algorithm for the optimal synthesis and design of networks of CHP units. *Energy*, 121 (2017) 403-426.
- [11] Reeves CR. Genetic algorithms for the operations researcher. *Inform Journal on Computing*, 9 (1997) 231-250.
- [12] Michalewicz Z. Genetic algorithms + data structure = evolution programs. *Springer* (1992).
- [13] Goldberg DE. Genetic algorithms. *Addison-Wesley*, (1989) Reading, MA.
- [14] Marshman DJ, Chmelyk T, Sidhu MS, Gopaluni RB, Dumont GA. Energy optimization in a pulp and paper mill cogeneration facility. *Applied Energy*, 87 (2010) 3514-3525.
- [15] Mitra S, Sun L, Grossmann IE. Optimal scheduling of industrial combined heat and power plants under time-sensitive electricity prices. *Energy*, 54 (2013) 194-211.
- [16] Carrión M, Arroyo JM. A computationally efficient mixed-integer linear formulation for the thermal unit commitment problem. *IEEE Transactions Power Systems*, 21 (2006) 1371-1378.
- [17] Nistor S, Wu J, Sooriyabandara M, Ekanayake J. Cost optimization of smart appliances. *IEEE PES international conference and exhibition on innovative smart grid technologies*, (2011) 1-5.

- [18] Rastegar M, Fotuhi-Firuzabad M, Zareipour H. Home energy management incorporating operational priority of appliances. *International Journal of Electrical Power and Energy Systems*, 74 (2016) 286-292.
- [19] Zhang D, Evangelisti S, Lettieri P, Papageorgiou LG. Economic and environmental scheduling of smart homes with microgrid: DER operation and electrical tasks. *Energy Conversion and Management*, 110 (2016) 113-124.
- [20] Nolde K, Morari M. Electrical load tracking scheduling of a steel plant. *Computers and Chemical Engineering*, 34 (2010) 1899-1903.
- [21] Mitra S, Grossmann IE, Pinto JM, Arora N. Optimal production planning under time sensitive electricity prices for continuous power-intensive processes. *Computers and Chemical Engineering*, 38 (2012) 171-184.
- [22] Hadera H, Harjunkski I, Sand G, Grossmann IE, Engell S. Optimization of steel production scheduling with complex time-sensitive electricity cost. *Computers and Chemical Engineering*, 76 (2015) 117-136.
- [23] Mohsenian-Rad A, León-García A. Optimal residential load control with price prediction in real-time electricity pricing environments. *IEEE Trans Smart Grid*, 1 (2010) 120-133.
- [24] Silvente J, Aguirre AM, Zamarripa MA, Méndez CA, Graells M, Espuña A. Improved time representation model for the simultaneous energy supply and demand management in microgrids. *Energy*, 87 (2015) 615-627.
- [25] Zhang D, Shah N, Papageorgiou LG. Efficient energy consumption and operation management in a smart building with microgrid. *Energy Conversion and Management*, 74 (2013) 209-222.
- [26] Wakui T, Kinoshita T, Yokoyama R. A mixed-integer linear programming approach for cogeneration-based residential energy supply networks with power and heat interchanges. *Energy*, 68 (2014) 29-46.
- [27] Belotti P, Kirches C, Leyffer S, Linderoth J, Luedtke J, Mahajan A. Mixed-Integer Nonlinear Optimization. *Cambridge University Press*, 22 (2013) 1-131.

6. Software EGO

In this chapter, the software EGO (Energy Grid Optimizer) – developed for the optimal scheduling definition within complex energy networks – will be presented. This calculation code is written in Visual Basic for Application (VBA) and it is based on genetic algorithms: for known energy demand and energy production systems, it allows the definition of the optimal load allocation with the purpose of minimizing the total costs of energy production, the heat dissipations and the electricity exchange with the national electric grid.

6.1 Calculation model

The realized software can simulate a complex energy grid as presented in Figure 6.1, consisting in (i) an arbitrary number of prime movers (PM) even in CHP (Combined Heat and Power) application, (ii) generators from renewable source (solar thermal panels – RGt – wind turbines and photovoltaic panels – RGe), (iii) energy storage devices for both electrical (EES) and thermal (TES) energy, (iv) thermal generators (auxiliary and biomass boilers – AB and BB – and heat pumps – HP) and (v) cooling machines (compression chillers – CC – and absorption chillers – AC). The previous generators are used to cover the electrical, thermal and cooling energy load requested by one or more users; the simulated grid can also be connected (if present) with the electric grid and with the gas distribution network.

The schematic flow chart of the realized software is presented in Figure 6.2; as it can be seen from the figure, the calculation core of the software consists of a *genetic algorithm* based on the minimization of an objective function which expresses the total cost of energy production.

In more details, the input section requires:

- electrical, thermal and cooling power required by the users. Furthermore, from Figure 6.1 it can be noted that it is also possible to define the gas demand (for direct use) for the users;
- the number, typology and main characteristics of:
 - prime movers (electrical and thermal design power output, efficiency, off-design behavior, etc.);
 - renewable source generators (peak power, performance, etc.);
 - heating and cooling systems (size, performance, off-design behavior, etc.);
 - electrical and thermal energy storage devices (maximum storable energy);
- the tariff scenario (purchased and sold electrical energy values, cost of the fuel, etc.);
- a series of parameters characteristic of the genetic algorithm (as better explained in the following of this paragraph).

As it regards the prime movers, the software is provided with a database of commercial models [1] including: Internal Combustion Engines (ICE), Organic Rankine Cycles (ORC), Micro Gas Turbines (MGT) and Gas Turbines (GT).

In Figure 6.3, the design electrical and thermal efficiencies of the about 300 prime movers collected in the software database are presented.

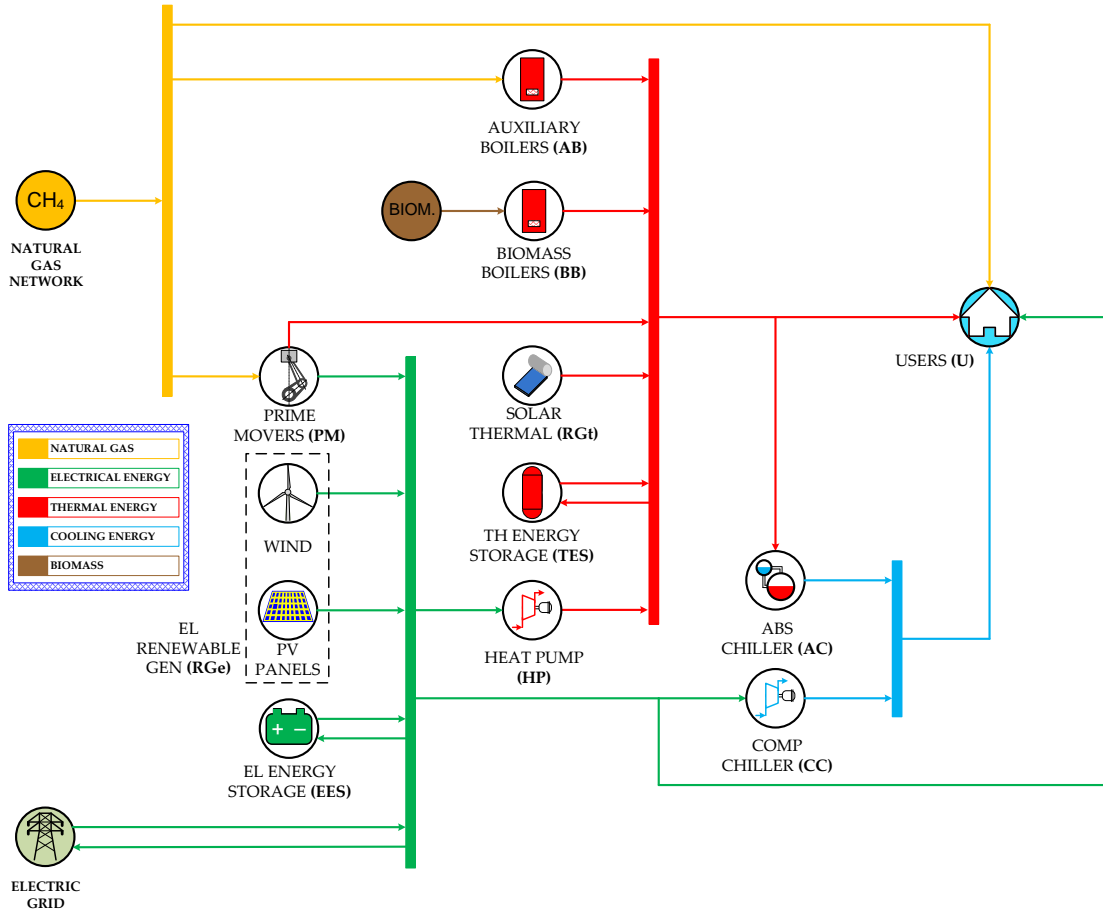


Figure 6.1 – EGO software calculation scheme.

The software's main output are the optimal load of each considered energy systems, in order to minimize the total cost of the energy supplied to the users, and the costs of energy production.

As it regards the calculation core, whit reference to Figure 6.1, the adopted genetic algorithm is based on the minimization of the following fitness function (FF):

$$FF = C_{\lambda} + C_M + C_E + C_F \quad E6.1$$

where C_{λ} represents the total cost of fuel, C_M the total maintenance cost of the energy systems, C_E the total cost of the electricity purchased from the national grid and C_F are the so-called fictitious costs.

In more detail, the total cost of fuel C_{λ} can be expressed as:

$$C_{\lambda} = \left[\sum_{i=1}^{n_{PM}} f_{\lambda,i}^{PM}(L_{PM,i}) + \sum_{i=1}^{n_{AB}} f_{\lambda,i}^{AB}(L_{AB,i}) \right] \cdot \lambda_{fuel} + \sum_{i=1}^{n_{BB}} f_{\lambda,i}^{BB}(L_{BB,i}) \cdot \lambda_{biomass} \quad E6.2$$

being λ_{fuel} the specific cost (€/kW) of the fuel introduced in prime movers and auxiliary boilers – usually natural gas – and $\lambda_{biomass}$ the biomass specific cost (€/kW), while $L_{PM,i}$, $L_{AB,i}$ and $L_{BB,i}$ are respectively the loads of the i^{th} prime mover, of the i^{th} auxiliary boiler and of the i^{th} biomass boiler. The functions $f_{\lambda,i}^{PM}$, $f_{\lambda,i}^{AB}$ and $f_{\lambda,i}^{BB}$ express the power introduced with fuel in the i^{th} prime

mover or auxiliary boiler or biomass boiler as function of the systems load ($L_{PM,i}$ or $L_{AB,i}$ or $L_{BB,i}$).

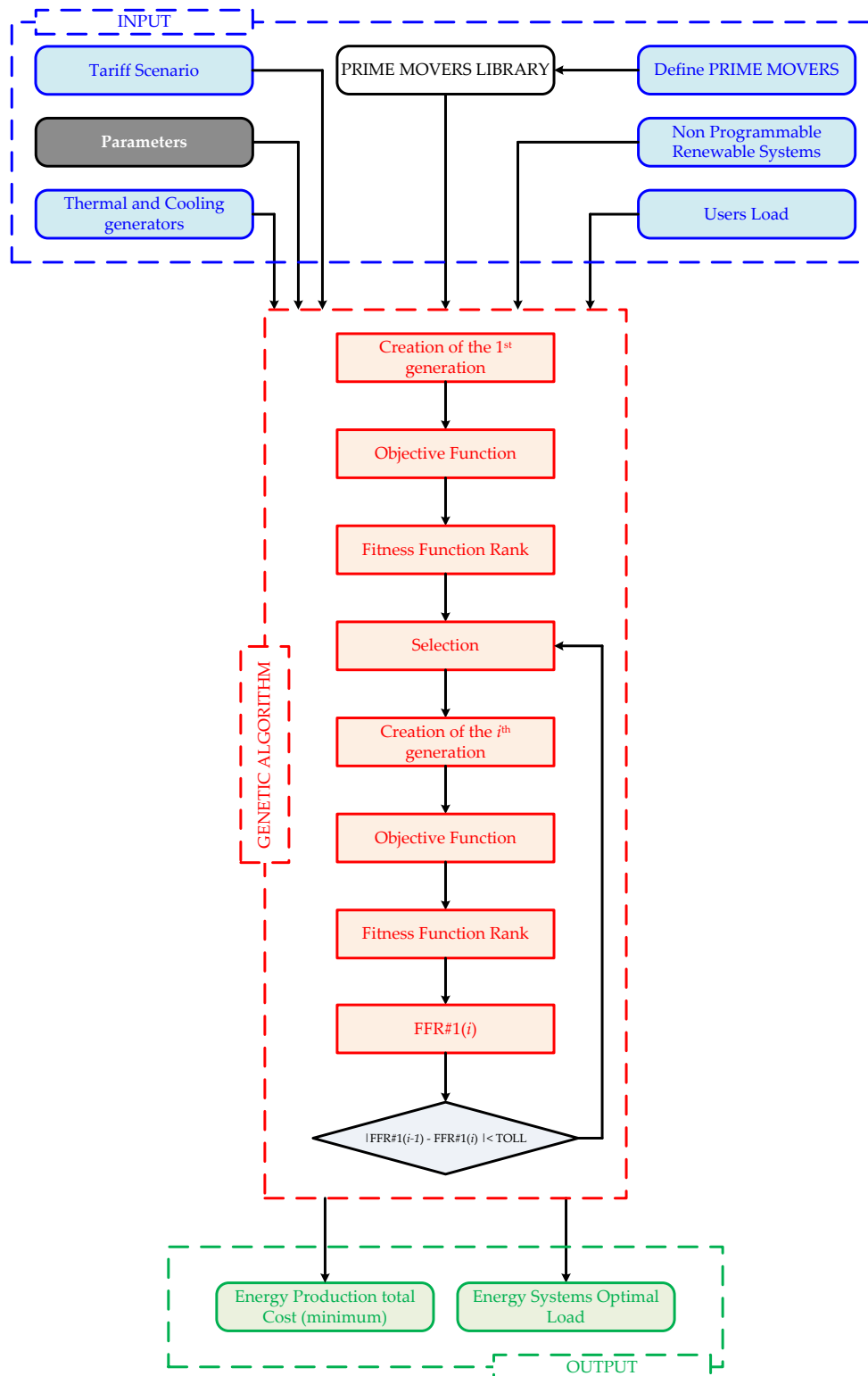


Figure 6.2 – EGO software calculation main flow chart.

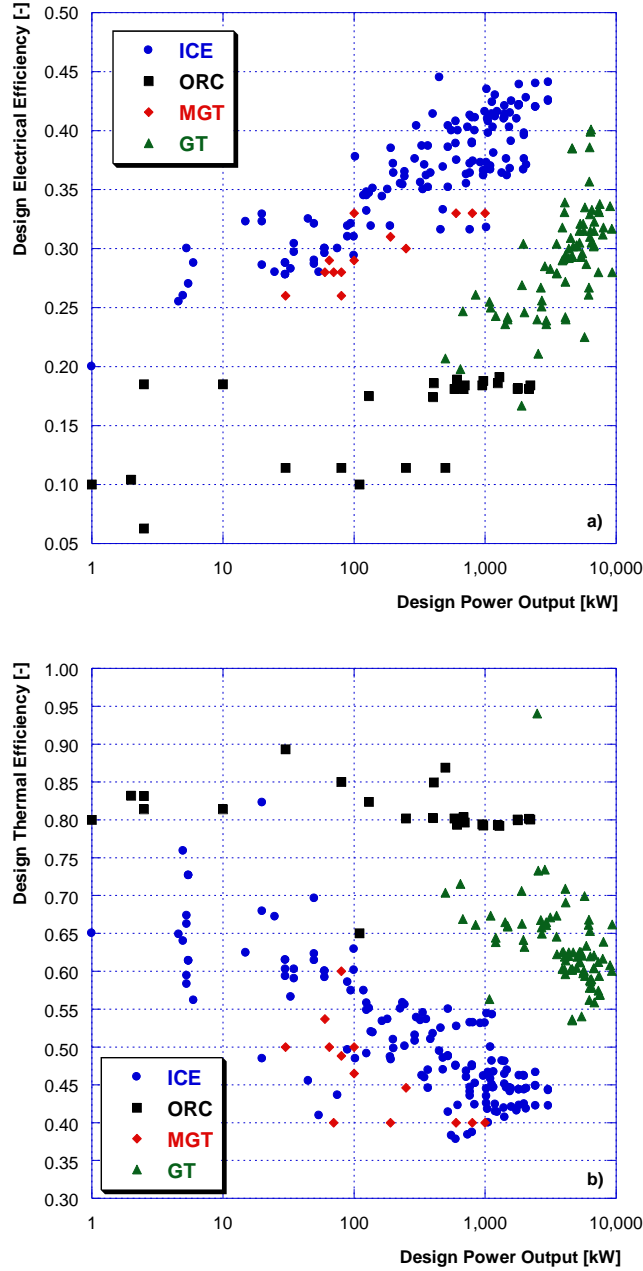


Figure 6.3 – EGO software prime movers database: electrical (a) and thermal (b) design efficiency as function of nominal electrical power output [1].

C_M expresses the maintenance cost of all the energy systems in the smart grid. This cost is accounted as function of the produced power – electrical (EL), thermal (TH) or cooling (FR) – of each system by using maintenance cost specific values (μ_i expressed in €/kW):

$$C_M = \sum_{i=1}^{n_{PM}+n_{RGe}} P_{EL,i} \cdot \mu_{EL,i} + \sum_{i=1}^{n_{RGt}+n_{AB}+n_{BB}+n_{HP}} P_{TH,i} \cdot \mu_{TH,i} + \sum_{i=1}^{n_{CC}+n_{AC}} P_{FR,i} \cdot \mu_{FR,i} \quad E6.3$$

where P_i is function of the load of each system $P_i = f(L_i)$.

C_E is the total cost of the electricity purchased from the network and can be estimated as:

$$C_E = P_{EL,P} \cdot \xi_{EL,P} \quad E6.4$$

being $\xi_{EL,P}$ the specific cost of purchased electricity (€/kW) and $P_{EL,P}$ the total electric power from the distribution network to the users. It can be seen that $P_{EL,P}$, if greater than zero, can be expressed as:

$$P_{EL,P} = \sum_{i=1}^{n_U} P_{EL,i}^U + \sum_{i=1}^{n_{CC}} \frac{P_{FR,i}^{CC}}{f_{EER,i}^{CC}(L_{CC,i})} + \sum_{i=1}^{n_{HP}} \frac{P_{TH,i}^{HP}}{f_{COP,i}^{HP}(L_{HP,i})} - \sum_{i=1}^{n_{RGe}} f_{EL,i}^{RGe}(L_{RGe,i}) - \sum_{i=1}^{n_{PM}} f_{EL,i}^{PM}(L_{PM,i}) - \sum_{i=1}^{n_{ES}} P_{EL,i}^{ES} \quad E6.5$$

which represents the sum of the electrical power required from (i) the users (U), (ii) the compressor chillers (CC) and (iii) the heat pumps (HP) minus the production (iv) of the renewable source generators (RG), (v) of the prime movers and minus (vi) the power recovered from electrical storage devices (ES). The terms $f_{COP,i}^{HP}$ and $f_{COP,i}^{HP}$ represent two functions which estimate respectively the cooling machines energy efficiency ratio (EER) and the heat pumps coefficient of performance (COP) as function of the systems loads ($L_{CC,i}$ and $L_{HP,i}$); furthermore, the function $f_{EL,i}^{PM}$ calculates the produced power of the i^{th} prime mover for a given load ($L_{PM,i}$).

Finally, C_F represents a term which forces the regulation strategy of the whole smart grid. In fact, the realized software allows to optimize the load distribution considering a (i) thermal priority or a (ii) electrical priority. In case of regulation with thermal priority, in order to minimize the environmental impact of the prime movers, a fictitious cost has been introduced to take into account the dissipation of thermal energy available from the prime movers and not used for the users. This cost is accounted as a multiple (p_T) of the corresponding fuel cost used in a conventional boiler to produce the same amount of dispersed heat. In case of multiple auxiliary boilers, the corresponding assumed conversion efficiency is the average value, $\eta_{AB,av}$. With this regulation strategy, if more electricity is generated compared to users' needs and storage availability, surplus can be sold to the network. The sale of electricity to the network is accounted as a reduction of the costs of electricity production considering a specific value $\xi_{EL,S}$ (€/kW). It follows that the term C_F can be expressed as:

$$C_F = \sum_{i=1}^{n_{PM}} \frac{Q_{disp,i}}{\eta_{AB,av}} \cdot \lambda_{fuel} \cdot p_T - P_{EL,S} \cdot \xi_{EL,S} \quad E6.6$$

Conversely, the regulation strategy with electrical priority discourages the sale of electricity to the grid by considering, opposite to the previous case, this option as a cost. Similarly, in this case, a multiplication factor (p_E) has been applied, while the dispersion of heat from the prime movers to the environment is not considered as a cost. Therefore, the term C_F becomes:

$$C_F = P_{EL,S} \cdot \xi_{EL,S} \cdot p_E \quad E6.7$$

This strategy can be adopted, as an example, in case of a smart grid not connected to the network or if the national grid is not suitable to accommodate energy.

With the aim to minimize the fitness function FF , the developed genetic algorithm creates and/or evolves a population of candidate solutions, in which the chromosomes of each individual are represented by the loads (L_i) of the systems installed within the grid. The values of L_i allow the estimation of the FF according to the previous equations.

As usual for a genetic algorithm, the evolution of the population starts from a first generation randomly generated.

The population size (p_S) is estimated as function of the total number of the systems (n_{tot}) included in the smart grid, according to this relation:

$$p_S = P_{FM} \cdot (L_{UP} - L_{LO}) \cdot n_{tot} \quad E6.8$$

where L_{UP} and L_{LO} are the upper and lower limits of the variation range of the terms L_i and P_{FM} is a multiplicative parameter (an integer number greater than 1). In more detail, P_{FM} is a tuning parameter which influences the convergence velocity of the algorithm: low values of P_{FM} mean few individuals for each generation, thus the convergence of the algorithm can require a large number of iterations. On the other hand, high number of individuals reduces the number of required iterations but increases the time necessary for each iteration.

After the creation of the first generation, the FF is estimated for each individual and a FF rank is created (see Figure 6.4). The individuals with lower values of FF (*i.e.* lower values of energy production cost) are recognized as high rank solutions, while the ones with higher values of FF become low rank solutions. A set percentage of the lower rank solutions is automatically eliminated from the generation. The remaining percentage of possible solutions is instead used to generate the individuals of the next generation. The developed algorithm adopts the crossover method (also known as recombination method) without mutation, in order to generate two new individuals from two parent individuals. The selection of the parent individuals is realized with a *roulette method*. This method guarantees that individuals with higher rank have higher probability (under the statistical point of view) of generating a new individual. With the exception of the first generation, the highest rank solution $FFR\#1(i)$ of each generation is compared with the corresponding of the previous generation, $FFR\#1(i - 1)$: the procedure ends when the absolute value of the difference between these two quantities is lower than a given tolerance value (TOL):

$$|FFR\#1(i) - FFR\#1(i - 1)| < TOL \quad E6.9$$

6.2 Software test versus alternative approach

The optimization method introduced in this Chapter, based on the genetic algorithm technique, has been tested, under simplified conditions, by comparing it with a conventional and widely used method, generally called as “equal incremental cost” criterion. The equal incremental cost (also known as marginal cost) criterion, is a deterministic approach used in the power generation sector to identify the economically “optimum” power generation mix, when a pool of power units is available to cover a given electric power demand profile.

This reference criterion is based on an economic assessment and on a comparison between the specific generation costs for all the available power units, as detailed below.

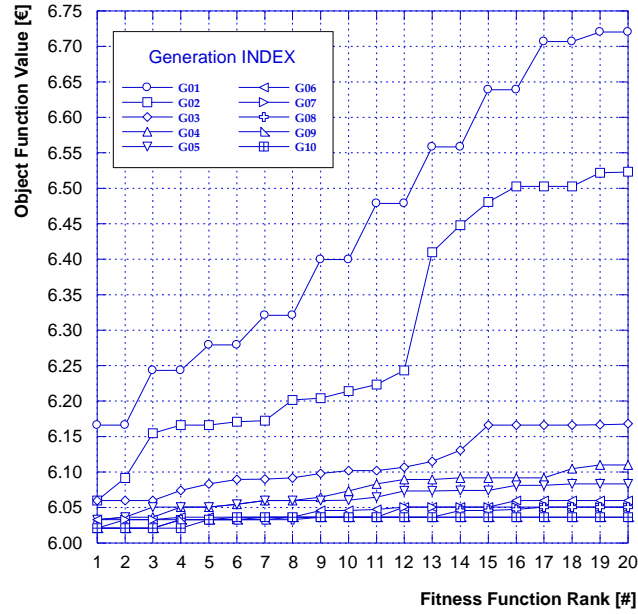


Figure 6.4 – Evolution of possible solutions for the EGO software.

The total generation cost, in a given operation time period (*e.g.* one year), for each prime mover – named here for simplicity as CT – is expressed, in general, as sum of fixed (CF) and variable (CV) costs, according to:

$$CT = CF + CV \quad \text{E6.10}$$

The CF term depends on the technology, on the size and on other characteristics of the unit, but it is not directly related with the unit operation and with the actual number of operating hours. On the other side, the CV term depends on the actual operation and it is the sum of variable costs contributions (CV_i) in each j -th time step of the plant operating period (hour, minute or else). As a consequence, the CV_i quantity is a function of the fuel cost per unit of fuel power input (λ_{fuel}), of the actual power output (P_j) and of the prime mover actual electric efficiency (η_j):

$$CV = \sum_j^N CV_j = \sum_j^N \frac{\lambda_{fuel}}{\eta_j} P_j \quad \text{E6.11}$$

where N is the number of time steps of the total operating period.

Thus, for a given j -th operating time interval or power output value, the incremental cost per unit of power output, IC_j , can be introduced, defined as:

$$IC_j = \frac{dCT_j}{dP_j} = \frac{dCV_j}{dP_j} = \lambda_{fuel} \left(\frac{1}{\eta_j} + \frac{d}{dP_j} \left(\frac{1}{\eta_j} \right) \cdot P_j \right) \quad \text{E6.12}$$

where CT_j is the total cost over the N steps and the CF term can be considered equally divided over the N steps and it does not depend on P_j .

The IC_j quantity expresses, for a given plant, the specific instantaneous cost per unit of produced power and it basically depends on (i) the efficiency trend versus power and (ii) on the fuel cost (assumed as constant for sake of simplicity).

The incremental cost profile versus the power output, $IC = IC(P)$, can be calculated for each prime mover once the trend of the efficiency versus the load is known. Thus, a comparison among the prime movers in terms of IC trend can be made.

For each power demand value in each j-th time step, the power unit with lower CT_j value is the more convenient power plant and, therefore, it can operate with priority in that time step. Moreover, the equal incremental cost criterion indicates that, if multiple units are in operation to fulfill a given power demand, the optimum condition in terms of power setpoint of each one is the case in which they are operated with load output corresponding to equal incremental cost.

In order to validate the developed software versus the “equal incremental cost” criterion a given simplified scenario has been considered. In this scenario two prime movers (PM#1 and PM#2) have been taken into account with the performance at design condition reported in Table 6.1.

The PM#1 and PM#2 incremental cost functions versus the power output are plotted in Figure 6.5. It can be seen that in this considered case the PM#2 electric efficiency and economic performance are preferable over its entire power range.

Table 6.1 – Prime movers design performance.

System	$P_{EL,DES}$ [kW]	$Q_{TH,DES}$ [kW]	$\eta_{EL,DES}$ [-]	$\eta_{TH,DES}$ [-]
PM#1	10.00	44.00	0.1850	0.8140
PM#2	15.00	29.00	0.3230	0.6245

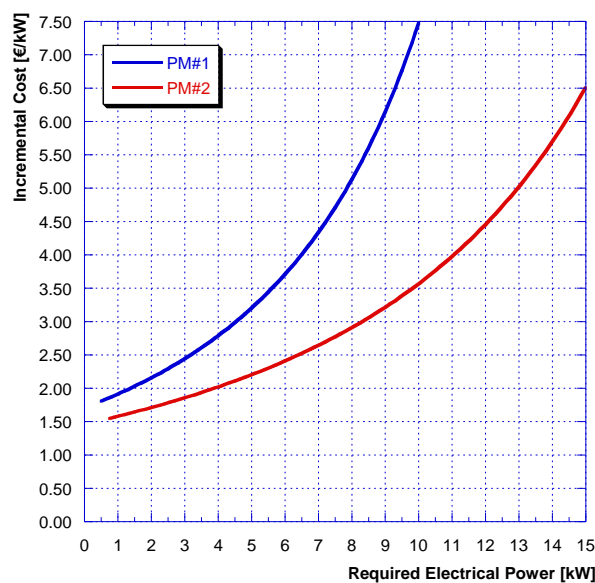


Figure 6.5 – Incremental cost trend as function of the power for the two considered prime movers.

The optimization method based on genetic algorithm has been applied to obtain the optimal PM#1 and PM#2 output loads versus the required electrical power (Figure 6.6, where GA results are indicated by blue dots for PM#1 and red dots for PM#2). This trend has been compared with the “equal incremental cost” criterion results (continuous lines, indicated as EICC in figure). A very good matching between the results of the two methods is obtained for both PMs. In particular, the obtained results show that PM#2 is the only operating prime mover for a demand power lower than the PM#2 design power (15 MW), while PM#1 is switched off. In case of a total required power higher than 15 MW, also PM#1 is activated and contextually the actual power of PM#2 is reduced. This result is confirmed by both the GA and EICC. In more details, the total incremental cost of the PM#1 and PM#2 assembly is shown in Figure 6.7 (with full agreement between GA and EICC), where a monotonic rising trend is obviously obtained and the slope changes at a load equal to the PM#2 design power 15 MW.

Thus, the results show that the GA method indicates to operate the PMs with variable incremental costs, depending on the load demand; moreover, there is a given load range, (between PM#2 design power and the sum of PM#1 and PM#2 design power), in which the optimal power of PM#1 and PM#2 is decided by the GA and in full agreement with the EICC method.

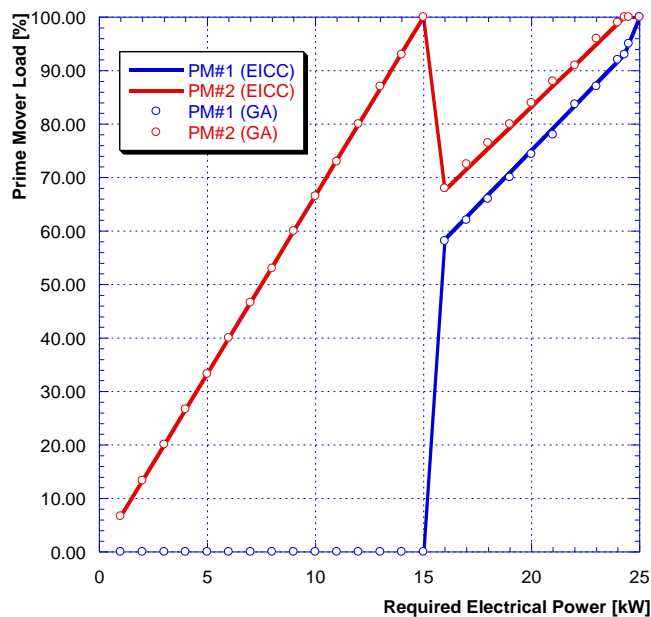


Figure 6.6 – Optimal PMs power output trend versus required electrical power.

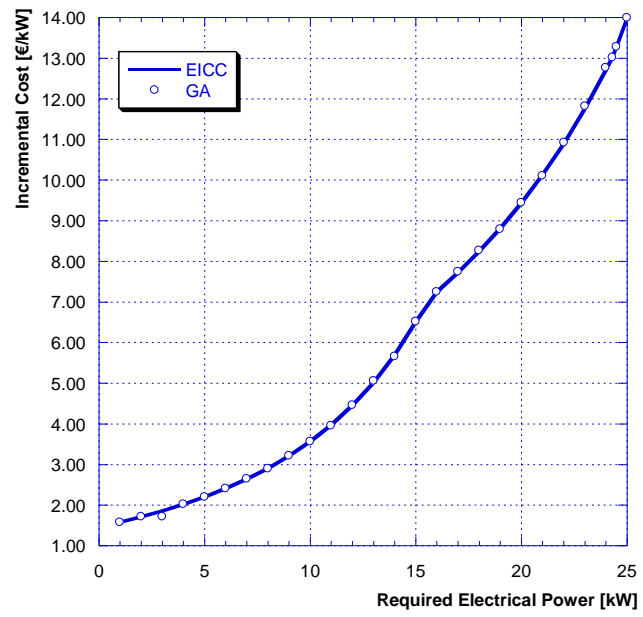


Figure 6.7 – Total incremental cost versus required electrical power.

References

- [1] Bianchi M, Spina PR, Tomassetti G, Forni D, Ferrero E. Le tecnologie innovative ed efficienti nei sistemi di generazione in assetto co-trigenerativo e nei sistemi integrati con unità a pompa di calore nelle applicazioni industriali e del terziario. Report RSE/2009/18.

7. Optimization analysis – case study I

The first presented case study relates to the study of an existing district heating network. As better explained in the following paragraphs, the current set-up of this network consists of a centralized production plant which guarantee – at present – the fulfillment of the connected users' thermal needs. No electricity nor cooling energy are supplied by the centralized station.

For this reason, the carried out analysis has been divided into two phases, both with the general aim to optimize the energy production (eventually by adding different energy systems to the current ones). In the first phase of the study, the current mode of operation of the network has been maintained. In other words, only the thermal needs are considered to be supplied by the centralized plant, while each user by itself purchases electricity from the national electric grid for electrical needs and, eventually, to produce cooling energy. On the other hand, the second phase is characterized by a modification in the mode of operation of the network: in this case it is supposed that thermal, electrical and cooling needs are fulfilled by the centralized power station. Deeper explanations will be given in the following of this chapter.

7.1 DHN current set-up

The considered district heating network is located in the Northern part of Italy, in the city of Bologna. It is a small-medium network and it supplies a group of 17 users in a neighborhood called Corticella, including 13 residential users, 2 schools, 1 day-hospital structure and 1 supermarket. A panoramic view of the area served by the DHN is presented in Figure 7.1.

The Corticella network is supplied by a thermal power station consisting of an Internal Combustion Engine (ICE), operating as Combined Heat and Power (CHP) unit, and four auxiliary boilers. Relating to the electric production of the CHP unit, it is used to move the pumping station of the plant and – when exceeding the pumps need – it is sold to the national electric grid. The current configuration of the thermal power station is shown in Figure 7.2, while the technical data of the before-mentioned installed generation systems are presented in Table 7.1.

The produced hot water is supplied to the network at 10 bar and $80^{\circ}\text{C}\div 90^{\circ}\text{C}$, while the pressure drop across all the network's path (feed line plus return line) is about 6 bar.

As aforementioned the considered DHN – presented in Figure 7.3 – supplies 17 thermal users, composed of 13 residential consumers (for a total of 960 housing units) and four tertiary users (two schools, 1 day-hospital building and 1 super-market). The correspondence between identification number and typology of user is listed in Table 7.2. Furthermore, the network's length is about 4 km, considering both the feed and the return paths. All the connected users are served by the DHN for both space heating and hot water needs, excepting for the super-market where only space heating is needed.



Figure 7.1 – Area of interest for the analyzed district heating network [1].

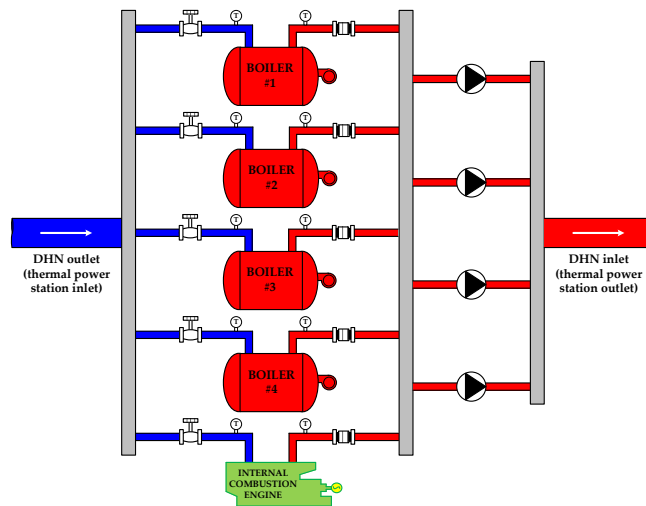


Figure 7.2 – Current configuration of the considered thermal power station.

Table 7.1 – Generation systems main parameters.

Internal Combustion Engine (CHP Unit)	
Model	Jenbacher JMS 420
Fuel type	Natural gas
Design Electric Power	1415 kW
Design Thermal Power	1492 kW
Design Electric Efficiency	41.9%
Design Thermal Efficiency	44.2%

Auxiliary Boilers (each one)	
Design Thermal Power	2900 kW
Design Thermal Efficiency	80%

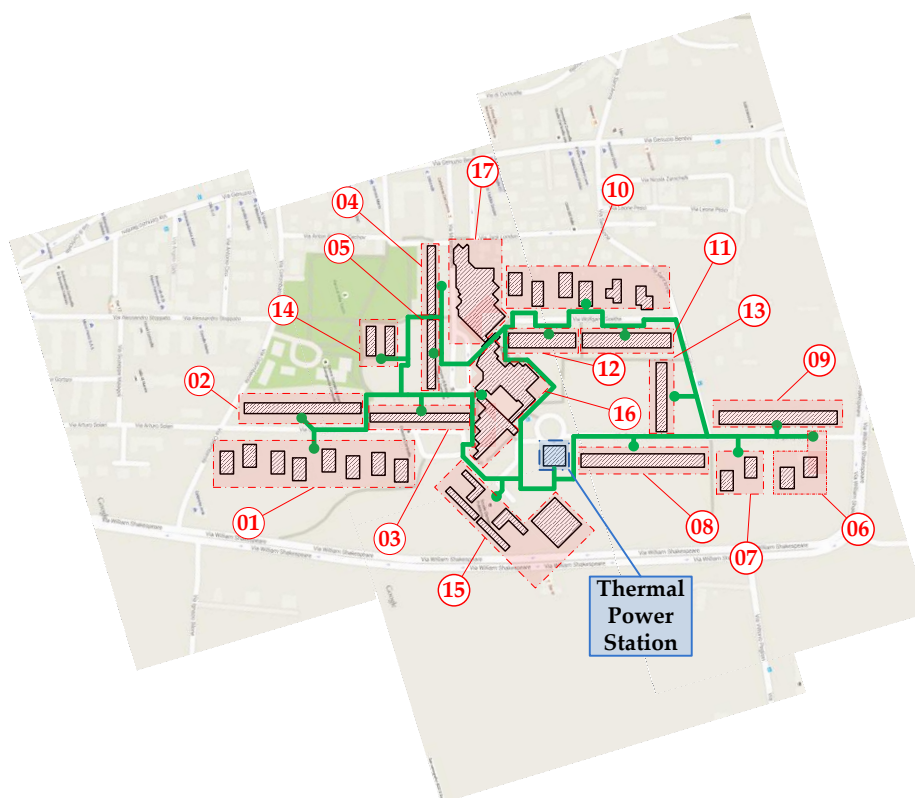


Figure 7.3 – Schematic of the district heating network.

7.2 Phase I: thermal needs fulfillment

In this first part of the analysis, only users thermal needs have been accounted. The aim of the study was the optimization of the energy production considering a whole year of operation. With this purpose, after the determination of the yearly profile of thermal energy to be produced by the thermal power station, different new configurations – in terms of installed energy production

systems – have been proposed and compared to the current plant configuration. It should be pointed out that the analysis involves only the possibility to add further generation systems to the current set-up. As a consequence, the ICE and the four auxiliary boilers have been maintained for each of the proposed new configurations.

7.2.1 Thermal needs profile definition

Based on the measured experimental data (*i.e.* for each utility substation: temperatures, mass flow rates, pressures,...), the peaks of thermal need for each user have been evaluated separately for space heating and hot water, as presented respectively in Figure 7.4 and in Figure 7.5. The values of the peak thermal needs had then enabled to determine, for each user, the daily hourly profile of thermal need for space heating and hot water by applying non-dimensional curves available in literature [2]. Obviously, as suggested in [2], different profiles have been considered depending on the considered typology of user as well as on the thermal need typology, as presented in Appendix A.

In particular, two representative days have been considered and set for the further optimization analysis: one winter typical day (space heating and hot water needs) and one summer typical day (only hot water is needed). Then, considering for the utility substations a thermal exchange effectiveness equal to the 99% and for the secondary distribution circuit an efficiency around the 95% (values evaluated through the in-house developed software IHENA), for a typical winter day and for a typical summer day, the real needs which the DHN has to guarantee have been determined. Thus, as imposed by the Italian framework [3] for the considered location, 183 days a year have been modeled with the winter typical day (both space heating and hot water are considered) and 182 days with the summer typical one. With these assumptions the hourly thermal need profiles in a whole year have been determined, for space heating and hot water separately and for each user.

Consequently, the network behavior has been analyzed by applying the software IHENA, enabling to obtain the thermal power to be produced by the centralized plant, the required electric power for the pumping station and the thermal dissipations through the network.

Once evaluated the hourly thermal power profile to be produced, the operation mode of the centralized station has to be set. With this purpose the software EGO has been applied in order to determine the optimal operation of the generation systems. Thus, the energy fluxes of the plant and the fuel costs for the whole year have been evaluated.

It must be highlighted that this solution, from here called as Reference Case, is already an optimized solution – in terms of operational management – for the existing network, due to the application of EGO. However, the change in the production plant configuration represents an interesting issue for the further optimization of the CHP-DHN operation and for the minimization of both the auxiliary boilers use and the operational costs.

Table 7.2 – Users identification numbers and associated typology.

ID	Typology
From #1 to #13	Residential User
#14	Infant School
#15	Primary School
#16	Day-Hospital
#17	Supermarket

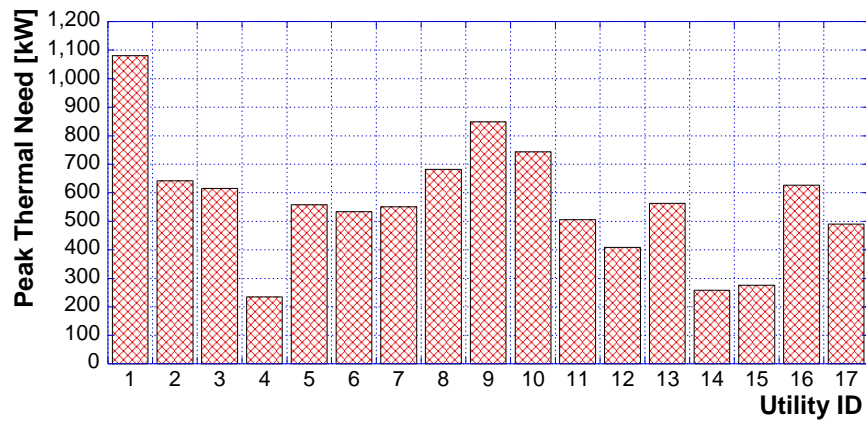


Figure 7.4 – Space heating peak needs for each user.

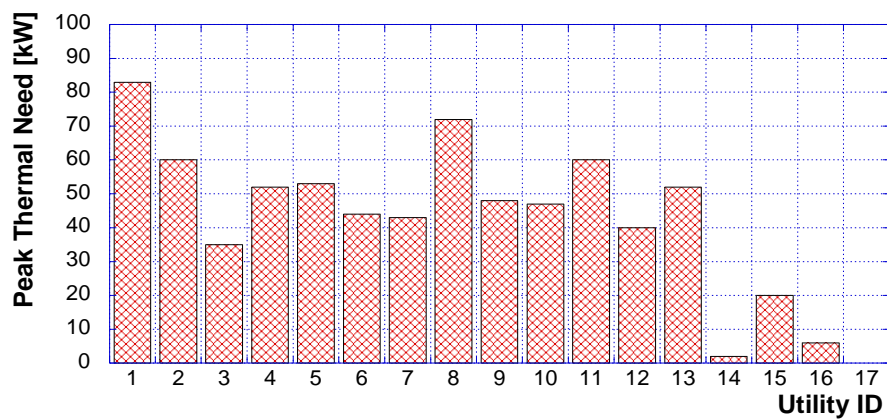


Figure 7.5 – Hot water peak needs for each user.

7.2.2 Case studies: characteristics and assumptions

With the aim to analyze the possibility of adding different electric and/or thermal generation systems and optimizing the management of the network, various scenarios in terms of considered production systems have been considered:

1. Case 1: in addition to the generation systems currently installed, this case considers the installation at the thermal power station of solar thermal panels and of a thermal energy storage system (Figure 7.6a);
2. Case 2: this scenario – in addition to the CHP units and the auxiliary boilers – considers the installation of photovoltaic (PV) panels feeding a heat pump (HP), both the systems installed at the thermal power station. The electric power input of the heat pump can be given by the PV panels (firstly) and by the CHP unit (as second option), while there is no connection between the national electric grid and the HP (Figure 7.6b);
3. Case 3: in the third proposed configuration the photovoltaic panels are installed, along with heat pumps, directly at the utility substations (Figure 7.6c). It must be highlighted that the installation of PV panels and HPs involves not the totality of the users but only a fraction of them. The choice of the involved users is part of the analysis and it has been made with the purpose of unloading the centralized thermal power station, in particular by closing one of the two rings of the network. Moreover, the avoidance of the produced heat dispersion and the minimization of the electric energy introduction into the grid have been maintained for the choice. After this preliminary investigation, the right ring of the network has been selected for the further analysis, *i.e.* the involved users are those with ID #6, #11, #13, #14, #16, #20, #25 and #29.

In order to give an immediate comprehension of the proposed configurations, all the analyzed cases are summarized in Table 7.3.

Table 7.3 – Summary of the analyzed configurations – Phase I.

	Ref. Case	Case 1	Case 2	Case 3
ICE	•	•	•	•
Aux. Boilers	•	•	•	•
Thermal Solar Panels		•		
Thermal Energy Storage		•		
PV Panels (centralized)			•	
PV Panels (distributed)				•
HP (centralized)			•	
HP (distributed)				•

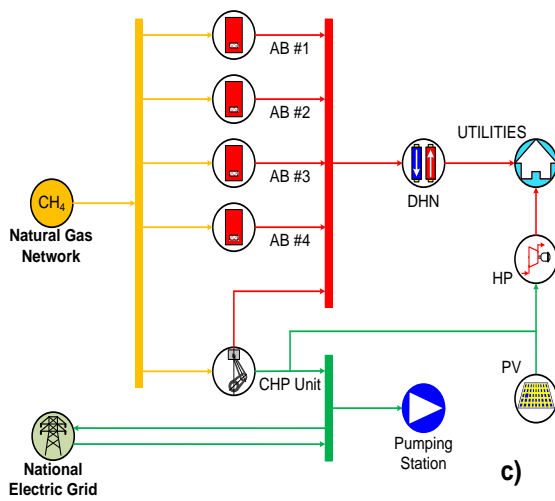
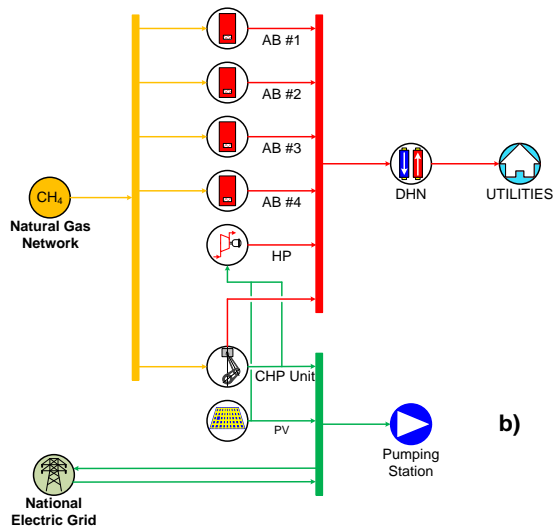
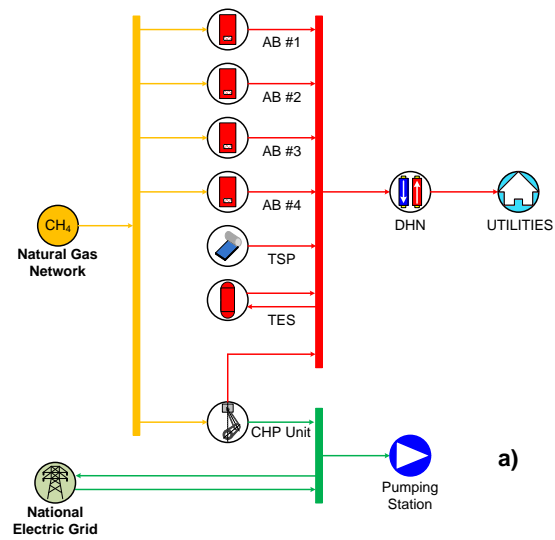


Figure 7.6 – Case studies configurations: a) Case 1; b) Case 2; c) Case 3.

The proposed cases have been simulated with the software EGO in order to evaluate the optimal yearly operational set-up. As well as for the Reference Case, the constraint of completely avoiding thermal energy dissipation has been imposed for the operation of the CHP unit.

All the simulations have been carried out considering for the users the same thermal needs of the Reference Case. This assumption entails that the hourly profile of the centralized thermal power station production remains the same of the Reference Case, excepting for Case 3. In the last proposed configuration, indeed, the solar PV panels and the heat pumps are placed at the final users (*i.e.* distributed generation systems are considered). Thus, in this case the users need is partially covered by the thermal energy produced directly at the users themselves, avoiding a part of the thermal dissipations through the DHN.

Moreover, further considerations can be made about the introduction of renewable energy generation systems (thermal or PV panels) as well as of the heat pumps and the thermal storage system. The main characteristics of the introduced systems – listed in Table 7.4 – have been defined as follows:

- Thermal Solar Panels (TSP) – Case 1: the size of the TSP has been set considering the real available surface at the thermal power station. The tilt and the azimuth angles have been chosen on the basis of the optimum for the considered city (latitude $44^{\circ}30'27''00$ N, longitude $11^{\circ}21'5''04$ E).
- Thermal Energy Storage (TES) – Case 1: the volume of the thermal storage tank has been defined as the minimum volume to obtain at the end of the day the complete restitution of the stored energy (*i.e.* every 24 hour the same conditions can be registered for the tank). This minimum value has been individuated by applying the software EGO with a trial and error procedure.
- Centralized PV panels – Case 2: similarly to the considerations made for the TSP, the available surface at the thermal power station has been considered to choose the PV size. The produced electric energy is used (*i*) for the centralized heat pump, (*ii*) for the pumping station and (*iii*) only the possible surplus is sold to the national electric grid.
- Centralized Heat Pump – Case 2: the Coefficient Of Performance (COP) has been chosen on the basis of the available literature [4] considering a large-scale Heat Pump (HP). The size of the HP, for this case, has been determined with the aim to completely recover the ICE available heat and contemporarily operate the HP with the electric energy produced by PV panels and ICE, in order to minimize the electric energy exchange with the grid. Thus, the size of the centralized heat pump becomes a result of the optimization analysis.
- Distributed PV panels – Case 3: as previously explained, the first step of the analysis related to Case 3 involved the choice of the users to be considered for the distributed generation. Once determined the involved substations (right ring of the DHN, users with ID #6, #11, #13, #14, #16, #20, #25 and #29), the surface of PV panels has been set on the basis of the roof available surfaces faced to South.
- Distributed Heat Pumps – Case 3: in this case, the distributed HPs are supplied by (*i*) the PV panels production and (*ii*) the ICE generated electric energy. Obviously, HPs are present only at the users where also distributed PV panels are installed. The considered COP, as it can be seen in Table 7.4, is lower than the one for Case 2, due to the lower HP sizes [4], which are defined on the basis of each user need.

The off-design of the ICE has been modeled as described in [5], while for other components efficiency parameters have been kept constant also in off-design operation. Finally, the model for the thermal storage tank can be found in [6].

Table 7.4 – Main systems parameters considered in the proposed variation scenarios – Phase I.

Thermal Solar Panels	
Typology	plate
S	300 m ²
η	80%
Peak Power	240 kW _P
Tilt Angle	30°
Facing	South

Thermal Storage Tank	
V	1 m ³
T_{min}	70 °C
T_{max}	130 °C
T_i	70 °C

Solar PV Panels	
S	300 m ²
η	10%
Peak Power	30 kW _P
Tilt Angle	30°
Facing	South

Centralized Heat Pump	
COP	4

Distributed PV Panels	
η	10%
Peak Power (total)	350 kW _P
Tilt Angle	30°
Facing	South

Distributed Heat Pumps	
COP	3

As it regards the production obtainable from the solar panels – for both thermal and PV panels – it has been evaluated starting from the measured data of solar irradiation profile on a horizontal surface [7] in the city of Bologna. The solar radiation etching on a surface with a tilt angle equal to 30° [8] and south-facing has been calculated, extracting the yearly solar irradiation profile to be applied for the analyzed cases. In Figure 7.7, the obtained profiles for a typical winter day (*i.e.*

January) and for a typical summer day (*i.e.* July) are shown. Different conversion efficiencies have been then considered (as it can be seen in Table 7.4) for the evaluation of the thermal solar production and for the PV case.

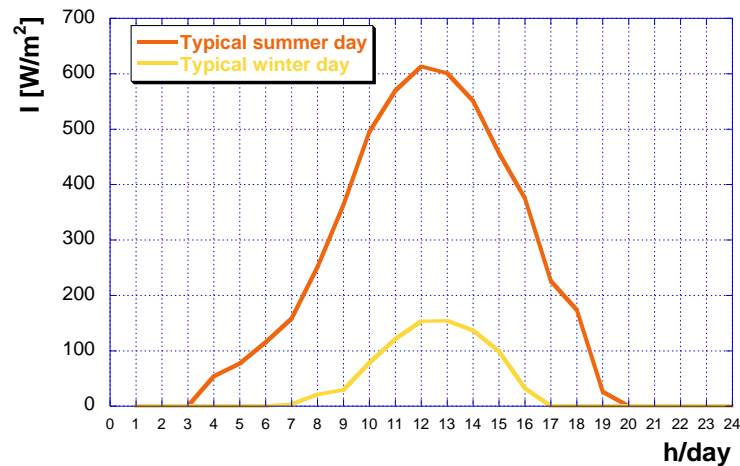


Figure 7.7 – Incident solar irradiation on a south-facing solar panel with a tilt angle equal to 30°, for a typical summer day (orange line) and for a typical winter day (yellow line) – Bologna case.

7.2.3 Results and discussion

The application of the software EGO led to the definition of the optimal energy systems scheduling for each considered case. Thus, from Figure 7.8 to Figure 7.11 the hourly profiles – for typical winter and summer days separately – of the thermal power production in the considered scenarios are shown, along with the production mix. In more detail, in the presented figures the centralized thermal production (by means of various generation systems, based on the considered case study) and the distributed thermal generation have been distinguished. All the plotted curves show the same qualitative trend with two peaks of thermal production (at 9 a.m. and 8 p.m. respectively), but different quantitative behavior can be observed.

As it can be clearly seen, indeed, the introduction of distributed generation systems (Case 3) allows to considerably unload the centralized thermal power station, both in winter (see Figure 7.11-a) and in summer seasons (see Figure 7.11-b). The remaining amount of thermal energy for the fulfillment of the users' need is guaranteed by the distributed heat pumps (Figures 7.11-c and 7.11-d, for winter and summer days respectively). On the other hand, relating to Reference Case, Case 1 and Case 2, the same trend of production can be seen at the thermal power station (see Figures from 7.8 to 7.10). However, as already discussed, this production is guaranteed by a different mix of production systems, that is a result of the optimization analysis depending on the considered case.

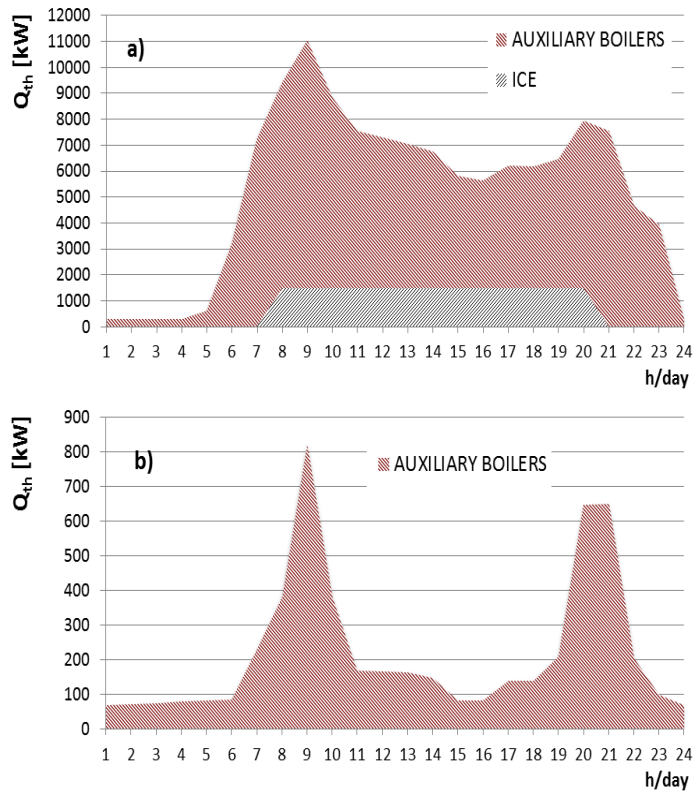


Figure 7.8 – Thermal production profiles (thermal power station) along with the production systems mix for the Reference Case: a) typical winter day, b) typical summer day.

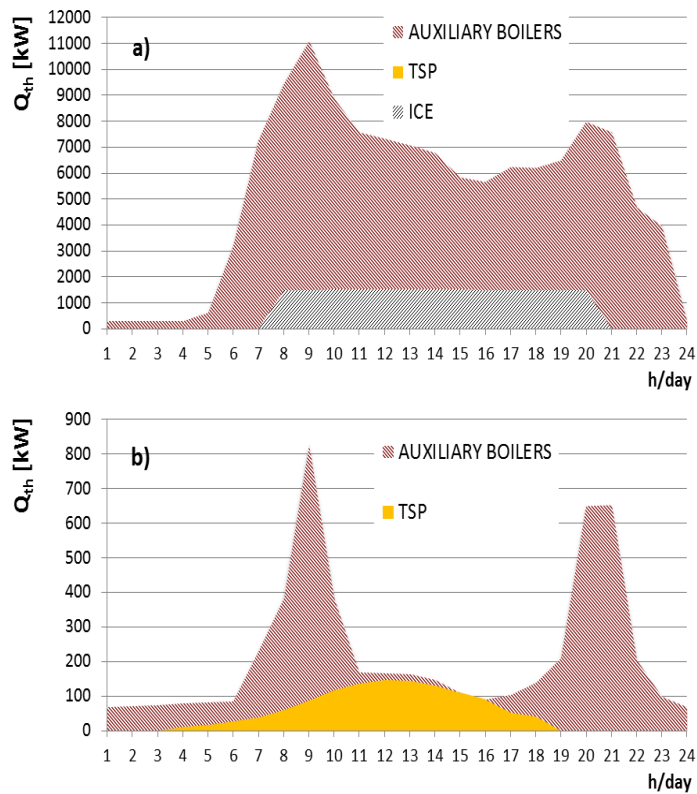


Figure 7.9 – Thermal production profiles (thermal power station) along with the production systems mix for the Case 1: a) typical winter day, b) typical summer day.

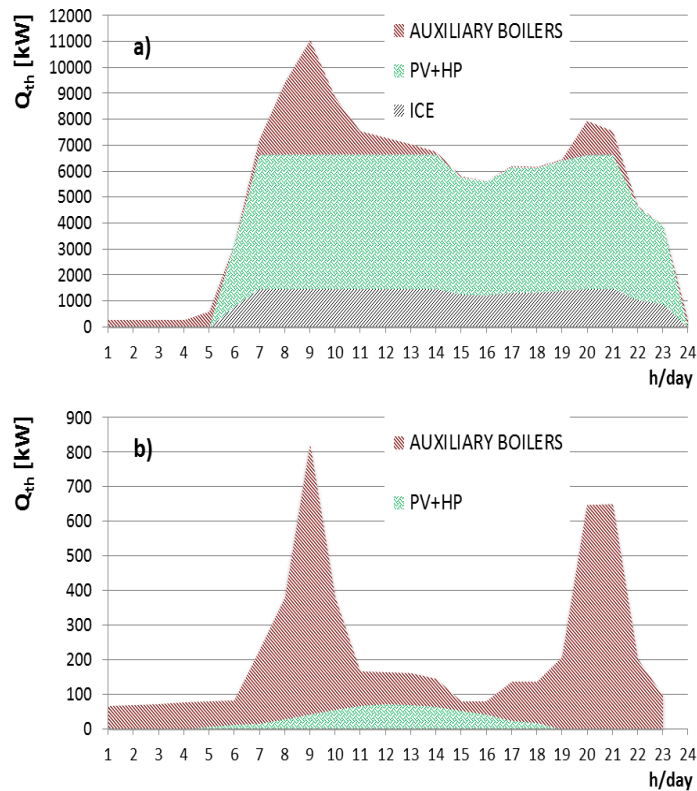


Figure 7.10 – Thermal production profiles (thermal power station) along with the production systems mix for the Case 2: a) typical winter day, b) typical summer day.

Focusing on the CHP unit, the optimization made with the software EGO allowed to set its optimal operation profile. In Figure 7.12 the results for all the analyzed cases during the typical winter day are presented. Relating to the summertime, instead, the optimal solution identified by the software is the complete shutdown of the internal combustion engine, due to the low thermal needs of the users. This evidence can be seen also in Figures from 7.8 to 7.11.

As it can be seen from Figure 7.12, for the Reference Case – Figure 7.12 a) – and for the Case 1 – Figure 7.12 b) – the ICE in winter operates from 8 a.m. to 8 p.m. included (when the users thermal needs are higher than the ICE capacity) and – when operating – it works always at the rated power. Relating to Case 2, instead, the internal combustion engine operation results extended, working from 6 a.m. to 11 p.m. included, for a total of around 3000 equivalent operating h/year. Furthermore, Figure 7.12 c) shows that in this case not only the rated power but also the off-design operation of the ICE is considered (as already explained, the complete off-design model can be found in [5]). This evidence is due to the will of contemporarily avoiding the thermal energy dissipations, operating the heat pump using the CHP unit produced electric energy and minimizing the introduction of electricity into the national electric grid. Further increase in the ICE operational range can be reached with Case 3 – see Figure 7.12 d) – in which the CHP unit works from 5 a.m. to 11 p.m. included, thanks to the introduction of the distributed generation systems.

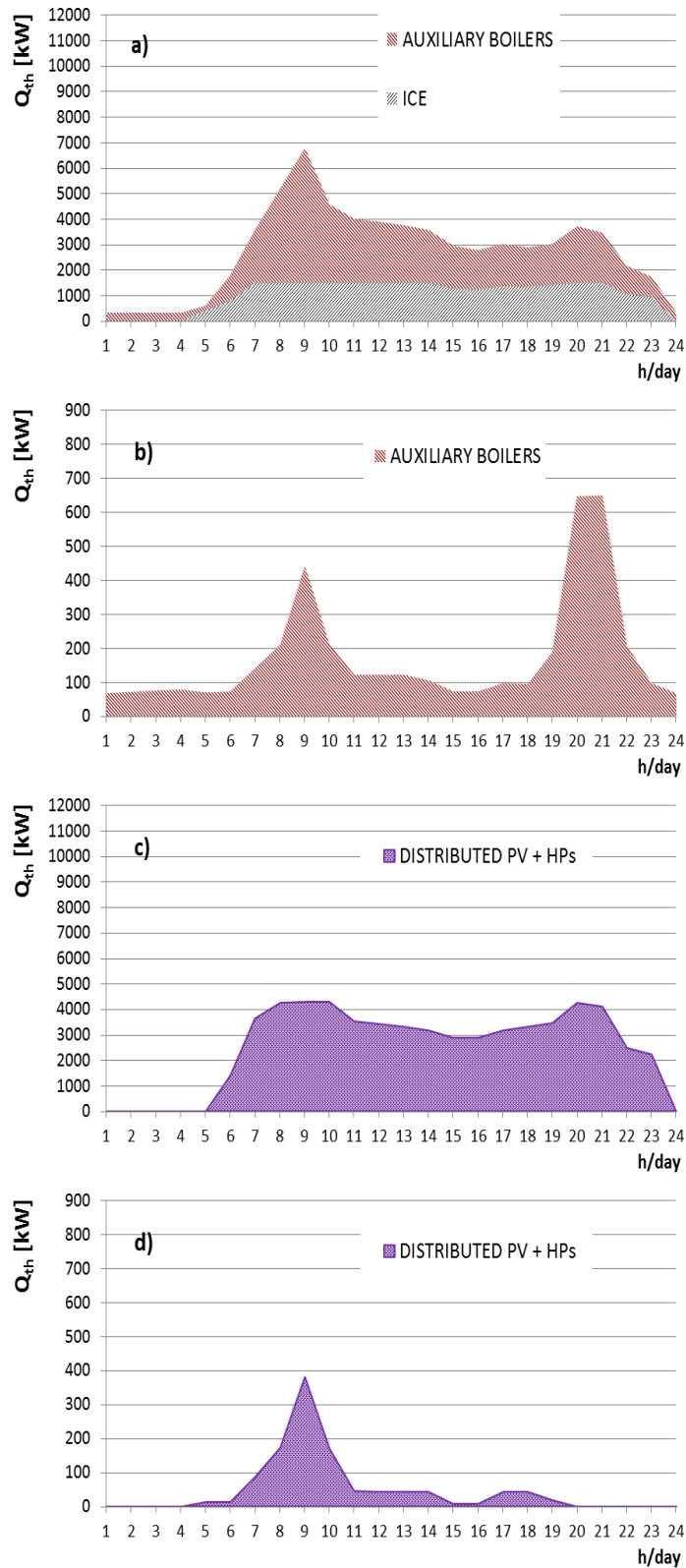


Figure 7.11 – Thermal production profiles along with the production systems mix for the Case 3: a) typical winter day (thermal power station), b) typical summer day (thermal power station), c) typical winter day (distributed generation units), d) typical summer day (distributed generation units).

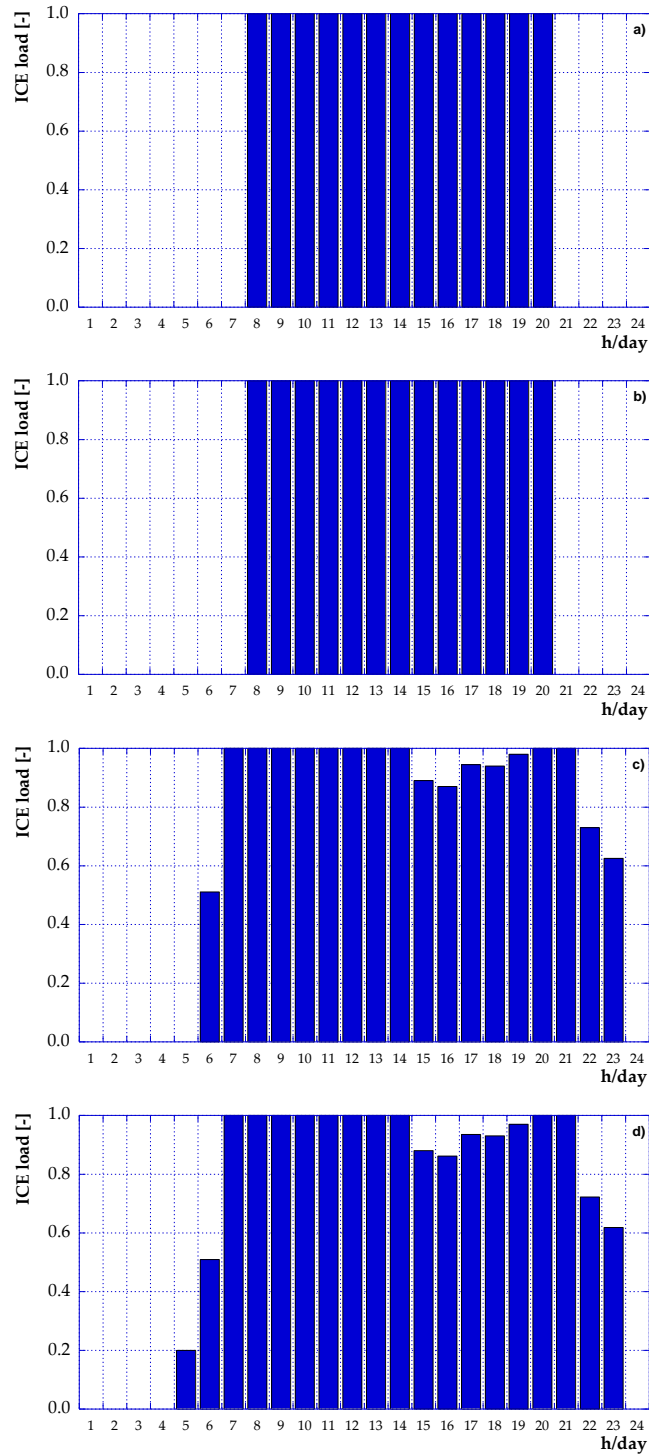


Figure 7.12 – Daily operation profile of the CHP unit in a typical winter day: a) Reference Case, b) Case 1, c) Case 2 and d) Case 3.

Relating to the Reference Case, evidently, only the auxiliary boilers provide in winter for the remaining amount of thermal energy to be produced – once the CHP heat is completely recovered – as well as they provide for the whole production in summer season. As it regards the Case 1, instead, the installed thermal solar panels along with the thermal energy storage contribute to the

thermal energy need fulfillment within the auxiliary boilers. This fact entails the reduction of the auxiliary boilers operation, with consequent benefits in fuel consumption (as better explained in the following of this paragraph). It is also essential to highlight that the thermal solar panels production and the stored thermal energy are completely recovered during the day (and every day/year), thus – as it happens for the ICE production – no thermal dissipation occurs. Similarly, in Case 2 and in Case 3, all the electric energy produced from renewable energy source (*i.e.* by means of the PV panels) is used for the thermal energy production through the centralized heat pump (Case 2) or the distributed HPs (Case 3). During winter, the PV-HPs contribute with the auxiliary boilers and the ICE to the thermal energy production, while during summertime only PV-HPs and boilers operate.

Based on the hourly results of the carried out simulations with the software EGO, the evaluation of the yearly fuel consumption, the yearly purchase of electric energy from the grid and the yearly sale of the exceeding electricity to the grid has been made. As a result, the yearly fuel consumption for each of the analyzed cases is shown in the bar graph of Figure 7.13. As it can be seen, all the elaborated configurations allow to decrease the fuel consumption with respect to the Reference Case (representing the current configuration of the considered CHP-DH network), with a maximum percentage saving equal to about the 57% achieved in Case 2 (fuel consumption decreasing from 35000 MWh to 15000 MWh).

Furthermore, in Figure 7.14 the yearly purchase of electric energy from the national electric grid is shown for the analyzed cases. As evident considering the CHP unit operation, the same amount of electric energy has to be annually purchased for the Reference Case and Case 1 (equal to 800 MWh/year), while a reduction can be seen for the Case 2 (around the 14%) and for the Case 3 (maximum reduction, equal to about the 30%). The decrease in electricity purchase reached in Case 2 and Case 3 is clearly due to the installation of the PV panels that – coupled with the heat pumps – enables to obtain the double advantage of fuel consumption and electric energy purchase decrease.

Finally, the electric energy annually sold to the national electric grid for each configuration is presented in Figure 7.15. Relating to Reference Case and Case 1, all the electric energy produced with the ICE is sold to the network excepting for the internal self-consumption of the pumping station (that requires only the 8% of the ICE capacity, thus a high excess of electricity is present). The introduction of the heat pumps with an optimum management, instead, allows to completely avoid the introduction of electricity into the national grid in Case 2 and to reduce the sale of about the 85% in Case 3 (see Figure 7.15). This condition is particularly desirable since a higher electric grid stability can be guaranteed.

As a consequence, these results seems to indicate the Case 2 as the best viable solution for the considered CHP-DH network, allowing contemporarily the reduction of the fuel consumption and of the purchase of electric energy, the elimination of the electricity sale and the avoidance of thermal energy dispersion through the chimney. Generally speaking, the developed analysis indicates that heat pumps coupled with RES generation can be regarded as a promising way for complex energy network efficiency improvement, even more when then the production is centralized.

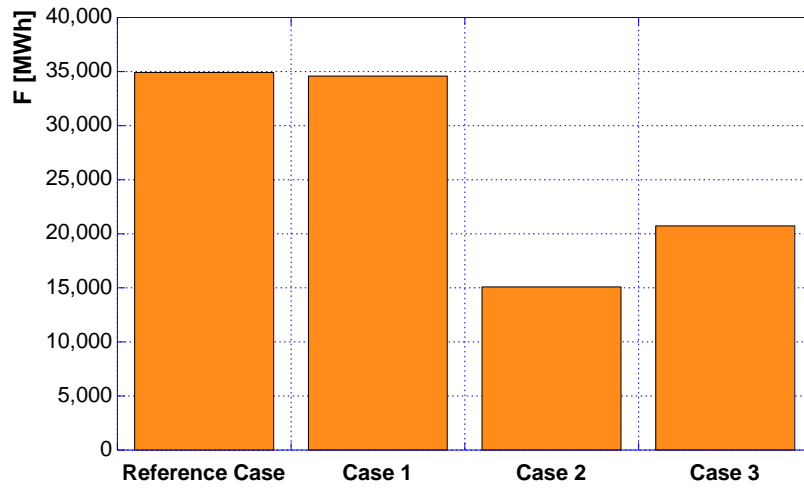


Figure 7.13 – Yearly fuel consumption (ICE plus auxiliary boilers).

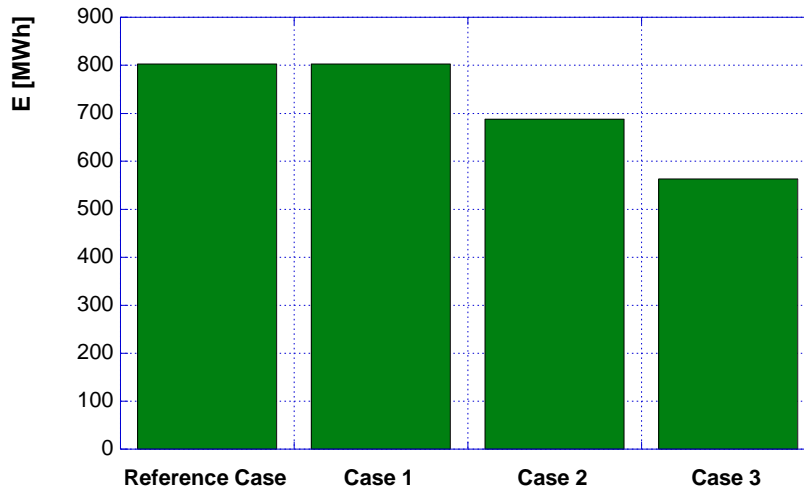


Figure 7.14 – Electric energy yearly purchased from the national electric grid.



Figure 7.15 – Electric energy yearly sold to the national electric grid.

7.3 Phase II: thermal, electrical and cooling energy fulfillment

The second stage of the analysis was focused on the optimization of the considered network set-up when not only thermal energy, but also electricity and cooling energy must be provided to the users. In particular, since a high excess of electricity production can be seen in the current operation of the network with respect to the pumping station need, the possibility of using this electricity to fulfill the users' needs and/or to produce cooling energy has been analyzed.

Considering the results discussed in the previous paragraph, the new proposed solutions involves mainly the centralized power plant. In other words, as will be better explained in the following of this paragraph, no energy production systems placed at final users have been considered (obviously excepting the cooling machines).

7.3.1 Energy needs analysis

In this case, three different typical days during a year have been considered, each one representative respectively of wintertime, summertime and middle season. This assumption has been made because – differently from the phase I in which only users thermal needs were accounted – the inclusion of electricity and cooling needs entails three different load profiles during the year. In fact, typically, during wintertime thermal needs are composed by space heating and hot water needs and no cooling energy is required, during middle season only hot water is present as thermal need and no cooling energy is required and, finally, during summertime only hot water is present as thermal need and cooling needs is present. Furthermore, the electricity demand slightly changes during the year, depending on the season.

Relating to the users thermal needs, the same profiles already presented and discussed in Paragraph 7.2.1 have been considered also for the second part of the analysis. The consideration of three typical days instead of two does not affect users thermal needs: summertime and middle season, indeed, are characterized by the same thermal need profile (for hot water production). However, due to different mean ambient temperatures, the heat dissipations across the district heating network varies depending on the season, thus three different profiles for the thermal energy to be produced by the centralized thermal power station have been calculated with the software IHENA and presented in Figure 7.16.

As it regards the electrical load evaluation, since no information of real needs of the users connected to the DHN was available, a literature analysis has been carried out. The detail of the non-dimensional profiles considered for the analysis is presented in Appendix B.

In particular, different non-dimensional – with respect to the peak of consumption – profiles have been set for each typical day (wintertime, middle season and summertime) and for each typology of user (residential, school, day-hospital and super-market). A further distinction has been made relating to residential users: for these kind of users, indeed, two different profiles have been distinguished, for the electricity consumption respectively of each residential apartment and of the common areas of each building (which is composed by a certain number of apartments). Moreover, for the day-hospital structure and for the super-market the same electricity need daily profile has been considered for the whole year.

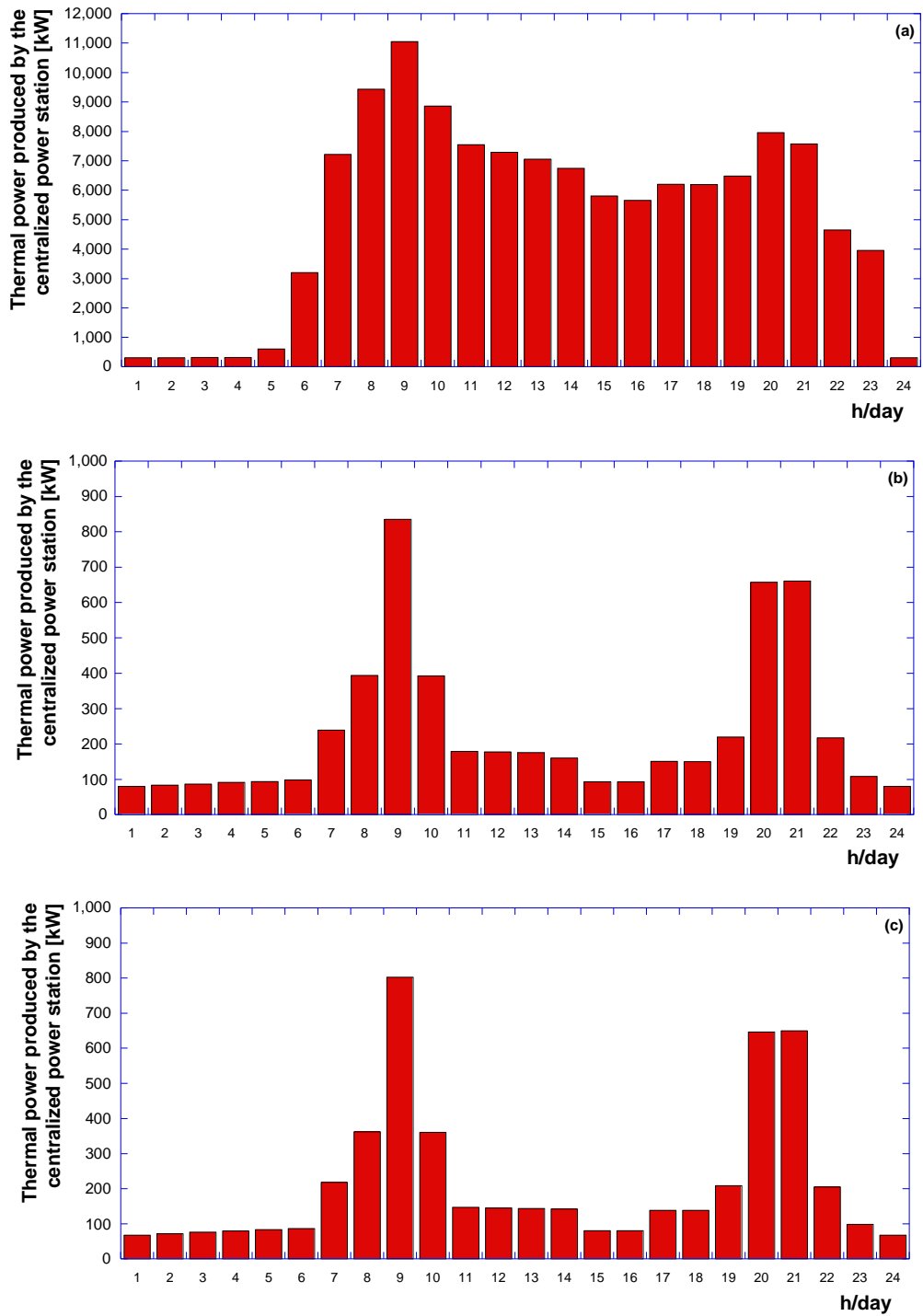


Figure 7.16 – Produced thermal power profile for a typical day in (a) wintertime, (b) middle season and (c) summertime.

In more detail, as it regards the single apartments composing the 13 residential users, the electrical need has been evaluated as the sum of each device (*i.e.* lighting, computers, appliances, audio/video devices, etc.) usually present in a typical apartment. Based on [2], the three non-dimensional curves presented in Appendix B (Figure B1) have been determined, one for each season. It must be highlighted that the electricity needs for air conditioning have been kept out of the electricity load profiles and accounted as cooling energy need, as explained in the following. Similarly, the electrical needs for buildings common areas have been evaluated accounting all the possible needs (lighting of staircases, garages, gardens, elevators, water circulation pumps, etc.), leading to the definition of the curves – for the three typical days – presented in Figure B2, Appendix B.

Based on the non-dimensional curves, the electrical load profiles for each of the 13 residential users can be determined, once estimated the peak powers. With this purpose, an electric energy consumption equal to 3000 kWh/y has been assumed for each apartment and a consumption reference value equal to 0.50 W/m³ has been fixed for the common areas. The result of these evaluations led to the determination of the electrical peak powers listed in Table 7.5.

Table 7.5 – Electric peak power for the residential users.

User ID	Electric peak power [kW]
1	75 (total apartments) + 19 (common areas)
2	54 (total apartments) + 12 (common areas)
3	32 (total apartments) + 14 (common areas)
4	47 (total apartments) + 11 (common areas)
5	48 (total apartments) + 11 (common areas)
6	40 (total apartments) + 9 (common areas)
7	40 (total apartments) + 10 (common areas)
8	65 (total apartments) + 18 (common areas)
9	44 (total apartments) + 10 (common areas)
10	42 (total apartments) + 13 (common areas)
11	54 (total apartments) + 11 (common areas)
12	36 (total apartments) + 8 (common areas)
13	47 (total apartments) + 11 (common areas)

As it regards the two schools connected to the network, a primary school and a kindergarten, the electrical need has been calculated by means of the non-dimensional curves presented in Figure B3, Appendix B [9]. The presented curves have been determined considering the schools opening hours during the academic year, the afternoon activities and the closure for summer holidays. On the basis of the assumed reference literature [9], no differentiation has been considered for the primary school and the kindergarten. As it concerns the peak powers, instead, referring to the mean scholastic electricity consumption in Italy, values equal to 63 kW and 67 kW have been assumed respectively for the kindergarten and the primary school.

Furthermore, the electricity need of the day-hospital structure has been determined considering the well-known non-dimensional load profile for hospital users [10] shown in Figure B4, Appendix B. On the basis of the available literature data, a peak power equal to 86 kW has been assumed, considering a ratio between the annual thermal and electrical energies equal to 3 [2]. It should be noted that, for this kind of users, a weak dependence on the season can be seen, thus the same load profile can be considered for every day of the year. Finally, as it regards the supermarket, the non-dimensional profile found in [2] has been considered (see Figure B5 in Appendix B) and a peak electrical power equal to 93 kW has been assumed (calculated considering a ratio between the annual thermal and electrical energies equal to 0.30). As for the day-hospital structure, the same electricity load profile during the whole year has been assumed.

Starting from the afore mentioned considerations, the evaluation of the hourly based peak power load curves for the total connected users has been made. The result is presented in Figure 7.17, for the typical days in wintertime, middle season and summertime. From the figure it can be noted that the maximum electrical power varies between a value slightly higher than 1400 kW (winter typical day) and a value slightly lower than 1500 kW (middle season typical day). The base load, instead, ranges between 520 kW (for the winter typical day) and 550 kW (for the summer typical day). Furthermore, since the electricity consumption for air conditioning is not considered, the electrical load profile do not importantly change depending on the season and presents the characteristic *M shape*.

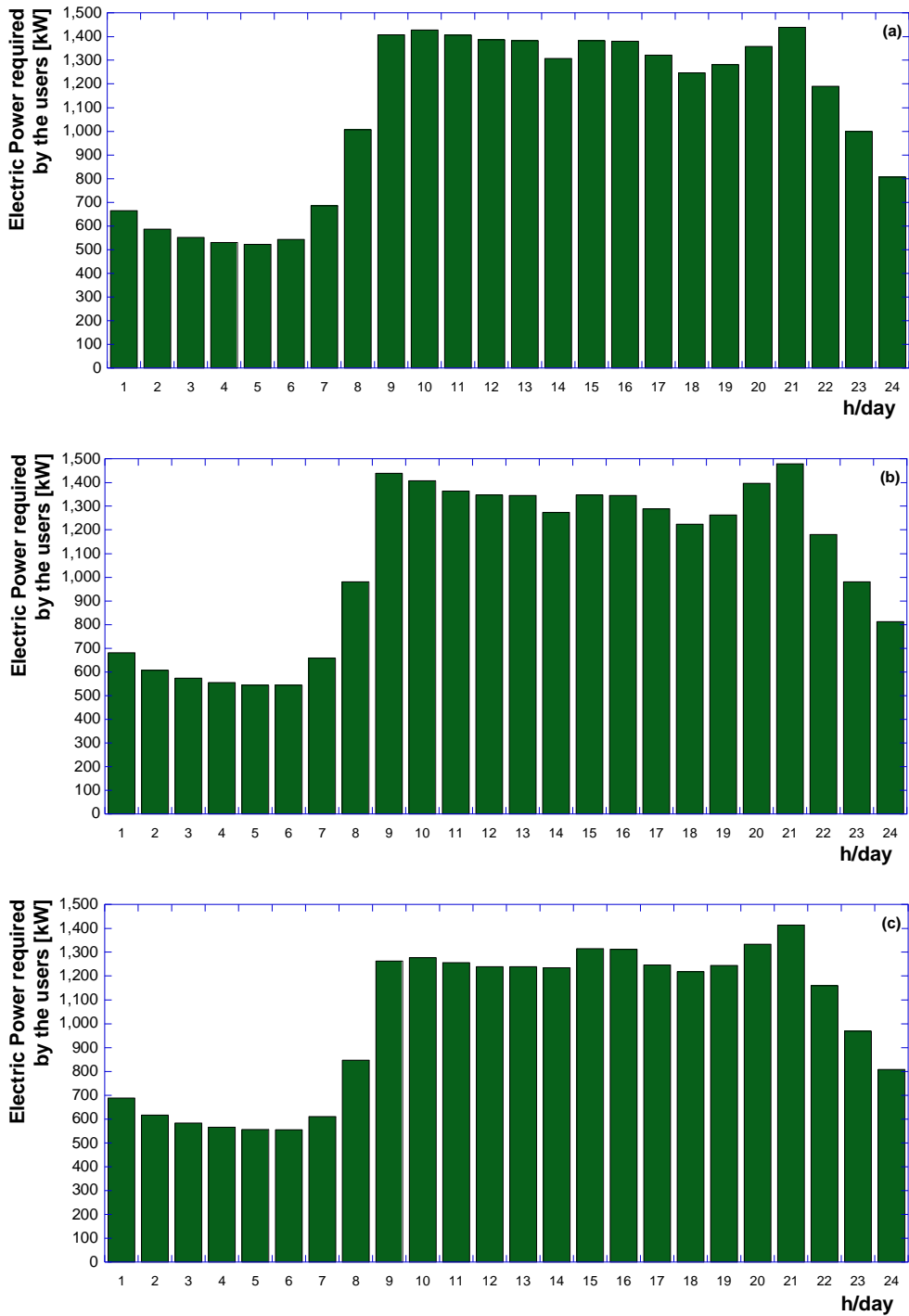


Figure 7.17 – Required electrical power profile for a typical day in (a) wintertime, (b) middle season and (c) summertime.

The last part of the loads analysis relates to the evaluation of the cooling power hourly profiles for the network connected users. Different cooling needs profiles have been determined for each typology of user, but only one typical day has been considered since, evidently, only during summertime the cooling energy request occurs.

Relating to the residential users, the Carrier method [11, 12] has been applied for the evaluation of the cooling energy needs. The day assumed for the calculation is the 21st of June and the external ambient temperature is equal to 33 °C (city of Bologna). The internal set point temperature, instead, is fixed at the value of 26 °C. Furthermore, thermal contribution of lighting and electrical appliances operation have been accounted, as well as the constant presence of people inside the apartments. Finally, an increase coefficient equal to 15% has been considered, in a cautious way. The obtained non-dimensional curve is shown in Figure C1, Appendix C, while the peaks of cooling power are listed in Table 7.6 for each residential user.

Table 7.6 – Cooling peak power for the residential users.

User ID	Cooling peak power [kW]
1	232
2	166
3	100
4	144
5	148
6	122
7	122
8	200
9	136
10	130
11	166
12	110
13	144

As it regards the schools, no cooling energy needs have been considered for the analysis, due to the fact that in summertime only few activities are done and the schools are closed for summer holydays for the most of the time.

On the other hand, the day-hospital structure operates from 7:30 a.m. to 6:30 p.m. every day. Even in this case, no data from the structure were available, thus a literature study has been considered [13]. This study refers to a hospital placed in the city of Cagliari (Sardinia, Italy). Based on the methodology applied in [13], considering the surface of the day-hospital and the different external ambient temperature to be considered for Bologna, the non-dimensional daily curve of the cooling load has been determined (see Figure C2 in Appendix C). The peak cooling power of the analyzed day-hospital structure is equal to 80 kW.

Finally, the non-dimensional cooling load curve for the super-market has been determined considering literature studies about structures placed in the northern part of Italy [14]. The result is presented in Figure C3, Appendix C. The super-market is open from 8:00 a.m. to 8:00 p.m. and the peak power is equal to 185 kW.

On the basis of all the considerations made, the hourly profile of the cooling power need for the typical day in summertime has been evaluated and presented in Figure 7.18. The major contribution to the total needs is attributable to the residential users, being the majority of the users. The peak of cooling need can be seen at 8:00 p.m. and it is equal to around 2100 kW, while the minimum request is slightly lower than 900 kW (at 5:00 a.m.).

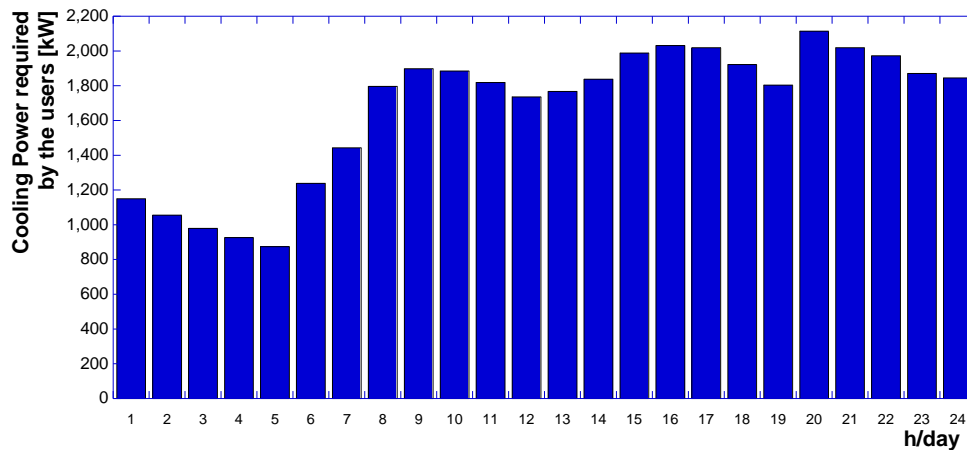


Figure 7.18 – Required cooling power profile for a typical day in summertime.

7.3.2 Optimal management strategies – Case studies

As previously explained, this second phase of the analysis about the Corticella district heating network aims to optimally manage a complex energy network, able to fulfill thermal, electrical and cooling needs of the connected users. The objective of optimization procedure – carried out by elaborating and comparing different solutions in terms of energy systems set-up, with the optimization software EGO – is the minimization of the total costs of energy production. This purpose can be detailed with the following further objectives: (i) the minimization (or avoidance) of the electricity exchange with the national grid, (ii) the minimization (or avoidance) of the heat dissipations through the chimney, (iii) the minimization of the auxiliary boilers employment, (iv) the optimization of the CHP units operation and (v) the maximization of the renewable sources exploitation. In more detail, starting from the Reference Case (*i.e.* the network current set-up and operation – obviously, this Reference Case is the same already presented and discussed in Paragraph 7.2), different alternatives have been proposed and analyzed. The proposed solutions consider the possibility of the energy production systems addition to the current ones and the production is aimed to the fulfillment of thermal, electrical and cooling energy needs of the 17 connected users. Furthermore, in order to maintain the current DHN layout and considering the non-convenience of DHN with 4 tubes (well-known in literature), when present the cooling machines (both compression and absorption chillers) are considered as installed at the final users. As a consequence, each utility substation will be composed of three heat exchangers, respectively for space heating, hot water and cooling circuits.

The different elaborated solutions are the following:

- Case A: in this first proposed alternative solution no energy systems have been added to the current plant configuration (1 internal combustion engine and 4 auxiliary boilers). However for this case, as well as for the following ones, the centralized power station has to fulfill the electricity and cooling energy needs of the users in addition to the thermal needs. With this purpose compression and/or absorption chillers installation at the final users is considered. The layout of this configuration is presented in Figure 7.19.
- Case B: with respect to the Case A, the addition of a further internal combustion engine (with a rated power equal to the one of the already installed engine), a thermal storage tank and a heat pump (HP) has been considered, as shown in Figure 7.20. The heat pump is coupled only with the CHP unit, so no grid connection is allowed.
- Case C: the centralized production plant is modified – with respect to Case A – by the addition of photovoltaic panels (PV) and a heat pump (see Figure 7.21). The electric power input of the heat pump can be given by the PV panels (firstly) and by the CHP unit (as second option), while there is no connection between the national electric grid and the HP.
- Case D: the last proposed solution consists in the addition of thermal solar panels (TSP), a thermal storage tank and a heat pump to the configuration proposed in Case A (see Figure 7.22).

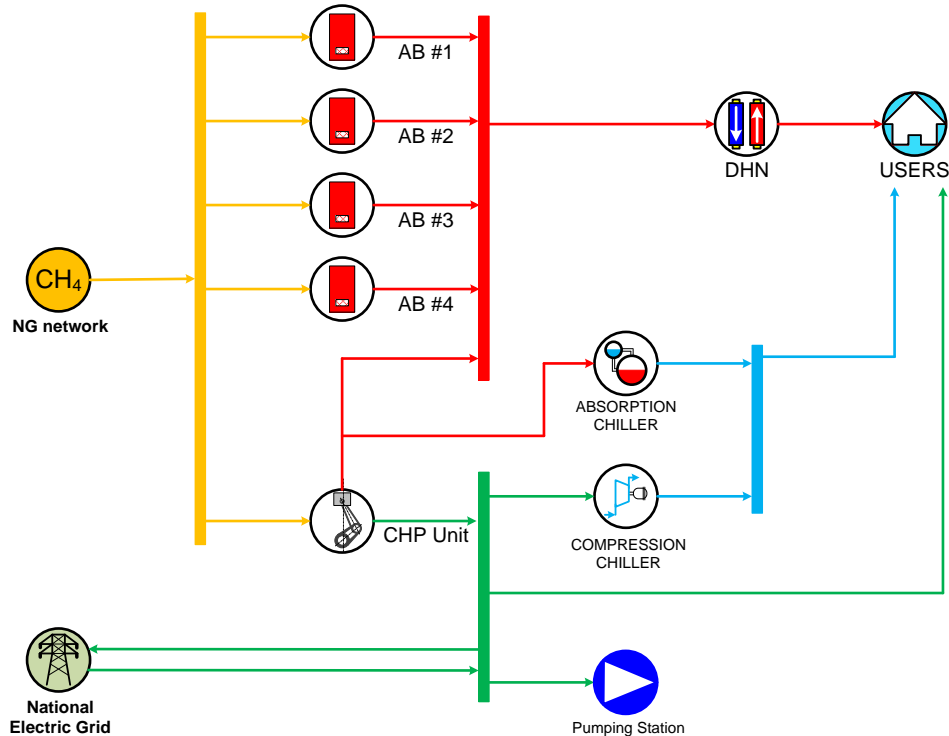


Figure 7.19 – Layout of the analyzed configuration Case A.

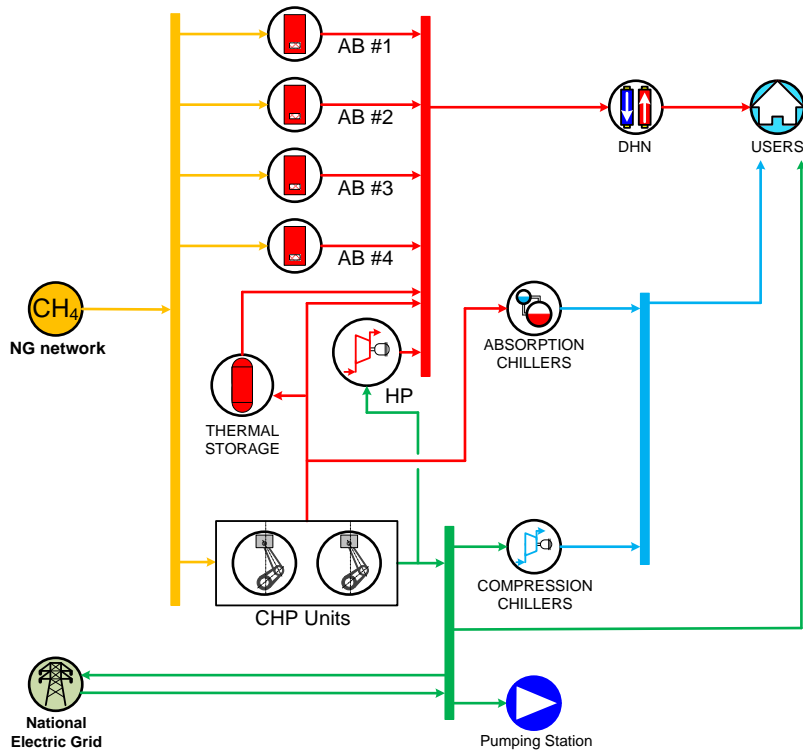


Figure 7.20 – Layout of the analyzed configuration Case B.

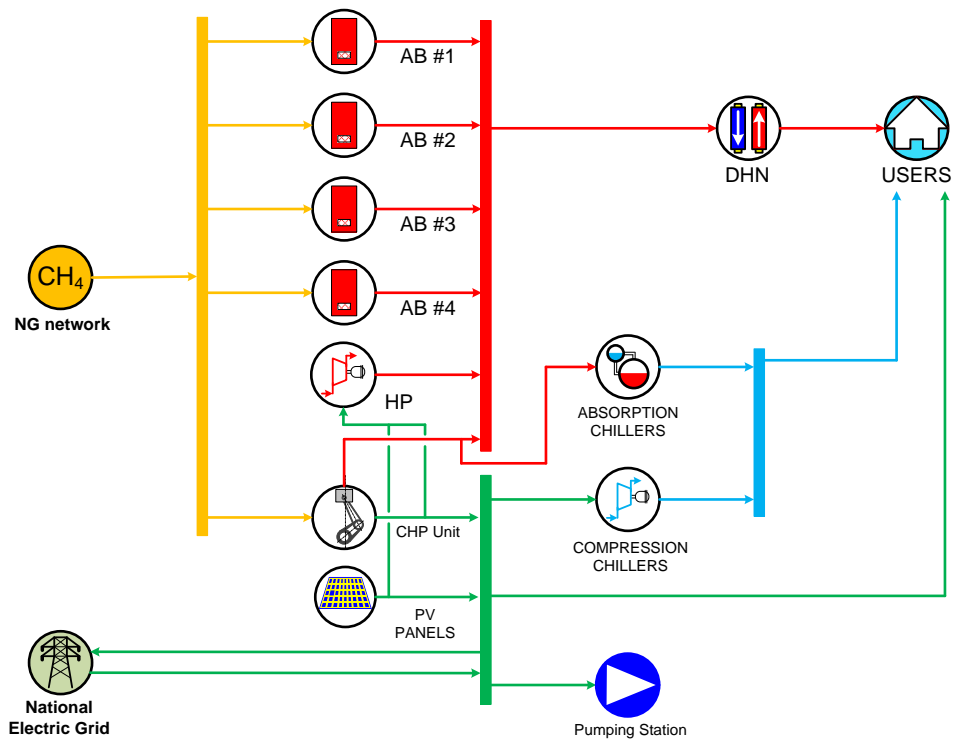


Figure 7.21 – Layout of the analyzed configuration Case C.

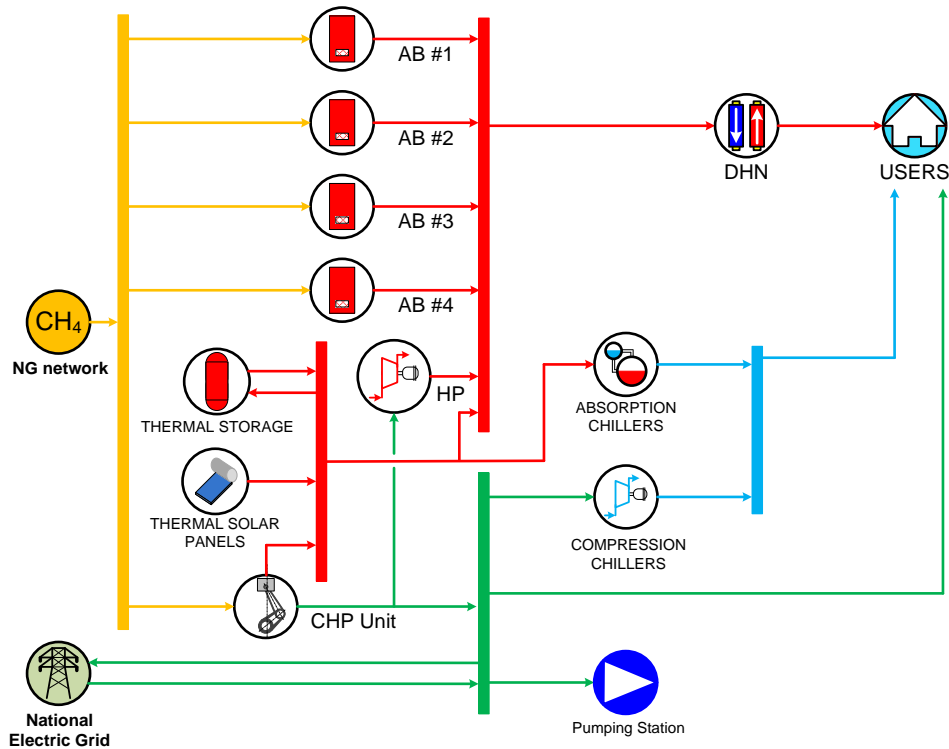


Figure 7.22 – Layout of the analyzed configuration Case D.

As it regards the logic of operation, as already said the electricity in input to the heat pump can be supplied only by – in order of priority – renewables (when present) and ICE production. Relating to the cooling machines, instead, the following constraints have been imposed to the mode of operation: (i) absorption chillers can be fed by the thermal power produced by means of TS panels (in Case D) and CHP units (for all the cases) – *i.e.* the auxiliary boilers and the heat pump cannot be employed to produce cooling energy, (ii) compression chillers are fed with the electricity produced by PV panels, CHP units and, finally, the national electrical grid. Since the cooling needs must always be satisfied, indeed, a connection between compression chillers and the grid has to be present.

In order to give an immediate comprehension of the proposed configurations, all the analyzed cases are summarized in Table 7.7.

The proposed cases have been simulated with the software EGO – in order to evaluate the optimal yearly operational set-up – and compared to the Reference Case. It should be highlighted that, for the Reference Case, only thermal energy needs are fulfilled by the centralized power station, while each user has to provide by itself for the fulfillment of electricity and cooling needs. As well as for the Reference Case, the constraint of completely avoiding thermal energy dissipation has been imposed for the operating of the CHP unit.

Table 7.7 – Summary of the analyzed configurations – Phase II.

	Ref. Case	Case A	Case B	Case C	Case D
ICE	•	•	•	•	••
Aux. Boilers	•	•	•	•	•
Thermal Solar Panels					•
Thermal Energy Storage			•		•
Photovoltaic Panels				•	
Heat Pump			•	•	•
Compression Chillers		•	•	•	•
Absorption Chillers		•	•	•	•

As previously mentioned, the second CHP unit introduced in the Case A is an internal combustion engines equal to the one already installed. As a consequence, the main design parameters for this system are the ones presented in Table 7.1.

Moreover, further considerations can be made about the introduction of renewable energy generation systems (thermal or PV panels), the heat pumps and the thermal storage system as well as for the cooling machines. The main characteristics of the introduced systems – listed in Table 7.8 – have been defined as follows:

- Compression Chillers (CC) – all cases: the installation of CC at the final users has been considered. Based on the available technology an Energy Efficiency Ratio (EER) equal to 4 has been assumed.
- Absorption Chillers (AC) – all cases: similarly, the possibility of installing AC, in addition or as an alternative to the CC, for the cooling energy production has been evaluated. The assumed EER is 0.67.
- Thermal Energy Storage (TES) – Case B and Case D: the volume of the thermal storage tank has been defined as the minimum volume to obtain at the end of the day the complete restitution of the stored energy (*i.e.* every 24 hour the same conditions can be registered for the tank). This minimum value has been individuated by applying the software EGO with a trial and error procedure and, as it can be seen in Table 7.8, it differs depending on the analyzed configuration.
- Heat Pump (HP) – Case B, Case C and Case D: the Coefficient Of Performance (COP) has been chosen on the basis of the available literature [4] considering a large-scale Heat Pump (HP). The size of the HP has been determined for each case, with the aim to completely recover the ICE available heat and contemporarily operate the HP with the electric energy produced by ICE and – in Case C – PV panels, in order to minimize the electric energy exchange with the grid. Thus, the size of the centralized heat pump becomes a result of the optimization analysis and it differs depending on the analyzed configuration.
- Photovoltaic Panels (PV) – Case C: as for the Phase I of the analysis, the available surface at the thermal power station has been considered to choose the PV size. The tilt and the azimuth angles have been chosen on the basis of the optimum for the considered city (latitude 44°30'27"00 N, longitude 11°21'5"04 E). The produced electric energy is used (*i*) for users' electricity needs, (*ii*) for the heat pump, (*iii*) for the pumping station,

- (iv) for the compression chillers and (v) only the possible surplus is sold to the national electric grid.
- **Thermal Solar Panels (TSP)** – Case D: similarly to the PV case, the size of the TSP has been set considering the real available surface at the thermal power station, while the tilt and the azimuth angles have been chosen on the basis of the optimum for the considered city.

Table 7.8 – Main systems parameters considered in the proposed variation scenarios – Phase II.

Thermal Solar Panels	
Typology	plate
S	300 m ²
η	80%
Peak Power	240 kW _p
Tilt Angle	30°
Facing	South
Thermal Storage Tank	
V	2 m ³ (Case B), 1 m ³ (Case D)
T_{min}	70 °C
T_{max}	120 °C
T_i	70 °C
Solar PV Panels	
S	300 m ²
η	10%
Peak Power	30 kW _p
Tilt Angle	30°
Facing	South
Heat Pump	
COP	4
Compression Chillers (each one)	
EER	4
Absorption Chillers (each one)	
EER	0.67

As it regards the production obtainable from the solar panels – for both thermal and PV panels – the same evaluations already presented in Phase I have been replied. Thus, in Figure 7.23 the obtained profiles relating to a typical winter day (*i.e.* January), for a typical day during middle season (considered as an average profile between winter and summer) and for a typical summer day (*i.e.* July) are shown. Evidently, the winter and summer profiles are the same already presented in Figure 7.7. Different conversion efficiencies have been then considered (as it can be seen in Table 7.8) for the evaluation of the thermal solar production and for the PV case.

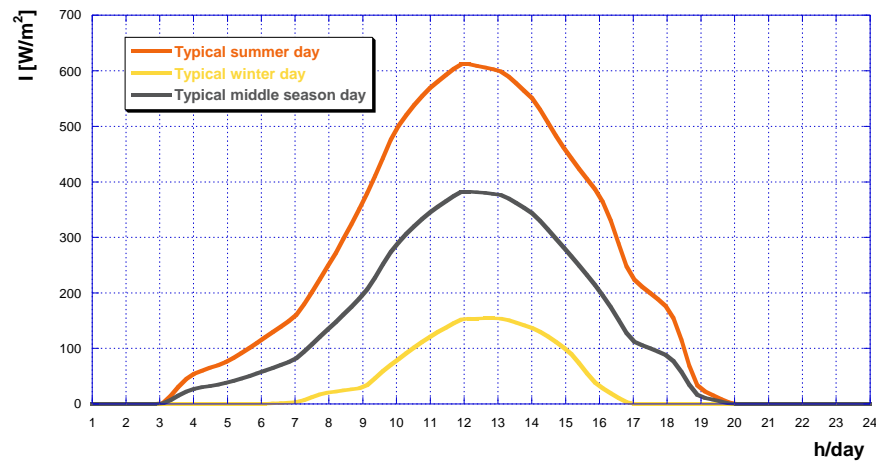


Figure 7.23 – Incident solar irradiation on a south-facing solar panel with a tilt angle equal to 30°, for a typical winter day (yellow line), for a typical middle season day (grey line) and for a typical summer day (orange line) – Bologna case.

7.3.3 Results and discussion

The energy systems scheduling optimization made with the software EGO led to the definition of the optimal energy production profiles (*i.e.* thermal, electrical and cooling energies) for each case. Thus, from Figure 7.24 to Figure 7.28 the hourly profiles – for typical (a) winter, (b) middle season and (c) summer days separately – of the thermal power production in the considered scenarios are shown, along with the production mix. From Figure 7.29 to Figure 7.33 (respectively for configurations from the Reference Case to the Case D), instead, the hourly profiles – for typical (a) winter, (b) middle season and (c) summer days separately – of the electrical power production are presented, along with the production mix. Finally, the hourly based cooling power production for a typical summer day is shown, along with the production mix, from Figure 7.34 (Case A) to Figure 7.37 (Case D). As it can be seen, no results are presented about the cooling power profile for the Reference Case: in the current plant set-up and operation, indeed, each user eventually provides by itself for the fulfillment of cooling needs. On the other hand, as it regards the electricity production, the users electrical needs have not been considered for the Reference Case; however, a self-consumption for the power plant pumping station is present.

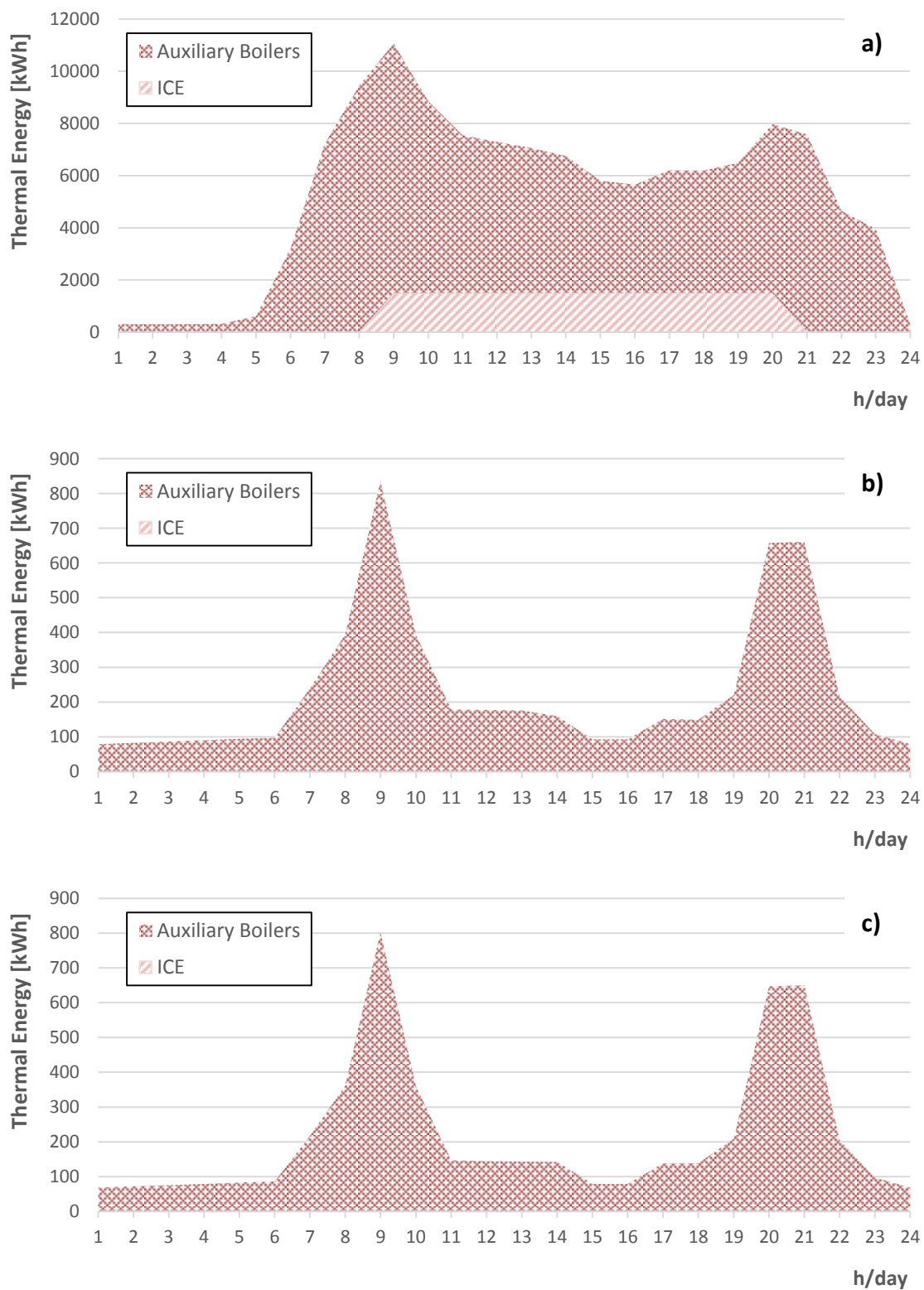


Figure 7.24 – Thermal production profiles (thermal power station) along with the production systems mix for the Reference Case: a) typical winter day, b) typical middle season day, c) typical summer day.

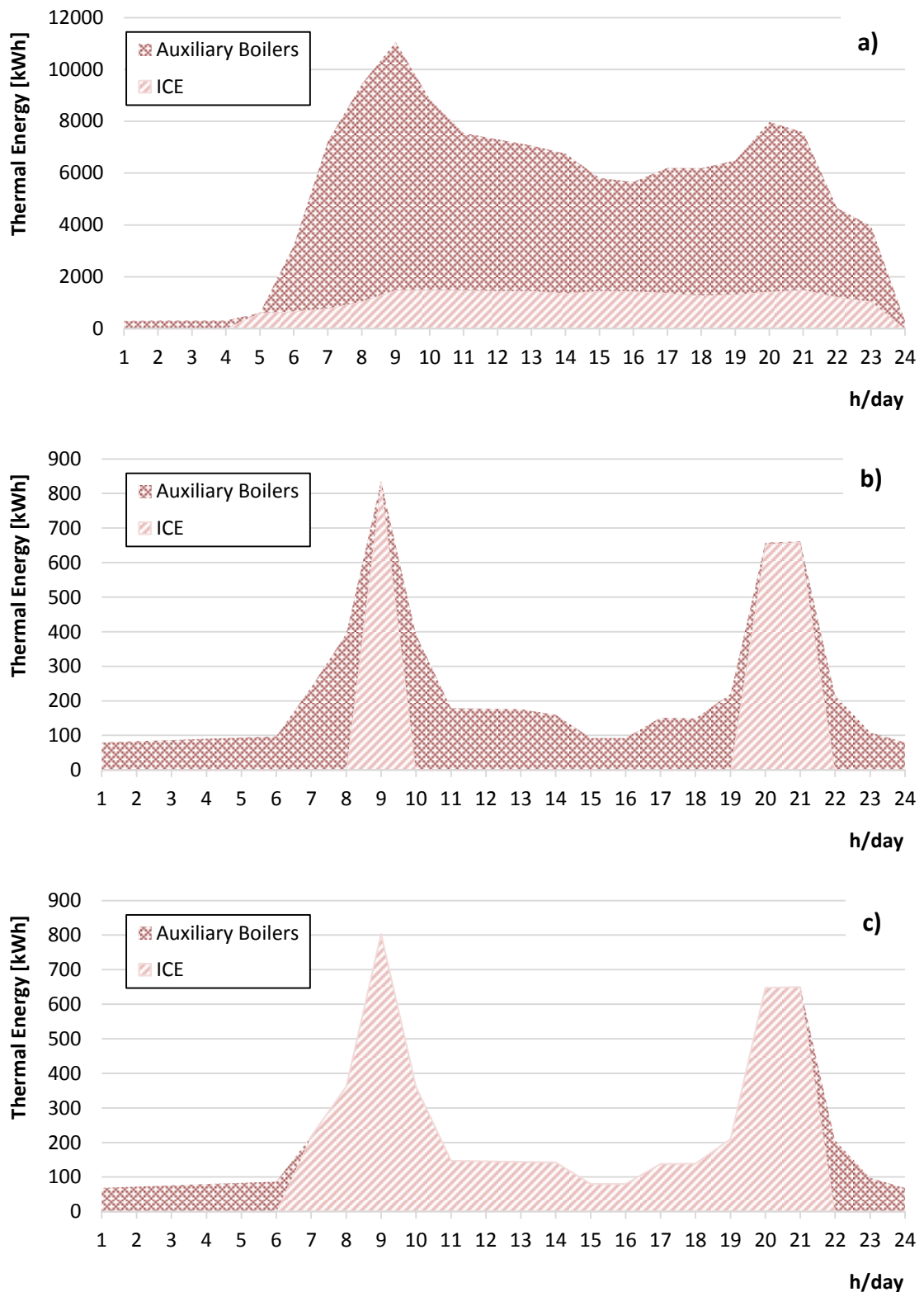


Figure 7.25 – Thermal production profiles (thermal power station) along with the production systems mix for the Case A: a) typical winter day, b) typical middle season day, c) typical summer day.

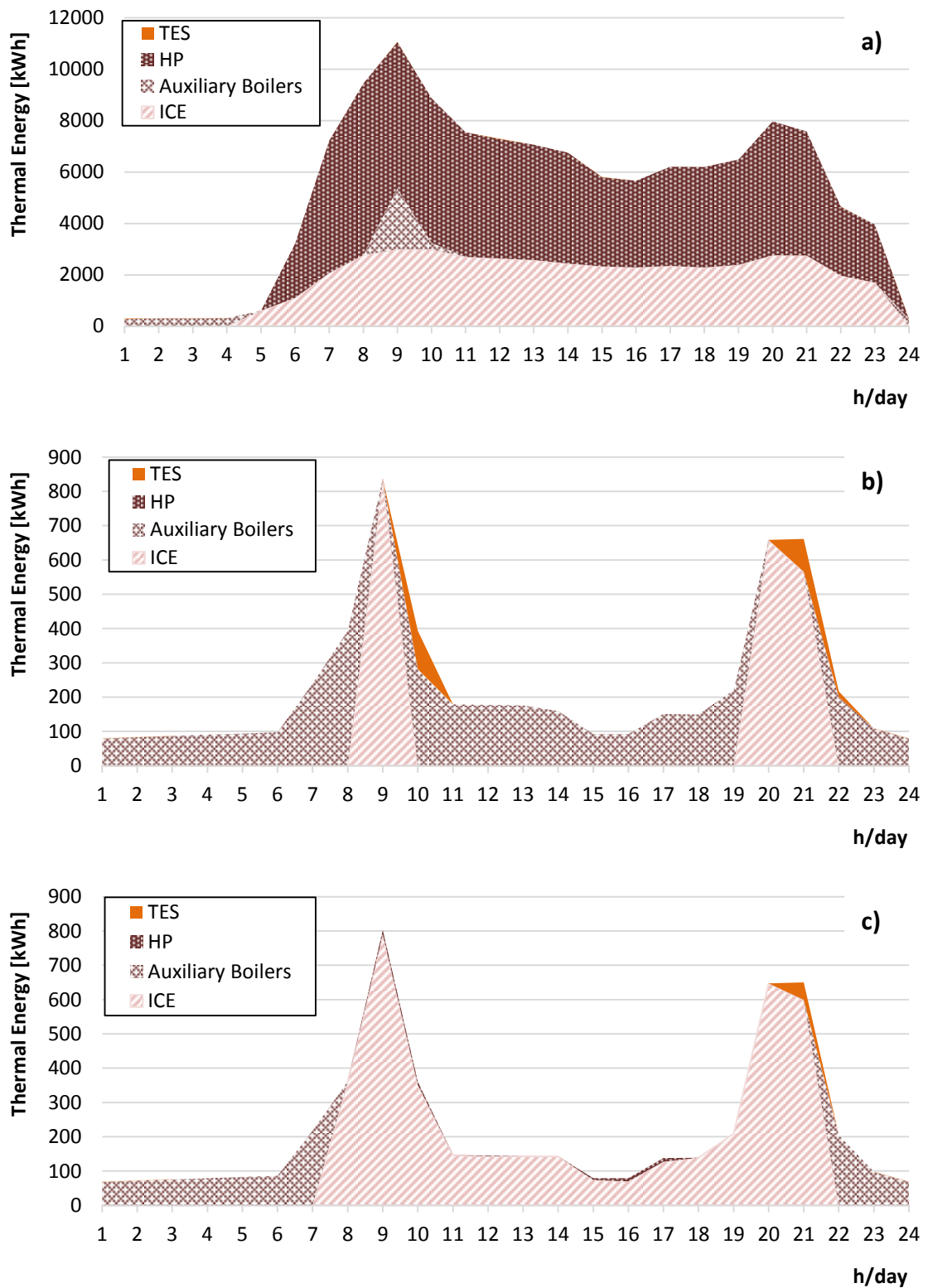


Figure 7.26 – Thermal production profiles (thermal power station) along with the production systems mix for the Case B: a) typical winter day, b) typical middle season day, c) typical summer day.

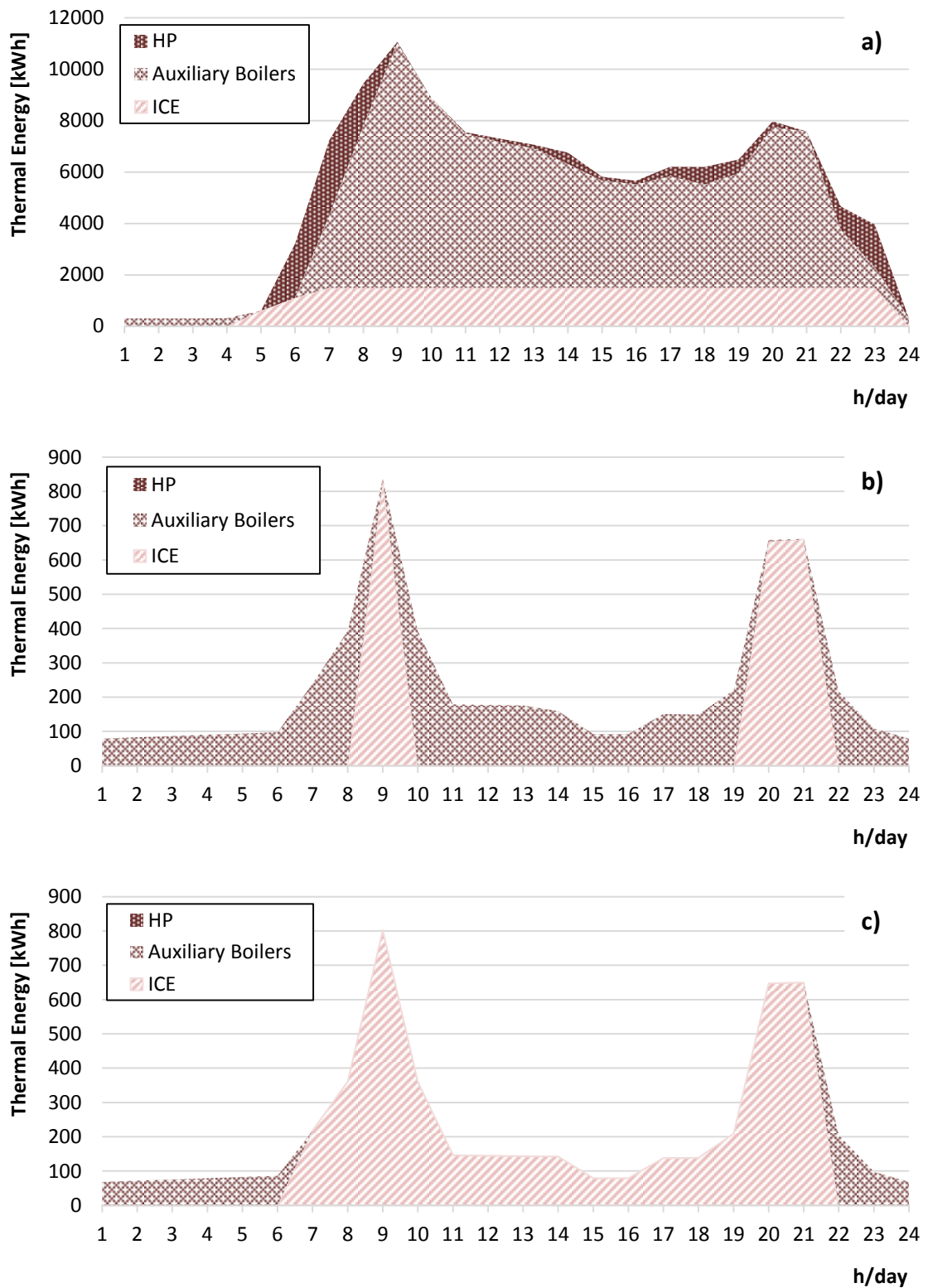


Figure 7.27 – Thermal production profiles (thermal power station) along with the production systems mix for the Case C: a) typical winter day, b) typical middle season day, c) typical summer day.

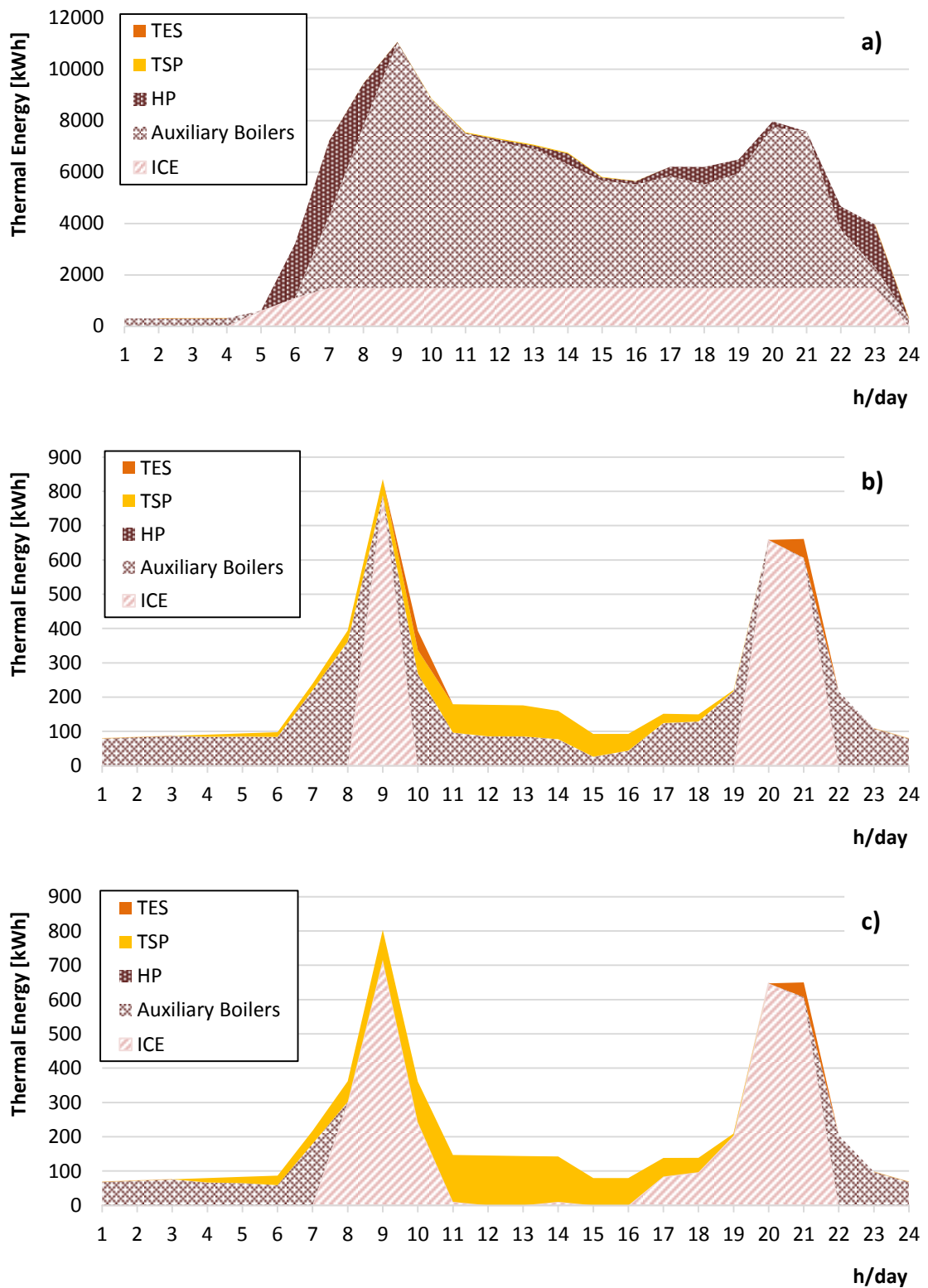


Figure 7.28 – Thermal production profiles (thermal power station) along with the production systems mix for the Case D: a) typical winter day, b) typical middle season day, c) typical summer day.

In more detail, relating to the thermal needs fulfillment and starting from the Reference Case (Figure 7.24), it can be seen that, only considering the additional fulfillment of electrical and cooling needs (*i.e.* without the introduction of further energy systems – see Case A in Figure 7.25), an increase in the ICE operation can be obtained. During wintertime, indeed, the ICE operation is extended up to 20 h/day (considering both design and off design operation). Furthermore, differently from the Reference Case, from Figure 7.25 it can be seen that the ICE operates also during middle season (when the peaks thermal needs occur) and summertime (from the 6 a.m. to the 10 p.m., allowing in this period the complete shutdown of the auxiliary boilers). Moving to Case B, the addition of a further CHP unit and of a heat pump allows to importantly reduce the auxiliary boilers operation during wintertime (see Figure 7.26-a). The auxiliary boilers, indeed, operates only during the night and during the peak hours in the morning of the winter typical day. Even in this case, CHP units operates in middle season and summertime. A slight contribution of the heat pump can be seen in summertime, while during middle season it does not operate. As it regards the thermal storage, instead, its employment can be seen mainly during middle season (Figure 7.26-b) and summertime (Figure 7.26-c), while no significant contribution is registered in wintertime. In particular, relating to the summer typical day, with respect to the Case A, a decrease in the ICE exploitation for thermal energy fulfillment can be observed when the TES operates. As better explained in the following, this fact allows a major employment of absorption chillers.

The results of the Case C shows the same thermal power profiles of the Case A during the typical days in middle season (Figure 7.27-b) and summertime (Figure 7.27-c). On the other hand, the presence of the heat pump allows to reduce, with respect to Case A, the auxiliary boilers operation during the winter typical day (Figure 7.27-a).

Finally, from Figure 7.28 it can be observed that – compared to the Case C – for Case D during wintertime a slight reduction in auxiliary boilers operation is obtained, due to thermal solar panels. In middle season and particularly in summertime, instead, a high production from TSP is registered, enabling to further decrease boilers operation.

As it concerns the electricity production, the hourly profiles for the Reference Case during typical days in wintertime, middle season and summertime are presented respectively in Figure 7.29-a, in Figure 7.29-b and in Figure 7.29-c. As already mentioned, for the Reference Case (which represents the current set-up and operation of the Corticella DHN) the only electricity need considered in the analysis is the one for the power plant pumping station. As it can be noted, this self-consumption is almost independent from the season and it is guaranteed (*i*) during wintertime by means of the ICE production (from 9 a.m. to 8 p.m.) and electricity purchase (from 9 p.m. to 8 a.m.), (*ii*) during middle season and summertime by means of electricity purchase.

The profiles of electrical energy needs significantly change for the other analyzed configurations, due to the will of users' needs fulfillment. It is important to highlight that the profiles shown from Figure 7.30 to Figure 7.33 do not include the electrical energy produced and employed for the compression chillers. In other words, these profiles include the users electricity needs (*i.e.* lighting, computers, appliances, audio/video devices, etc.) while the electricity needs for air conditioning have been kept out of the electricity load profiles and accounted as cooling energy need. As it can be seen, since the pumping station need is very low with respect to the ICE rated power, the introduction of the users electrical and cooling needs fulfillment allows to increase the ICE production and contemporarily its employment during summertime and middle season, both in Case A and Case B (see Figure 7.30 and Figure 7.31). The introduction of the heat pump in Case B affects the summertime profile, slightly reducing the amount of ICE electrical production employed for electrical needs fulfillment.

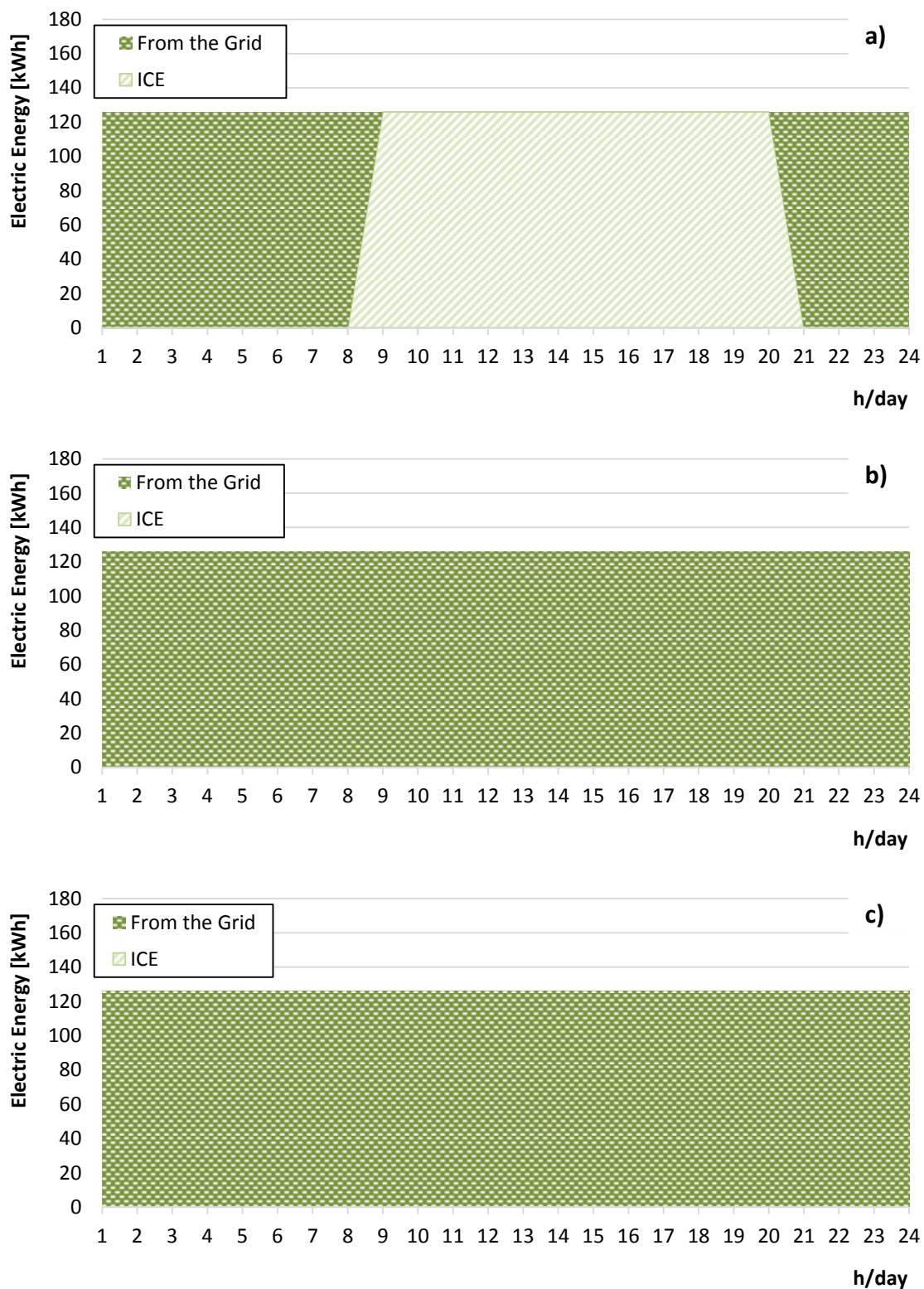


Figure 7.29 – Electricity production profiles (thermal power station) along with the production systems mix for the Reference Case: a) typical winter day, b) typical middle season day, c) typical summer day.

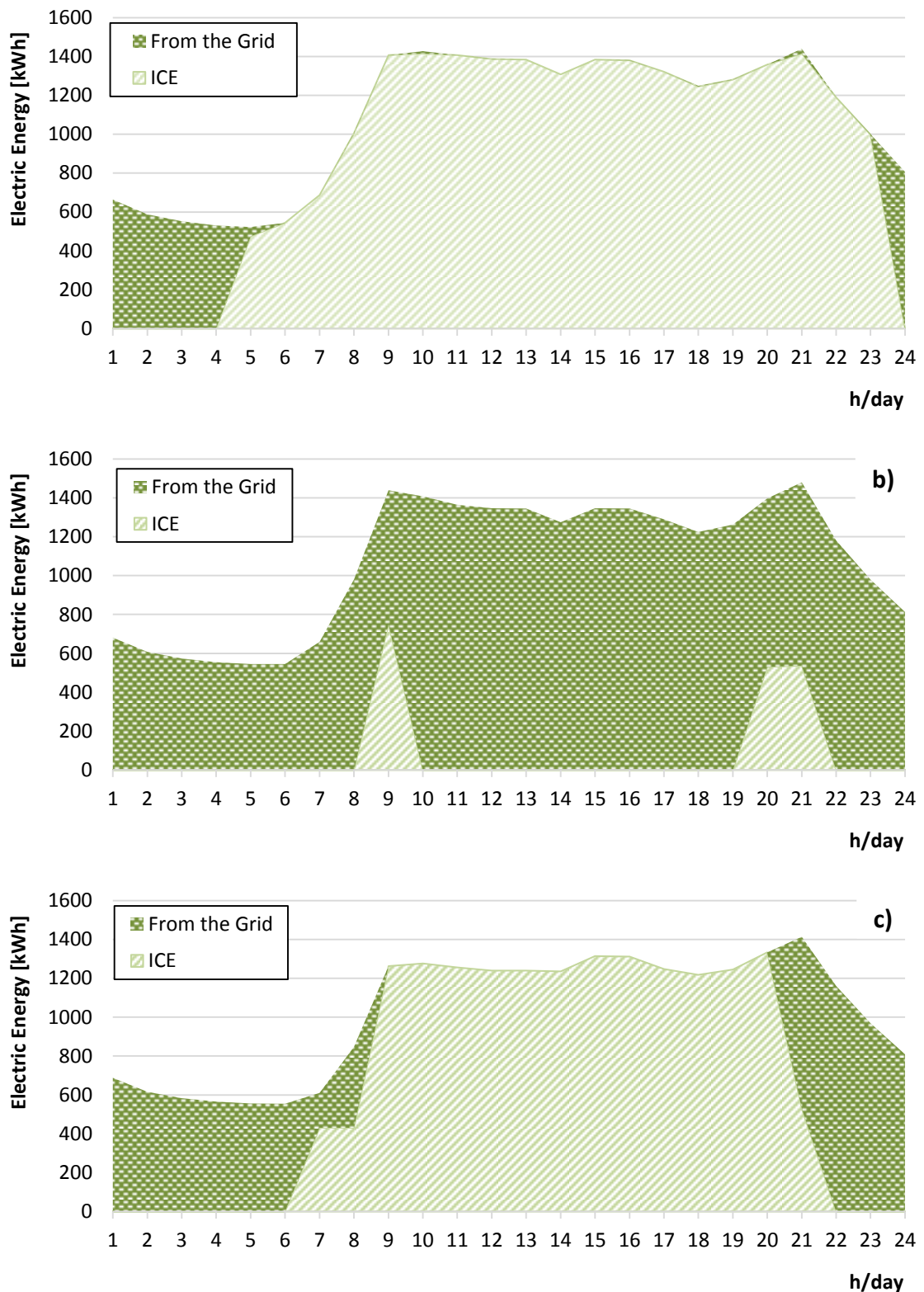


Figure 7.30 – Electricity production profiles (thermal power station) along with the production systems mix for the Case A: a) typical winter day, b) typical middle season day, c) typical summer day.

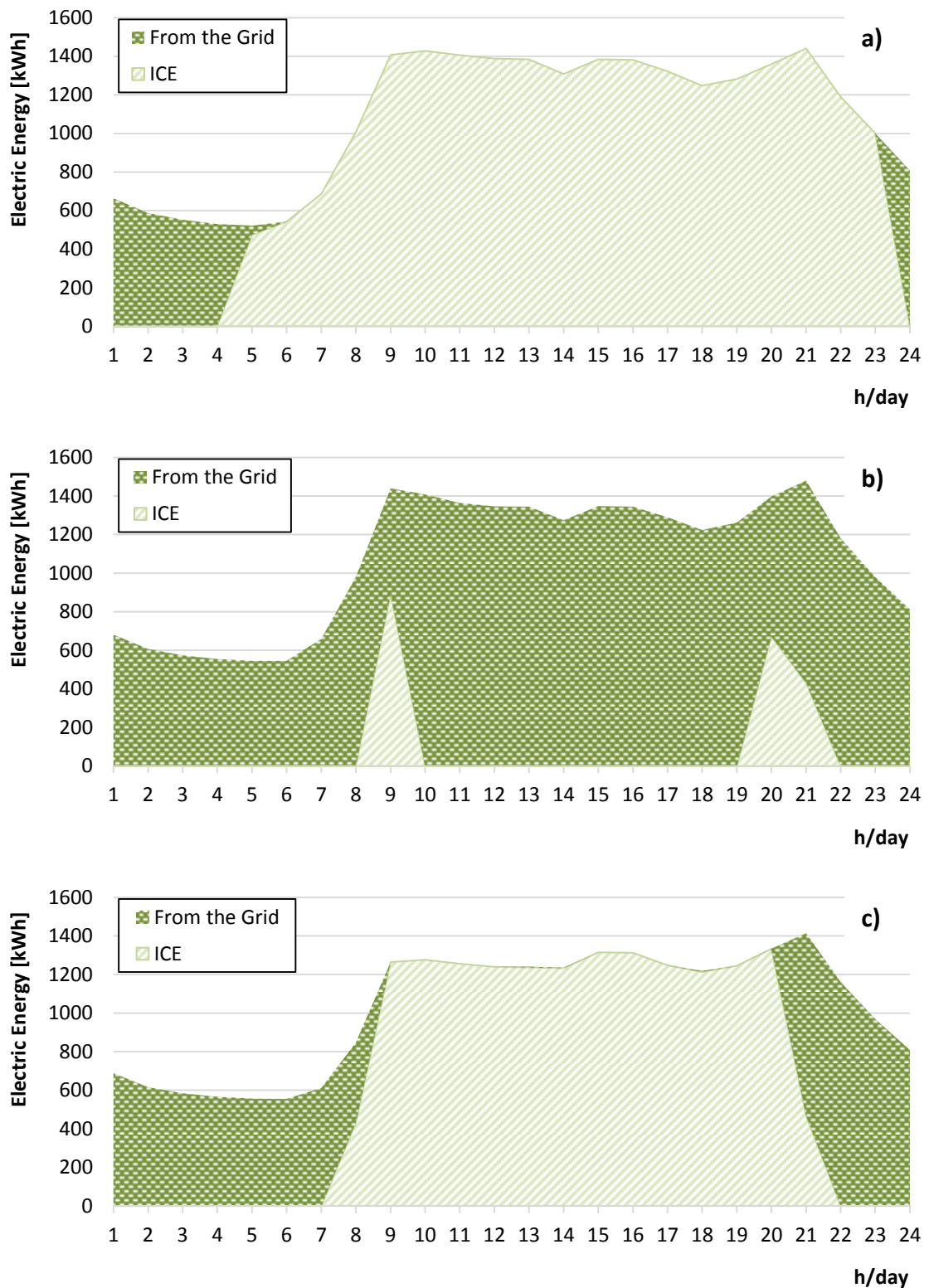


Figure 7.31 – Electricity production profiles (thermal power station) along with the production systems mix for the Case B: a) typical winter day, b) typical middle season day, c) typical summer day.

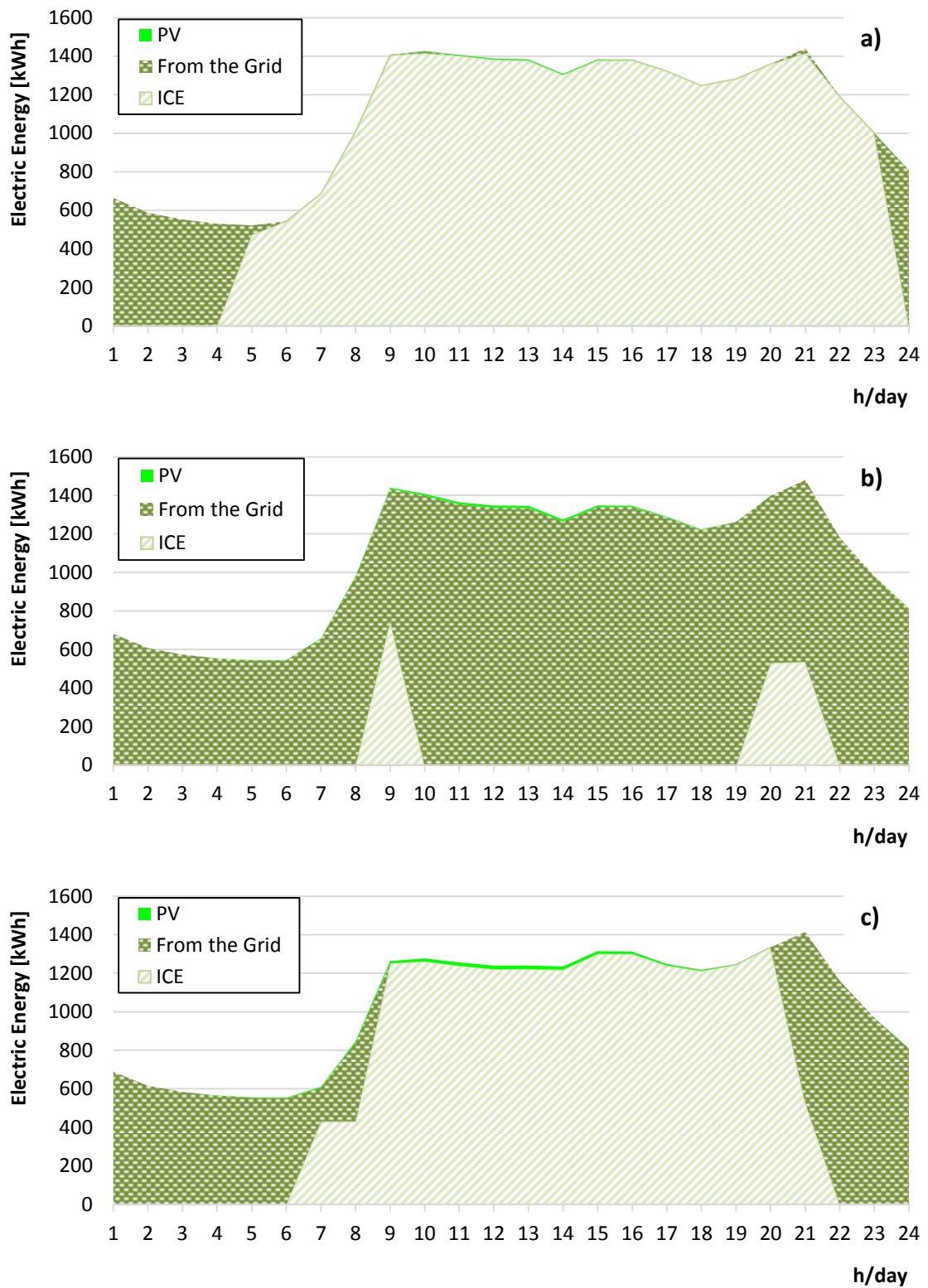


Figure 7.32 – Electricity production profiles (thermal power station) along with the production systems mix for the Case C: a) typical winter day, b) typical middle season day, c) typical summer day.

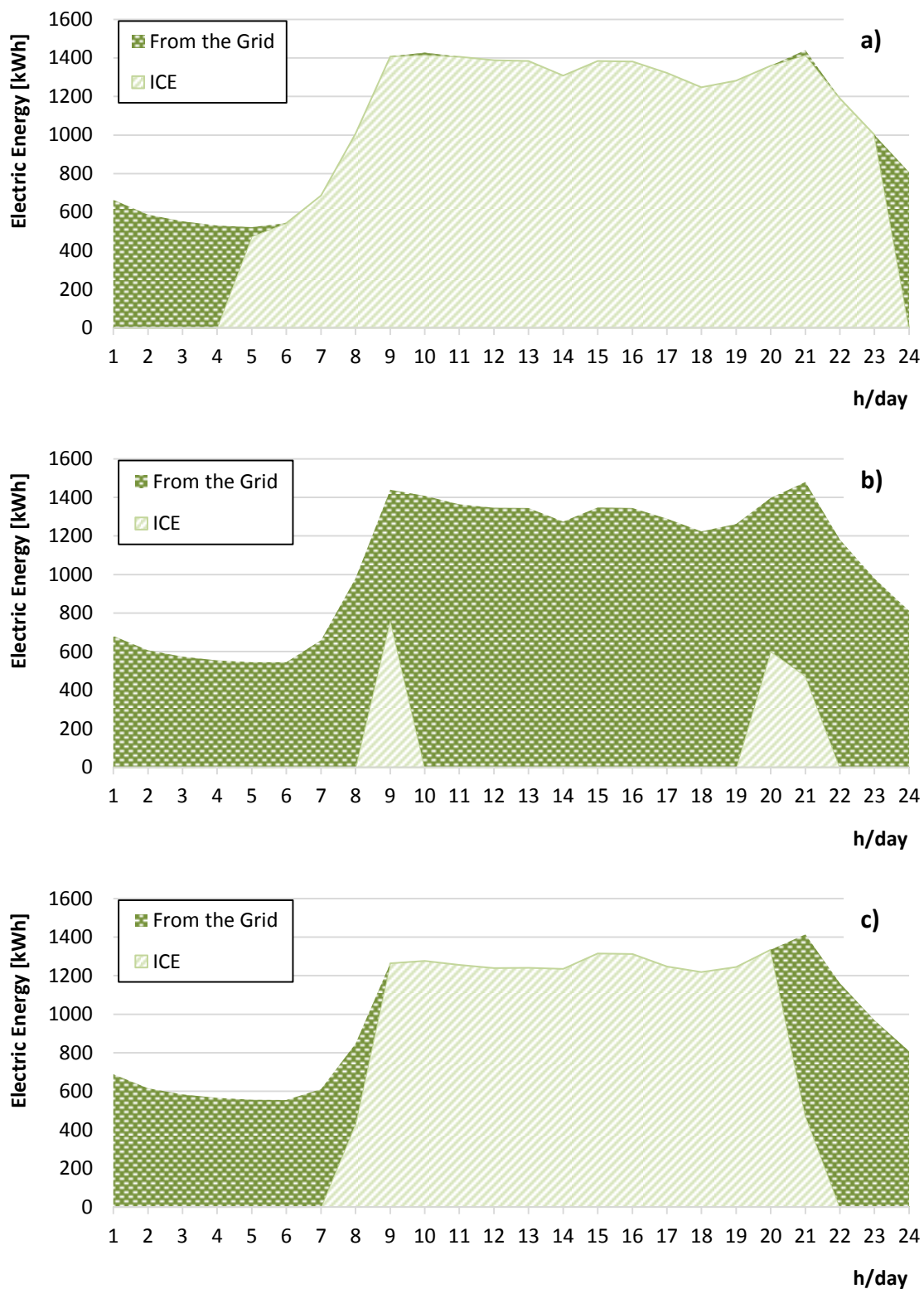


Figure 7.33 – Electricity production profiles (thermal power station) along with the production systems mix for the Case D: a) typical winter day, b) typical middle season day, c) typical summer day.

The PV panels allow in Case C (Figure 7.32) a further reduction in the electricity purchase from the national electric grid, as well as a decrease in the ICE employment for electric needs fulfillment especially during summertime. Finally, Figure 7.33 presents the results for the Case D: profiles very similar to the ones discussed for the Case B can be observed for the typical days in summertime and in middle season, while the same profile of the Case A is obtained for wintertime.

Relating to the cooling energy production mix, the following main considerations can be made:

- The optimization of the scheduling for the currently installed production systems led to the cooling energy production mix shown in Figure 7.34. As it can be seen, absorption chillers operate between 6 a.m. to 9 p.m., but the major load is satisfied by means of compression chillers;
- due to the introduction of the second internal combustion engine, for Case B the compression chillers employment increases in the morning, between 6 a.m. and 8 a.m., but it decreases in the other hours (Figure 7.35);
- the PV panels installed in Case C allow to reduce the ICE production during summertime, with a consequent increase in the absorption chillers operation with respect to Case B (see Figure 7.36);
- the thermal solar panels installation produces an increase in the absorption chillers operation (Figure 7.37).

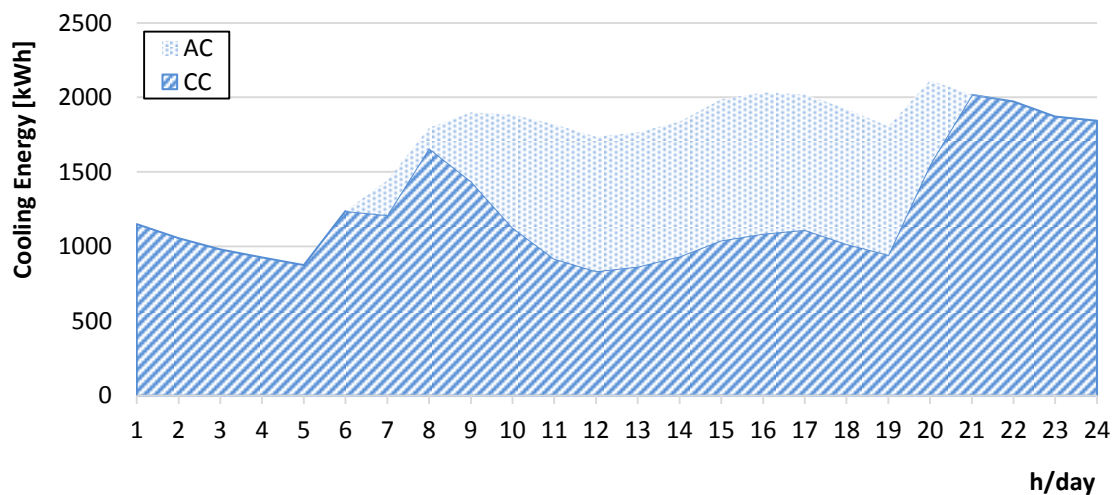


Figure 7.34 – Cooling energy production profiles (thermal power station) along with the production systems mix for the Case A during a typical summer day.

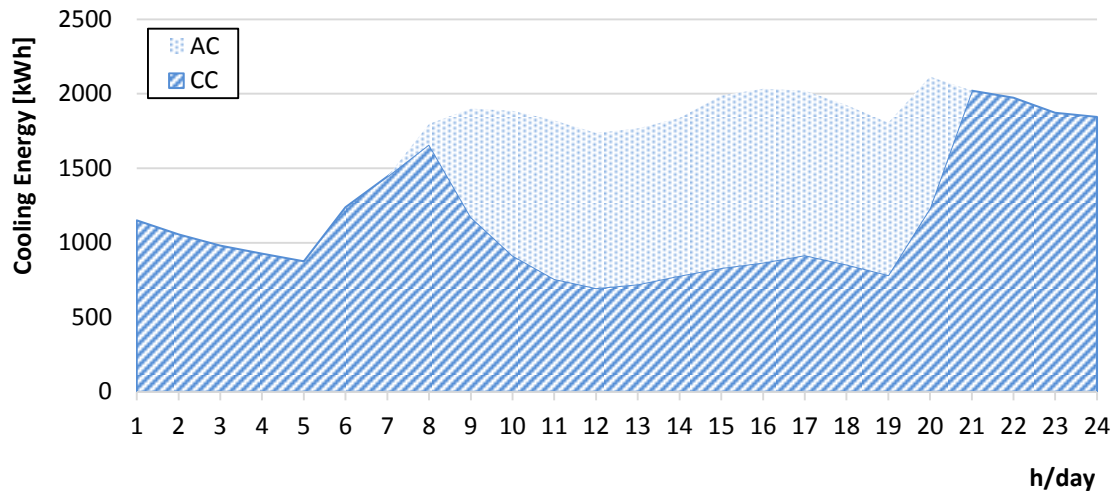


Figure 7.35 – Cooling energy production profiles (thermal power station) along with the production systems mix for the Case B during a typical summer day.

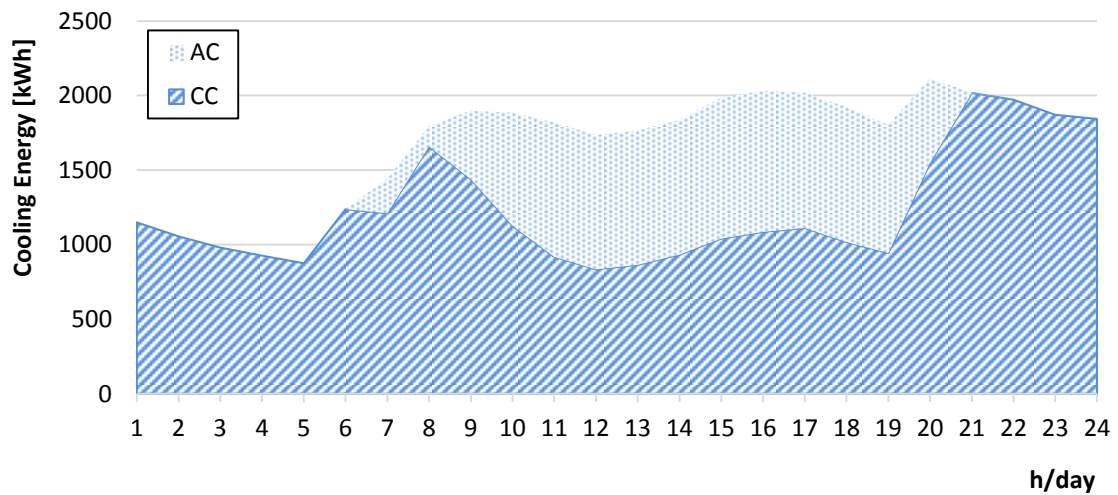


Figure 7.36 – Cooling energy production profiles (thermal power station) along with the production systems mix for the Case C during a typical summer day.

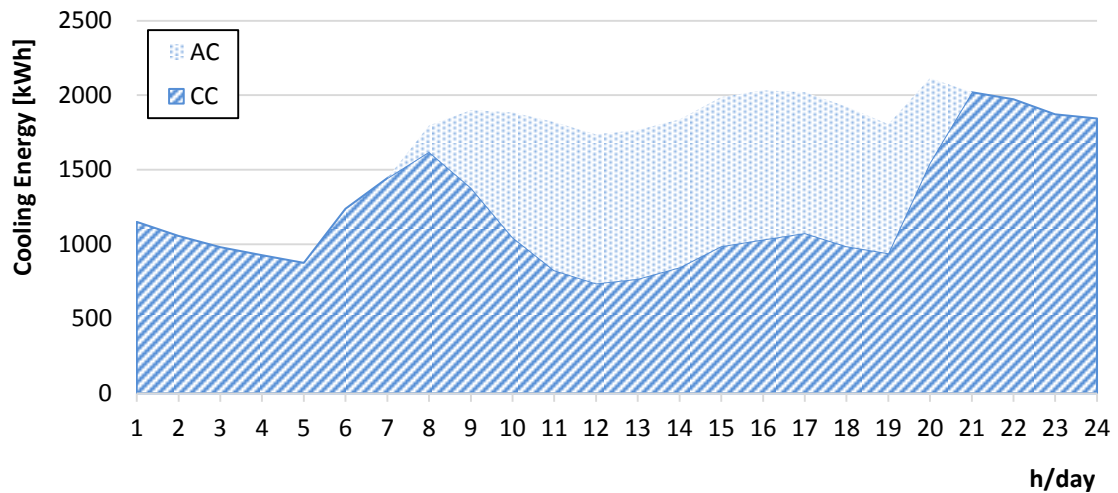


Figure 7.37 – Cooling energy production profiles (thermal power station) along with the production systems mix for the Case D during a typical summer day.

Based on the hourly results of the simulations carried out with the software EGO, the evaluation of the yearly fuel consumption at the centralized power plant, the yearly purchase of electric energy from the grid and the yearly sale of the produced electricity surplus to the grid has been made. In detail, the winter period consists in 183 days (as defined by the national regulations for the considered location), while the middle season and the summer period are composed respectively by 90 days and 92 days. Thus, the obtained annual fuel consumption (ICE and auxiliary boilers) for each of the analyzed cases is presented in Figure 7.38. As it can be noted, excepting for the Case B, a fuel consumption increase is registered with respect to the Reference Case, with a maximum consumption slightly lower than 38'000 MWh/y for the Case A. However, this evidence does not reflect the fact that in the proposed configurations the power station fulfills thermal, electric and cooling needs of the users, whereas in the Reference Case only the thermal ones are accounted. As it can be seen in the bar graph presented in Figure 7.39, indeed, the electrical energy to be purchased during a year from the national electric grid importantly decrease (a reduction equal to more than the 50% is obtained, from 10'000 MWh/y of the Reference Case to around 4'500 MWh/y of the proposed configurations). Furthermore, the Case B seems to be the most promising one, due to the decrease of both fuel consumption and electricity purchase with respect to the Reference Case.

Finally, as presented in Figure 7.40, all the proposed set-up and their scheduling optimization allow, during the whole year, to completely avoid the introduction of electric energy into the national grid, with the consequent benefits for its stability and management.

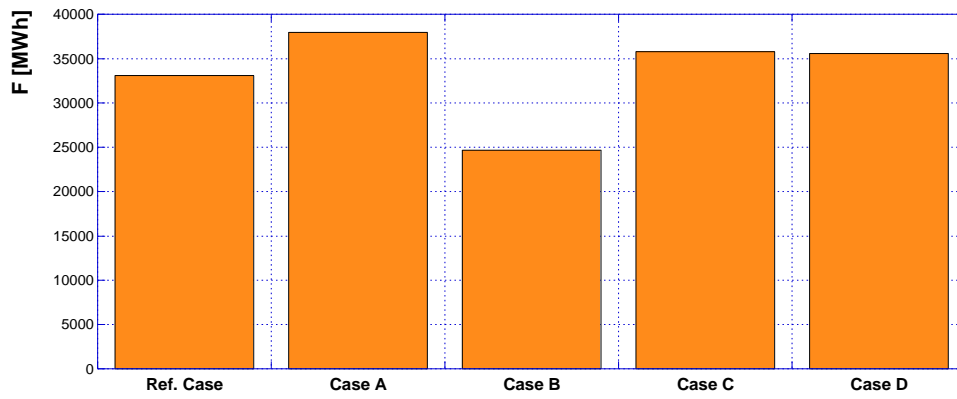


Figure 7.38 – Yearly fuel consumption (ICE and auxiliary boilers).

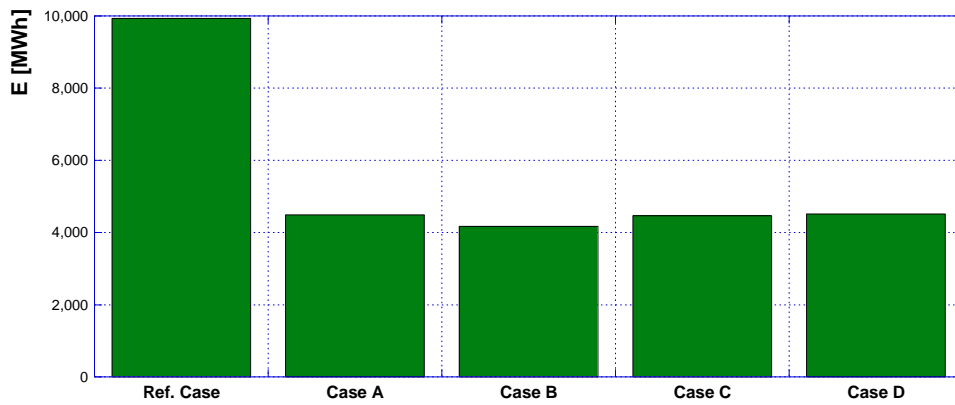


Figure 7.39 – Yearly electricity purchase from the National Electric Grid.

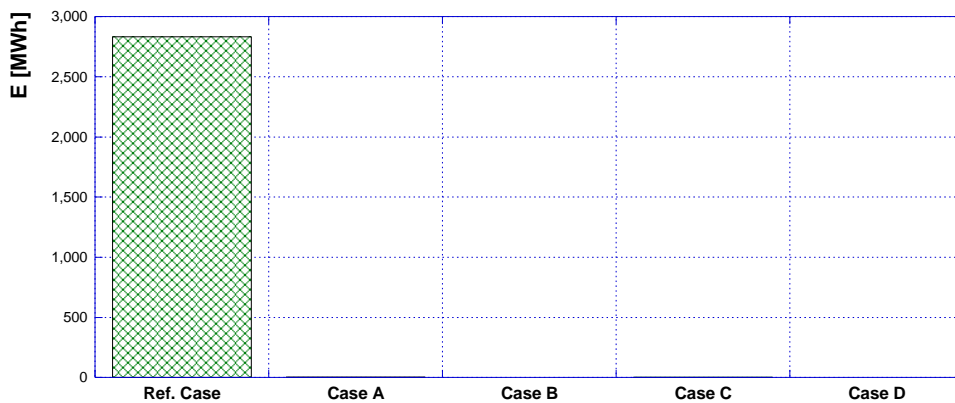


Figure 7.40 – Yearly electricity sold to the National Electric Grid.

In order to better compare the new proposed solutions with the Reference Case, the total fuel consumption required for the complete fulfillment of thermal, electrical and cooling needs of the network connected users has been calculated. In other words, in addition to the Corticella power plant fuel consumption presented in Figure 7.38, also the fuel consumption required to produce the purchased electricity has been accounted. This latter amount has been determined assuming that the electricity purchased from the national grid is produced only by thermo-electric systems (so the worst case in terms of fuel consumption is analyzed in a conservative manner) and considering a mean conversion efficiency for the national thermo-electric fleet equal to 40.2% [15]. The results are presented in Figure 7.41: as it can be seen, a reduction of both the total fuel consumption for the users' needs fulfillment and of the fuel consumption at a national level for electricity production is registered. This result is particularly positive considering national and international objectives in the energy field. Finally, it should be pointed out that the fuel saving presented in Figure 7.41 has been evaluated based only on the electricity purchase reduction, but further benefits related to the distribution losses are achieved.

Furthermore, the calculated fuel saving allows the determination of the CO₂ avoided emissions (see Figure 7.42), achievable with the analyzed configurations with respect to the Reference Case. For the sake of simplicity, the calculation has been carried out considering natural gas employment. The developed evaluations show the possibility of achieving a CO₂ emissions reduction ranging from slightly more than 1700 tons/y (Case A) to around 4500 tons/y (Case B). These final considerations confirm the Case B as the most promising case for the analyzed network.

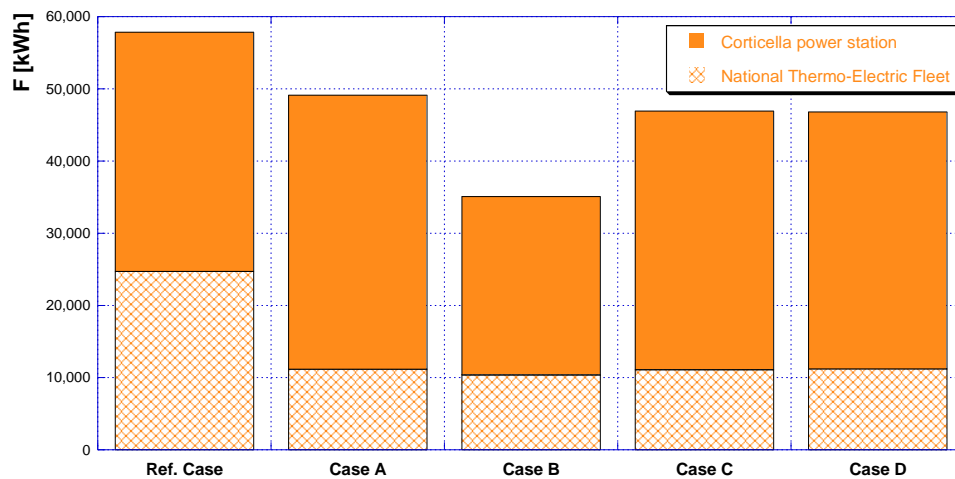


Figure 7.41 – Total yearly fuel consumption for the production of thermal, electrical and cooling energies (centralized power station of the network and National Thermo-Electric Fleet).

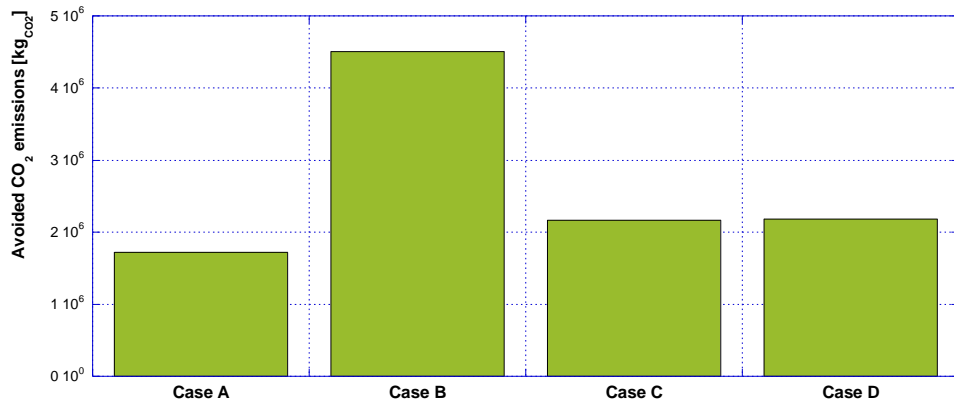


Figure 7.42 – CO₂ avoided emissions with respect to the Reference Case.

References

- [1] Ancona MA, Melino F. Analisi di soluzioni progettuali per la trasformazione di reti di teleriscaldamento esistenti in reti poligenerative con presenza di scambio attivo. Report Ricerca di Sistema Elettrico, Accordo di Programma Ministero dello Sviluppo Economico – ENEA, Piano Annuale di Realizzazione 2014, Area: Razionalizzazione e risparmio nell'uso dell'energia, Progetto: C.1. Risparmio di energia elettrica nei settori: civile, industria e servizi, Report RdS/PAR2014/019.
- [2] Macchi E, Campanari S, Silva P. La microgenerazione a gas naturale. 2005, Polipress ISBN: 8873980163.
- [3] Italian framework on heating and cooling, UNI 10349. http://uni.com/index.php?option=com_content&view=article&id=4819%3Ariscaldamento-o-e-raffrescamento-degli-edifici-pubblicata-la-serie-nazionale-uni-10349&catid=170&Itemid=2612.
- [4] Bianchi M, Spina PR, Tomassetti G, Forni D, Ferrero E. Le tecnologie innovative ed efficienti nei sistemi di generazione in assetto co-trigenerativo e nei sistemi integrati con unità a pompa di calore nelle applicazioni industriali e del terziario. Report RSE/2009/18.
- [5] Baldi F, Ahlgren F, Melino F, Gabrielli C, Anderson K. Optimal Load Allocation of Complex Ship Power Plant. *Energy Conversion and Management*, 124 (2016) 344-356. doi:10.1016/j.enconman.2016.07.009.
- [6] Ancona MA, Bianchi M, Diolaiti E, Giannuzzi A, Marano B, Melino F, Peretto A. A Novel Solar Concentrator System For Combined Heat And Power Application In Residential Sector. *Applied Energy*, 185 (2017) 1199-1209. doi: 10.1016/j.apenergy.2016.03.026.
- [7] <http://www.solaritaly.enea.it/>
- [8] Bianchi M, Branchini L, Ferrari C, Melino F. Optimal Sizing Of Grid-Independent Hybrid Photovoltaic-Battery Power Systems For Household Sector. *Proceedings of ICAE 2013*. Pretoria, South Africa. July 1-4, 2013.
- [9] Bianchi F, Altomonte M, Cannata ME, Fasano G. Definizione degli indici e livelli di fabbisogno dei vari centri di consumo energetico degli edifici adibiti a scuole - consumi energetici delle scuole primarie e secondarie, Report RSE/2009/119.
- [10] Ancona MA, Bianchi M, Biserni C, Melino F, Salvigni S, Valdiserri P. Optimum Sizing of Cogeneration for a Hospital Facility: Multi-Objective Analysis Applied to a Case Study. *Proceedings of 16th International Conference on Sustainable Energy Technologies*, SET 2017. July 17-20, 2017, Bologna, Italy.
- [11] UNI/TS 11300, Prestazione energetica degli edifici - Calcolo del fabbisogno di energia per il riscaldamento e il raffrescamento.
- [12] UNI EN ISO 7730, Ergonomia degli ambienti termici – Determinazione analitica e interpretazione del benessere termico mediante il calcolo degli indici PMV e PPD e dei criteri di benessere termico locale.

- [13] Caredda FV. Diagnosi Energetica dell'Azienda Ospedaliera "G. Brotzu", Tesi di Dottorato di Ricerca, Università degli Studi di Cagliari, Anno Accademico 2011/2012.
- [14] Arteconi A, Brandoni C, Polonara F. Distributed generation and trigeneration: Energy saving opportunities in Italian supermarket sector. *Applied Thermal Engineering*, 29 (2009) 1735-1743.
- [15] <http://data.enel.com/node/4748?language=it>

8. Optimization analysis – case study II

In this chapter a further case study will be presented and discussed, consisting of an isolated energy grid. This case – represented by a cruise ship – is particularly interesting due to the lack of connection with both the electricity grid and the gas distribution network. The software EGO – opportunely adapted – has been applied in order to optimize the cruise ship energy systems set-up and operation.

8.1 Case Study

The aim of this analysis was the scheduling optimization for an existing cruise ship, operating in the Baltic Sea between Stockholm (in Swedish mainland) and Mariehamn (in the Åland islands). The vessel of the considered ship is 177 meters long and about 28 meters wide, operating with a design speed equal to 21 knots. Because of its capacity – up to 1'800 passengers – this vessel can be considered as a medium size cruise ship. Furthermore, the ship is equipped with restaurants, clubs and bars, as well as saunas and pools.

The daily route made every day by the ship during the whole year (365 days/year) is the one shown in Figure 8.1. On the basis of this route and according to the available information, the ship annual operation can be divided among (i) sea going, (ii) port and sea stay and (iii) maneuvering, as presented in Figure 8.2. These three different operation phases account, respectively, for the 59%, 33% and 8%. Thus, it can be noted that – even if the sea going obviously represents the majority of the ship mode of operation – the port and sea stay operation accounts for around one third of the total operational profile.

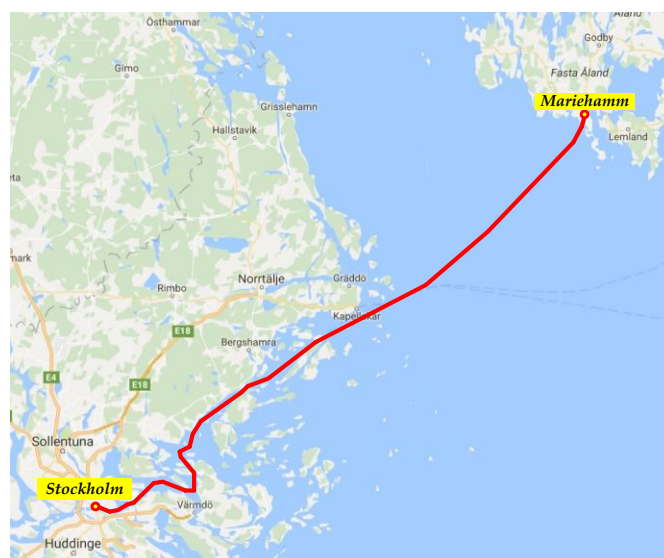


Figure 8.1 – Schematic of the cruise ship route.

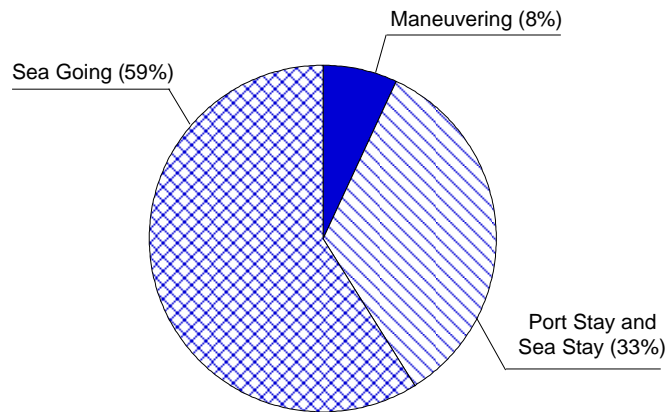


Figure 8.2 – Cruise ship mode of operation during a year.

The energy demand of the considered ship consists of (i) mechanical energy (for propulsion), (ii) electrical energy (for lighting, cold appliance, hot appliance, auxiliary systems, etc.), (iii) thermal energy (mainly for space heating and hot water production) and (iv) cooling energy (only during the summer period). Obviously, as detailed in the following, the energy needs varies depending on the season and the mode of operation of the ship.

As for the vessel typical operational profile, it is the same every day: the departure from Stockholm is scheduled around 6:00 p.m., then the ship reaches the open sea, where it stops for few hours during the night before reaching Mariehamn port early in the morning. Then, the ship leaves Mariehamn around 9:00 a.m., to go back to Stockholm where the arrivals is scheduled around 4:00 p.m..

As previously said, the thermal and cooling energy requests are different depending on the considered season – since the travel's conditions (*i.e.* weather condition) change. As it regards the mechanical energy demand, instead, no variations can be appreciated during the year.

The characterization of the energy needs of the ship could be done according to the ship operational modes and with the following considerations:

- when the cruise ship is at the harbor (*port stay*) or it lays in open sea (*sea stay*), the demand consists of electrical and thermal energy (and cooling energy during the summertime), in order to guarantee the ship services for the boarding and alighting procedures of the passengers (*port stay*) and for their comfort on board (*sea stay*);
- during the sailing (*sea going*) the demand reaches its maximum values in terms of mechanical demand;
- when the ship enters or leaves the port (*maneuvering*) the mechanical demand is intermediate between the one of sea going and the one corresponding to port stay or sea stay;
- the electrical and thermal (for space heating and/or hot water production) demands are not influenced by the operational profiles of the ship, but only by the season.

The aforementioned considerations, together with an experimental data collection made on board [1], allowed to estimate the hourly load profile curves of mechanical, thermal, electrical and

cooling powers for typical days during wintertime, summertime and middle season, as presented in Figure 8.3. More details about the elaboration of these curves can be found in [1].

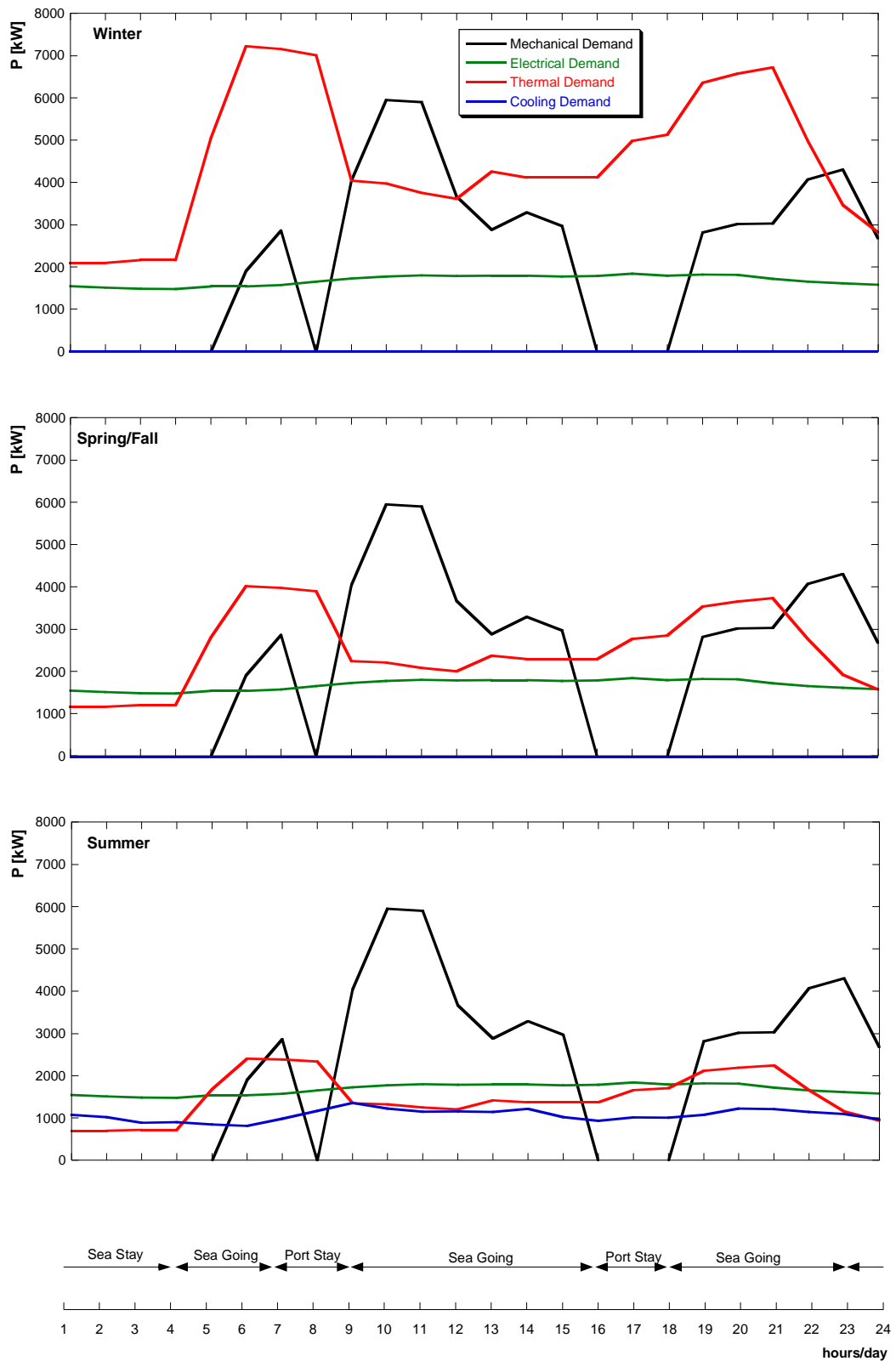


Figure 8.3 – Hourly load curves for typical days in wintertime, summertime and middle season.

Relating to the duration of each season, according to the average monthly temperatures in Sweden [2], the following assumptions can be made:

- wintertime: 182 days (since January the 1st to April the 15th and since October the 16th to December the 31st);
- summertime: 62 days (since July the 1st to August the 31st);
- middle season: 121 days (since April the 16th to June the 30th and since September the 1st to October the 15th).

From Figure 8.3 it can be observed that both the mechanical power (for propulsion) and the electrical power demands maintain the same daily profile for each season. Furthermore, as for the mechanical power, it is possible to note that it is equal to zero during the port stay and when the ship is drifting offshore. This behavior is consistent with the fact that the movement of the propellers, generated by the mechanical power, is stopped when it is not necessary to the movement of the ship.

As it regards the thermal power, the summertime need is almost entirely due to hot water request, while during wintertime and also in middle season space heating accounts for a large part of the thermal needs. The peak of thermal power is equal to slightly more than 7 MW and obviously occurs in wintertime around 7:00 a.m..

Finally, it can be observed that electrical and thermal powers are always present. This evidence can be explained considering that the continued operation of safety systems (smoke detectors, gas detectors, fixed fire-fighting equipment, alarms, emergency lights, etc.) and minimum comfort on-board (lighting, entertainment, space heating, hot water, etc.) are ensured. Moreover, being the analyzed vessel used for passengers transport, electrical power (in addition to lighting, also for equipment for the preservation and preparation of food, refrigerators, etc.) and thermal power (for example for the heating of the cabins) must always be guaranteed, also during the port stay phase. On the other hand, during the summer a cooling power is required and, as it can be noted from the figure, its trend is almost constant with an average value around 1'000 kW.

8.2 Energy systems

The ship is currently equipped with eight marine diesel engines (PM) according to the scheme presented in Figure 8.4, named Base Case. Four *main engines* (4× Wärtsilä 6L46 – from PM#01 to PM#04 in Figure 8.4), for mechanical power production, and four *auxiliaries engines* (4× Wärtsilä 6L32 – from PM#05 to PM#08 in Figure 8.4), for electrical power production, are installed. The PMs design performance are presented in Table 8.1.

Table 8.1 – Internal combustion engines design performance [3, 4].

Model	Wärtsilä 6L46	Model	Wärtsilä 6L32
Mechanical Power [kW]	5850	Electrical Power [kW]	2760
Thermal Power [kW]	6081	Thermal Power [kW]	3049
Mechanical Efficiency [-]	0.44	Electrical Efficiency [-]	0.43
Thermal Efficiency [-]	0.46	Thermal Efficiency [-]	0.47

All the on board engines are medium speed engines [5, 6] characterized by 500 RPM and 750 RPM, respectively for main and auxiliary engines.

As it can be observed from Figure 8.4, the main engines are divided into two groups (gearboxes), each one providing energy to only one propeller. The mechanical load has to be equally divided between the two propellers: it follows that at least two main engines are always operated when mechanical power is requested.

The ship thermal demand can be satisfied by recovering waste heat from all the eight engines and by the use of two auxiliary boilers. The latter are characterized by a maximum thermal power output equal to 4 500 kW (each) and by a thermal efficiency in design condition equal to the 80%. Furthermore, a compression chiller is included for cooling power production. This chiller shows a maximum cooling power output equal to 2 000 kW, with a design EER assumed equal to 3.5.

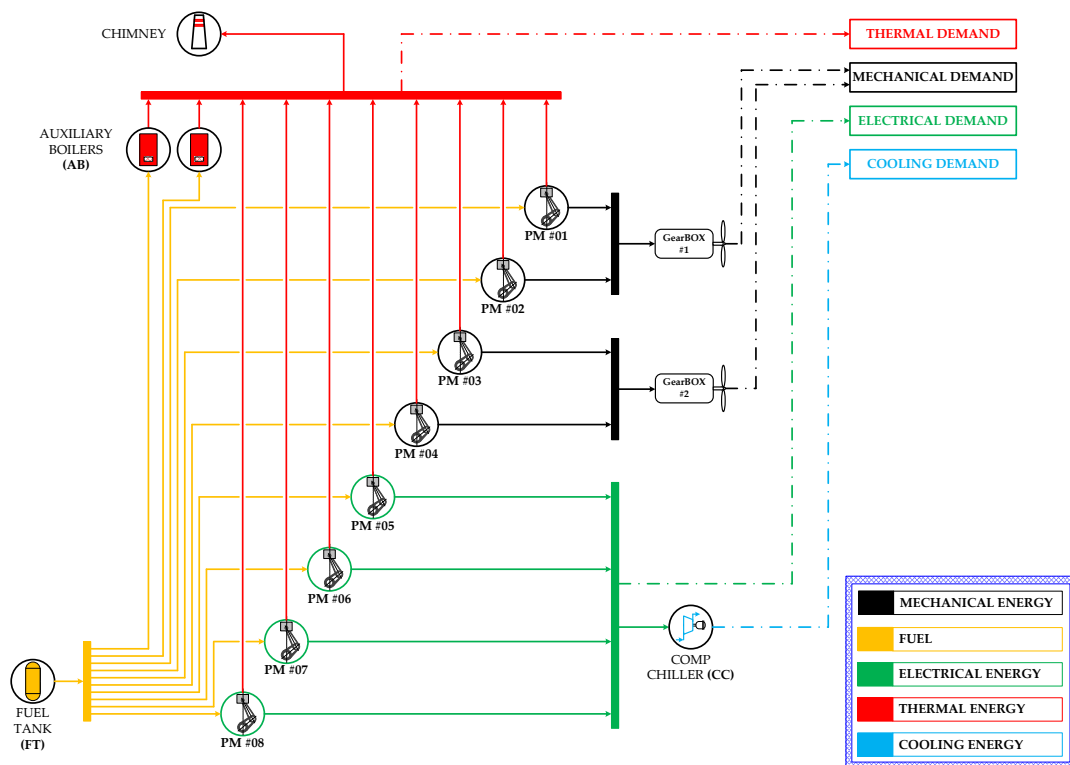


Figure 8.4 – Base Case (BC) layout.

In order to determinate the optimal configuration and operational strategy for the energy systems of the considered ship, five different configurations have been proposed and analyzed in addition to the Base Case. The Base Case and the first two new proposed strategies are characterized by a standard configuration, typical for this kind of ships. On the other hand, the remaining three

strategies, are characterized by a hybrid engines configuration, which at present is broadly used on the military ships.

In detail:

- Base Case (BC) – the first strategy considers the energy system scheme presented in Figure 8.4, corresponding to the current configuration of the vessel, and performs the current mode of operation of the ship. In this case, both the mechanical and electrical powers are satisfied by equally sharing the production among the corresponding engines.
- Optimized Load (OL) – in this second strategy the energy systems set-up is again the one shown in Figure 8.4. However, differently from the previous case, the load of each engine is determined by the developed optimization software, in order to minimize the fuel consumption and the wasted thermal energy.
- Optimized Load with Storage (OL-S) – in this case, with respect to the previous energy systems configuration (see Figure 8.4), a thermal storage device has been added. The related set-up scheme is shown in Figure 8.5. As for the case OL, also in this case the load of each engine is determined by the software EGO.
- Hybrid (HY) – compared to the previous ones, this strategy is characterized by a different engines mode of operation – as is shown in Figure 8.6. In this case, indeed, a hybrid system has been considered, in which all the engines produce electrical power and the propulsion is realized by means of two electrical engines instead of the two gearboxes.
- Hybrid with Storage (HY-S) – the engines configuration is the same of the previous case HY with the addition of a thermal storage tank (see Figure 8.7).
- Hybrid with Storage and Absorption Chiller (HY-S-AC) – in this last strategy, the engines configuration derives from the previous HY and HY-S, with the further introduction of an absorption chiller unit, as presented in Figure 7.8.

Each of these configurations has been implemented in the software EGO considering the energy demand profiles presented in Figure 8.3. The calculation has been carried out considering – as already explained – three different typical days (wintertime, summertime and middle season typical days).

Furthermore, relating to the configurations OL-S, HY-S and HY-S-AC, the thermal storage volume has been part of the optimization analysis. The storage volume, indeed, has been estimated in order to minimize both the auxiliary boilers fuel consumption and the thermal energy from the internal combustion engines dispersed through the chimney.

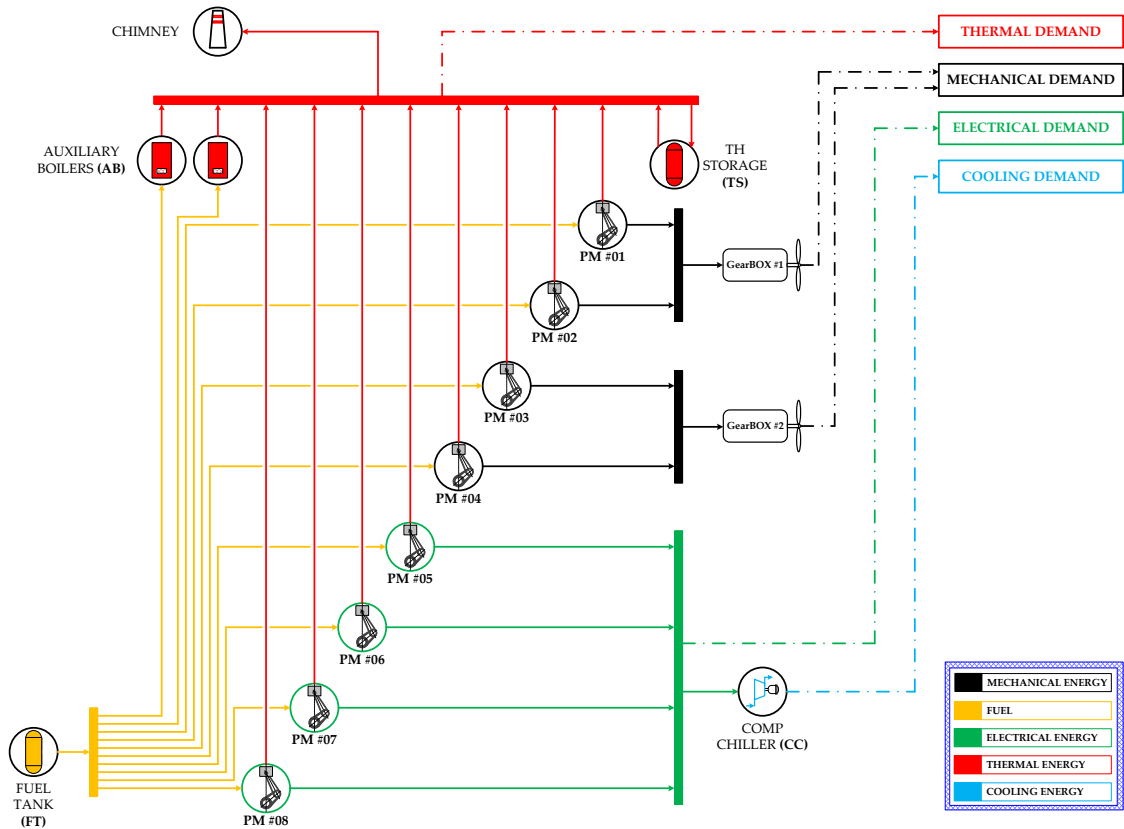


Figure 8.5 – Optimized load with storage (OL-S) layout.

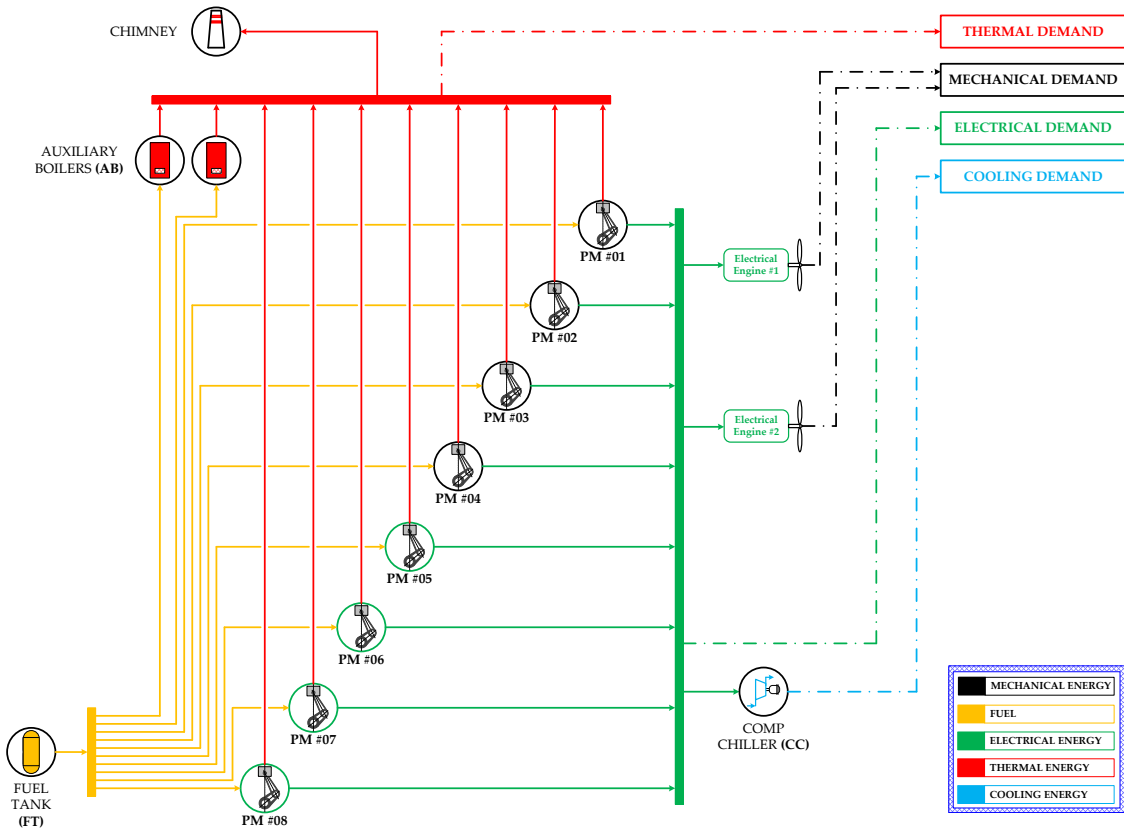


Figure 8.6 – Hybrid (HY) layout.

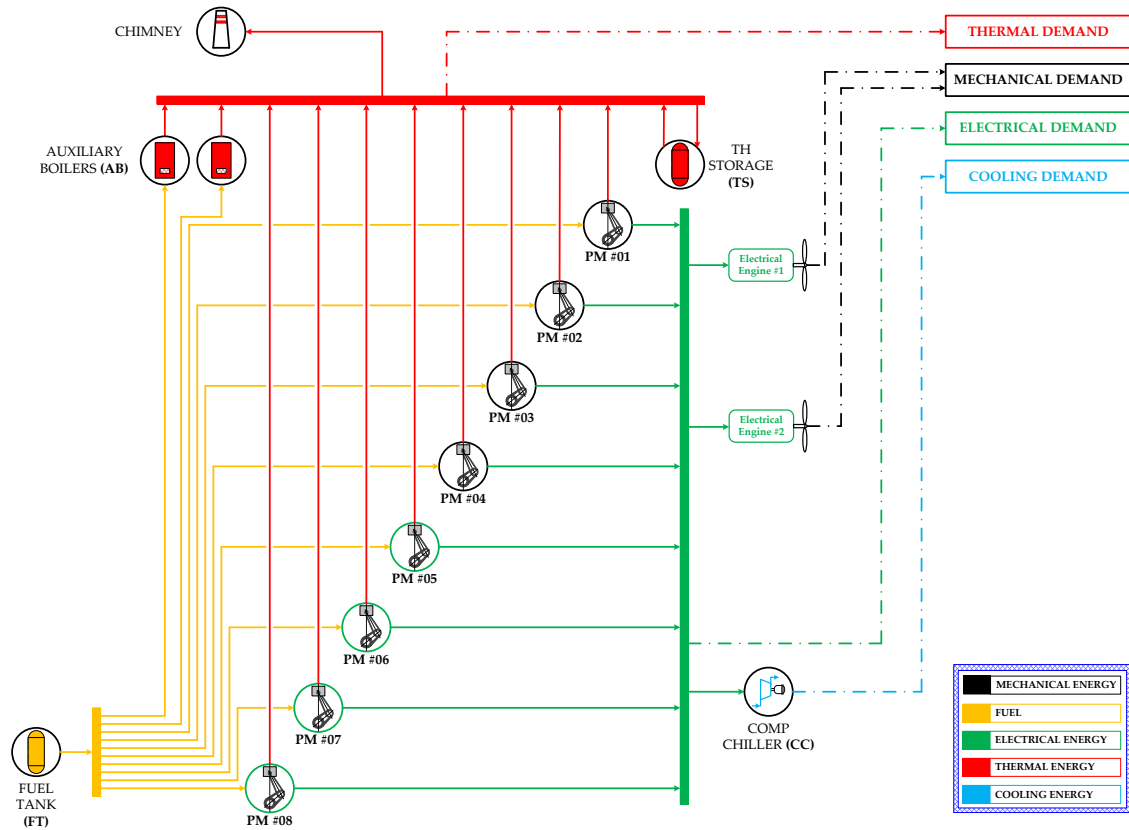


Figure 8.7 – Hybrid with storage (HY-S) layout.

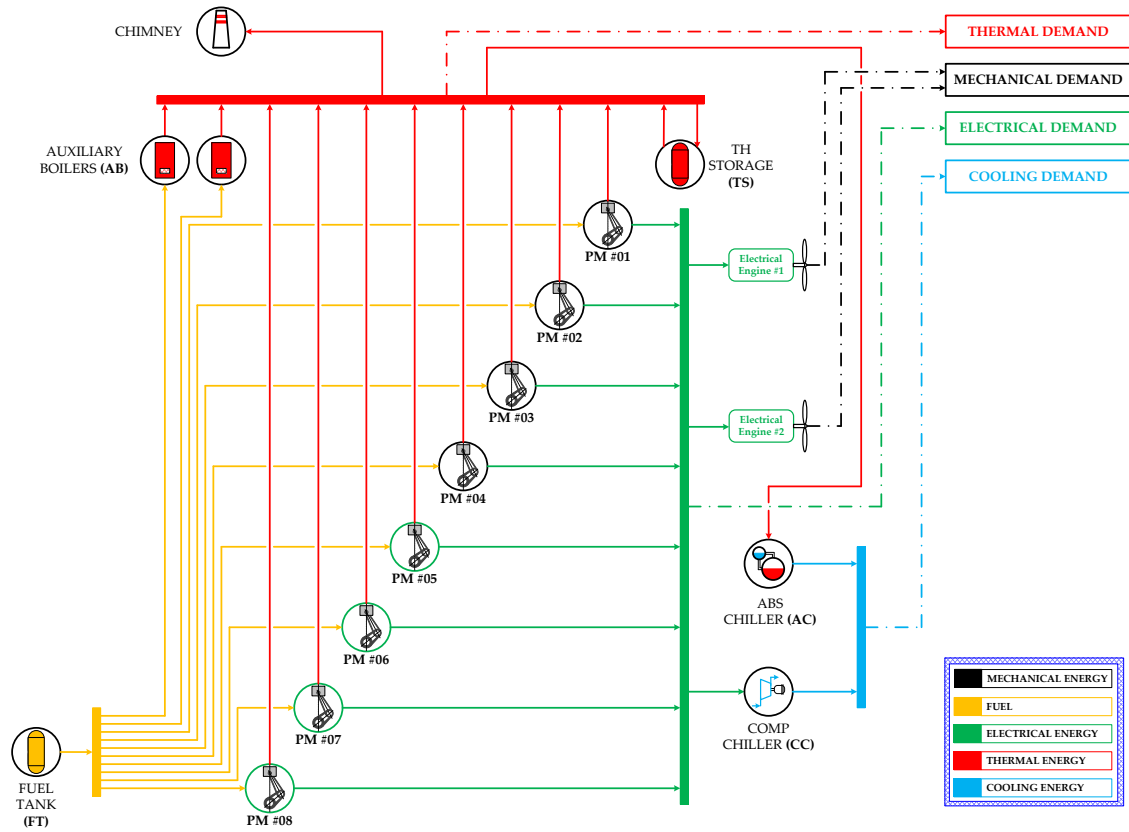


Figure 8.8 – Hybrid with storage and absorber chiller (HY-S-AC) layout.

8.3 Energy Systems Off-design Operation and Others Assumptions

The off-design behavior of the main and of the auxiliary engines has been evaluated according to the curves respectively presented in Figure 8.9 and in Figure 8.10.

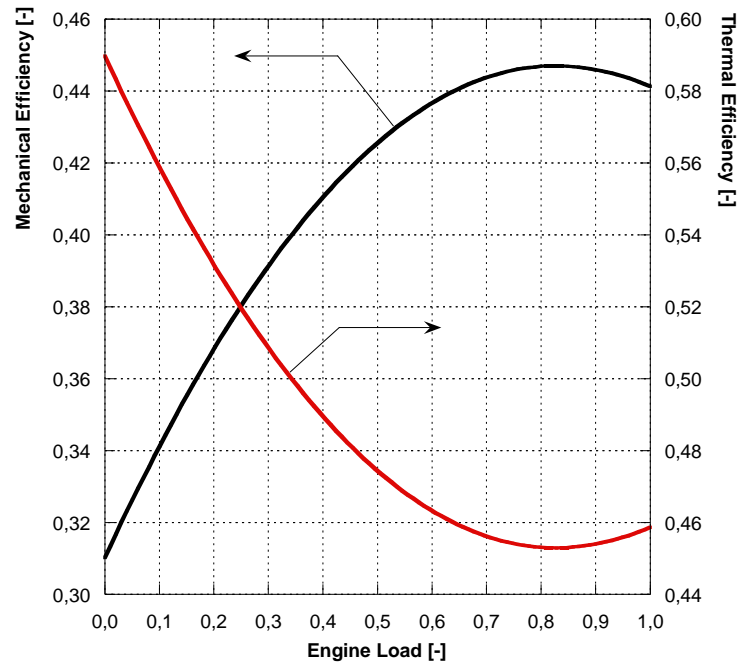


Figure 8.9 – Mechanical and thermal efficiency as function of the load for main engines.

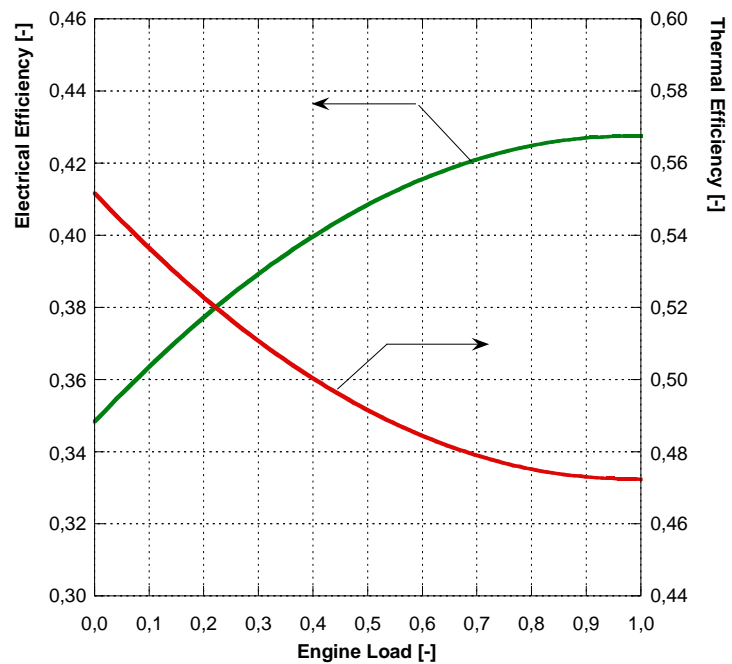


Figure 8.10 – Electrical and thermal efficiency as function of the load for auxiliary engines.

It can be observed that the main engines show a maximum value of the mechanical efficiency (44.7%) for a load equal to the 80%, while – again with reference to the 80% load – the thermal efficiency reaches its minimum value (45.3%). Differently, the auxiliary engines are characterized by a maximum value of electrical efficiency (42.8 %) and a minimum value of thermal efficiency (47.2 %) in correspondence to full load. Further details about the calculation methodology of the curves presented in Figure 8.9 and in Figure 8.10 can be found in [1].

As it regards the auxiliary boilers, instead, the trend of the thermal efficiency as function of the load is presented in Figure 8.11. This curve, which shows the maximum value of the 80% for a load equal to 30%, has been estimated according to the evidence that generally – for marine applications – boilers are characterized by high performance, even at very low loads [7]. Furthermore, the EER trend as function of compression chiller load is presented in Figure 8.12. The plotted trend is typical of this kind of machines and was estimated according to the literature on this matter [8]. Finally, as it regards the EER of the absorption chiller (see HY-S-AC strategy in Figure 8.8), a constant value equal to 0.67 has been considered [8].

Furthermore, as it concerns the thermal storage, a cylindrical insulated tank has been considered with an assumed global heat exchange coefficient equal to 0.5 W/m²K [9]. As previously mentioned, the choice of the optimal volume of the tank is object of the developed analysis. It has been assumed that the storage temperature can vary between a minimum temperature $T_{TES,min}=100^{\circ}\text{C}$ and a maximum temperature $T_{TES,max}=300^{\circ}\text{C}$ [9].

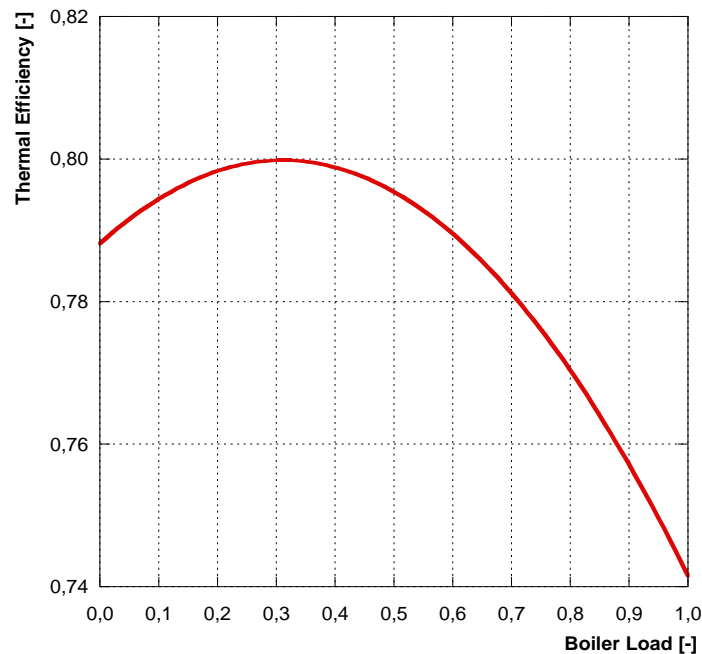


Figure 8.11 – Thermal efficiency as function of the load for auxiliary boilers.

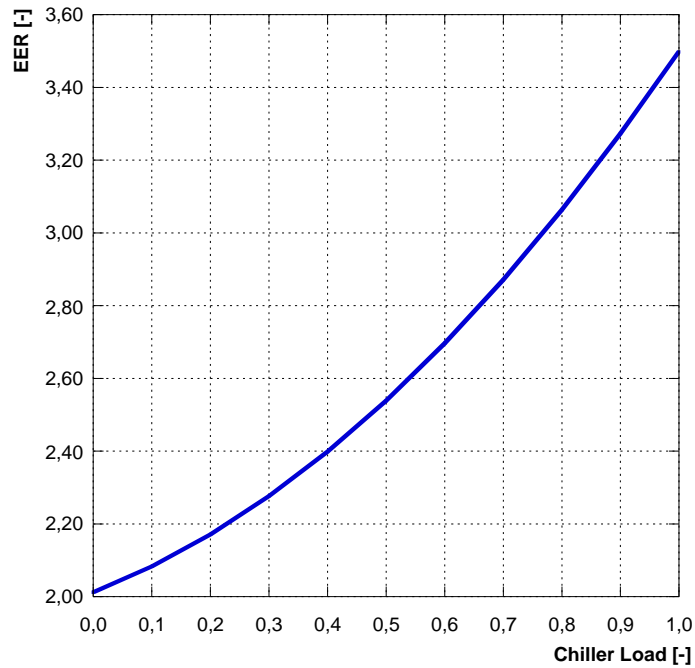


Figure 8.12 – EER as function of the load for the compression chiller.

Relating to the auxiliary components, such as gearbox, frequency converter, etc. (for simplicity not included in the schemes from Figure 8.4 to Figure 8.8, with the exception of electrical engines and of gearboxes between main engines and propellers), a constant value of the efficiency has been taken into account. The assumed values are presented in Table 8.2 [10-12].

Moreover, a constant value of efficiency (equal to 0.97) has been assumed for the distribution of thermal and cooling energies from the production systems to the final users.

Table 8.2 – Auxiliary components efficiencies [10-12].

Component	η_{des}
Gearbox	0.98
Generator	0.97
Electrical Engine	0.96
Frequency converter	0.98
Shaft	0.98

8.4 Energy Results

The two main quantities of interest for the energy production and management optimization of a cruise ship are the fuel consumption and the heat dispersion through the chimney. With the purpose of evaluating these two quantities, their annual amounts on varying the thermal storage volume have been evaluated. Thus, respectively in Figure 8.13 and in Figure 8.14, the yearly fuel consumption of the auxiliary boilers and the annual dispersed thermal energy trends are presented as function of the storage volume, for both standard (BC, OL and OL-S) and hybrid configurations (HY, HY-S and HY-S-AC). As evident, no thermal storage is installed in case of BC, OL and HY configurations (and so the corresponding markers lie on the y-axis), while the optimal storage volumes for the OL-S, HY-S and HY-S-AC strategies are the ones which avoid the auxiliary boilers operation and minimize the heat dispersion. However, as it can be seen from Figure 8.13 and Figure 8.14, these optimal volumes – being equal to 61 m³ and 69 m³, respectively for OL-S strategy and for HY-S and HY-S-AC configurations – are very big and, in some cases, the on board available space may not lead to their installation. Related to this aspect, it should be highlighted that even with lower storage volumes a convenience can be reached. The trends presented in Figure 8.13, indeed, show that the annual fuel consumption of OL and HY configurations increases in comparison with the one of the Base Case strategy (BC), but, with the introduction of the storage tank with thermal storage volumes beyond certain values, the yearly fuel consumption decreases below the BC reference value. As a consequence, a decrease in the annual fuel consumption can be achieved starting from a storage tank of around 12 m³ for the OL-S configuration and around 23 m³ for HY-S and HY-S-AC configurations.

Relating to the thermal energy dispersion through the chimney, instead, from Figure 8.14 it can be seen that all the proposed strategies allow to decrease the analyzed quantity. The best case results the HY-S-AC case, with the optimal storage volume (69 m³).

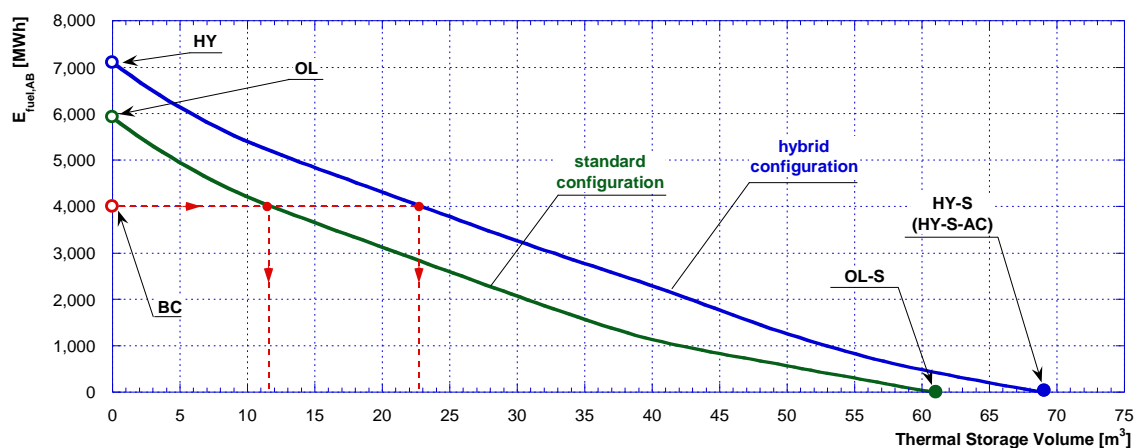


Figure 8.13 – Annual auxiliary boilers fuel consumption as function of the storage volume.

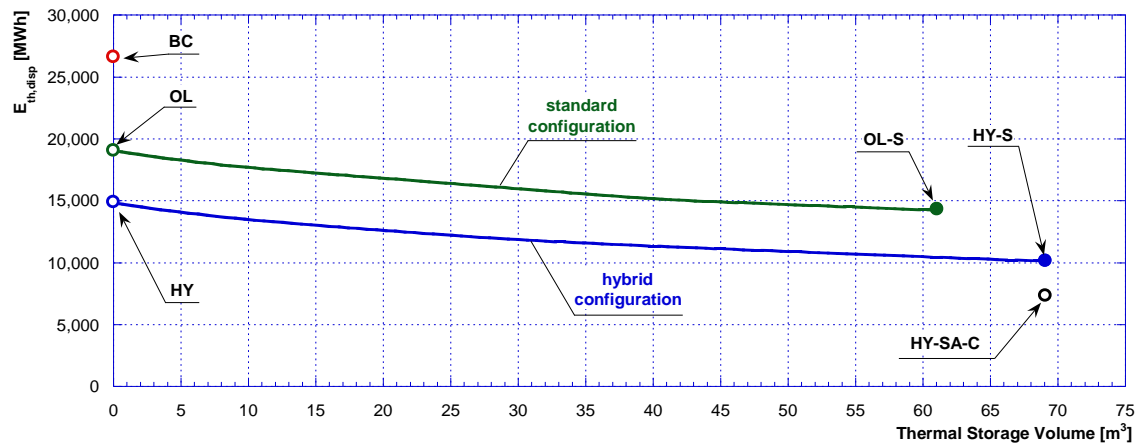


Figure 8.14 – Annual thermal dissipations as function of the storage volume.

On the basis of all the previous considerations, the minimum and the optimal volumes can be fixed for each case. In particular, for the standard configuration they are respectively 11.5 m^3 and 61 m^3 , while for the hybrid configuration they correspond to 22.7 m^3 and 69 m^3 . In detail, the optimal thermal storage volumes (that avoid the boilers fuel consumption) evidently correspond to the maximum volumes which allow to recover all the heat discharged from the engines. In other words, the previous assumption means that the maximum values of thermal storage volumes do not necessarily nullify the dispersed thermal energy (see Figure 8.14). In addition, it should be obviously verified the possibility to install these devices on board, according to the available space.

Furthermore, from Figure 8.13 can be observed that, compared to the standard configuration and the Base Case, the hybrid configuration is always characterized by a higher auxiliary boilers fuel consumption (being the same the storage tank volume) and a higher optimal storage volume. This evidence seems to indicate that better performance can be obtained with the standard configuration. However, for a complete evaluation of the proposed strategies, deeper investigation should be done.

With this purpose, the yearly total fuel consumption, divided between auxiliary boilers and engines, is shown in Figure 8.15, while the annual dispersed thermal energy is reported in Figure 8.16. It must be pointed out that the results presented in these figures refer to the optimal volumes of thermal energy storage devices aforementioned, where implemented (OL-S, HY-S and HY-S-AC strategies). As further proof of this fact, indeed, in these cases no boilers consumption is observed.

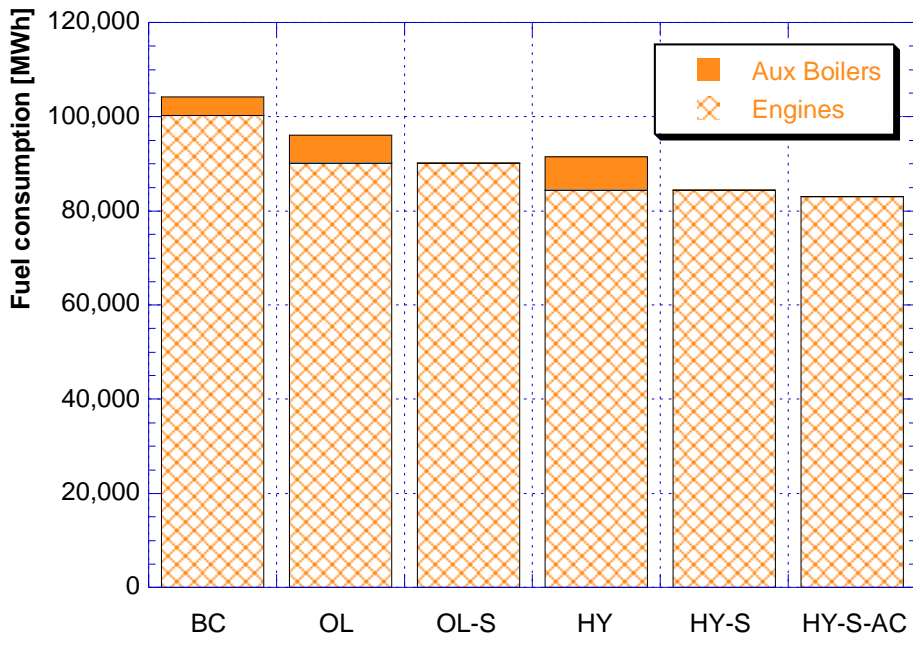


Figure 8.15 – Annual total fuel consumption, divided between auxiliary boilers and engines contributions.

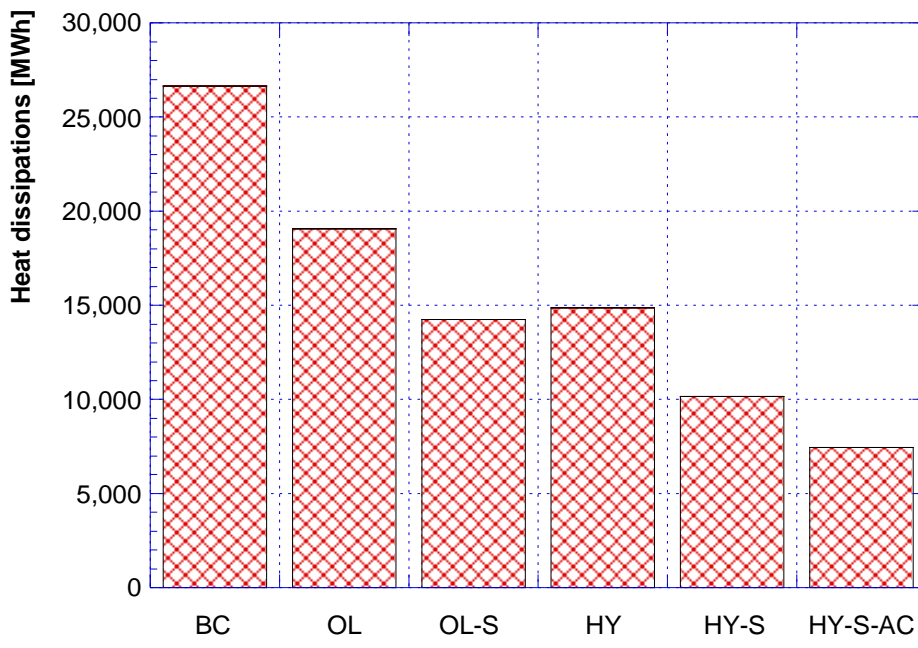


Figure 8.16 – Annual total heat dissipations through the chimney.

From Figure 8.15 it can be noted that the maximum total fuel consumption is achieved with the Base Case, for an overall amount slightly higher than 104'000 MWh/y. In this case the total dispersed thermal energy is equal to more than 26'000 MWh/y (see Figure 8.16). These values decrease with the adoption of an optimal management strategy, as it results from the developed calculation code application (OL). The reductions in fuel consumption and dispersed thermal energy, indeed, are respectively close to 8% and less than 29%. With this regard, it must be noted that the fuel consumption reduction is due to the fact that, moving from BC to OL strategy, a consumption increase equal to around the 47% can be observed for auxiliary boilers (as aforementioned for Figure 8.13), but it is counterbalanced by a consumption decrease for the engines equal to about the 10%. This evidence can be explained considering that the optimal operation of the engines – which results in a different load allocation with respect to the BC – increases the conversion efficiency. As a consequence, being the total produced energy (mechanical, electrical, thermal and cooling energy) equal for each configuration, the available thermal energy from the engines is reduced. In addition, the adoption of the thermal energy storage (OL-S) further reduces the fuel consumption by completely shutting down the auxiliary boilers (as said for Figure 8.13), while the operation of both main and auxiliary engines remains the same of case OL-S. As expected, the optimal volume of thermal storage allows to reduce the dissipated thermal energy down to a value slightly higher than 14'000 MWh for the standard configuration (OL-S strategy), which corresponds to about a 57 % reduction with respect to the BC strategy.

As it regards the hybrid configurations, similarly to the OL case, even the HY strategy allows a reduction of the annual total fuel consumption with respect to the base case (resulting from the increase in auxiliary boilers consumption and from the decrease in engines consumption). However, the total amount of both fuel consumption and dissipated thermal energy is slightly higher than for OL-S configuration. The adoption of a hybrid configuration, in any case, allows a greater flexibility for the engines load allocation: it follows that the engines fuel consumption from OL-S to HY reduces from more than 90'000 MWh/y to 84'400 MWh/y, even if an increase in dispersed thermal energy occurs (equal to about the 4%).

It should be considered that the increase in thermal losses, moving from standard to hybrid configuration, is observed only without considering the thermal storage. The absence of thermal storage, indeed, entails the adoption of auxiliary boilers: in the HY case about 7'100 MWh of fuel consumption are accounted, representing the highest value among all the analyzed configurations. This evidence confirms the fact that the optimization of load allocation involves a reduction in the engines fuel consumption and a contemporary increase in the auxiliary boilers employment. Thus, considering the HY-S strategy, the adoption of the thermal storage allows to nullify the auxiliary boilers fuel consumption and to reduce the dispersed thermal energy down to about 10'000 MWh/y. Furthermore, as already observed for OL and OL-S, also moving from HY to HY-S the thermal storage allows the complete boilers shut down but it does not affect the engines load allocation. Finally, the introduction of absorption chiller (HY-S-AC), enables the further reduction of the dissipated thermal energy (with a decrease of about the 72% and the 27% compared to BC and HY-S respectively). As it regards the fuel consumption, HY-S-AC shows a slightly reduction with respect to HY-S, mainly due to the lower electrical demand of the compression chiller.

In Figure 8.17, the yearly operational equivalent hours (defined as the ratio between the annual produced energy and the design power) are presented for each system (absorption chiller, compression chiller, auxiliary boilers, main engines – from PM#01 to PM#04 – and auxiliary

engines – from PM#05 to PM#08) and for each strategy. It should be highlighted that the reduction of the operational equivalent hours, for a given system, means a reduction of its maintenance costs. Furthermore, from Figure 8.17 it can be noted that – moving from BC to OL and OL-S – no variations occur in the operational equivalent hours of the main engines, the auxiliary engines and the compression chiller. The only difference, in these three cases, stands in the equivalent hours of operation of the auxiliary boilers. Similarly, HY and HY-S are characterized by the same values of operational equivalent hours both in case of main and auxiliary engines. Comparing HY and HY-S with the previous three strategies (BC, OL and OL-S), it can be observed an increase in the operational equivalent hours of the main engines and a decrease in the auxiliary engines ones. This is due to the application of the optimization software, which favors the engines with a greater mechanical conversion efficiency (see Table 8.1). Furthermore, HY strategy shows an increase in auxiliary boilers’ operating hours with respect to the base case (BC), while for the HY-S configuration – as already explained – this value is equal to zero. Obviously, the equivalent hours of operation for the compression chiller do not show any changes referring to strategies from BC to HY-S, while a reduction is obtained for HY-S-AC, due to the use of the absorption chiller. This fact clearly results in a reduction of the electrical load, with a consequent decrease in the operation of auxiliary engines. Finally, a slightly increase in the equivalent hours of the main engines is observed.

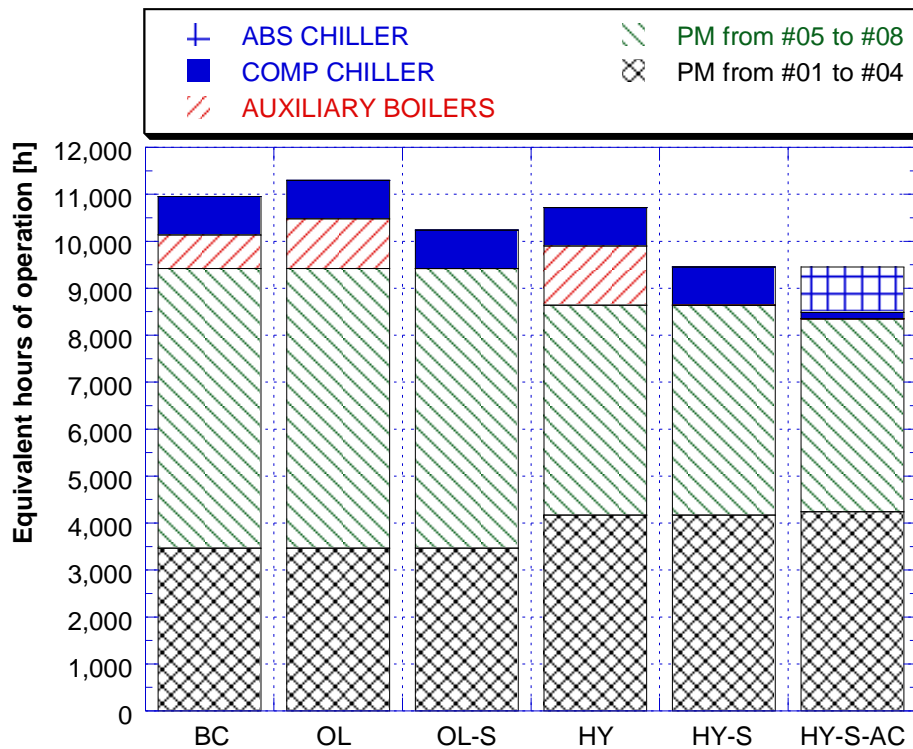


Figure 8.17 – Annual equivalent hours of operation for each strategy and each energy system.

8.5 Economic and Environmental Results

In order to evaluate the annual operational costs for each proposed configuration, the specific costs (for the fuel and for the energy systems maintenance) listed in Table 8.3 have been considered [13, 14]. The obtained results are shown in Figure 8.18.

Table 8.3 – Specific variable costs [13, 14].

	Costs [€/kWh]
Fuel	0.0843
Main Engines maintenance	0.0150
Auxiliary Engines maintenance	0.0150
Auxiliary Boilers maintenance	0.0060
Compression Chiller maintenance	0.0050
Absorption Chiller maintenance	0.0025

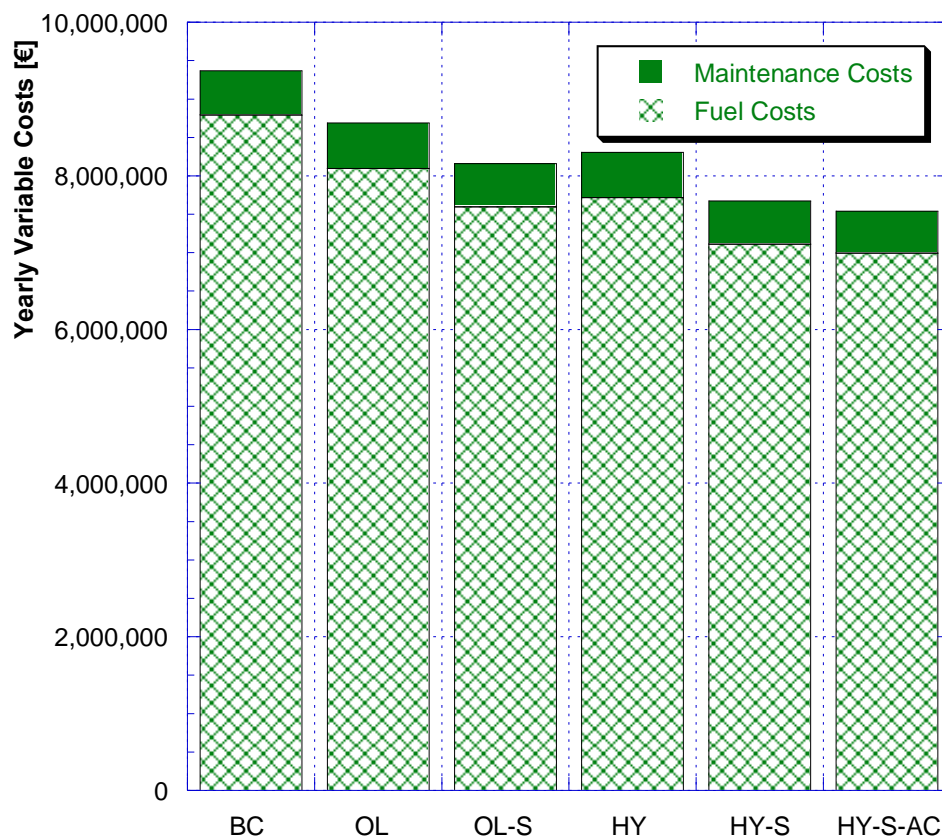


Figure 8.18 – Annual fuel consumption and maintenance costs.

From Figure 8.18 it can be noted that the main contribution to the total variable costs is ascribable to the fuel costs. The total maintenance costs value, indeed, varies between 550'000 € and 580'000 €, representing a small percentage (around 7%) of the total variable costs. Based on this consideration, the maintenance costs can be considered quite constant with the considered strategy. Furthermore, with reference to Figure 8.18, it can be noted that OL-S strategy involves a performance improvement in terms of yearly variable costs (around 13% reduction). Evidently, the increase in the investment costs due to the presence of the storage tank should be accounted, but it can be considered as moderate with respect to the variable costs decrease. Compared to the current layout of the ship, the engines configuration remains the same, while the main change is indeed represented by the installation of a tank for the thermal energy storage.

Relating to HY-S and HY-S-AC strategies, instead, a further reduction in the annual variable costs, consisting in the reduction in fuel costs, can be reached (equal to around 18% and 20% respectively for HY-S and HY-S-AC). In this case, however, in addition to the storage tank installation, also a reconfiguration of the engines from the traditional to the hybrid operation must be considered. Furthermore, HY-S-AC strategy requires the absorption chiller unit installation, with the consequent related costs.

Based on the economic results presented in Figure 8.18, the annual money saving for each developed strategy compared to the base case can be determined. Thus, the maximum investment cost sustainable to pay back the expenditure in 2 years and in 5 years has been evaluated (see Figure 8.19). For the analysis a discount rate equal to 7% has been assumed.

From Figure 8.19 it can be observed that the minimum viable investment cost is obtained for the standard configuration OL-S and it ranges from a value slightly higher than 2'000'000 € to a value equal to about 5'000'000 €. With the increase in the complexity of the adopted strategy, the maximum sustainable investment increases up to 7'000'000 € (HY-S-AC). This result is particularly appreciated since the HY-S-AC configuration requires the installation of the major number of components with respect to the other analyzed solutions.

Furthermore, it should be highlighted that the investment costs for the OL strategy have to be considered as a money saving, since the OL strategy does not change the energy systems set-up, but involves only the optimization. In any case, this saving is relatively low, ranging from around 1'000'000 € to around 3'000'000 €.

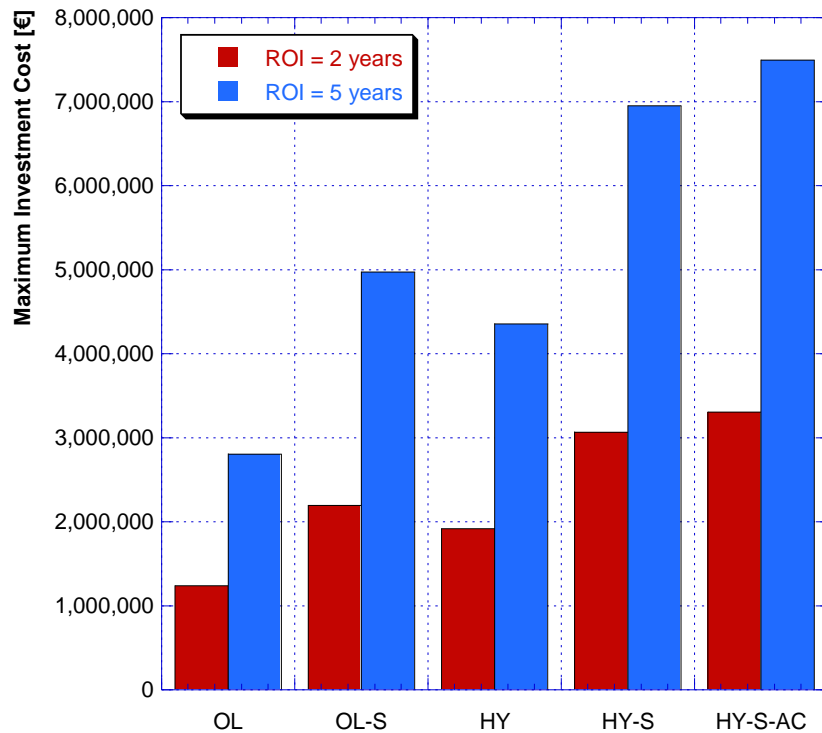


Figure 8.19 – Maximum viable investment costs in order to have a return of the investment in 2 years (red bars) or 5 years (blue bar), for each strategy.

Since a key point for naval sector relates to the pollutant emissions, an environmental analysis has been carried out for the proposed different operational strategies. Indeed even if, from a global point of view, shipping industry seems to play a minor role representing only the 3% of the whole CO₂ emissions [15], it has to be considered that more than the 40% of the total shipping costs is attributed to fuel consumption. Furthermore, despite of its current low contribution, many predictions indicate for the next future an increase in shipping volumes (which means, obviously, emissions increase) [16]. With this purpose, recently the International Maritime Organization (IMO) has introduced relevant regulations and is continuously improving the standards of ship energy saving and emission reduction [17, 18]. The achievement of the energy saving and emission reduction goals – through effective ship energy efficiency management measures – became the new challenge for the development of shipping technology. With regard to this goal, even the European Union is starting actions to realize a reduction of transport’s carbon emissions of 60% by 2050. In particular, concerning the European shipping industry, the goal is the reduction of CO₂ pollutant emissions for values ranging from 40% up to 50% [19].

The emissions factors applied for the analysis are listed in Table 8.4 for the main considered pollutant. According to the Third IMO Greenhouse Gases study [16], Carbon Oxide (CO), Carbon Dioxide (CO₂), Nitrogen Oxides (NO_x), Sulphur Oxides (SO_x), Particulate Matter (PM) and Non-Methane Volatile Organic Compounds (NMVOC) have been reported in Table 8.4. These values – representing the average emissions related to the specific naval sector – refers to marine diesel oil (MDO) considered as input fuel used for all the energy systems: main engines, auxiliary

engines and boilers. It has to be noted that these values depends on the engines speed: in this case, as aforementioned, the engines can be classified as medium-speed engines.

Table 8.4 – Emission factors for the MDO fuel [16].

Emission substance	Emission Factor [kg/kg fuel]
CO	0.00277
CO₂	3.20600
NO_x	0.08725
SO_x	0.00264
PMs	0.00102
NMVOC	0.00308

Starting from these emission factors values, the corresponding emissions quantities – for each developed strategy – have been calculated and presented in Figure 8.20a, in Figure 8.20b and in Figure 8.20c. In detail, Figure 8.20a shows the annual emissions of CO₂ for the various strategies: it can be seen that their value ranges from a maximum of about 30'000 tons_{CO2}/y for the Base Case to a minimum of about 24'000 tons_{CO2}/y corresponding to the HY-S-AC strategy. Because of these high values, the carbon dioxide can be considered the main pollutant.

Another significant pollutant is represented by the Nitrogen Oxides (NO_x), shown in Figure 8.20b. The NO_x emissions, indeed, varies between a value equal to about 650 tons/y (HY-S-AC strategy) and a value equal to quite more than 800 tons/y (BC).

Other minor but non negligible pollutant emissions – such as the ones related to PMs, CO, NMVOC and SO_x – are presented in Figure 8.20c. From this figure it can be observed that moving from the BC strategy to the HY-S-AC one, the Particulate Matter varies from 10 tons/y to around 8 tons/y. As it regards the other pollutants, instead, the SO_x emissions vary from about 25 tons/y to 20 tons/y, the CO emissions from 26 tons/y to 21 tons/y and, finally, the NMVOC emissions vary from 29 tons/y to 23 tons/y – always moving from the BC to the HY-S-AC strategy. On the whole, it can be observed that the standard configurations (BC, OL and OL-S) can reach a maximum decrease of the pollutant emissions equal to 14%. Furthermore, with the hybrid configurations the emissions further decrease for a total value equal to 20 % (from BC to HY-S-AC).

In conclusion, not only from an energy point of view, but also considering both economic and environmental aspects, the hybrid configurations seems to be the most promising solutions for this kind of applications. These solutions, indeed, allow to decrease fuel consumption and maintenance costs, as well as the pollutant emissions, due to an increase in the global systems conversion efficiency.

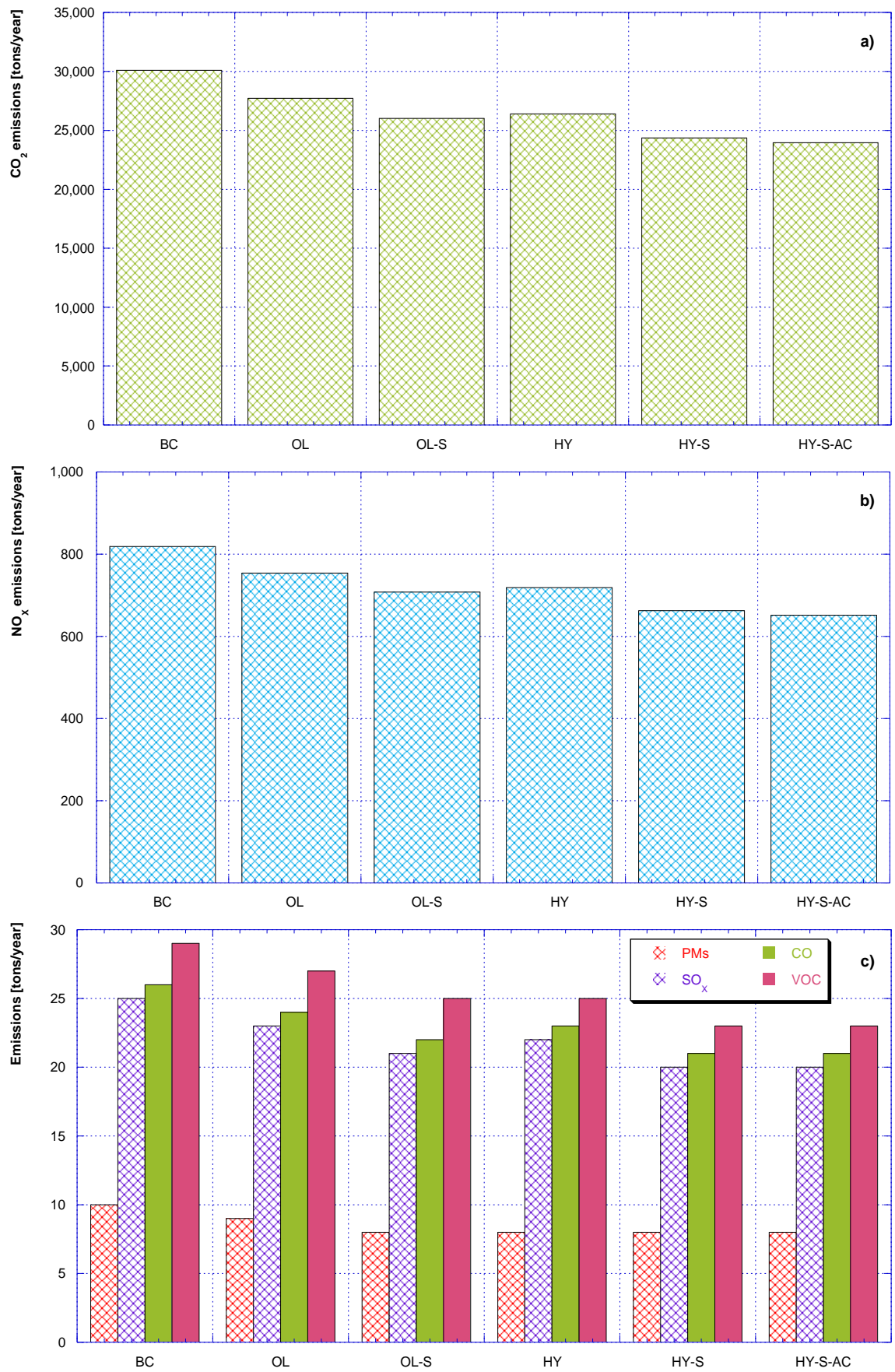


Figure 8.20 – Main pollutant emissions: a) CO₂, b) NO_x and c) CO, PMs, SO_x, and VOC.

References

- [1] Baldi F, Ahlgren F, Melino F, Gabrieli C, Andersson K. Optimal load allocation of complex ship power plants. *Energy Conversion and Management*, 124 (2016) 344-356.
- [2] Climate Change Knowledge Portal – <http://sdwebx.worldbank.org/climateportal/>
- [3] Wärtsilä 46 – Project guide for marine application.
- [4] Wärtsilä Engines – Wärtsilä 32.
- [5] Ntziachristos L, Saukko E, Lehtoranta K, Rönkkö T, Timonen H, Simonen P, Keskinen J. Particle emissions characterization from a medium-speed marine diesel engine with two fuels at different sampling conditions. *Fuel*, 186 (2016) 456-465.
- [6] Andersson K, Brynolf S, Lindgren JF, Wilewska-Bien M. Shipping and the Environment: Improving Environmental Performance in Marine Transportation. *Springer* (2016).
- [7] Cohen L, Fritz WA. Efficiency determination of marine boilers: input-output versus heat-loss method. *J Eng Power* 1962:39–43.
- [8] Macchi E, Campanari S, Silva P. La microgenerazione a gas naturale. Polipress (2005) p.304. ISBN: 8873980163.
- [9] Ancona MA, Bianchi M, Diolaiti E, Giannuzzi A, Marano B, Melino F, Peretto A. A novel solar concentrator system for combined heat and power application in residential sector. *Applied Energy*, 185 (2017) 1199-1209.
- [10] Shi W, Stapersma D, Grimmeli HT. Analysis of energy conversion in ship propulsion system in off-design operation conditions. *WIT Trans Econogy Environ*, 121 (2009) 461-72.
- [11] Dedes E, Hudson DA, Turnock SR. Assessing the potential of hybrid energy technology to reduce exhaust emissions from global shipping. *Energy Policy*, 40 (2012) 204-18.
- [12] Ådanes, A.K. Maritime electrical installations and diesel electric propulsion. ABB AS Marine 2003.
- [13] Andreoni V, Miola A, Perujo A. Cost effectiveness analysis of the emission abatement in the shipping sector emissions. *European Commission Joint Research Centre Institute for Environment and Sustainability*, Luxembourg (2008).
- [14] Gunnarsson G, Skúlason JB, Sigurbjarnarson Á, Enge S. Regenerative electric/hybrid drive train for ships – RENSEA II, Nordic innovation publication (2016).
- [15] Johnson H, Styhre L. Increased energy efficiency in short sea shipping through decreased time in port. *Transportation Research Part A: Policy and Practice*, 71 (2015) 167-178.
- [16] Smith TWP, Jalkanen JP, Anderson BA, Corbett JJ, Faber J, Hanayama S et al. Third IMO GHG Study. London, UK; 2014.
- [17] Anderson K, Bows A. Executing a Scharnow turn: reconciling shipping emissions with international commitments on climate change. *Carbon Manage*, 3 (2012) 615-628.

- [18] Lindstad HE, Eskeland GS. Environmental regulations in shipping: Policies leaning towards globalization of scrubbers deserve scrutiny. *Transportation Research Part D: Transport and Environment*, 47 (2016) 67-76.
- [19] European Commission (EC). Roadmap to a single European transport area – towards a competitive and resource efficient transport system. Brussels, Belgium; 2011.

9. MILP optimization – comparison

In this chapter the methodology applied for the comparison between genetic algorithms and MILP models is shown. In more detail, the case study selected for the analysis is presented and the main characteristics of the two software – the first in-house developed and based on genetic algorithms (*i.e.* the software EGO), the second developed by the IPESE (Industrial Process and Energy Systems Engineering) research group at EPFL – are described.

9.1 Case Study

In order to compare the two different optimization approaches, namely genetic algorithms (GA) and MILP, a portion of an existing district heating network has been chosen as case study.

The considered DHN – presented in Figure 9.1 – supplies 10 thermal users, composed of residential consumers and four tertiary users (two schools, 1 day-hospital building and 1 super-market). Furthermore, the network's length is about 3 km, considering both the supply and the return paths. All the connected users are served by the DHN for both space heating and hot water needs, excepting for the super-market where only space heating is needed. The thermal need is known for each of the considered users. In particular, two typical days can be considered for the analysis, respectively for wintertime (space heating and hot water needs) and for summertime (only hot water need). As an example, the thermal need for space heating during wintertime is shown in Figure 9.2 for the 10 users.

The comparison has been carried out considering different scenarios, in terms of installed energy production systems, including combined heat and power units and renewable energy sources, as well as traditional fossil fuel technologies. The analysis has been carried out by comparing the results obtained with the software EGO with the ones of the software MEGS, described in the following paragraph.

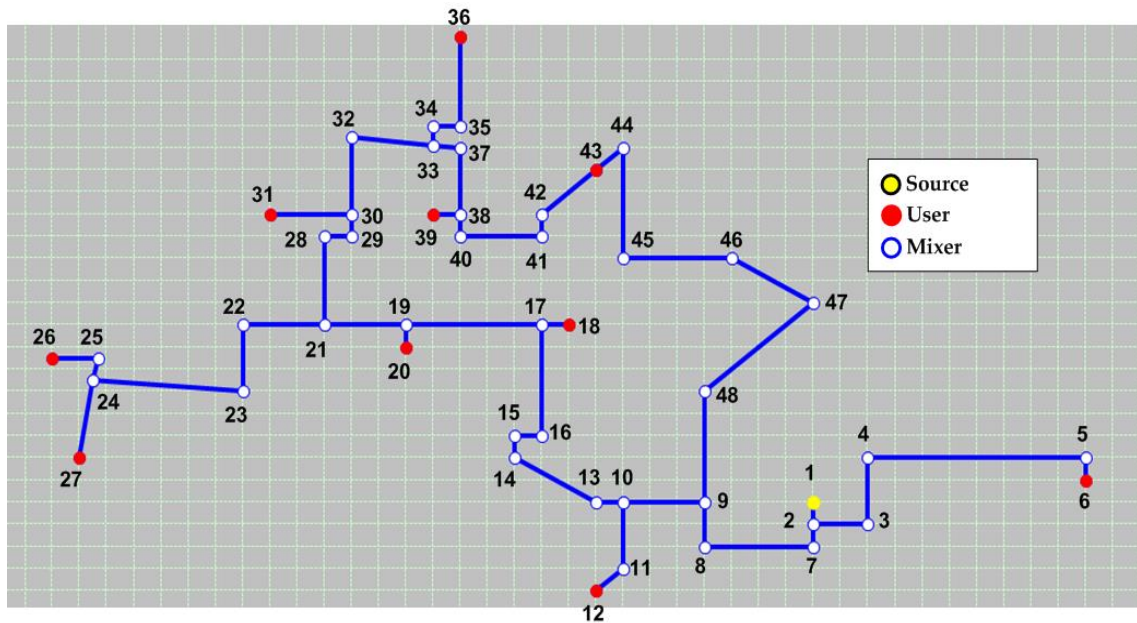


Figure 9.1 – District Heating Network considered for the analysis.

9.2 Software MEGS

The software MEGS (Multi Energy Grid Systems) is a user oriented tool for designing and retrofitting energy systems. The aim is the optimization of the network design and of the production systems scheduling by means of a mixed integer linear programming (MILP) problem. As a consequence, the optimization process consists in a multi-objective function: the first level is the minimization of the capital costs, while the second level is the minimization of the operative costs. In Figure 9.3 a schematic of the MEGS tool flow chart along with the input and results sheets screenshots.

The main input of the software are:

- the location of each node of the network (*i.e.* sources, users and mixers);
- the set of thermal and electrical users for each geographic location with given demands;
- the set of components (heat pumps, boilers, CHP units, GTs, thermal storage, batteries, transformers, PV panels, solar thermal panels,...) with their performance curves, operating and capital costs;
- the costs of district heating network and electricity lines.

District heating network is modeled without considering pressure losses and the performances in off-design of the production systems are linearized.

At the end of the iterative procedure the main output are:

- the optimal sets of components to be installed;
- the optimal operations scheduling of components (taking into account minimum and maximum capacity, rump-up and rump-down constraints);
- the optimal DHN and electricity network configurations.

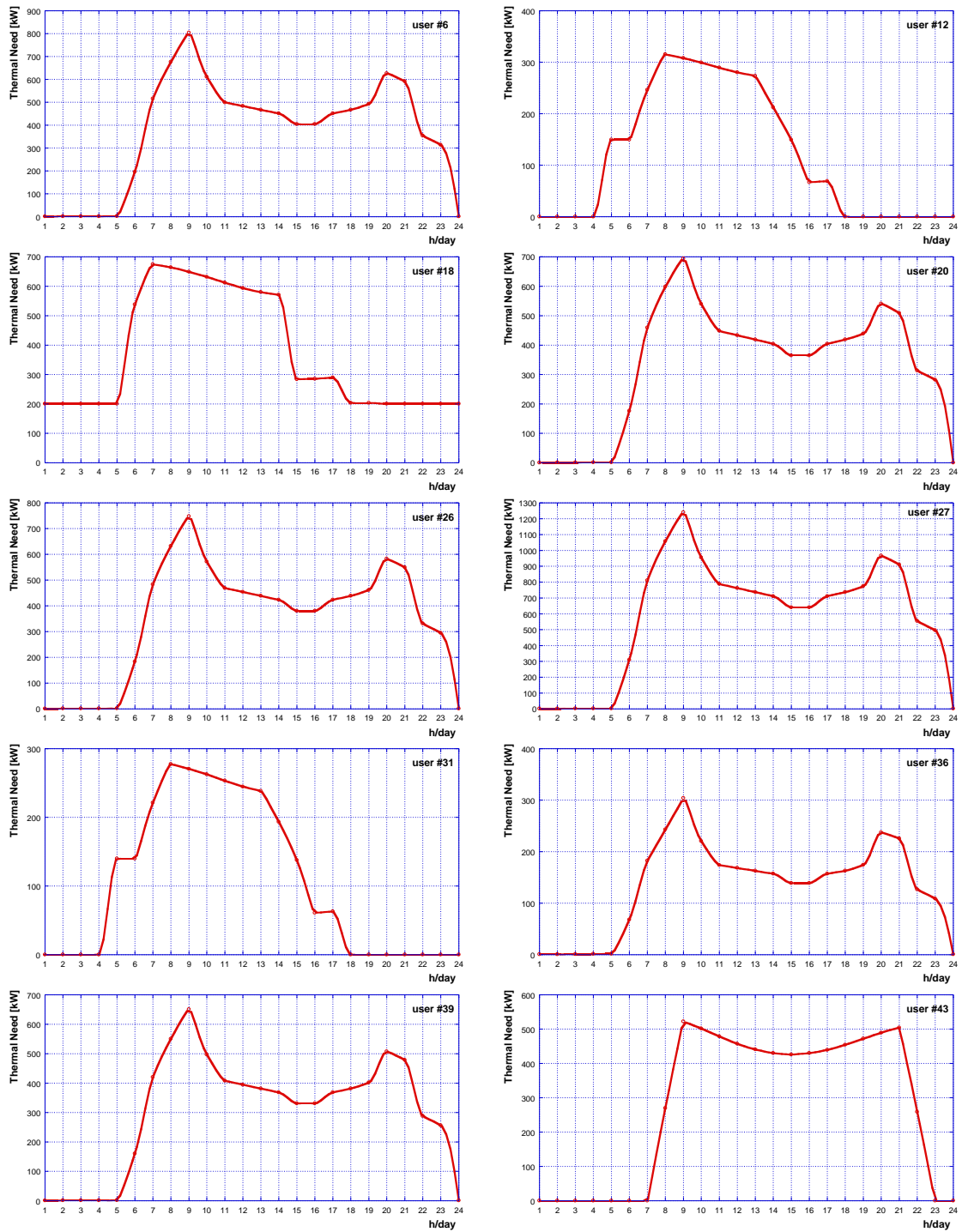


Figure 9.2 – Users thermal needs for space heating during wintertime.

Define -> Solve -> Analyze approach:

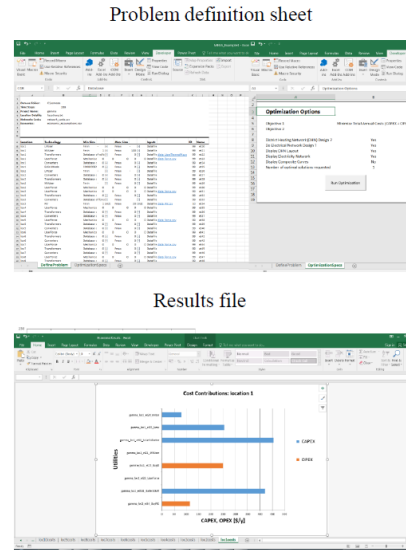
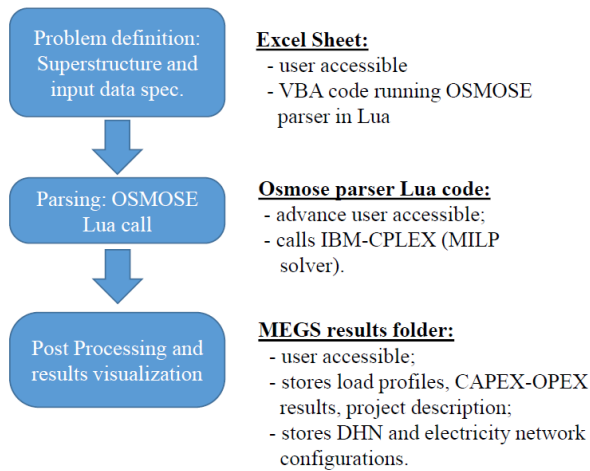


Figure 9.3 – Main flow chart of the MEGS calculation code.

9.3 Results

The main results obtained from the comparison allow to highlight some advantages and criticism for both the analyzed approaches, as described in this section. In addition, three different possible ways of integration between the exact linear optimization method (MILP) and the heuristic nonlinear optimization one (GA) are presented.

9.3.1 DHN design

First of all, as it regards the design of the network, considering the genetic algorithm approach the network path is an input and it is a ring network. In fact, with our approach the design relates only to the diameters of the pipes and it is done by means of a *try & error* procedure. On the other hand, with MEGS tool the design is a result of the minimization of DHN costs, with fixed pipes costs per unit length. As a consequence, the optimal DHN path based on MILP seems to be the one proposed in Figure 9.4, without the ring. Thus, in order to analyze the variation in the thermo-hydraulics aspects starting from this result, the new network layout has been implemented in the tool developed by University of Bologna and evaluated again. In our approach, indeed, the network is modeled in detail with the Todini-Pilati algorithm generalized by the use of Darcy-Weisbach equation [1], allowing the evaluation of pressures and temperatures calculated for each node of the DHN by means of nonlinear equations. The MILP model, instead, considers for each pipe a maximum given mass flow rate in order to select the design diameters, but – since the model is linear – no pressure losses are considered.

This procedure allowed to point out an important criticism of the MILP model: indeed, keeping the diameter of each pipe as constant and eliminating the network ring, the hydraulics of the network is completely changed and this aspect cannot be detected with the MEGS tool. In more

detail, the pressure at the outlet of the centralized pumping station (*i.e.* the pressure of the water supplied to the network) cannot be maintained, in order to guarantee the correct flow across the network. In particular the following considerations can be done:

- the pressure at the source should be increased from 10 bar to 182 bar in order to guarantee the correct flow across the network. Obviously this very high increase in pressure is not viable;
- the two possible viable solutions are the modification of the diameters of each pipe (higher diameters with consequent increase in network design costs) or the addition of pumps along the DHN.

Since the MILP approach does not consider pressure losses and hydraulics aspects, the result in terms of network design could not be always the optimal one. In order to solve this problem a first step can be the implementation of pressure losses within the MEGS tool, even if considering the linearization of the nonlinear pressure losses equation. The next challenge is the development of a MINLP based model.

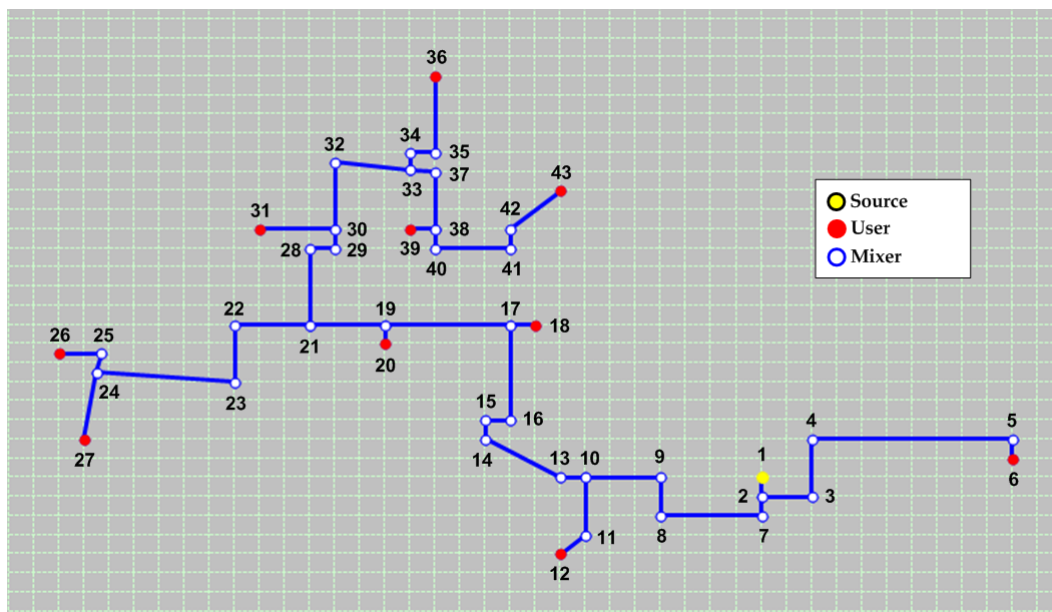


Figure 9.4 – District Heating Network design, as a result of MEGS application.

9.3.2 Energy systems operation

The main characteristic of the two approaches as it concerns the energy systems operation can be summarized as follows. In the EGO approach:

- the off-design behavior considered for each energy system is modeled with a non-linear problem;

- there is the possibility to consider a fictitious cost in order to account the regulation scenario;
- the location for the production systems installation is an input.

On the other hand, for the MILP model:

- a linear behavior is considered for off-design operation;
- the scheduling results are based only on the efficiency;
- for the production systems installation the location is an output.

The most important thing that appears considering the scheduling comparison is that the optimization based only on efficiency – without accounting for fictitious costs of heat dissipation or electricity production surplus – excludes the possibility of operation for some kinds of energy production systems, such as CHP units. In fact, the thermal efficiency of a CHP unit is always lower than the one of natural gas boilers. Thus, the fuel consumption to produce the same amount of heat is lower for the natural gas boilers and the results of the pure real cost based optimization with MEGS gives the complete shut-down of CHP units. However, cogeneration is promoted by international and national regulations and, for this reason, the cost of fuel in a CHP scenario is lower. This can be accounted with the fictitious costs considered within the GA approach.

The main advantage of the MILP approach, instead, consists in the higher flexibility due to the possibility of evaluation of several scenarios with one simulation. In more detail, since with EGO the location of energy production systems is an input, the evaluation of different configurations – in terms of generation systems set-up and size – has to be carried out running different simulations. On the other hand, with MEGS a set of possible installed systems has to be indicated as input, but the optimal installation configuration is an output of a single simulation.

9.3.3 Computational time

Relating to the calculation time, with the application of the genetic algorithm it importantly increases with the complexity of the problem and with the considered number of time steps. In order to have a reasonable computational time, the maximum number of time steps is 24. On the other hand, the MEGS tool is very fast even for high number of time steps, particularly due to the two level optimization structure: at the first level the optimal design is realized, while the optimal scheduling is evaluated at a second stage of the iterative procedure. Furthermore, higher time for data processing is needed in case of GA application.

9.3.4 Integration between GA and MILP approaches

At the end of the comparison, considering the individuated pro and cons, the individuation of a way for the integration between the two approaches seems to be the best solution in order to optimize complex network design and operation. Three different solutions are proposed:

- I. The two methods can be applied in cascade: pre-design with the MILP, feasibility of the network (hydraulic problem in-depth analysis) and operation with the non-linear model. This cascade approach is basically the one employed for the comparison of the case study presented in the previous paragraphs.
- II. Introduction of the pressure losses evaluation inside the MILP: pressure losses can be accounted by applying a piecewise linearization [2] of the pressure losses equation. Two variables are involved in the non-linearity, respectively mass flow rates and diameters; for this reason the development of this model is particularly challenging. This approach has been partially implemented during the period at EPFL and it will be completed in future works.
- III. Elaboration of a MINLP problem: pressure losses, off-design behavior of the production systems and electrical/thermal priority strategies accounted within a non-linear problem. The major challenge stands in the computational time.

References

- [1] Ancona MA, Bianchi M, Branchini L, Melino F. District Heating Network Design and Analysis. *Energy Procedia*, 45 (2014) 1225-1234.
- [2] D'Ambrosio C, Lodi A, Martello S. Piecewise linear approximation of functions of two variables in MILP models. *Operation Research Letters*, 38 (2010) 39-46.

Conclusions

The growing attention to energy efficiency increase, pollutant emissions decrease and fossil fuel consumption reduction had led to a rapid increase in distributed generation spread, both for electrical and thermal energy production. This evidence had entailed – as it regards the electrical grids – the birth of the so called *smart grids*. At the same time, in the heat sector district heating is seen as an interesting solution, considering both environmental and safety aspects, in order to reduce pollutant and thermal emissions within the city area, contemporarily increasing the safety (due to the elimination of combustion systems at the final users) and the conversion efficiencies.

In this context, the idea to replicate in the heat sector the smart grid concept has been developed, by the integration of thermal energy distributed generators with the district heating networks (*smart district heating*). As a consequence, the concept of complex energy network has been defined as a network for energy supply, consisting in electrical, thermal and cooling networks with centralized and distributed generation – eventually in presence of storage systems. The complexity of these kind of networks poses new issues, related to the operation and management of all the connected energy systems, in order to prevent networks instability and malfunction. As a consequence, it is fundamental to optimize the production mix and the operation of each system, in order to maximize the renewable energies exploitation, minimize the economic costs (in particular the fossil fuel consumption) and the environmental impact. As it regards the scheduling optimization, several optimization algorithms can be applied: at present, the most promising ones are genetic algorithms (GA), Mixed Integer Linear Programming (MILP) and Mixed Integer Non Linear Programming (MINLP) problems.

As a first part of this research activity, a thermo-hydraulic analysis on district heating networks has been carried out. In particular, an in-house developed software (called Ca.R.Di.F. – Calcolo Reti Distribuzione Fluidi) for the design and analysis of district heating and cooling networks has been applied to a case study and validated. Furthermore, in order to promote and investigate the smart district heating concept, four innovative configurations for users substations have been elaborated and implemented within the software (the new version is called IHENA – Intelligent Heat Energy Network Analysis), allowing to guarantee the bidirectional heat exchange:

1. scheme 1 (feed to return): a mass flow rate is extracted from the feed line of the network and it is heated by decentralized production system before the reintroduction in the return line;
2. scheme 2 (feed to feed): the thermal energy transfer from the decentralized production system towards the distribution network concerns only the feed line;
3. scheme 3 (return to return): the transfer of thermal energy from the user to the network involves only the return line;
4. scheme 4 (return to feed): a mass flow rate is taken from the return line, heated from the decentralized production system and reintroduced in the feed line of the network.

By means of this new software, the effects of the four configurations on the network have been thermodynamically analyzed, with the help of a case study, allowing to highlight the advantages and the possible criticism of each configuration. Evidently, the introduction of heat into the network produces a temperature modification and – in some cases – a change in the network flows. Generally speaking, the analysis show that the increase in the temperature on the return

circuit of distribution network implies the necessity of modifications in control and regulation strategy of the whole network (with a consequent reduction of the conversion efficiency for the centralized production plant). For this reason, even if this problem concerns the simpler configurations, the return temperature increase is not appreciated by the network management. On the other hand, when the increase in the temperature is obtained on the feed line, unwelcome effects could be registered for downstream users (if they need a constant temperature flow and/or for others distributed generation systems which can be excluded from the possibility of thermal energy feed-in). The most promising configuration, instead, is the one in which a mass flow rate from the return line is heated and inserted in the feed line: this is the most complex configuration due to the flows modification, but it does not necessary implies the increase of the feed temperature, avoiding particular regulation problems related to the temperature profile.

Then, two different transformation hypotheses for the conversion of an existing user substation into a smart one have been conceived and projected, defining for each one the logic of operation and carrying out a techno-economic analysis. The hypotheses consider respectively solar thermal panels or a CHP unit as distributed generation system to be installed at the final user. A techno-economic analysis has been carried out, leading to the definition of the plant projects. The results highlight in particular the economic convenience of cogeneration-district heating integration.

Starting from the district heating analysis results and focusing on complex energy networks on the whole, the software EGO (Energy Grid Optimizer) – based on genetic algorithm – has been developed for the optimal scheduling definition of the connected energy production systems. The main objectives at the basis of the software mode of operation are: (i) the minimization (or avoidance) of the electricity exchange with the national grid, (ii) the minimization (or avoidance) of the heat dissipations through the chimney, (iii) the minimization of the auxiliary boilers employment, (iv) the optimization of the cogeneration units operation and (v) the maximization of the renewable sources exploitation. In this study, two applications of the software EGO have been presented, relating to a small-medium size district heating network and to an isolated grid respectively.

The first presented case study relates to the study of an existing district heating network. The current set-up of this network consists of a centralized production plant which guarantee – at present – the fulfillment of the connected users' thermal needs. No electricity nor cooling energy are supplied by the centralized station. The carried out analysis has been divided into two phases, both with the general aim to optimize the energy production (eventually by adding different energy systems to the current ones). In the first phase of the study, the current mode of operation of the network has been maintained. In other words, only the thermal needs are considered to be supplied by the centralized plant, while each user by itself purchases electricity from the national electric grid for electrical needs and, eventually, to produce cooling energy. On the other hand, the second phase is characterized by a modification in the mode of operation of the network: in this case it is supposed that thermal, electrical and cooling needs are fulfilled by the centralized power station.

As it regards the Phase I, three different cases have been analyzed considering, in addition to the generation systems currently installed (a CHP unit and four auxiliary boilers), the installation of: *Case 1* - thermal solar panels and a thermal energy storage system (installed at the thermal power station); *Case 2* - photovoltaic panels feeding a heat pump (installed at the thermal power station); *Case 3* - photovoltaic panels coupled with heat pumps, installed directly at the final users (opportunistically chosen). The results of the analysis show that all the proposed alternative configurations enable to decrease the fuel consumption with respect to the starting Reference

Case, with a maximum percentage saving equal to about the 57% (Case 2) achieved when centralized PV panels and heat pump are considered in addition to the current thermal power station set-up (CHP unit and four auxiliary boilers). Furthermore, in this case the electric energy sale to the grid results eliminated and the purchase of electricity reduced (around the 14%). Thus, Case 2 seems to represent the best solution for the considered existing network, considerably reducing the operating costs. In any case, all the proposed set-up allow to improve the CHP-DH network efficiency relating to the current plant configuration performance.

Relating to the Phase II, the analysis was focused on the optimization of the considered network set-up when not only thermal energy, but also electricity and cooling energy must be provided to the users. In addition to the current energy systems, in this second phase four alternatives have been analyzed, considering the installation of compression and absorption chillers at the final users plus – at the centralized power station: *Case A* - no further systems are considered; *Case B* - a further internal combustion engine (with a rated power equal to the one of the already installed engine), a thermal storage tank and a heat pump; *Case C* - photovoltaic panels and a heat pump; *Case D* - thermal solar panels, a thermal storage tank and a heat pump. Based on the simulations carried out with the software EGO, the yearly fuel consumption at the centralized power plant, the yearly purchase of electric energy from the grid and the yearly sale of the produced electricity surplus to the grid has been evaluated. Furthermore, with the purpose to properly compare the new solutions with the Reference Case, the fuel consumption required to produce the purchased electricity has been calculated considering a mean conversion efficiency for the national thermo-electric fleet. Finally, the CO₂ avoided emissions, achievable with the analyzed configurations with respect to the Reference Case, have been calculated. The results show that the Case B seems to be the most promising one, due to the decrease of both fuel consumption (around 22760 kWh/y, namely around the 39%) and electricity purchase (around the 50%), as well as of the CO₂ emissions (reduction around 4500 tons/y) with respect to the Reference Case. Furthermore, all the proposed set-up and their scheduling optimization allow, during the whole year, to completely avoid the introduction of electrical energy into the national grid, with the consequent benefits for its stability and management. This result confirms the benefits of the integration of cogeneration/tri-generation systems within the district heating scenario.

The second presented case study refers to a cruise ship, which is a particular case of isolated grid. The ship is currently equipped with eight marine diesel engines, four dedicated to electricity production and four for mechanical energy production (for propulsion). Also for this case study, different solutions have been proposed in terms of production systems set-up and the scheduling optimization has been made with the software EGO. The most relevant obtained result is that – not only from an energy point of view, but also considering both economic and environmental aspects – hybrid configurations seems to be the most promising solutions for this kind of applications. These solutions, indeed, allow to decrease fuel consumption and maintenance costs, as well as the pollutant emissions, due to an increase in the global systems conversion efficiency.

Finally, a comparison between the EGO approach and the MILP one for the design and scheduling of complex energy networks, developed by IPESE Research Group of the École Polytechnique Fédérale de Lausanne (EPFL), has been carried out during a research period abroad, at the EPFL laboratory. The comparison had allowed to highlight pro and cons for both the approaches: the non-linearity (*e.g.* for pressure losses and energy systems off-design performances) maintained by genetic algorithms is preferable and enables to model the problem with a high complexity level, however the computational time is importantly lower for MILP. As a consequence, in order to maintain the advantages from both the optimization methods, different

ways of integration between the two approaches have been investigated as the basis for future approaches definition.

List of Tables

Table 3.1 – Comparison between Termis and Ca.R.Di.F. software.

Table 4.1 – Main users and source parameters assumed for the analysis.

Table 4.2 – Distributed generation system parameters.

Table 4.3 – Heat exchanger main characteristics.

Table 4.4 – Heat exchanger design operation.

Table 4.5 – Hypothesis and assumptions for the Case 1 – thermal solar panels integration.

Table 4.6 – List of components selected for the smart utility substation transformation - Case 1.

Table 4.7 – Micro-GT available on the market.

Table 4.8 – List of components selected for the smart utility substation transformation - Case 2.

Table 6.1 – Prime movers design performance.

Table 7.1 – Generation systems main parameters.

Table 7.2 – Users identification numbers and associated typology.

Table 7.3 – Summary of the analyzed configurations – Phase I.

Table 7.4 – Main systems parameters considered in the proposed variation scenarios – Phase I.

Table 7.5 – Electric peak power for the residential users.

Table 7.6 – Cooling peak power for the residential users.

Table 7.7 – Summary of the analyzed configurations – Phase II.

Table 7.8 – Main systems parameters considered in the proposed variation scenarios – Phase II.

Table 8.1 – Internal combustion engines design performance [3, 4].

Table 8.2 – Auxiliary components efficiencies [10-12].

Table 8.3 – Specific variable costs [13, 14].

Table 8.4 – Emission factors for the MDO fuel [16].

List of Figures

Figure 1.1 – Example of a complex energy networks.

Figure 1.2 – Evolution of energy networks concept.

Figure 1.3 – Technologies for electrical energy generation as function of the size.

Figure 1.4 – Top ten Countries for federal smart grid investment at 2010 [17].

Figure 2.1 – Percentage of population supplied by district heating [15].

Figure 2.2 – Thermal energy supplied to the users via DHN in 2011, for several Countries [15].

Figure 2.3 – Trend of the DHN connected volumetry in Italy from 1972 to 2015 [16].

Figure 2.4 – Fossil primary energy savings with DHNs [16].

Figure 2.5 – CO₂ emissions [16].

Figure 3.1 – Example of a portion of a DHN.

Figure 3.2 – Main Calculation code flow chart.

Figure 3.3 – Case study layout selected for software validation.

Figure 3.4 – Comparison between the mass flow rates results of the two considered software.

Figure 3.5 – Comparison between the pressure results of the two considered software at the inlet of the pipes, considering the network path from the source to the user #43.

Figure 3.6 – Comparison between the temperature results of the two considered software at the inlet of the pipes, considering the network path from the source to the user #43.

Figure 4.1 – Scheme 1, feed to return configuration.

Figure 4.2 – Scheme 2, feed to feed configuration.

Figure 4.3 – Scheme 3, return to return configuration.

Figure 4.4 – Scheme 4, return to feed configuration.

Figure 4.5 – Software IHENA main flow chart.

Figure 4.6 – Primary circuit temperature increase as function of the ratios $Q_{TH,U}/Q_{TH,SP}$ and M_P/M_T , in case of $T=80$ °C and schemes 1 and 2.

Figure 4.7 – Primary circuit temperature increase as function of the ratio $Q_{TH,U}/Q_{TH,SP}$ and of the primary circuit inlet temperature, in case of $M_P/M_T=1.0$ and schemes 1 and 2.

Figure 4.8 – Primary circuit temperature increase as function of the ratios $Q_{TH,U}/Q_{TH,SP}$ and M_P/M_T , in case of $T=80$ °C and scheme 3.

Figure 4.9 – Primary circuit temperature increase as function of the ratio $Q_{TH,U}/Q_{TH,SP}$ and of the primary circuit inlet temperature, in case of $M_p/M_T=1.0$ and scheme 3.

Figure 4.10 – Primary circuit temperature increase as function of the ratios $Q_{TH,U}/Q_{TH,SP}$ and M_p/M_T , in case of $T=80$ °C and scheme 4.

Figure 4.11 – Primary circuit temperature increase as function of the ratio $Q_{TH,U}/Q_{TH,SP}$ and of the primary circuit inlet temperature, in case of $M_p/M_T=1.0$ and scheme 4.

Figure 4.12 – Layout of the DHN chosen as case study.

Figure 4.13 – Temperature profiles along the critical path of the network – for both the feed and the return lines – for the case $Q_{th,u}/Q_{th,sp} = 0.0$ and when the user substation at the node #12 can be represented with (a) scheme 1, (b) scheme 2, (c) scheme 3 or (d) scheme 4. In dotted lines the temperature profiles when no thermal production occurs are presented as comparison.

Figure 4.14 – Schematic of the current utility substation (traditional thermal exchange: from the network to the user).

Figure 4.15 – Thermal exchange diagram for the heat exchanger HE1 in design conditions.

Figure 4.16 – Heat exchanger HE1 off-design operation: a) primary circuit mass flow rate and b) primary circuit outlet temperature as function of the exchanged heat, for different values of the primary circuit inlet temperature $T_{IN,P}$.

Figure 4.17 – Plant of the selected user for the implementation of smart user substations and rooftop surfaces exposed to south, south-east and south-west (highlighted in blue).

Figure 4.18 – Case 1: thermal solar panels integration: smart user substation schematic (scheme 1 – feed to return configuration).

Figure 4.19 – Temperature T_3 as function of the ratio between user need and thermal solar production, for different values of the primary circuit inlet temperature $T_{IN,P}$.

Figure 4.20 – Heat transferred from the distributed generation system to the DHN as function of the ratio between user need and thermal solar production, for different values of the primary circuit inlet temperature $T_{IN,P}$.

Figure 4.21 – Trend of the maximum thermal power transferred from the distributed generation system to the DHN as function of the network supply temperature $T_{IN,P}$.

Figure 4.22 – Plant schematic for the Case 1 – integration with thermal solar panels.

Figure 4.23 – Case 2: combined heat and power unit integration: smart user substation schematic (scheme 4 – return to feed configuration).

Figure 4.24 – Trends of the mass flow rate to the heat exchanger HE3 on the secondary circuit (*i.e.* user side) – blue line – and of the mass flow rate through the heat exchanger HE2 on the network side (*i.e.* the mass flow rate withdrawn from the DHN return and introduced – after being heated – into the DHN supply) – red dotted line.

Figure 4.25 – Trend of the HE2 inlet temperature on the CHP side (TC), as function of the ratio between user need and CHP production.

Figure 4.26 – Portion of the district heating network circuit which involves the considered user (infant school) as currently set.

Figure 4.27 – Detail of the current status of the district heating network portion involved in the required modifications in order to convert the considered utility substation in a smart substation.

Figure 4.28 – Portion of the district heating network circuit which involves the considered user (infant school).

Figure 4.29 – Plant schematic for the Case 2 – integration with CHP unit.

Figure 5.1 – Example of the composition of a population in the GA model.

Figure 5.2 – Roulette structure in the GA model.

Figure 5.3 – Crossover process for new individuals creation in the GA model.

Figure 5.4 – Mutation process for new individuals creation in the GA model.

Figure 5.5 – Summary of the whole GA process.

Figure 5.6 – Schematic of a MILP model for a cogeneration-based energy supply network [26].

Figure 6.1 – EGO software calculation scheme.

Figure 6.2 – EGO software calculation main flow chart.

Figure 6.3 – EGO software prime movers database: electrical (a) and thermal (b) design efficiency as function of nominal electrical power output [1].

Figure 6.4 – Evolution of possible solutions for the EGO software.

Figure 6.5 – Incremental cost trend as function of the power for the two considered prime movers.

Figure 6.6 – Optimal PMs power output trend versus required electrical power.

Figure 6.7 – Total incremental cost versus required electrical power.

Figure 7.1 – Area of interest for the analyzed district heating network [1].

Figure 7.2 – Current configuration of the considered thermal power station.

Figure 7.3 – Schematic of the district heating network.

Figure 7.4 – Space heating peak needs for each user.

Figure 7.5 – Hot water peak needs for each user.

Figure 7.6 – Case studies configurations: a) Case 1; b) Case 2; c) Case 3.

Figure 7.7 – Incident solar irradiation on a south-facing solar panel with a tilt angle equal to 30°, for a typical summer day (orange line) and for a typical winter day (yellow line) – Bologna case.

Figure 7.8 – Thermal production profiles (thermal power station) along with the production systems mix for the Reference Case: a) typical winter day, b) typical summer day.

Figure 7.9 – Thermal production profiles (thermal power station) along with the production systems mix for the Case 1: a) typical winter day, b) typical summer day.

Figure 7.10 – Thermal production profiles (thermal power station) along with the production systems mix for the Case 2: a) typical winter day, b) typical summer day.

Figure 7.11 – Thermal production profiles along with the production systems mix for the Case 3: a) typical winter day (thermal power station), b) typical summer day (thermal power station), c) typical winter day (distributed generation units), d) typical summer day (distributed generation units).

Figure 7.12 – Daily operation profile of the CHP unit in a typical winter day: a) Reference Case, b) Case 1, c) Case 2 and d) Case 3.

Figure 7.13 – Yearly fuel consumption (ICE plus auxiliary boilers).

Figure 7.14 – Electric energy yearly purchased from the national electric grid.

Figure 7.15 – Electric energy yearly sold to the national electric grid.

Figure 7.16 – Produced thermal power profile for a typical day in (a) wintertime, (b) middle season and (c) summertime.

Figure 7.17 – Required electrical power profile for a typical day in (a) wintertime, (b) middle season and (c) summertime.

Figure 7.18 – Required cooling power profile for a typical day in summertime.

Figure 7.19 – Layout of the analyzed configuration Case A.

Figure 7.20 – Layout of the analyzed configuration Case B.

Figure 7.21 – Layout of the analyzed configuration Case C.

Figure 7.22 – Layout of the analyzed configuration Case D.

Figure 7.23 – Incident solar irradiation on a south-facing solar panel with a tilt angle equal to 30°, for a typical winter day (yellow line), for a typical middle season day (grey line) and for a typical summer day (orange line) – Bologna case.

Figure 7.24 – Thermal production profiles (thermal power station) along with the production systems mix for the Reference Case: a) typical winter day, b) typical middle season day, c) typical summer day.

Figure 7.25 – Thermal production profiles (thermal power station) along with the production systems mix for the Case A: a) typical winter day, b) typical middle season day, c) typical summer day.

Figure 7.26 – Thermal production profiles (thermal power station) along with the production systems mix for the Case B: a) typical winter day, b) typical middle season day, c) typical summer day.

Figure 7.27 – Thermal production profiles (thermal power station) along with the production systems mix for the Case C: a) typical winter day, b) typical middle season day, c) typical summer day.

Figure 7.28 – Thermal production profiles (thermal power station) along with the production systems mix for the Case D: a) typical winter day, b) typical middle season day, c) typical summer day.

Figure 7.29 – Electricity production profiles (thermal power station) along with the production systems mix for the Reference Case: a) typical winter day, b) typical middle season day, c) typical summer day.

Figure 7.30 – Electricity production profiles (thermal power station) along with the production systems mix for the Case A: a) typical winter day, b) typical middle season day, c) typical summer day.

Figure 7.31 – Electricity production profiles (thermal power station) along with the production systems mix for the Case B: a) typical winter day, b) typical middle season day, c) typical summer day.

Figure 7.32 – Electricity production profiles (thermal power station) along with the production systems mix for the Case C: a) typical winter day, b) typical middle season day, c) typical summer day.

Figure 7.33 – Electricity production profiles (thermal power station) along with the production systems mix for the Case D: a) typical winter day, b) typical middle season day, c) typical summer day.

Figure 7.34 – Cooling energy production profiles (thermal power station) along with the production systems mix for the Case A during a typical summer day.

Figure 7.35 – Cooling energy production profiles (thermal power station) along with the production systems mix for the Case B during a typical summer day.

Figure 7.36 – Cooling energy production profiles (thermal power station) along with the production systems mix for the Case C during a typical summer day.

Figure 7.37 – Cooling energy production profiles (thermal power station) along with the production systems mix for the Case D during a typical summer day.

Figure 7.38 – Yearly fuel consumption (ICE and auxiliary boilers).

Figure 7.39 – Yearly electricity purchase from the National Electric Grid.

Figure 7.40 – Yearly electricity sold to the National Electric Grid.

Figure 7.41 – Total yearly fuel consumption for the production of thermal, electrical and cooling energies (centralized power station of the network and National Thermo-Electric Fleet).

Figure 7.42 – CO₂ avoided emissions with respect to the Reference Case.

Figure 8.1 – Schematic of the cruise ship route.

Figure 8.2 – Cruise ship mode of operation during a year.

Figure 8.3 – Hourly load curves for typical days in wintertime, summertime and middle season.

Figure 8.4 – Base Case (BC) layout.

Figure 8.5 – Optimized load with storage (OL-S) layout.

Figure 8.6 – Hybrid (HY) layout.

Figure 8.7 – Hybrid with storage (HY-S) layout.

Figure 8.8 – Hybrid with storage and absorber chiller (HY-S-AC) layout.

Figure 8.9 – Mechanical and thermal efficiency as function of the load for main engines.

Figure 8.10 – Electrical and thermal efficiency as function of the load for auxiliary engines.

Figure 8.11 – Thermal efficiency as function of the load for auxiliary boilers.

Figure 8.12 – EER as function of the load for the compression chiller.

Figure 8.13 – Annual auxiliary boilers fuel consumption as function of the storage volume.

Figure 8.14 – Annual thermal dissipations as function of the storage volume.

Figure 8.15 – Annual total fuel consumption, divided between auxiliary boilers and engines contributions.

Figure 8.16 – Annual total heat dissipations through the chimney.

Figure 8.17 – Annual equivalent hours of operation for each strategy and each energy system.

Figure 8.18 – Annual fuel consumption and maintenance costs.

Figure 8.19 – Maximum viable investment costs in order to have a return of the investment in 2 years (red bars) or 5 years (blue bar), for each strategy.

Figure 8.20 – Main pollutant emissions: *a*) CO₂, *b*) NO_x and *c*) CO, PMs, SO_x, and VOC.

Figure 9.1 – District Heating Network considered for the analysis.

Figure 9.2 – Users thermal needs for space heating during wintertime.

Figure 9.3 – Main flow chart of the MEGS calculation code.

Figure 9.4 – District Heating Network design, as a result of MEGS application.

Figure A1 – Non-dimensional thermal power profile for a single residential unit for (a) space heating and (b) hot water needs. The request during wintertime is composed by both space heating and hot water needs, while in middle season and summertime only hot water is required.

Figure A2 – Non-dimensional thermal power profile for space heating in case of school user.

Figure A3 – Non-dimensional thermal power profile for hot water in case of school user, for a typical day during (a) wintertime and (b) summertime.

Figure A4 – Non-dimensional thermal power profile for (a) space heating and (b) hot water, in case of day-hospital structure.

Figure A5 – Non-dimensional thermal power profile for space heating in case of super-market.

Figure B1 – Non-dimensional electrical power profile for a single residential unit during a typical day in (a) wintertime, (b) middle season and (c) summertime.

Figure B2 – Non-dimensional electrical power profile for the building common areas during a typical day in (a) wintertime, (b) middle season and (c) summertime.

Figure B3 – Non-dimensional electrical power profile for a school during a typical day in (a) wintertime, (b) middle season and (c) summertime.

Figure B4 – Non-dimensional electrical power profile for a day-hospital structure: this profile is maintained for the whole year.

Figure B5 – Non-dimensional electrical power profile for a super-market: this profile is maintained for the whole year.

Figure C1 – Non-dimensional cooling power profile for a single residential unit during a typical day in summertime.

Figure C2 – Non-dimensional cooling power profile for a day-hospital structure during a typical day in summertime.

Figure C3 – Non-dimensional cooling power profile for a super-market during a typical day in summertime.

Appendix A

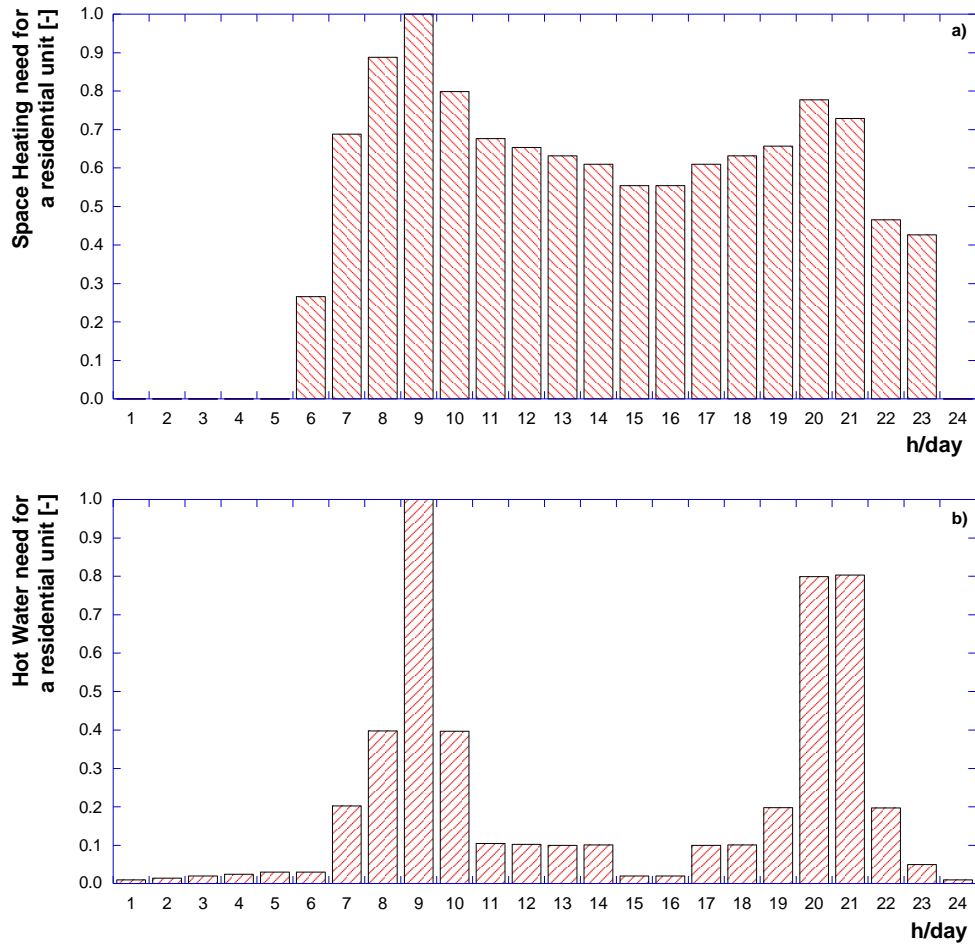


Figure A1 – Non-dimensional thermal power profile for a single residential unit for (a) space heating and (b) hot water needs. The request during wintertime is composed by both space heating and hot water needs, while in middle season and summertime only hot water is required.

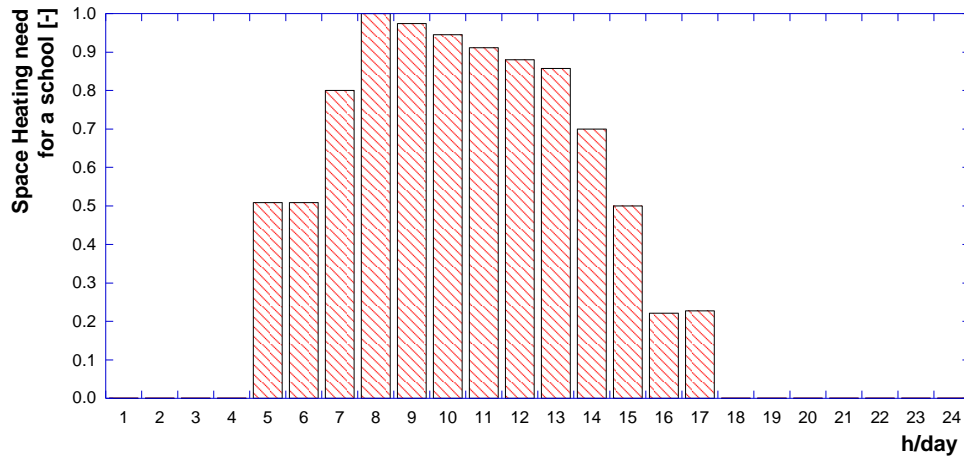


Figure A2 – Non-dimensional thermal power profile for space heating in case of school user.

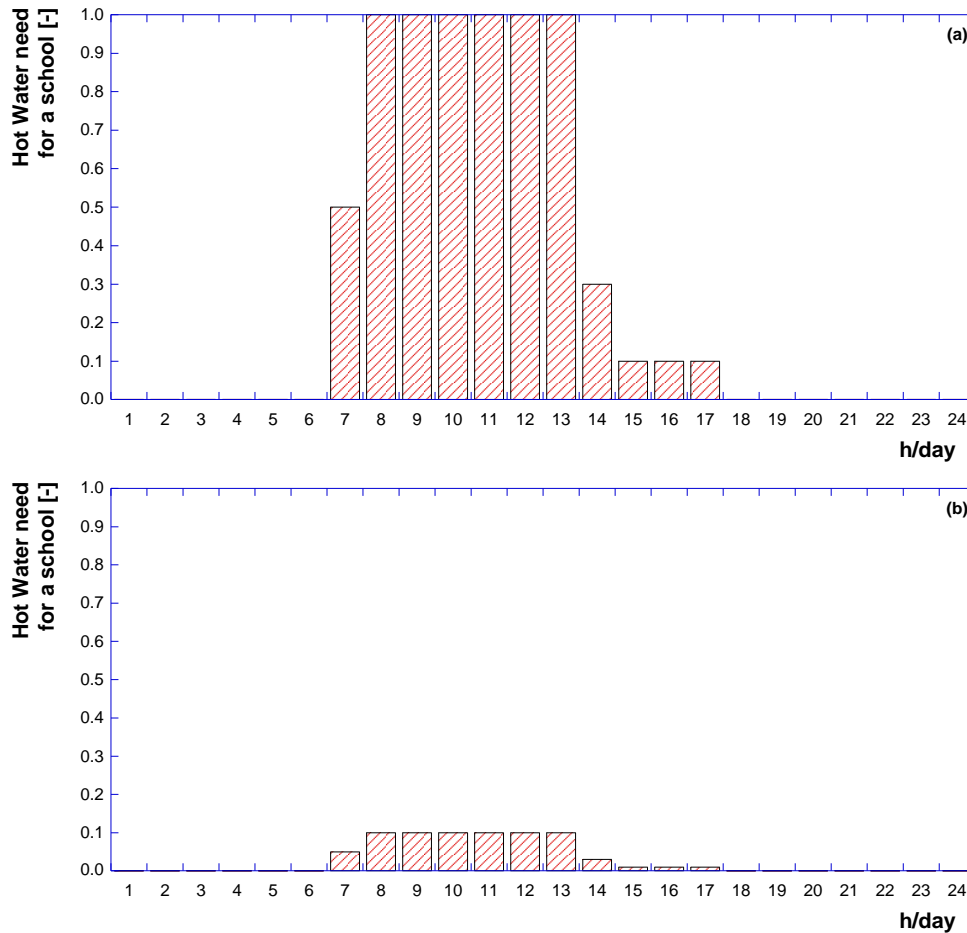


Figure A3 – Non-dimensional thermal power profile for hot water in case of school user, for a typical day during (a) wintertime and (b) summertime.

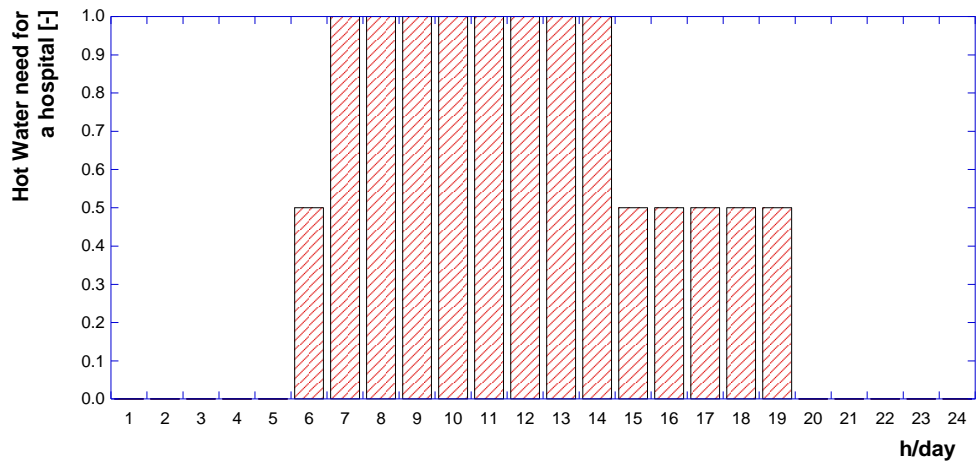
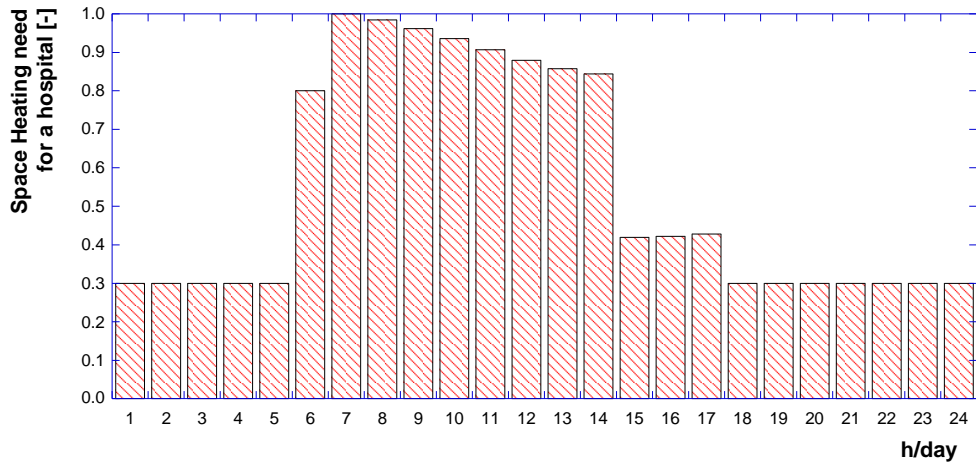


Figure A4 – Non-dimensional thermal power profile for (a) space heating and (b) hot water, in case of day-hospital structure.

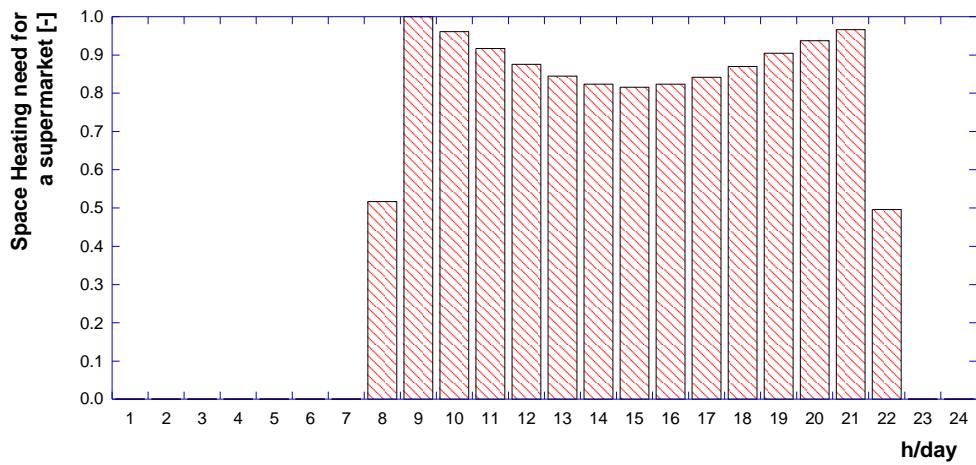


Figure A5 – Non-dimensional thermal power profile for space heating in case of super-market.

Appendix B

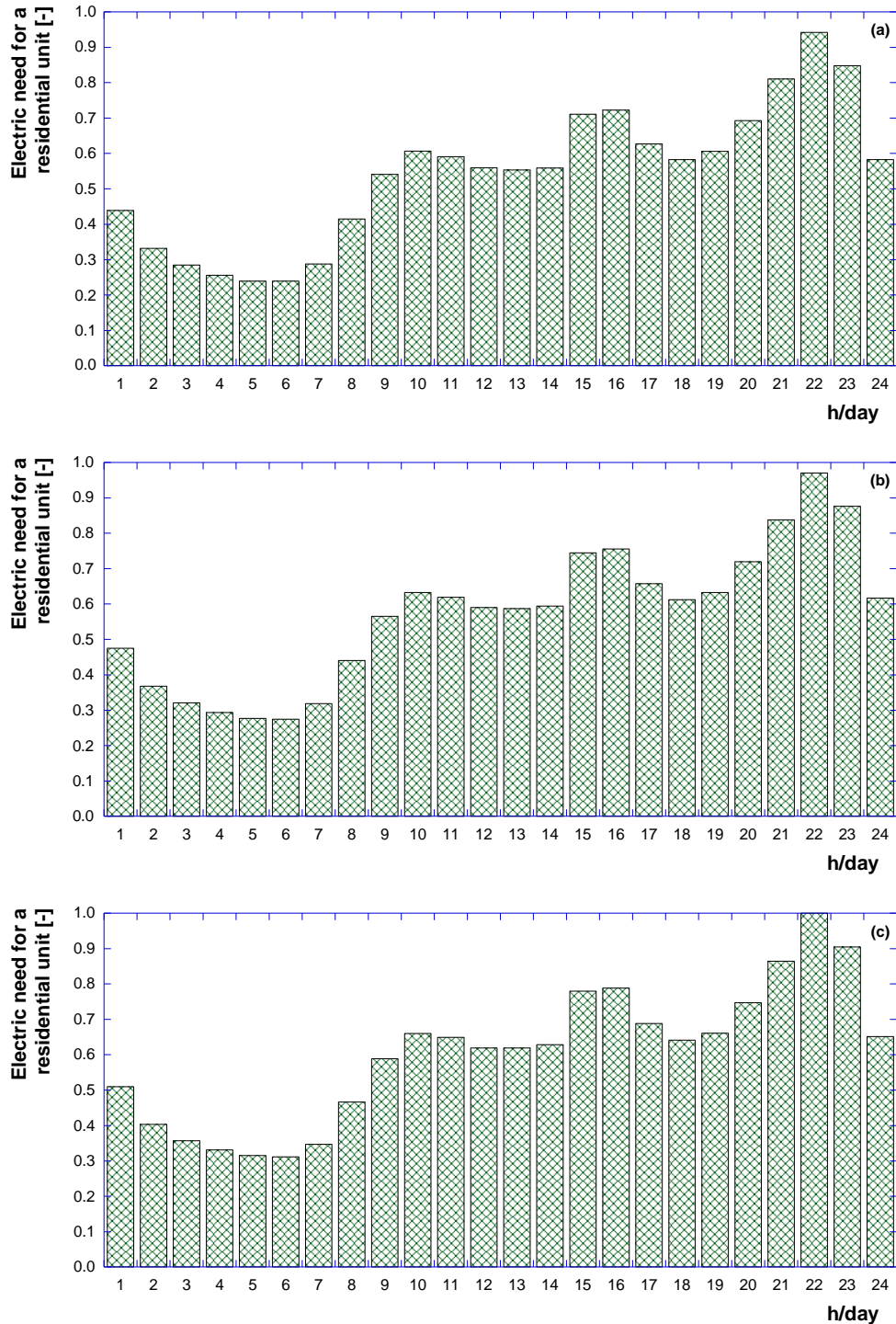


Figure B1 – Non-dimensional electrical power profile for a single residential unit during a typical day in (a) wintertime, (b) middle season and (c) summertime.

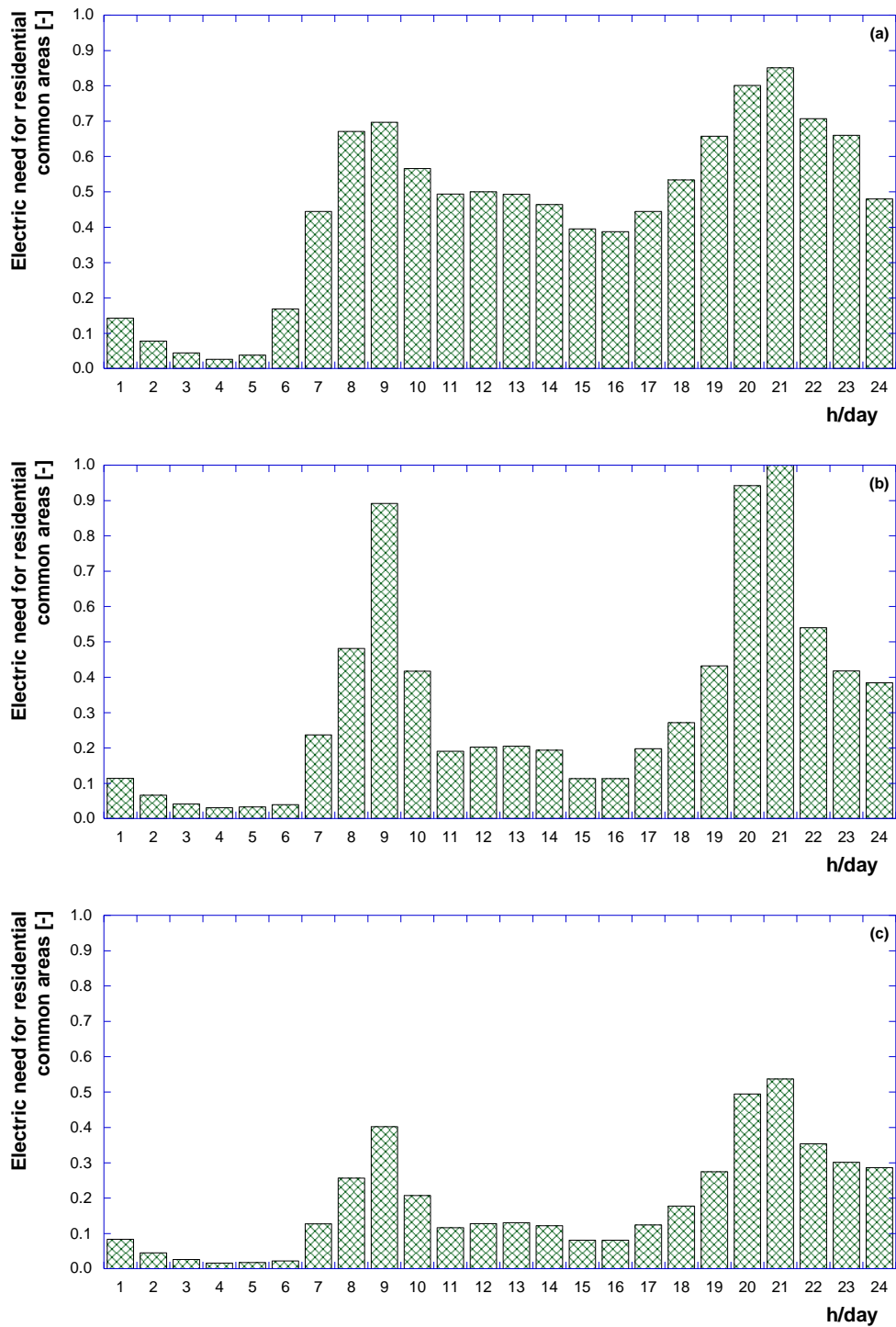


Figure B2 – Non-dimensional electrical power profile for the building common areas during a typical day in (a) wintertime, (b) middle season and (c) summertime.

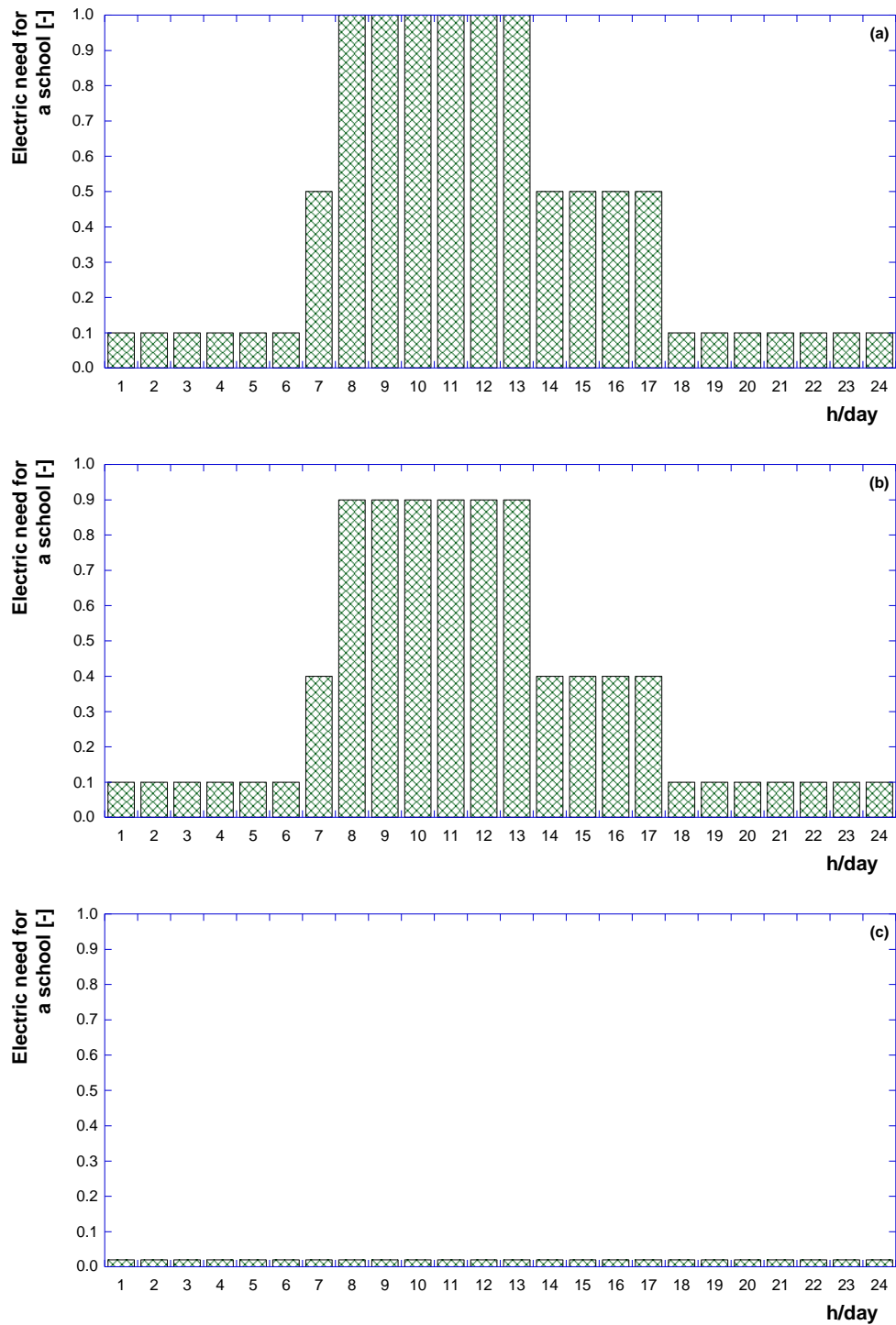


Figure B3 – Non-dimensional electrical power profile for a school during a typical day in (a) wintertime, (b) middle season and (c) summertime.

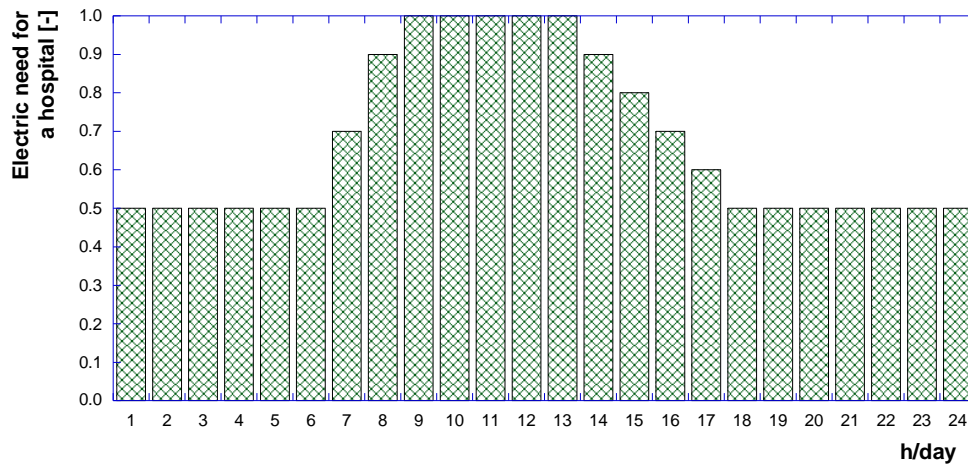


Figure B4 – Non-dimensional electrical power profile for a day-hospital structure: this profile is maintained for the whole year.

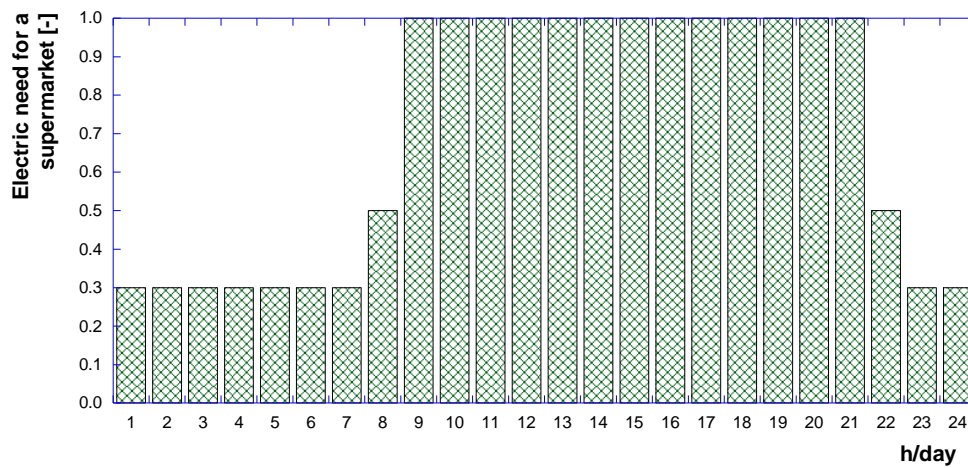


Figure B5 – Non-dimensional electrical power profile for a super-market: this profile is maintained for the whole year.

Appendix C

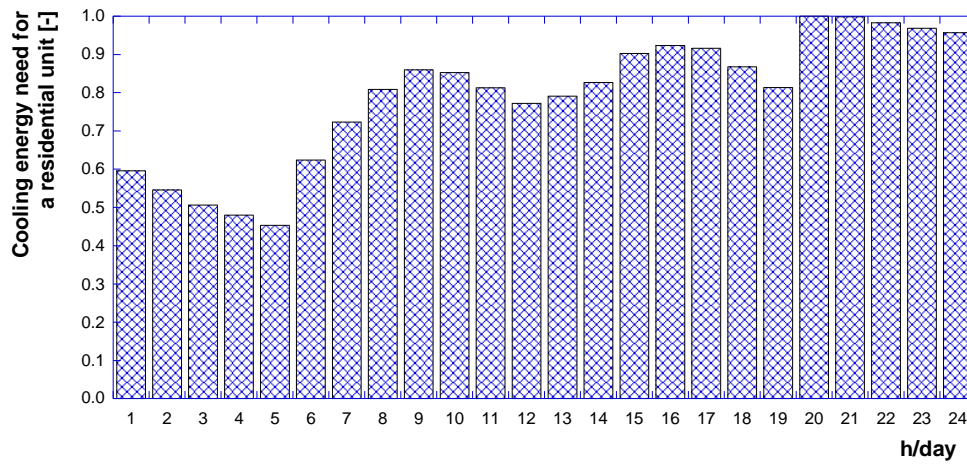


Figure C1 – Non-dimensional cooling power profile for a single residential unit during a typical day in summertime.

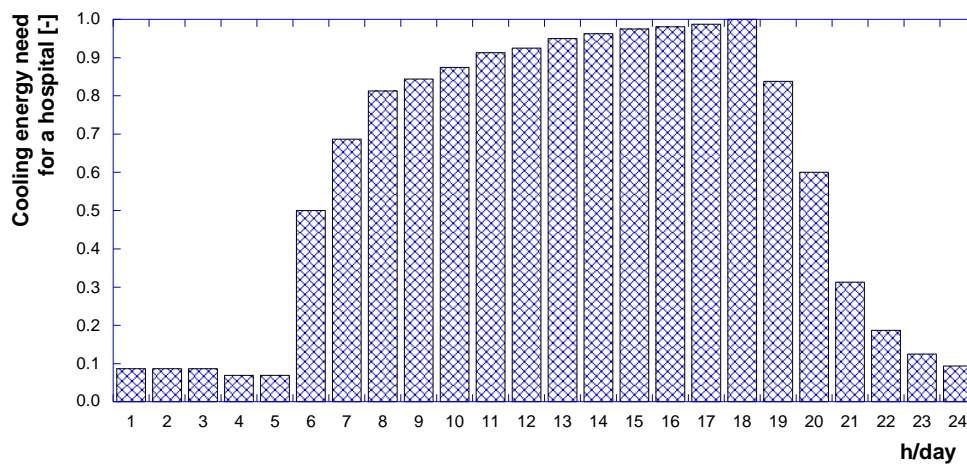


Figure C2 – Non-dimensional cooling power profile for a day-hospital structure during a typical day in summertime.

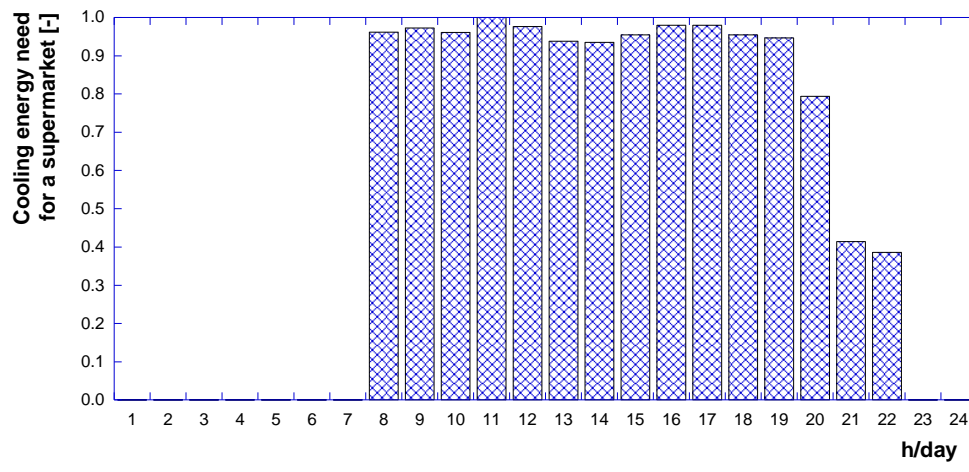


Figure C3 – Non-dimensional cooling power profile for a super-market during a typical day in summertime.